

FINISHING OF ADVANCED CERAMIC BALLS FOR BEARING  
APPLICATIONS BY MAGNETIC FLOAT POLISHING (MFP)  
INVOLVING FINE POLISHING FOLLOWED BY  
CHEMO-MECHANICAL POLISHING (CMP)

By

MING JIANG

Bachelor of Science  
HuaQiao University  
FuJian, China  
1991

Master of Science  
HuaQiao University  
FuJian, China  
1994

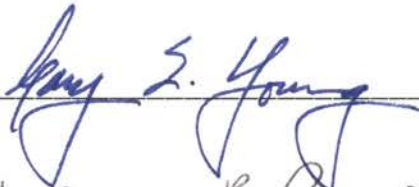
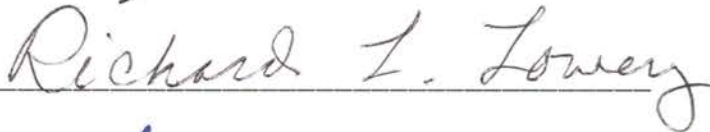
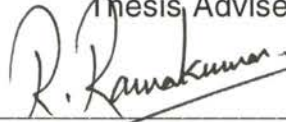
Submitted to the Faculty of the  
Graduate College of the  
Oklahoma State University  
in partial fulfillment of  
the requirements for  
the Degree of  
DOCTOR OF PHILOSOPHY  
July, 1998

FINISHING OF ADVANCED CERAMIC BALLS FOR BEARING  
APPLICATIONS BY MAGNETIC FLOAT POLISHING (MFP)  
INVOLVING FINE POLISHING FOLLOWED BY  
CHEMO-MECHANICAL POLISHING (CMP)

Thesis Approved:



Thesis Adviser



Wayne B. Powell

Dean of the Graduate College

## PREFACE

Advanced ceramics, such as silicon nitride ( $\text{Si}_3\text{N}_4$ ) are being considered actively for ball and roller applications in high-speed, high-temperature bearings in jet turbines and high speed spindles in precision machine tools. This is due to their unique properties, such as lower density, higher hardness, higher elastic modulus (higher stiffness), higher thermal and chemical stability, and higher fracture toughness among advanced ceramics. However, the application of ceramic bearings, either all ceramic or hybrid, are still limited as they are expensive to manufacture and lack sufficient reliability after finishing by conventional grinding and polishing techniques.

Magnetic float polishing (MFP) combined with mechanical and chemo-mechanical polishing (CMP) is an efficient and cost effective manufacturing technology for producing high quality  $\text{Si}_3\text{N}_4$  balls for bearing applications, due to high polishing speed, small and controlled polishing force, flexible support, and chemo-mechanical action between the balls and abrasives. The primary objective of this investigation is to develop a methodology for finishing  $\text{Si}_3\text{N}_4$  balls for bearing applications with good sphericity ( $0.15 \mu\text{m}$ ) and surface finish ( $4 \text{ nm Ra}$ ) by magnetic float polishing (MFP) technology.

Experimental design and analysis based on Taguchi's method is applied to determine the optimum processing conditions (within the range of parameters

and levels tested) for improving the surface quality of the ceramic balls by magnetic float polishing. High material removal rates ( $1 \mu\text{m}/\text{min}$ ) with minimal subsurface damage are possible using abrasives harder than the workmaterial, such as  $\text{B}_4\text{C}$  or  $\text{SiC}$  due to rapid accumulation of minute amounts of material removed by mechanical microfracture at low loads but high polishing speeds in the MFP process. The best surface finish obtained using fine mechanical polishing with fine, harder  $\text{B}_4\text{C}$  abrasive ( $1\text{-}2 \mu\text{m}$ ) is  $20 \text{ nm}$  for  $R_a$  and  $200 \text{ nm}$  for  $R_t$ ; The best surface finish obtained using fine, harder  $\text{SiC}$  abrasive ( $1 \mu\text{m}$ ) (fine mechanical polishing) is  $15 \text{ nm}$  for  $R_a$  and  $150 \text{ nm}$  for  $R_t$ ; To improve the final surface finish, further, polishing was carried out involving chemo-mechanical polishing (CMP).

There are three stages involved in polishing, namely, initial roughing stage where the emphasis is on high material removal rate with minimal surface-subsurface damage, intermediate semi-finishing stage where material removal rate, sphericity, and surface roughness have to be closely monitored, and the final finishing stage with emphasis is on the final required size, sphericity, and finish. CMP is a cost effective process for final finishing of  $\text{Si}_3\text{N}_4$  balls for bearing applications. The result of CMP depends on the polishing conditions used, abrasive-workmaterial combination, and the environment.

Various abrasives were investigated systematically to determine their effectiveness for the CMP of  $\text{Si}_3\text{N}_4$  bearing balls for obtaining extremely smooth and damage-free surface.  $\text{CeO}_2$  and  $\text{ZrO}_2$  abrasives were found to be most effective abrasives followed by  $\text{Fe}_2\text{O}_3$  and  $\text{Cr}_2\text{O}_3$ . It is also found that CMP of  $\text{Si}_3\text{N}_4$  is particularly effective in a water-based environment rather than oil-based environment. Thermodynamic analysis (Gibbs free energy of formation) indicated the feasibility of chemical reactions between the following abrasives,

CeO<sub>2</sub>, ZrO<sub>2</sub>, Fe<sub>2</sub>O<sub>3</sub>, Cr<sub>2</sub>O<sub>3</sub>, and Si<sub>3</sub>N<sub>4</sub> workmaterial leading to the formation a extremely thin SiO<sub>2</sub> layer. Since the hardness of these abrasives is closer to that of SiO<sub>2</sub> layer and lower than Si<sub>3</sub>N<sub>4</sub> workmaterial, the SiO<sub>2</sub> reaction layer is effectively removed without damaging the Si<sub>3</sub>N<sub>4</sub> substrate by subsequent mechanical action by the abrasives on the workmaterial. The kinetic action, which involves the removing of the reaction products from the interface is critical in the CMP process. The chemical reaction can be continued only after the passivating layers are removed continuously by the subsequent mechanical action. It is found that there is very little, if any, of CMP occurring in an oil-based polishing environment. The conductivity and dissolution value of an oil-based polishing fluid is nearly zero. The oil film between the abrasive and the workmaterial prevents any chemical reactions between them as well as the removal of reaction layer formed, if any, thus minimizing CMP. It has been found that CMP of Si<sub>3</sub>N<sub>4</sub> is particularly effective in a water environment. Water from water-based polishing fluid not only facilitates chemo-mechanical interaction between the abrasive and the workmaterial but also participates directly in the chemical reaction with the Si<sub>3</sub>N<sub>4</sub> workmaterial (hydrolysis) leading to the formation of the SiO<sub>2</sub> softer layer thereby enhancing the CMP.

An extremely smooth and damage-free surface with a finish R<sub>a</sub> of 4 nm and R<sub>t</sub> of 40 nm have been obtained with CeO<sub>2</sub> and ZrO<sub>2</sub> abrasives in the CMP of Si<sub>3</sub>N<sub>4</sub> balls. It may be noted that CeO<sub>2</sub> and ZrO<sub>2</sub> are much softer than Si<sub>3</sub>N<sub>4</sub> and could not cause any mechanical damage or scratching on the Si<sub>3</sub>N<sub>4</sub> workmaterial. In the case of Cr<sub>2</sub>O<sub>3</sub> abrasive which was reported as the most effective polishing media [Baghavatula, et al, 1996], the mechanical abrasion caused by Cr<sub>2</sub>O<sub>3</sub> could not be eliminated completely, in spite of its chemo-mechanical polishing ability, because Cr<sub>2</sub>O<sub>3</sub> is slightly harder than the Si<sub>3</sub>N<sub>4</sub>

workmaterial. Consequently, while CMP can take place effectively between  $\text{Si}_3\text{N}_4$  and  $\text{Cr}_2\text{O}_3$ , possibility exists for mechanical abrasion and subsequent microchipping. Further,  $\text{CeO}_2$  and  $\text{ZrO}_2$  and their various reaction products formed during polishing are much more safer than the compounds formed by the reaction of  $\text{Cr}_2\text{O}_3$  with  $\text{Si}_3\text{N}_4$  workmaterial from an environmental point of view. It has been reported that the best abrasives for polishing glasses are  $\text{CeO}_2$  and  $\text{ZrO}_2$  [Cook, 1990]. There are many similarities between polishing glass and polishing  $\text{Si}_3\text{N}_4$  workmaterial including the role of water, polishing environment (pH value 7-9), and abrasive hardness (~ Mohs 7) for effective polishing. It is somewhat coincidental, that in general, chemical effectiveness and mechanical hardness of abrasives for CMP of  $\text{Si}_3\text{N}_4$  are similar to those for glass. This is not altogether surprising as the material removal mechanism in the case of  $\text{Si}_3\text{N}_4$  is through the formation of  $\text{SiO}_2$  and in the case of glass which is basically  $\text{SiO}_2$  (Mohs 6.5). From an analysis of CMP of  $\text{Si}_3\text{N}_4$ , it appears reasonable to extend this mechanism to the polishing of silicon wafers,  $\text{SiO}_2$ -based glasses, and advanced SiC ceramics. This is based on the similarity in the formation of  $\text{SiO}_2$  on the surface and its subsequent removal by mechanical action.

$\text{CeO}_2$  is found to be the most effective polishing medium in the CMP of  $\text{Si}_3\text{N}_4$  balls. It has two important functions, first, it directly reacts chemically (oxidization-reduction reaction) with  $\text{Si}_3\text{N}_4$  workmaterial and leads to the formation of  $\text{SiO}_2$  layer, second, its hardness (Moh 6) is close to the  $\text{SiO}_2$  layer (Moh 6.5) and significantly lower (~ 1/3) than  $\text{Si}_3\text{N}_4$  workmaterial. So, the  $\text{Si}_3\text{N}_4$  substrate can hardly be scratched or damaged by  $\text{CeO}_2$  but the  $\text{SiO}_2$  layer can be removed under subsequent mechanical action of  $\text{CeO}_2$  on the  $\text{Si}_3\text{N}_4$  workmaterial. The  $\text{CeO}_2$  polishing media is particularly effective in a water

environment as it causes hydrolysis and leads to the formation of  $\text{SiO}_2$  layer which is removed from the  $\text{Si}_3\text{N}_4$  by subsequent mechanical action of  $\text{CeO}_2$ . Possible chemical reactions during this process are studied in detail using Gibbs free energy change (thermodynamic analysis) using the HSC Chemistry Software developed in Finland [Outokumpu research, 1997]. The flash temperature generated and the corresponding flash times in the polishing process were calculated using the moving disc heat source model developed by Hou and Komanduri (1998). It can be seen that the estimated temperatures generated and the flash durations at the contact zone of the CMP process are adequate for the generation of specific reactions obtained from the thermodynamic analysis. The  $\text{Si}_3\text{N}_4$  surface after CMP would consist of an outer  $\text{SiO}_2$  layer and an intermediary layer of silicon oxinitride ( $\text{Si}_x\text{O}_y\text{N}_z$ ) on the  $\text{Si}_3\text{N}_4$  substrate. The layers composed of amorphous and crystalline  $\text{SiO}_2$ ,  $\text{Si}_2\text{N}_2\text{O}$ , and  $\text{MgSiO}_3/\text{MgO} \cdot \text{SiO}_2$  form by the reaction with the sintering aid (1 wt.% MgO). This is not much different from the surface of  $\text{Si}_3\text{N}_4$  workmaterial which invariably has a natural oxidation layer in air even at room temperature.

MFP can be a cost effective process for finishing  $\text{Si}_3\text{N}_4$  balls for bearing applications. The roughing stage depends on the amount of material to be removed from the as-received condition to the final requirements. The material removal rate is  $\sim 1 \mu\text{m}/\text{min}$ . The semifinishing and finishing stages can be accomplished in about 4 hours. In any case, a batch of balls can be finished (actual polishing times, not including the time taken for characterizations, periodic replacement of magnetic fluids and abrasives, and cleaning) in about 20 hours compared to several weeks by conventional polishing. Also, diamond abrasive is not required for the process. Faster polishing times and use of abrasives other than diamond would significantly reduce the overall costs of

manufacture of the  $\text{Si}_3\text{N}_4$  balls for bearing applications. Also, the implementation of this technology would not be very capital intensive as it can be incorporated in an existing equipment. Attempts are currently underway to increase the batch size close to hundred balls (3/8 inch dia.) with the next generation prototype equipment. Besides, an additional advantage of the magnetic float polishing (MFP) apparatus used in this investigation is that it is capable of finishing a small batch (10-20 balls) to the finish requirements without the need for sorting them from a large batch of balls or use different equipment as in conventional lapping. Such an apparatus would be beneficial especially when small batches are needed for specific low volume applications or for evaluation of materials in the development of new materials for bearing applications. A methodology of obtaining silicon nitride balls of required tolerance for bearing application has been developed in this investigation.



## ACKNOWLEDGMENTS

I would like to thank my advisor Dr. R. Komanduri for his support and guidance. I would also like to show my appreciation to Dr. R. G. Ramakumar, Dr. R. L. Lowery, and Dr. G. E. Young for serving on my doctoral advisory committee. My special thanks to Drs. Zhen-Bing Hou and Yin-Ming Wang for valuable discussions. I would also thank Dr. N. Umehara, Assoc. Prof. at Tohoku University, Japan, Dr. R. Makaram, a former graduate student at OSU, and all my colleagues at MAERL for their help and useful discussions. Thanks are also due to Ms. Margaret Mitchell and Mr. Jerry Dale of MAERL for their help.

This project is sponsored by grants from the National Science Foundation on "Tribological Interactions in Polishing of Advanced Ceramics and Glasses," (CMS-9414610), "Design, Construction, and Optimization of Magnetic Field Assisted Polishing," (DMI-9402895), DoD's DEPSCoR Program on "Finishing of Advanced Ceramics" (DAAH04-96-1-0323), and CATT's program on "Finishing of Silicon Nitride Balls for Bearing Applications" (F34601-95-D-0376). This project was initiated by a DARPA contract on the "Ceramic Bearing Technology Program" (F33615-92-5933). Thanks are due to Drs. J. Larsen Basse, B. M. Kramer, Ming Leu, and D. Durham of NSF and Dr. K. R. Mecklenburg of WPAFB, Dr. W. Coblenz of DARPA, and Dr. Nelson Wood of TASC for their interest and support of this work.

## TABLE OF CONTENTS

Chapter		Page
1.	INTRODUCTION	1
	1.1 Hybrid Advanced Ceramic Bearings	1
	1.2 Fundamental Problems in the Finishing of Advanced Ceramics	11
	1.3 Conventional Finishing Method and Its Limitations	15
	1.4 "Gentle" Finishing of Ceramic Balls for Bearing Applications	21
2.	LITERATURE REVIEW	29
3.	PROBLEM STATEMENT	52
4.	APPROACH	55
	4.1 Magnetic Float Polishing (MFP) Apparatus	55
	4.2 Silicon Nitride Workmaterial	60
	4.3 Abrasives	63
	4.4 Experimental Work	66
	4.5 Surface Integration Evaluation	67
5.	APPLICATION OF TAGUCHI METHOD TO DETERMINE OPTIMUM POLISHING CONDITIONS	77
	5.1 Introduction	77
	5.2 The Design of Experiments and Taguchi Method	80
	5.3 Experimental Approach	82
	5.4 Experimental Results and Evaluation	86

5.5	Experimental Analysis	90
5.6	Optimum Settings	107
5.7	Single-Factor By Single-Factor Approach	108
5.8	Brittle Fracture Model of Mechanical Polishing	123
6.	INVESTIGATION OF CHEMO-MECHANICAL POLISHING (CMP) SILICON NITRIDE ( $\text{Si}_3\text{N}_4$ ) WITH VARIOUS ABRASIVES	129
6.1	Introduction	129
6.2	Chemo-mechanical Polishing (CMP)	129
6.3	Experimental Details	133
6.4	CMP Test Results	136
6.5	Discussion of CMP	148
7.	ON THE CHEMO-MECHANICAL POLISHING (CMP) OF $\text{Si}_3\text{N}_4$ WITH WATER-BASED $\text{CeO}_2$ SLURRY	155
7.1	Introduction	155
7.2	Cerium Oxide ( $\text{CeO}_2$ ) Abrasive	156
7.3	CMP of $\text{Si}_3\text{N}_4$ With Water-based $\text{CeO}_2$ Slurry	158
7.4	Thermodynamic Analysis of CMP	165
7.5	Mechanism of CMP of $\text{Si}_3\text{N}_4$ With $\text{CeO}_2$	177
8.	METHODOLOGY OF FINISHING $\text{Si}_3\text{N}_4$ BALLS BY MFP FOR BEARING APPLICATIONS	181
8.1	Introduction	181
8.2	Polishing Conditions and Procedure	182
8.3	Polishing Results	187
8.4	Discussion	202
8.5	Precision Manufacturing Process	204
8.6	Conclusions	222

9.	FUTURE WORK	224
10.	CONCLUSIONS	233
	REFERENCES	239
	APPENDIX	250

## LIST OF FIGURES

Figure		Page
Figure 1.1	Under similar conditions, the hybrid (ceramic ball-M50 race) bearing balls (CENTER) kept going where the all-M50 steel bearing balls (LEFT and RIGHT) failed [Lynch, 1991]	4
Figure 1.2	High-speed spindle unit with hybrid ceramic bearings (from HSK) for precision high speed cutting machines	5
Figure 1.3	(a) The M50 ball with significant fatigue after about first 25 hour induced-defect test	7
	(b) Typical condition of silicon nitride ball without signs of fatigue after the first 25 hour induced-defect test	7
	(c) SEM photo of spalled area on silicon nitride ball after fourth induced-defect test	8
Figure 1.4	(a) Mechanisms of material removal	14
	(b) Chip formation of advanced ceramics [Usui, 1990]	14
Figure 1.5	Conventional V-groove lapping apparatus for the grinding and polishing of bearing balls	16
Figure 1.6	SEM micrograph of a best commercially finished Si <sub>3</sub> N <sub>4</sub> ball surface (AFBMA Grade 3)	20
Figure 1.7	Principle of hydrodynamic float polishing [Watanabe and Suzuki, 1981]	22

Figure 1.8	Principle of magnetic float polishing [Tani and Kawata, 1984]	22
Figure 1.9	Principle of chemo-mechanical polishing [Yasunaga, Imanaka, et al, 1978]	22
Figure 2.1	When a magnetic field is applied to the magnetic fluid, the magnetic particles move to high field side and push non-magnetic body towards lower field side and thus (a) the abrasive grains and (b) the float being non-magnetic are floated up. (c) Magnet arrangement in this study	32
Figure 2.2	The effect of float on polishing load, sphericity, and stock removal [Umehara and Kato, 1990]	
	(a) Magnetic float polishing set-up	37
	(b) variation of polishing load with clearance	38
	(c) variation of sphericity with polishing time	39
	(d) variation of the stock removal with polishing time	39
Figure 2.3	Dynamic model of magnetic float polishing [Zhang et al, 1996]	40
Figure 2.4	Eccentric magnetic float polishing apparatus [Zhang et al, 1997]	41
Figure 2.5	Material removal mechanism in magnetic float polishing [Childs et al, 1994]	
	(a) kinematic model of ball motion during MFP	42
	(b) Abrasives embedded in the drive shaft show two-body abrasion of material removal mechanism in MFP	43
	(c) Diagram of two-body abrasion	43
Figure 2.6	Electromagnetic float polishing apparatus	44
Figure 2.7	Magnetic float polishing of Alumina flat surfaces [Umehara et al, 1992]	45

Figure 2.8	Schematic of the magnetic float polishing of HIP'ed Si <sub>3</sub> N <sub>4</sub> rollers apparatus.[Umehara and Komanduri, 1996]	47
Figure 2.9	X-ray diffraction analysis of the wear debris showing the presence of CrN and Cr <sub>2</sub> SiO <sub>4</sub> [Bhagavatula and Komanduri, 1996]	50
Figure 4.1	Schematic of the magnet float polishing (MFP) apparatus for finishing advanced ceramic balls	57
Figure 4.2	(a) SEM micrograph of SiC (#400 grit) abrasives (b) SEM micrograph of B <sub>4</sub> C (#500 grit) abrasives	65 65
Figure 4.3	Four different reference circles available for out-of-roundness	69
Figure 4.4	Schematic diagram of Talyrond electronic measuring system and the principle of its variable inductance pick-up	70
Figure 4.5	Derivation of some surface roughness parameters (Ra and Rt)	72
Figure 4.6	Schematic diagram of Form Talysurf traverse unit with laser interferometric transducer system	75
Figure 5.1	(a) Plots of the response of each polishing parameter level on the surface finish Ra (b) Plots of the response of each polishing parameter level on the surface finish Rt	94 95
Figure 5.2	(a) Plots of the S/N ratios showing the effect of each parameter level on the surface finish Ra (b) Plots of the S/N ratios showing the effect of each parameter level on the surface finish Rt	99 100

Figure 5.3	Talysurf surface roughness trace after polishing with load (a) 0.5 N/ball, (b) 1 N/ball, and (c) 1.5 N/ball, with SiC (1 $\mu\text{m}$ grit) abrasive, concentration 5%, speed 2000 rpm	110
Figure 5.4	SEM morphologies of a $\text{Si}_3\text{N}_4$ ball surface after polishing with load (a) 0.5 N/ball, (b) 1 N/ball, and (c) 1.5 N/ball, with SiC (1 $\mu\text{m}$ grit) abrasive, concentration 5%, speed 2000 rpm	111
Figure 5.5	The schematic of 3-body and 2-body abrasion models	112
Figure 5.6	Talysurf surface roughness trace after polishing with speed (a) 2000 rpm, (b) 4000 rpm, and (c) 6000 rpm, with SiC (1 $\mu\text{m}$ grit) abrasive, load 1 N/ball, concentration 5%	114
Figure 5.7	Talysurf surface roughness trace after polishing with abrasive concentration (a) 5 %, (b) 10%, and (c) 20 %, with SiC (1 $\mu\text{m}$ grit) abrasive, load 1 N/ball, speed 2000 rpm	116
Figure 5.8	(a) Abrasive size vs surface roughness, and (b) Abrasive size vs material removal rate with SiC (1 $\mu\text{m}$ grit) abrasive, load 1 N/ball, speed 2000 rpm, concentration 10%	118
Figure 5.9	Profile of transversal cross-section after polished by small size abrasive and large size abrasive	119
Figure 5.10	SEM micrograph of the $\text{Si}_3\text{N}_4$ ball polishing with $\text{B}_4\text{C}$ (#500 grit) abrasive at 2000 rpm, 10% abrasive vol%, and 1 N/ball showing the material removal from 3 body abrasion brittle microchipping	121
Figure 5.11	SEM micrograph of the $\text{Si}_3\text{N}_4$ ball polishing with $\text{B}_4\text{C}$ (#1500 grit) abrasive at 2000 rpm, 10% abrasive	



	vol%, and 1 N/ball showing the material removal from brittle microfracture pits	121
Figure 5.12	SEM micrograph of the Si <sub>3</sub> N <sub>4</sub> ball polishing with diamond (#500 grit) abrasive at 4000 rpm, 10% abrasive vol%, and 1 N/ball showing the material removal from 2 body abrasion brittle scratching	122
Figure 5.13	Formation of cracks in a brittle surface under point indentation [Lawn and Wilshaw, 1975]	124
Figure 5.14	Lateral cracking and median cracking of a moving point indentation [Swain, 1979]	124
Figure 5.15	Lateral cracks and radial / median cracking in vickers indentation (A) Lateral cracks > Radial cracks (B) Lateral cracks < Radial cracks [Marshall et al, 1982]	126
Figure 6.1	(a) Initial surface finish prepared by polishing with B <sub>4</sub> C (1500)	138
	(b) Talysurf surface roughness profiles after polishing by Al <sub>2</sub> O <sub>3</sub>	138
	(c) Talysurf surface roughness profiles after polishing by CuO	138
	(d) Talysurf surface roughness profiles after polishing by Y <sub>2</sub> O <sub>3</sub>	139
	(e) Talysurf surface roughness profiles after polishing by SiO <sub>2</sub>	139
	(f) Talysurf surface roughness profiles after polishing by Mo <sub>2</sub> O <sub>3</sub>	139
	(g) Talysurf surface roughness profiles after polishing by Cr <sub>2</sub> O <sub>3</sub>	140
	(h) Talysurf surface roughness profiles after polishing by Fe <sub>2</sub> O <sub>3</sub>	140
	(i) Talysurf surface roughness profiles after polishing by CeO <sub>2</sub>	140

	(j) Talysurf surface roughness profiles after polishing by $ZrO_2$	141
Figure 6.2	(a) SEM micrograph of the surface of a $Si_3N_4$ ball finished by $B_4C$ (#1500 grit) abrasive	142
	(b) SEM micrograph of the surface of a $Si_3N_4$ ball finished by $CeO_2$ abrasive	142
Figure 6.3	(a) Initial surface finish prepared by polishing with $SiC$ (#8000 grit) abrasive	144
	(b) Talysurf surface roughness profiles after polishing by $ZrO_2$	144
	(c) Talysurf surface roughness profiles after polishing by $CeO_2$	144
Figure 6.4	SEM micrograph of the surface of a $Si_3N_4$ ball finished by $SiC$ (#8000 grit) abrasive followed by $CeO_2$	145
Figure 6.5	(a) Initial surface finish prepared by polishing with $B_4C$ (#1500 grit) abrasive	146
	(b) Surface finish after polishing by $CeO_2$ in an oil-based mag. fluid	146
	(c) Surface finish after polishing by $CeO_2$ in a water-based mag. fluid	146
Figure 7.1	(a) SEM micrograph of a $Si_3N_4$ ball surface after finishing by $Cr_2O_3$	161
	(b) Talysurf surface roughness profile of a $Si_3N_4$ ball surface after finished by $Cr_2O_3$	161
Figure 7.2	(a) SEM micrograph of a $Si_3N_4$ ball surface after finishing by $CeO_2$	162
	(b) Talysurf surface roughness profile of a $Si_3N_4$ ball surface after finished by $CeO_2$	162
Figure 7.3	The flash temperatures generated at the contact zone in MFP with $CeO_2$	164

Figure 7.4	(a) Variation of the mole fractions of various species with temperature of the chemical reaction system consisting of 1 mol of $\text{Si}_3\text{N}_4$ and 1 mol of $\text{H}_2\text{O}$	167
	(b) Variation of various chemical species with temperature for 1 mol of $\text{Si}_3\text{N}_4$ and increasing amounts of $\text{H}_2\text{O}$	168
Figure 7.5	(a) Variation of the reaction products with temperature of the chemical reaction system consisting of 1 mol of $\text{Si}_3\text{N}_4$ and 1 mol of $\text{CeO}_2$	170
	(b) Variation of the reaction products with increasing mole fraction of $\text{CeO}_2$	171
Figure 7.6	(a) Variation of the reaction products with temperature for the chemical reaction system of 1 mol of $\text{Si}_3\text{N}_4$ , 1 mol of $\text{CeO}_2$ , and 1 mol of $\text{H}_2\text{O}$	173
	(b) Variation of the reaction products with pressure for the chemical reaction system of 1 mol of $\text{Si}_3\text{N}_4$ , 1 mol of $\text{CeO}_2$ , and 1 mol of $\text{H}_2\text{O}$	174
Figure 8.1	(a) SEM micrograph of a commercially finished $\text{Si}_3\text{N}_4$ ball surface	188
	(b) Talysurf surface roughness profiles of of a commercially finished $\text{Si}_3\text{N}_4$ ball surface	188
	(c) AFM image of a commercially finished $\text{Si}_3\text{N}_4$ ball surface	189
	(d) High magnification AFM image of a commercially finished $\text{Si}_3\text{N}_4$ ball surface	190
Figures 8.2	Talysurf surface roughness profiles of a $\text{Si}_3\text{N}_4$ ball after polishing (a) by $\text{B}_4\text{C}$ (500 grit) abrasive (b) by $\text{SiC}$ (400 grit) abrasive (c) by $\text{SiC}$ (1000 grit) abrasive (d) by $\text{SiC}$ (1200 grit) abrasive (e) by $\text{SiC}$ (8000 grit) abrasive (f) by $\text{CeO}_2$ (5 $\mu\text{m}$ ) abrasive	195
Figure 8.3	(a) ZYGO plot of the surface of a $\text{Si}_3\text{N}_4$ ball after finishing by softer $\text{CeO}_2$ abrasive.	196

	(b) AFM image of the surface of a Si <sub>3</sub> N <sub>4</sub> ball after finishing by softer CeO <sub>2</sub> abrasive	197
	(c) AFM image at high magnification showing an extremely smooth surface of a Si <sub>3</sub> N <sub>4</sub> ball after finishing by softer CeO <sub>2</sub> abrasive	198
Figure 8.4	(a) SEM micrograph of the surface of a Si <sub>3</sub> N <sub>4</sub> ball after polishing by SiC (8000 grit) abrasive	200
	(b) SEM micrograph of the surface of a Si <sub>3</sub> N <sub>4</sub> ball after polishing by CeO <sub>2</sub> abrasive	200
Figure 8.5	(a) SEM micrographs of the the stainless steel shaft in cntact with Si <sub>3</sub> N <sub>4</sub> balls in MFP showing the presence of B <sub>4</sub> C (500 grit) particles and abrasion marks on the shaft materials	201
	(b) SEM micrographs of the the stainless steel shaft in cntact with Si <sub>3</sub> N <sub>4</sub> balls in MFP showing the presence of B <sub>4</sub> C (1500 grit) particles and abrasion marks on the shaft materials	201
Figure 8.6	TalyRond roundness profile of a Si <sub>3</sub> N <sub>4</sub> ball with a typical triangle shape (3 lobe) after poishing with B <sub>4</sub> C #500 due to eccentricity between the polishing drive shaft (tool) and guide ring (track) (Roundness: 6 μm)	207
Figure 8.7	Large batch magnetic float polishing apparatus	209
Figure 8.8	(a) TalyRond roundness profile of an as-received Si <sub>3</sub> N <sub>4</sub> ball showing a 200 μm x 5 mm band at the parting line due to uniaxial pressing process (Roundness: 200 μm)	213
	(b) TalyRond roundness profile of a Si <sub>3</sub> N <sub>4</sub> ball after polishing with B <sub>4</sub> C #500 in Test A (Roundness: 82 μm)	214

	(c) TalyRond roundness profile of a Si <sub>3</sub> N <sub>4</sub> ball after polishing with B <sub>4</sub> C #500 in Test B (Roundness: 46 μm)	214
	(d) TalyRond roundness profile of a Si <sub>3</sub> N <sub>4</sub> ball after after polishing with B <sub>4</sub> C #500 in Test D (Roundness: 16 μm)	215
	(e) TalyRond roundness profile of a Si <sub>3</sub> N <sub>4</sub> ball after after polishing with B <sub>4</sub> C #500 in Test F (Roundness: 7 μm)	215
	(f) TalyRond roundness profile of a Si <sub>3</sub> N <sub>4</sub> ball after after polishing with B <sub>4</sub> C #500 in Test H (Roundness: 2.4 μm)	216
	(g) TalyRond roundness profile of a Si <sub>3</sub> N <sub>4</sub> ball after after polishing with B <sub>4</sub> C #500 in Test J (Roundness: 1.6 μm)	216
	(h) TalyRond roundness profile of a Si <sub>3</sub> N <sub>4</sub> ball after after polishing with B <sub>4</sub> C #500 in Test L (Roundness: 0.6 μm)	217
	(i) TalyRond roundness profile of a Si <sub>3</sub> N <sub>4</sub> ball after polishing with SiC #1200 in Test N (Roundness: 0.3 μm)	217
	(j) TalyRond roundness profile of a Si <sub>3</sub> N <sub>4</sub> ball after polishing with SiC # 8000 in Test O (Roundness: 0.2 μm)	218
	(k) TalyRond roundness profile of a Si <sub>3</sub> N <sub>4</sub> ball after polishing with CeO <sub>2</sub> (5 μm) in Test Q (Roundness: 0.15 μm)	218
Figure 8.9	(a) TalySurf surface roughness profile of a Si <sub>3</sub> N <sub>4</sub> ball after polishing with B <sub>4</sub> C #500 in Test L	219
	(b) TalySurf surface roughness profile of a Si <sub>3</sub> N <sub>4</sub> ball after polishing with SiC #1200 in Test N	219
	(c) TalySurf surface roughness profile of a Si <sub>3</sub> N <sub>4</sub> ball after polishing with SiC #8000 in Test O	220
	(d) TalySurf surface roughness of a Si <sub>3</sub> N <sub>4</sub> ball after polishing with CeO <sub>2</sub> (5 μm) in Test Q	220

Figure 8.10	Variation of sphericity with polishing time	221
Figure 9.1	(a) An initial surface finish of a zirconia ( $ZrO_2$ ) ball	227
	(b) A surface finish of a zirconia ( $ZrO_2$ ) ball after polishing with SiC (#8000 grit) abrasive	227

## LIST OF TABLES

Table		Page
Table 1.1	The properties of some of the advanced ceramics and conventional bearing steel materials	2
Table 1.2	Features, benefits, and applications of the hybrid ceramic bearings	10
Table 1.3	The bonding nature of advanced ceramic materials	13
Table 1.4	Comparison of properties between metals and advanced ceramics	13
Table 1.5	Comparison of parameters used in conventional lapping and magnetic float polishing	26
Table 2.1	MFP research activities in Kato and Umehara's group in Japan	34
Table 2.2	MFP research activities in Childs' group in the UK	35
Table 2.3	MFP research activities in Komanduri's group in the USA	36
Table 4.1	Chemical composition of NBD-200 Silicon Nitride	63
Table 4.2	Mechanical and thermal properties of Si <sub>3</sub> N <sub>4</sub> workpiece	63
Table 4.3	Abrasives used in this study	64
Table 4.4	AFBMA grading charts of metal balls for bearing	76

Table 5.1	Test condition used in the investigation	79
Table 5.2	Test parameters and their levels	79
Table 5.3	$L_9(3^4)$ Orthogonal arrays	85
Table 5.4	Experimental design	85
Table 5.5	Experimental results	87
Table 5.6	Level average analysis using average effect	92
Table 5.7	Level average analysis using S/N	97
Table 5.8	Values of S/N and $(S/N)^2$	106
Table 5.9	Analysis of variance (ANOVA) for Ra	106
Table 5.10	Analysis of variance (ANOVA) for Rt	106
Table 6.1	Properties of the various abrasives used in this investigation	134
Table 6.2	Test conditions used in this investigation	134
Table 6.3	Effect of abrasives on improveing surface finish	137
Table 6.4	Surface finish after CMP	143
Table 6.5	Surface finish after CMP with different based magnetic fluid	143
Table 7.1	Properties of $CeO_2$ polishing abrasive/medium	159
Table 7.2	Test conditions in this investigation	159
Table 7.3	Flash times for different flash temperature	163
Table 7.4	Chemical reaction systems in water-based CMP of $Si_3N_4$ with $CeO_2$	180



Table 8.1	Properties of the various abrasives used in this investigation	183
Table 8.2	Test conditions used for different stages of polishing	183
Table 8.3	Surface finish and material removal rates during various progressive stages of polishing	192
Table 8.4	Polishing procedure and results	212
Table 9.1	Properties of zirconia (Ytria stabilized) balls	225
Table 9.2	Polishing conditions for MFP of zirconia ( $ZrO_2$ ) balls	226
Table 9.3	Test result sof finishing Zirconia ( $ZrO_2$ ) balls by MFP with SiC (#8000 grit) abrasive	226
Table 9.5	Chemical properties of AISI 440C	228
Table 9.5	Mechanical properties of AISI 440C	228
Table 9.6	Polishing conditions used for finishing stainless steel balls by MFP	229
Table 9.7	Test results of finishing stainless steel balls by MFP	230
Table 9.8	Polishing conditions used for finishing stainless stee balls by MFP with a $Si_3N_4$ Shaft	231
Table 9.9	Test results of finishing stainless steel balls by MFP with a $Si_3N_4$ shaft	231
Table 9.10	A comparison of polishing results of finishing stainless steel balls by MFP with 304 stainless steel and $Si_3N_4$ shafts	231

## LIST OF SYMBOLS

R	Roughness profiles
W	Waviness profiles
T	Total profiles
R <sub>a</sub>	Arithmetic average roughness height
R <sub>q</sub>	RMS(Root Mean Square) average roughness height
R <sub>y</sub>	Maximum roughness height in one cutoff: Maximum peak-to-valley height within one sampling length, has also called R <sub>max</sub>
R <sub>p</sub>	Maximum peak height in one cutoff
R <sub>v</sub>	Maximum valley depth in one cutoff
R <sub>tm</sub>	The mean value of the R <sub>y</sub> of five consecutive cutoffs
R <sub>t</sub>	Maximum roughness height in five cutoffs: the vertical height between the highest and lowest points of the profile within the evaluation length
R <sub>z</sub>	Ten point roughness height
S	Mean spacing of adjacent local peaks of the profile
S <sub>m</sub>	Mean spacing between profile peaks at mean line in one cutoff
tp%	Bearing length ratio, statistical parameters, given as a percent: the ratio of the length of material surface (cut by a line parallel to the mean line of the profile) to the sampling length
A	Amplitude distribution

# CHAPTER 1

## INTRODUCTION

### 1.1 HYBRID OR ADVANCED CERAMIC BEARINGS

Advanced ceramics, such as silicon nitride are being actively considered for high speed/high temperature precision bearing applications, such as in aircraft engines, in high-speed spindles, and in precision machine tools. Silicon nitride is the material of choice because of its many superior properties, including lower density, harder hardness, higher elastic modulus (higher stiffness), and higher thermal and chemical stability compared to the traditional steel balls for bearing applications, and higher fracture toughness among advanced ceramics. Table 1.1 shows for comparison the properties of some of the advanced ceramics as well as a conventional bearing steel material. Since advanced ceramics have high compressive strength but low tensile strength, they are excellent for bearing balls but may not be as appropriate for bearing races. Also, an all-ceramic bearing may have a problem from the difference in the thermal expansion coefficient between the ceramic inner race and the metal drive shaft. Consequently, it may be preferable to use steel bearing races, i.e., hybrid bearings with ceramic balls and steel races.

Hot-pressed silicon nitride rolling elements for aircraft gas turbine was initially developed in the late 1960's [Katz and Hannoosh, 1985]. These bearings could survive under the operating conditions that an all-steel bearing would be destroyed or are at the border of their metallurgical safety range. Both

Table 1.1 Properties of some advanced ceramics and bearing steel

	Si <sub>3</sub> N <sub>4</sub> (HIP)	B <sub>4</sub> C	SiC	Al <sub>2</sub> O <sub>3</sub>	ZrO <sub>2</sub>	Bearing Steel
Density	3.24 g/cm <sup>3</sup>	2.52 g/cm <sup>3</sup>	3.06 g/cm <sup>3</sup>	3.78 g/cm <sup>3</sup>	5.9 g/cm <sup>3</sup>	7.85 g/cm <sup>3</sup>
Young's Modulus	314 GPa	448 GPa	410 GPa	360 GPa	200 GPa	200 GPa
Hardness (Hv10kg)	16 GPa	28 GPa	24 GPa	22 GPa	12.5 GPa	7 GPa
Flexural Strength	700 MPa	300 MPa	450 MPa	240 MPa	500 MPa	2500 MPa
Fracture Toughness	7 MNm <sup>-3/2</sup>	3 MNm <sup>-3/2</sup>	4.5 MNm <sup>-3/2</sup>	4.9 MNm <sup>-3/2</sup>	8 MNm <sup>-3/2</sup>	20 MNm <sup>-3/2</sup>
Therm. Exp. Coeff.	3.2x10 <sup>-6</sup> /°C	5.8x10 <sup>-6</sup> /°C	4.6x10 <sup>-6</sup> /°C	8x10 <sup>-6</sup> /°C	9.8x10 <sup>-6</sup> /°C	11.6x10 <sup>-6</sup> /°C
Therm. Conductivity	32 W/m°K	26 W/m°K	85 W/m°K	25 W/m°K	38 W/m°K	40 W/m°K
Maximum Work Temp.	1100 °C	1750 °C	1700 °C	1200 °C	950 °C	200 °C
Corrosion Resistance	High	High	High	High	High	Moderate
Failure Mode	Spalling	Fracture	Fracture	Fracture	Spalling	Spalling

\* The density of advanced ceramics is much lower than steel, and their elastic modulus and hardness are higher than steel. Among the advanced ceramics, the fracture toughness of HIP-Si<sub>3</sub>N<sub>4</sub> is higher than the other ceramics except ZrO<sub>2</sub>. But the density of ZrO<sub>2</sub> is much higher than Si<sub>3</sub>N<sub>4</sub>. So, the HIP-Si<sub>3</sub>N<sub>4</sub> is recommended for the material of bearing balls.

high grade all-M50 steel bearings and hybrid bearing (HIP silicon nitride balls with high-strength steel races) were tested in turbine starters under the worst-case conditions in which the temperature was raised from 0 to 900 °F in a few seconds when it restarts a windmilling engine during flight [Lynch, 1991]. The results showed that an all-steel bearing failed catastrophically after 15 minutes but hybrid bearings were undamaged even after a 45 minutes of test. Figure 1.1 shows that under similar conditions, the hybrid bearing (ceramic balls and M50 race) (center) kept going while the all-M50 steel bearing (left and right) failed. The key findings are (1) less skidding (mainly due to low density of ceramic balls) in hybrid ceramic bearing reduces friction, heat, and wear, and thus allows lower bearing preloads, (2) galling in an all-steel bearing caused by transient microscopic welding of the steel balls to the steel race which can be avoided or reduced in a hybrid ceramic bearing. The chemical inertness of the ceramic balls with respect to the steel race in resisting welding even at high frictional temperatures and pressures, (3) lower rolling friction because of the smaller contact region of the balls, and less heat generated by viscous shear in the lubricant in hybrid ceramic bearings, and (4) smaller ball deformations in the case of ceramic balls decreases the internally generated heat. These allow the high temperature application of ceramic bearing without lubrication in applications where traditional all-steel bearings need complicated and expensive oil-lubrication equipment as in jet turbine engine for aircraft or for rocket motors in the space shuttle.

A major application of advanced silicon nitride balls is spindle bearings for high-speed, high-precision machine tools (half the world market is projected to be in this area) [Gottschalk and Bak, 1995]. Figure 1.2 shows a high-speed spindle unit with hybrid ceramic bearings (from HSK), for precision high speed

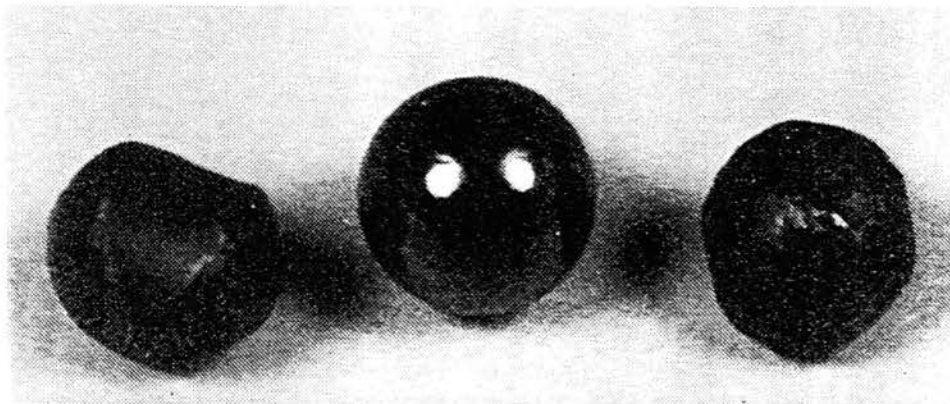
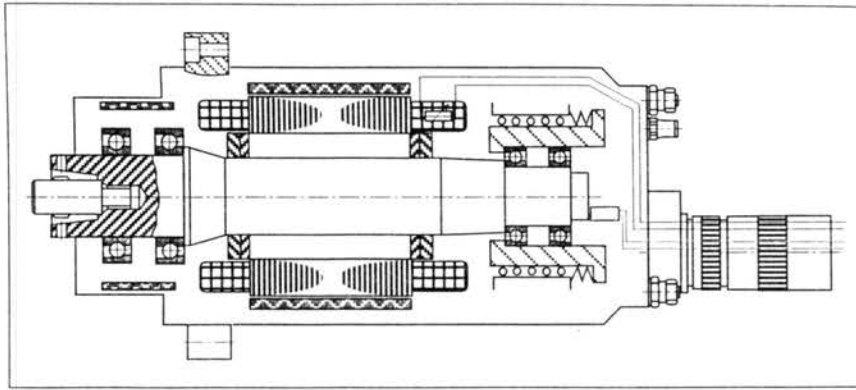


Figure 1.1 Under similar condition, the hybrid (ceramic ball-M50 race) bearing balls (CENTER) kept going where the all-M50 steel bearing balls (LEFT and RIGHT) failed.[Lynch, 1991]



# HIGH FREQUENCY SPINDLES for Precision Cutting

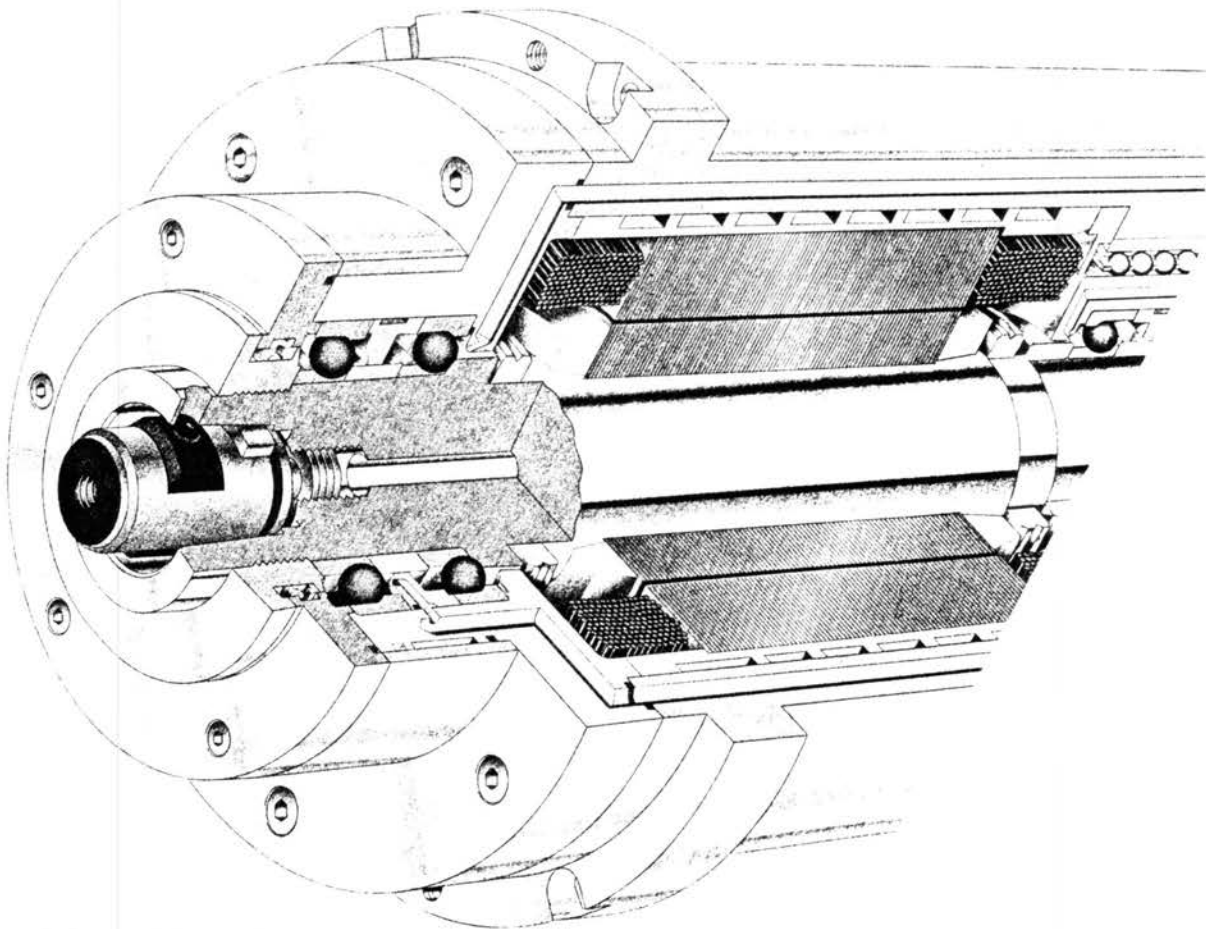


Figure 1.2 High-speed spindle unit with hybrid ceramic bearings (from HSK), for precision high speed cutting machines.

cutting machines, exhibited at the IMTS-96 (International Manufacturing Technology Show, 1996). The maximum rotation speed of this precision spindle can reach 180,000 rpm. The low density (~ 40% of bearing steel balls) of silicon nitride ball, for example, results in reducing the high centrifugal loading, gyroscopic moment, and spinning motion at the high rotational speeds which are considered as the main reasons for the failure of steel ball bearing at high speed [Buchner, 1993]. The DN value [dia.(mm) x rpm] of hybrid silicon nitride bearings can reach  $5 \times 10^6$ . A reduction in the heat generation and the possibility of lubrication starvation of silicon nitride balls are also helpful for high speed operation. Future extensive uses of hybrid bearings in high-speed and ultra-high speed spindles seem to be a natural progression.

To demonstrate the reliability of ceramic balls for withstanding shock-loading conditions experienced, such as during race spalling, both a high grade all-steel bearings and a hybrid bearing (NBD200 silicon nitride balls and steel races) were tested under severe shock loading conditions, namely, the induced-defect test. In this test, an artificial defect (a notch 0.5 mm wide and 0.25 mm deep) across the outer race is made by electrical-discharge machining (EDM). Figure 1.3 shows (a) the M50 ball with significant fatigue after the first 25-hours of induced-defect test, (b) typical condition of silicon nitride ball with no signs of fatigue after the first 25-hours of induced-defect test, (c) SEM photo of spalled area on silicon nitride ball after the fourth induced-defect test [Burrier and Burk, 1995].

In summary, the hybrid (silicon nitride - steel) bearings have a longer bearing service life (2-5 times longer than steel bearing), higher running speed (up to  $5 \times 10^6$  DN), favorable failure mode. The failure of high quality silicon nitride bearing balls is generally caused by spalling due to higher fracture



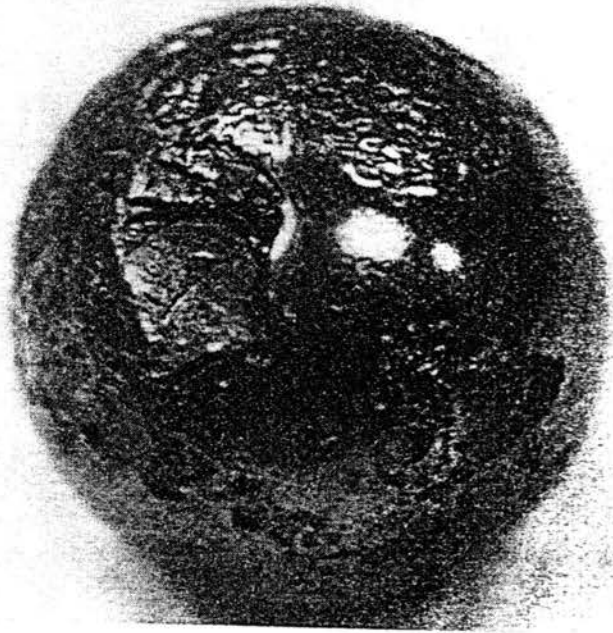


Figure 1.3(a)  
The M50 ball with  
significant fatigue after  
about first 25 hour  
induced-defect test

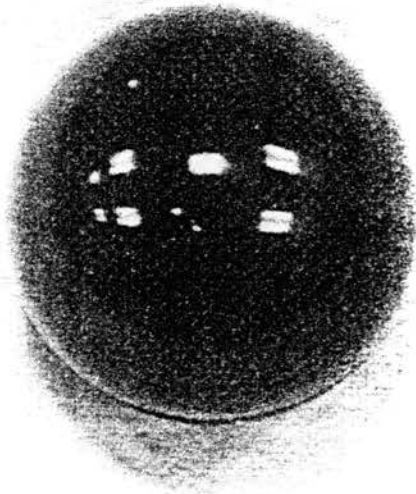


Figure 1.3(b)  
Typical condition  
of silicon nitride ball  
without signs of fatigue  
after the first 25 hour  
induced-defect test

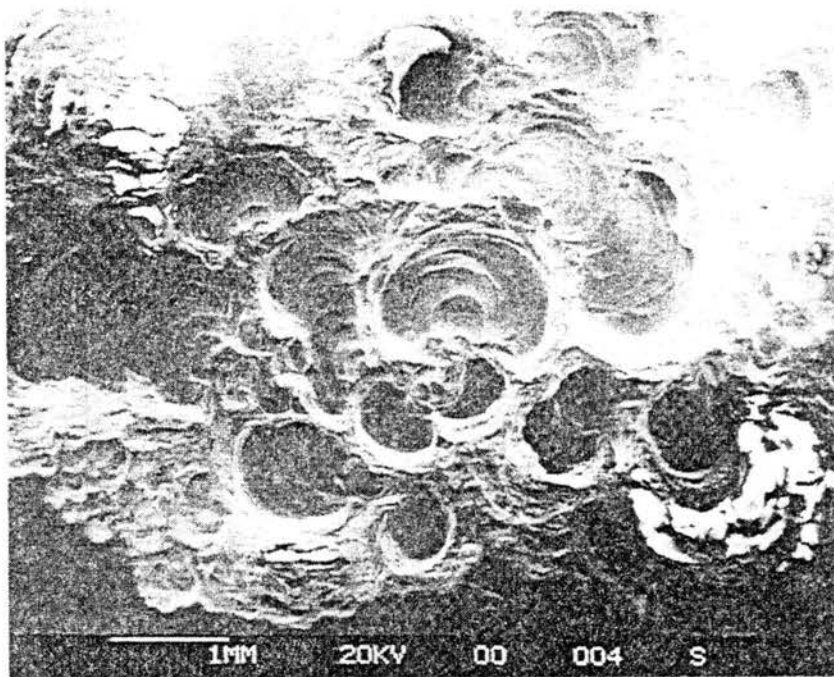


Figure 1.3(c)  
SEM photo of  
spalled area on  
silicon nitride ball  
after fourth  
induced-defect test.

toughness (among advanced ceramics) rather than by the catastrophic failure which takes place with the other advanced ceramics which have lower fracture toughness. It may be noted that failure in steel bearing balls is also generally by spalling due to their higher fracture toughness. In addition, hybrid bearings provide higher overall accuracy and quality, higher temperature capability and non-magnetic characteristics [Buchner, 1993]. Various applications, essential features, and advantages of the hybrid ceramic bearings are given in Table 1.2 [Barden, 1995]. Once the industry recognizes the potential of hybrid ceramic bearings, it is anticipated that they (hybrid bearings with silicon nitride balls and steel races) could replace 50 - 60% of traditional all-steel bearings currently in use for high-speed, high precision applications [Gardos and Pratt, 1991].

Although the concept of hybrid ceramic bearing could date back to some 20 years, advanced silicon nitride balls did not become available in commercial quantities until early 1990's. The acceptance of hybrid ceramic bearing in industry such as high-speed spindles in machine tools is even more recent [Gottschalk and Bak, 1995]. The application of ceramic bearings is still quite limited because the cost of finishing ceramic balls remain much higher compared to the cost of steel balls. This is due to the difficulty of machining the brittle and hard ceramic balls by conventional lapping. Current techniques for finishing ceramic bearing balls use conventional V-groove lapping machine with expensive diamond abrasives, low polishing speed/long finishing time, and high loads. Consequently, it is difficult to obtain good accuracy and surface finish.

A critical factor affecting the performance and reliability of ceramics for bearing applications is the quality of the resulting surface. It is well known that ceramics are extremely sensitive to surface defects resulting from grinding and

Table 1.2 The features, benefits, and applications  
of the hybrid ceramic bearings

### Features

60% lighter than steel balls

- Centrifugal forces reduced
- Lower vibration levels
- Less heat build up
- Reduced ball skidding
- Fatigue life increased

50% higher modulus of elasticity

- Improved spindle rigidity
- Naturally fatigue resistant

Tribochemically inert

- Low adhesive wear
- Improved lubricant life
- Superior corrosion resistance

### Benefits

- Bearing service life is two to five times longer
- Running speeds are 50% higher
- Overall accuracy and quality improves. Better work-piece finish characteristics
- Lower operating costs
- Boost productivity
- High temperature capability
- Cutting tool life is increased

### Applications

Applications where ceramic hybrids are highly recommended include:

Machine tools

- Grinding
- Milling
- Boring
- Drilling

Aircraft accessories/aerospace

- Generators
- Gyros
- Gearboxes
- APU's
- Turbine engines
- Radar
- Weapon systems
- Satellites

Industrial machinery

- Turbomolecular pumps
- Diesel fuel injection pumps
- Textile machines
- Woodworking machinery
- Food processing equipment
- Drilling equipment

Medical equipment

- Dental drills
- Centrifuges
- X-ray tubes

polishing processes owing to their high hardness and inherent brittleness. Since fatigue failure of ceramic parts is driven by surface imperfections, it is paramount that the quality and finish of the ceramic bearing elements be as best as possible with minimal defects so that reliability in performance of bearings in service can be achieved.

## 1.2 FUNDAMENTAL PROBLEMS IN THE FINISHING OF ADVANCED CERAMICS

The properties (physical, mechanical and thermal) of advanced ceramic materials are determined by the nature of atomic bonding as well as the manufacturing processes used in the syntheses of these materials, namely, sintering, chemical vapor deposition, reaction bonding, hot pressing, and hot isostatic pressing. The atomic structure of advanced ceramics, such as SiC, Si<sub>3</sub>N<sub>4</sub>, Al<sub>2</sub>O<sub>3</sub> and ZrO<sub>2</sub> are either covalent, ionic, or a combination of these two. They are thus significantly different from metals with a metallic bonding. Due to the covalent or ionic bonding system of advanced ceramics, their inter-atomic distances are larger than that of metals. This less closed-packed structures make advanced ceramics low in density, low in ductility, and high in brittleness. As the covalent or ionic bond is a strong bonding system, advanced ceramics have higher strength (compressive strength) and higher melting temperature. Due to low density and mobility of dislocations in advanced ceramic materials, they have high hardness. Furthermore, higher the ratio of covalent bonding to ionic bonding, the less affected they are by elevated temperature [Inasaki, 1987]. For example, the SiC, whose covalent bonding to ionic bonding ratio is 9:1, exhibits a better heat resisting performance (of avoiding thermal damage)

than  $\text{Si}_3\text{N}_4$ , whose ratio is 3:1, and both are better than typical oxide ceramics, e.g.,  $\text{Al}_2\text{O}_3$ , which has the ratio of 2:3. The low thermal coefficient of expansion and relatively high thermal conductivity are the special features of these advanced materials with covalent bonding (carbon atom bonding in diamond is an example of 100% covalent bonding). The bonding nature of advanced ceramic materials is given in Table 1.3 [Komanduri, 1996].

The nature of bonding of the advanced ceramics determine not only the desirable engineering properties but also cause difficulty in machining. Material removal of both single and polycrystalline advanced ceramic materials is predominantly by microfracture due to their high hardness and brittleness, i.e., from their strong covalent/ionic bonding, low symmetry crystal structure, and fewer dislocation systems. It is different from metals in which plastic deformation, instead of brittle fracture, is the predominant mode of material removal because of their uniform metallic bonding, high symmetry crystal structure, and numerous slip (planes and directions) systems [Komanduri, 1996]. A comparison of the properties between metals and advanced ceramics is shown in Table 1.4. The main crack in cutting (or abrading) polycrystalline ceramic materials originates along the direction of normal stress of cutting motion and the minimum material strength of workpiece [Usui, 1990]; The material removal (along the grain boundaries or through the grains) is by chipping resulting from the propagation of cracks or pitting by the grain dislodgements. In cutting metals, the materials is removed by the plastic deformation along the maximum shear stress of cutting (Figure 1.4). It is because the material shear strength  $\tau$  is smaller (2 times) than the material normal strength  $\sigma$  in metals due to large amount of dislocations, but the material shear strength  $\tau$  is similar to normal strength  $\sigma$  in advanced ceramic materials due to their small amounts of dislocations, and therefore, the direction and

Table 1.3 The bonding nature of advanced ceramic materials

	Ionic bonding	Covalent bonding
Al <sub>2</sub> O <sub>3</sub>	90%	10%
ZrO <sub>2</sub>	75%	25%
SiO <sub>2</sub>	50%	50%
Si <sub>3</sub> N <sub>4</sub>	25%	75%
SiC	10%	90%

Table 1.4 Comparison of properties between metals and advanced ceramics

	Metals	Advanced Ceramics
Atomic bonds	Metallic bond	Ionic / Covalent bond
Crystal structure	High in symmetry	Low in symmetry
Fracture behavior	Ductile	Brittle
Fatigue mechanism	Plastic deformation	Growth of crack
Density	High	Low
Hardness (kg/mm <sup>2</sup> )	Several hundreds	2,000
Toughness (MN.m <sup>-3/2</sup> )	210 (Carbon steel)	4.2 (HIP Si <sub>3</sub> N <sub>4</sub> )

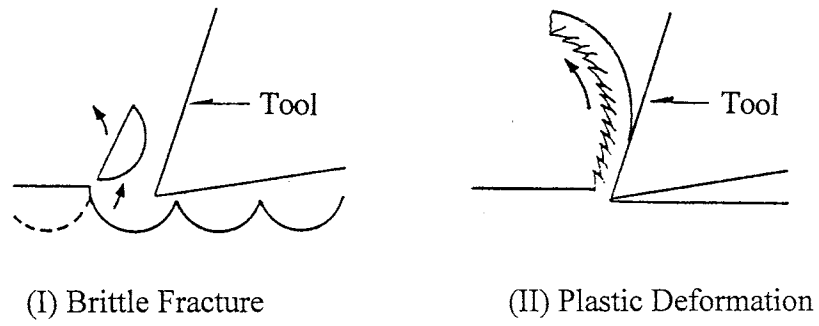


Figure 1.4 (a) Mechanisms of material removal

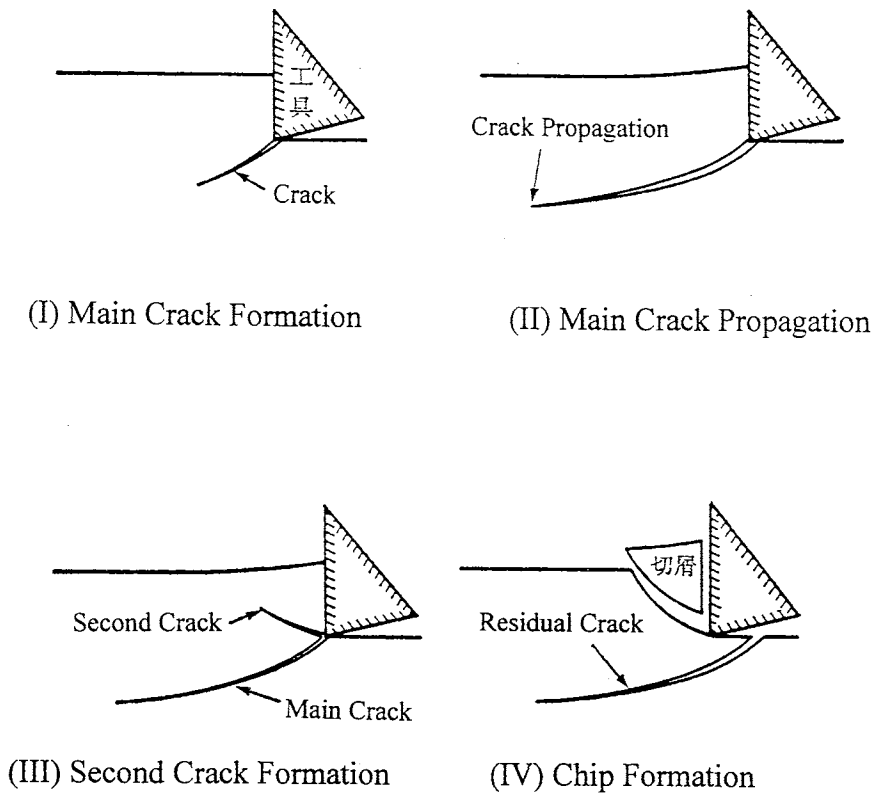


Figure 1.4 (b) Chip formation of advanced ceramics [Usui, 1990]



magnitude of the propagation of cracks and brittle fractures is random. Thus, in conventional machining methods, the machined quality of advanced ceramic materials are very difficult to be controlled due to their high brittleness, and also expensive diamond tools or abrasives and strong stiffness machine are required because of their high hardness.

### **1.3 CONVENTIONAL FINISHING METHOD AND ITS LIMITATIONS**

Advanced ceramics are currently finished by conventional grinding with diamond wheels followed by lapping and polishing with again diamond abrasive. The conventional apparatus used for V-groove lapping (including grinding and polishing) of steel bearing balls is currently used in lapping of ceramic balls for bearings with diamond abrasives as shown in Figure 1.5. In the lapping process, the abrasives can be either loose (for polishing process) or bonded (for grinding process). They are operated at low pressures and low speeds to achieve high geometric accuracy and good surface finish. The upper and/or lower lapping plates can be either diamond or SiC grinding wheel for the grinding process and cast iron lapping plates charged with fine and loose diamond abrasives (0.25  $\mu\text{m}$ ) for polishing process.

It is well known that a specific characteristic that shows a major difference between advanced ceramic materials and metals is the fracture toughness. The fracture toughness of advanced ceramics is extremely low, i.e. low resistance to the propagation of brittle cracks. While advanced ceramics have higher stiffness/higher elastic modulus,  $E$  than metals. Consequently, the elastic deformation of advanced ceramic materials during grinding would be less than metals. As a result, advanced ceramic materials can be machined to obtain

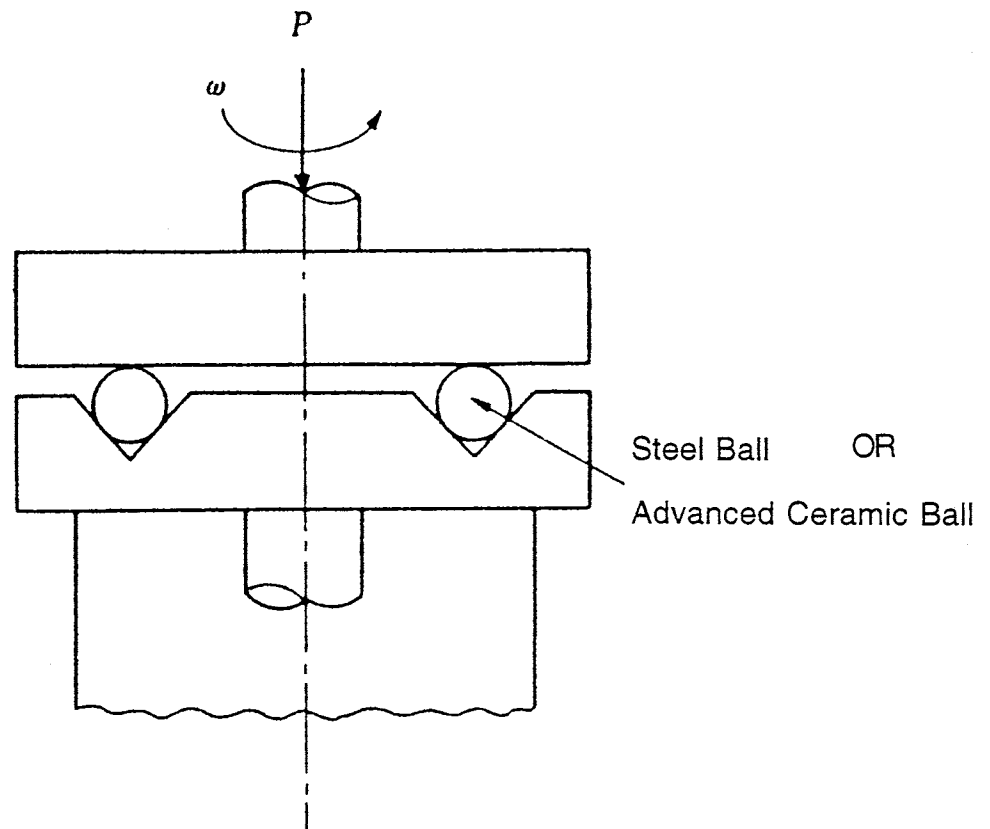


Figure 1.5 Conventional V-groove lapping apparatus for the grinding and polishing of bearing balls

higher geometrical accuracy than metals. Thus, the critical problem in the grinding of precision ceramic parts is their naturally low fracture toughness/low resistance to the propagation of brittle cracks. This causes the strength degradation of the finished part from surface and subsurface damages. It is found that the influence of grinding conditions on the surface finish of grinding advanced ceramics is basically similar to that of grinding metals [Inasaki, 1987].<sup>12</sup> The smaller depth of cut, lower workpiece feed speed, and higher grinding speed are helpful to improve the surface roughness. Fine grinding (fine abrasive and low force) can reduce the generation and propagation of cracks during the grinding of advanced ceramics. For the application of grinding metals, the most common abrasives used are aluminum oxide and silicon carbide; for grinding advanced ceramics, diamond abrasive is the primary choice [Subramanian et al, 1987].<sup>13</sup>

There are two grinding modes for the application of advanced ceramics: speed-stroke grinding (high workpiece speed and a small depth of cut) and creep-feed grinding (very low workpiece speed and high depth of cut). The high material removal rate without sacrificing the material strength and surface finish in creep-feed grinding is attributed to the long cutting length with low chip thickness of the individual abrasive grain in the creep-feed grinding process [Subramanian and Robert, 1988].<sup>14</sup> But the more powerful machine with greater machine rigidity is required to minimize deflections and loss of accuracy because of the resultant force on the grinding wheel is large. The need to design systems to increase the access of the grinding fluid, such as special slotted wheel is also required due to the long contact length in this grinding mode. For brittle materials, down-grinding is employed to subject as much material in compression as possible. Progressing towards the bottom of the

grinding wheel, the cutting forces fall off rapidly and the grinding depth is reduced.

The difference between polishing and grinding is that the abrasives are loose (or free) in the polishing process and bonded (or fixed) in the grinding process. The polishing process is more flexible than grinding/lapping. It is traditionally applied after prior grinding/lapping to remove surface damage and achieve very smooth surface. Recent developments in polishing of advanced ceramics have focussed on the abrasive size uniformity, flexible machining design, and chemical and mechanical process combination. In the mechanical polishing process, some of abrasive particles are embedded into the polishing tool surface or at least are restricted to roll by the polishing tool surface, and produce a cutting action (stroke/sliding) on the workpiece [Childs, 1995]. Some particles may roll between the two surfaces and may also get involved in the material removal process. Consequently, the predominant polishing motion is considered as rolling rather than sliding by some other researchers [Indge, 1990]. They proposed that rolling of the irregular particles is accompanied by repeated indentation of the surface. Fracture, particularly around indentations, is the mode of material removal for polishing [Indge, 1990]. But anyway it is clear that the grain size uniformity of abrasives is important in polishing. High precision and good surface finish can be achieved by abrasives with uniform grain size because the depth of the deep scratch on the polished surface by the oversized abrasive particle is minimized. The most common abrasives for the polishing (and lapping) of harder materials is fine grain size silicon carbide, boron carbide, and diamond.

**LIMITATIONS OF CONVENTIONAL LAPPING:** Although grinding and polishing may be conducted at fine depths of cut thereby reducing the

depth of cracks and amount of damage on advanced ceramics, serious surface damage (relative to bearing requirement) still can not be avoided by the conventional grinding and polishing methods because the stiffness,  $k (= \Delta p / \Delta x)$  of the system is very high. Thus small local out-of-roundness of the polished surface of the ceramic balls will generate large loads which will damage significantly the surface of the ceramic workmaterial because of the inherent brittleness of ceramics. Diamond abrasives used will also scratch the machined surface deeply because it is significantly harder than the ceramic workmaterial. Figure 1.6 shows the typical micro-damage on the surface of a best commercially finished silicon nitride ball (from conventional diamond abrasive V-groove lapping).

In summary, the current finishing of ceramic balls is by the V-groove lapping similar to the methods used for making the steel bearing balls. This includes the use of diamond abrasive, relatively high load (about 10 N/ball), and relatively low polishing speeds (about 50 rpm). In practice, it takes considerable time (some 12-16 weeks) to finish a batch of ceramic balls. The long processing time and use of expensive diamond abrasives result in high processing costs. Furthermore, the use of diamond abrasives at high loads can result in surface damages such as deep pits, scratches, and microcracks and subsurface damage, such as the large lateral and radial/median cracks. These surface defects may cause catastrophic failure of silicon nitride balls by propagation of larger brittle fracture.

~ approximately  
10,000 balls.

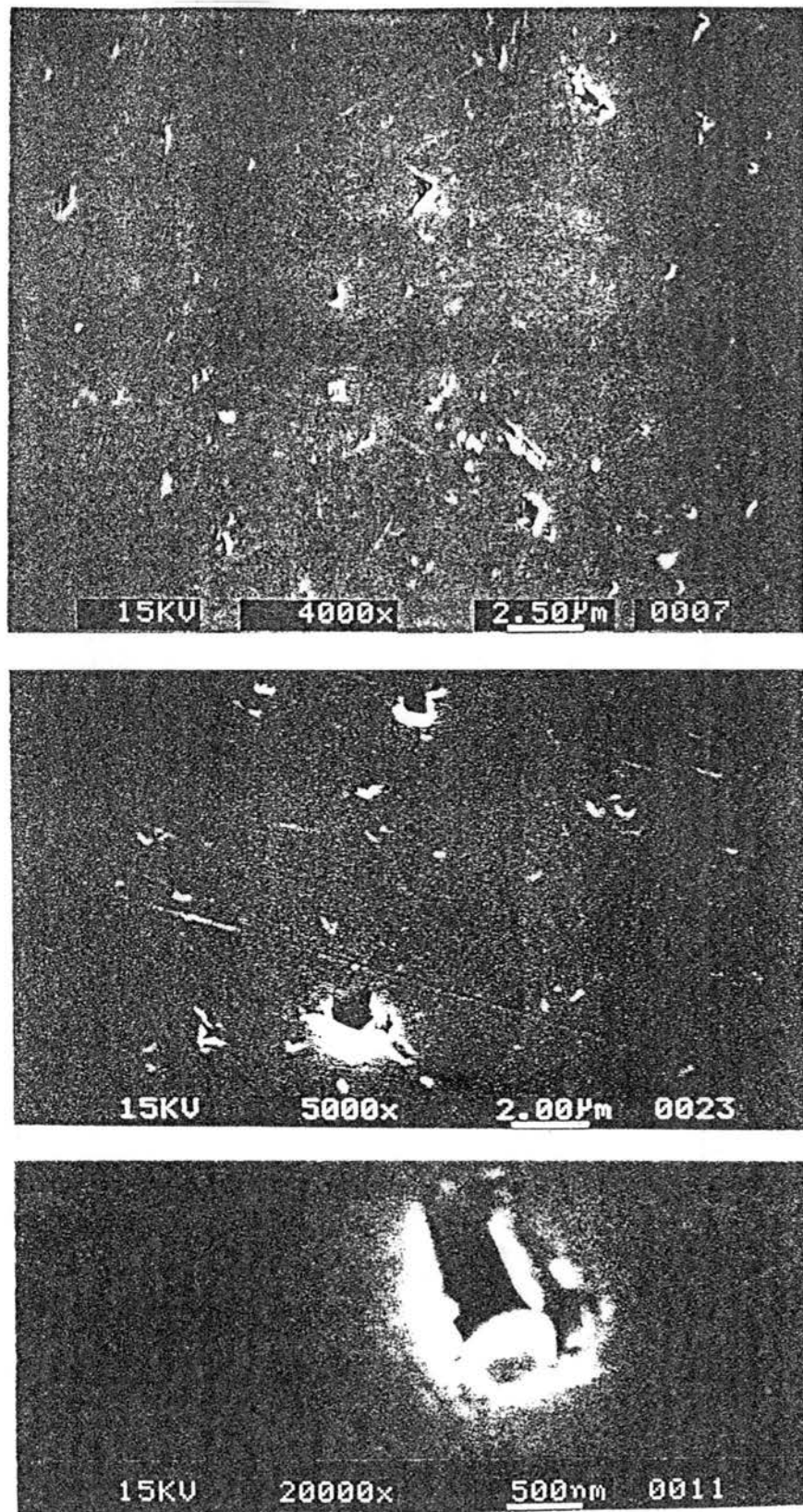


Figure 1.6 SEM micrograph of a best commercially finished  $\text{Si}_3\text{N}_4$  ball surface (ABMA Grade 3)

## 1.4 "GENTLE" FINISHING OF ADVANCED CERAMIC BALLS FOR BEARING APPLICATION

To minimize the surface damages, 'gentle' or 'flexible' machining method methods and conditions are required, i.e., low level value of stiffness  $k$  in  $\Delta p = k \Delta x$  in machining process is preferred and thus the amplitude of abrasing force is flexible, steady, and controllable, and also abrasives are not much harder, and even softer than workmaterial. High removal rates and shorter polishing cycles may be considered to obtain by high polishing speeds (from high frequency of cutting/abrasing). And thus, material removal and surface finish can be brought out by results of large amount of microscopic fractures in mechanical polishing at any point of the work surface where a large number of abrasive grains passed (or acted), other than some large instant fractures.

In the finishing of advanced ceramics, the flexibility of the grinding for obtaining the required geometry and subsequent polishing for obtaining good surface finish system should be emphasized to avoid deep brittle cracks on the surface and subsurface damage from local uncontrolled force due to out-of-shape of workpiece. It is seen that hydrodynamic behavior [Watanabe and Suzuki, 1981] and magneto-hydrodynamic behavior [Tani et al, 1984] are two particularly promising principles to be considered for abrasive machining of brittle materials, such as advanced ceramics, optics, and semi-conductor materials, for superfinished surface requirements.

Hydrodynamic float polishing method is shown in Figure 1.7 [Watanabe and Suzuki, 1981]. When the shaft rotates, dynamic pressure and laminar flow are generated between the slopes and the workpiece, like a dynamic pressure

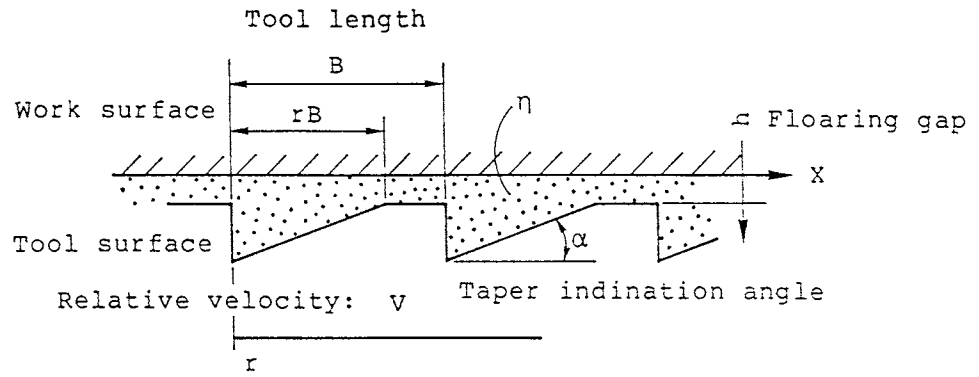


Figure 1.7 Principle of hydrodynamic float polishing [Watanabe and Suzuki, 1981]

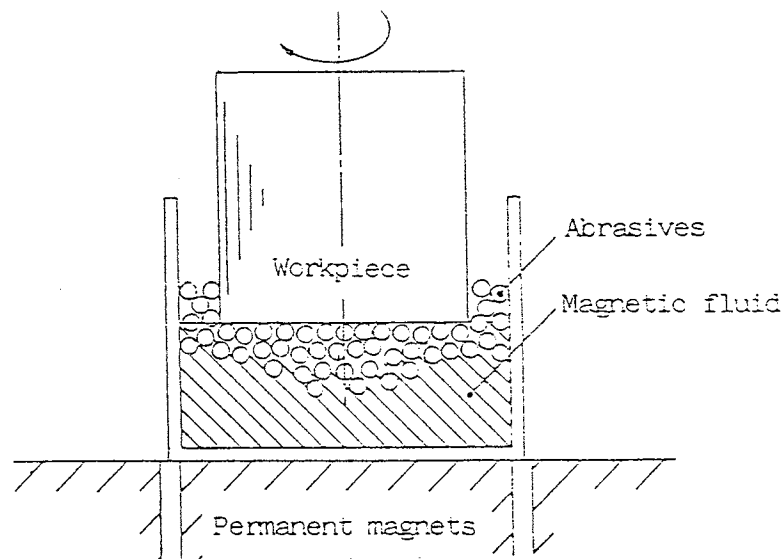


Figure 1.8 Principle of magnetic float polishing [Tani and Kawata, 1984]

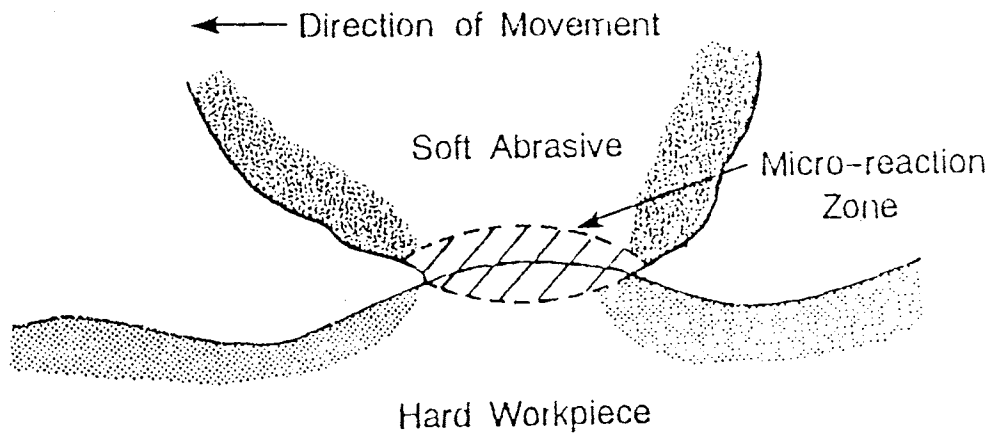


Figure 1.9 Principle of chemo-mechanical polishing [Yasunaga, Imanaka, et al, 1978]



bearing to float the abrasive grains toward the machined surface. Polishing is accomplished by these abrasive grains carried by laminar liquid flow passing the machined surface. In this process, the workmaterial is polished by hydrodynamic action without contact with the polishing lap. Because the grain size of abrasive used is very fine ( $0.1 \mu\text{m}$ ), the kinetic energy hitting the machined surface is very small. Also, the stress distribution area is limited because of shooting the abrasive particles almost parallel to the work surface.

This float polishing process actually removes atoms on the workpiece surface by elastically deformation (rather than plastic deformation) by the impacting abrasives. Material removal on the order of molecules or atoms can be obtained without damaging the crystallinity on the surface.  $\text{ZrO}_2$  abrasive was found to be suitable for polishing silicon workpiece while  $\text{Al}_2\text{O}_3$  for polishing glass. Surface roughness of  $5 \text{ \AA}$  can be achieved by this process [Hatta, 1988].

This method is being applied widely in the semi-conductor and optical industries.

Magneto-hydrodynamic behavior is more stable for machining support and more suitable for ball polishing with higher material removal than hydrodynamic action. A technique for fine finishing using a magnetic fluid is shown in the Figure 1.8 [Tani and Kawata, 1984]. The magnetic float polishing technique is based on the magneto-hydrodynamic behavior of a magnetic fluid that can float non-magnetic abrasives under the magnetic field, pressing abrasives against the machined surface. The forces applied by the abrasive to the workpiece are extremely small and highly controllable. The details will be discussed in the following chapters.

Besides mechanical polishing, chemo-mechanical polishing method can be applied to the above two polishing methods [Hatta, 1988; Bhagvatula and

20  
Komanduri, 1996]. In this technique abrasives which are mechanically softer than the workmaterials to be polished but react chemical with them can be selected. The process can produce extremely fine surfaces. The softer abrasives used in chemo-mechanical polishing process can avoid the surface damage on the machined surface of advanced ceramic materials, such as microcracking, scratchings and pitting, which are typical surface damage modes in traditional grinding and polishing because the abrasive used ( $B_4C$ , SiC, and diamond) are much harder than the hardness of the workpiece. In chemo-mechanical polishing, a very small amount of material is removed from the surface as a result of chemo-mechanical action at the contacting area between the soft abrasives and polished material (Figure 1.9). Chemical reaction is caused by the mechanical friction energy, and polishing is done when this very small reaction part is removed by the friction [Yasunaga, Imanaka, et al, 1978]. It is also called tribo-chemical polishing [Fishcher, 1988]. The removal amount of material in this process can be on the order of a few molecules or atoms. A concise review of literature on the chemo-mechanical polishing of various materials in general and that of silicon nitride in particular has been presented recently by Komanduri et al (1996).

The purpose of this investigation is to develop a 'gentle' but fast material removal process for finishing advanced ceramic balls for bearing applications that are superior and economical compared to balls manufactured by conventional diamond V-groove lapping. This is accomplished in our study by a new and effective process known as magnetic float polishing (MFP) in which cutting force is controlled by the flexible magnetic field. Magnetic field assisted polishing using a magnetic fluid was originally developed by Tani et al [Tani and Kawata, 1984]. However, the forces developed were so low that only soft

materials could be finished. Umehara and Kato in Japan made a major breakthrough by incorporating a float [Umehara and Kato et al, 1990, 1994] that improved the effectiveness of the process significantly. This was followed by the works of Childs et al in the UK [Childs et al, 1994, 1995] and Komanduri et al in the USA [Komanduri et al, 1996; Bhagvatula and Komanduri, 1996; Komanduri, 1997; Raghundan and Komanduri, 1997, 1998; Jiang and Komanduri, 1997, 1998 a, b, c; Hou and Komanduri, 1998 a, b, c].

Magnetic float polishing (MFP) is a very effective at the same time economical manufacturing technology. Table 1.5 shows a comparison of parameters used in conventional lapping and magnetic float polishing. The material removal rate by magnetic float polishing (MFP) is ~ 50 times higher than the conventional V-groove lapping owing to higher polishing speed (1,000-10,000 rpm) used in MFP compared to lapping (generally, 50 rpm) Furthermore, due to small but controlled force (~1 N/ball), surface and subsurface damage on the polished ceramic balls can be minimized. The number of balls required for each batch is also small (~ 10-20) and abrasives used to remove material are boron carbide (B<sub>4</sub>C) or silicon carbide (SiC) instead of diamond.

Table 1.5 Comparison of Lapping and Magnetic Float Polishing Condition  
[Child et al, 1995] [Komanduri et al, 1996]

	Lapping	Magnetic Float Polishing
Abrasives	Diamond	B <sub>4</sub> C, SiC, CeO <sub>2</sub>
Load	50-100 N/ball	0.5-1 N/ball
Speed	50 rpm	5000 rpm
Number of ball needed	1000-5000	10-50

Number of ball !

This investigation deals with the methodology for finishing superior (good sphericity and excellent surface finish) silicon nitride ( $\text{Si}_3\text{N}_4$ ) balls for bearing applications by magnetic float polishing (MFP) technology using mechanical polishing with fine and harder abrasives for removing materials to reach desired diameter and geometry fast but with minimal surface damage followed by chemo-mechanical polishing (CMP) with an appropriate softer abrasives to obtain final superior surface finish of ceramic balls for bearing applications.

The review of literature on magnetic float polishing is given in chapter 2.

The problem statement of this investigation is given in chapter 3.

Chapter 4 deals with the technical approach used in the MFP of ceramic balls. This includes a description of the magnetic float polishing apparatus, characterization of the silicon nitride workmaterial and the abrasives, details of the experimental work, and the evaluation of the surface generated by MFP.

Chapter 5 deals with the application of Taguchi method for determining the optimum polishing conditions. This includes the purpose and the parameters tested, experimental design and analysis methods, experimental approach used, details of the Taguchi experimental design and analysis, experimental results and evaluation, and finally experimental analysis and optimum settings.

Chapter 6 deals with the investigation of various abrasives and polishing environments to determine their suitability for chemo-mechanical finishing silicon nitride materials. The purpose is to determine the most effective abrasive and polishing environment to finish silicon nitride bearing balls with extremely smooth and damage-free surfaces. This includes the fundamentals of chemo-

mechanical polishing, characteristics of various abrasive, polishing results, various possible chemical reactions involved, the mechanism of CMP of  $\text{Si}_3\text{N}_4$  discussion.

Chapter 7 deals with the chemo-mechanical polishing (CMP) of silicon nitride ( $\text{Si}_3\text{N}_4$ ) balls with cerium oxide ( $\text{CeO}_2$ ) abrasive. This includes the purpose, characteristics of  $\text{CeO}_2$  abrasive, polishing results, polishing temperature calculation, various chemical reactions from thermodynamic analysis, the mechanism of CMP of  $\text{Si}_3\text{N}_4$  with  $\text{CeO}_2$  from thermodynamic and kinetic discussion.

Chapter 8 deals with the methodology and process for finishing  $\text{Si}_3\text{N}_4$  balls for bearing applications. This includes the polishing procedure and test conditions, details of methodology and test results, the mechanism of material removal in magnetic float polishing (MFP), the manufacturing process, and the discussion and conclusions of MFP process.

Chapter 9 deals with the future work involving extension of the magnetic float polishing (MFP) technology to finish other advanced ceramics, such as zirconium oxide ( $\text{ZrO}_2$ ) balls for flow control applications and ferritic stainless steel balls for bearing applications.

Chapter 10 deals with conclusions arrived from this investigation.

## CHAPTER 2

### LITERATURE REVIEW

Magnetic field assisted finishing process was initially developed in the U.S. in the 1940's to finish gun barrels [Coats, 1940]. This technology was applied in the the former USSR in the late 1950's and early 1960's for finishing some of the difficult-to-machine materials, especially large workpieces [Baron, 1975]. Following this, in the late 1980's, Japanese researchers [Shinmura et al, 1990; Kato and Umehara, 1990] applied this technology to value-added fine finishing of various workpieces to obtain good surface finish and accuracy. This work was further advanced in the early 1990's by Komanduri, et al [DARPA Report, 1995] in the U. S.

Magnetic field assisted finishing can be classified into two groups: i. <sup>①</sup>magnetic abrasive finishing (MAF) and ii. <sup>②</sup>magnetic float polishing (MFP). Magnetic abrasive finishing (MAF) is performed with abrasives mixed with fine iron particles which form a 'brush' between the magnetic poles in the case of non-magnetic workmaterial. The workpiece surface is polished by the action of the abrasive 'brush' against the workpiece. This method can be applied for finishing internal as well as external cylindrical surfaces and flat surfaces [Shinmura et al., 1990; Fox et al, 1994; Fox, 1994; Thomas, 1997].

The magnetic float polishing (MFP) technique is based on the magneto-hydrodynamic behavior of a magnetic fluid that can float non-magnetic materials under the magnetic field. The workpiece surface is polished by the magnetic buoyancy force of abrasives generated by applying a magnetic field to

a mixture of abrasives and magnetic fluid. The forces applied by the abrasive to the workpiece are extremely small and highly controllable. This method can be applied for finishing any shaped surface including flat, cylindrical, and spherical surfaces. [Kato and Umehara, 1990; Umehara, 1990; Childs et al, 1994, 1995; Komanduri et al, 1996; Bhagvatula and Komanduri, 1996; Umehara and komanduri, 1996; Raghundan and Komanduri, 1997 a, b; Jiang and Komanduri, 1997 a, b, c; Hou and Komanduri, 1998 a, b, c].

Magnetic fluid used in MFP is made of a stable colloidal suspension of extremely fine ferromagnetic particles (usually  $\text{Fe}_3\text{O}_4$ ,  $\sim 100\text{-}150 \text{ \AA}$ , coated with a stably dispersing surfactant to prevent particle agglomeration) in a suitable carrier fluid, such as water (W-40) or kerosene (EMG 909). It is also called ferrofluid because of its iron base [Rosenweig, 1966, 1985]. When a magnetic field is applied, the magnetic particles in the magnetic fluid are attracted downward to the area of higher magnetic field and an upward buoyant force is exerted on all non-magnetic materials inside the ferrofluid to push them to the area of lower magnetic field. The maximum magnetization of magnetic fluid can be up to 100 kA/m. The buoyancy force in the magnetic fluid is proportional to the gradient of the magnetic field and possesses susceptibility up to 10,000 times greater than natural liquids. Figures 2.1(a) and (b) show the principle of magnetic float polishing. When a magnetic field is applied to the magnetic fluid, the magnetic particles move to the high field side and push the non-magnetic body towards lower field side. As a result of this magnetic buoyancy/ levitational force, the abrasive grains and the float being non-magnetic are floated to a certain height. When the magnetic field is removed, the magnetic particles randomize in the fluid and thus there is not magnetic buoyancy (levitational) force and therefore the float and the abrasive will stay at the bottom.



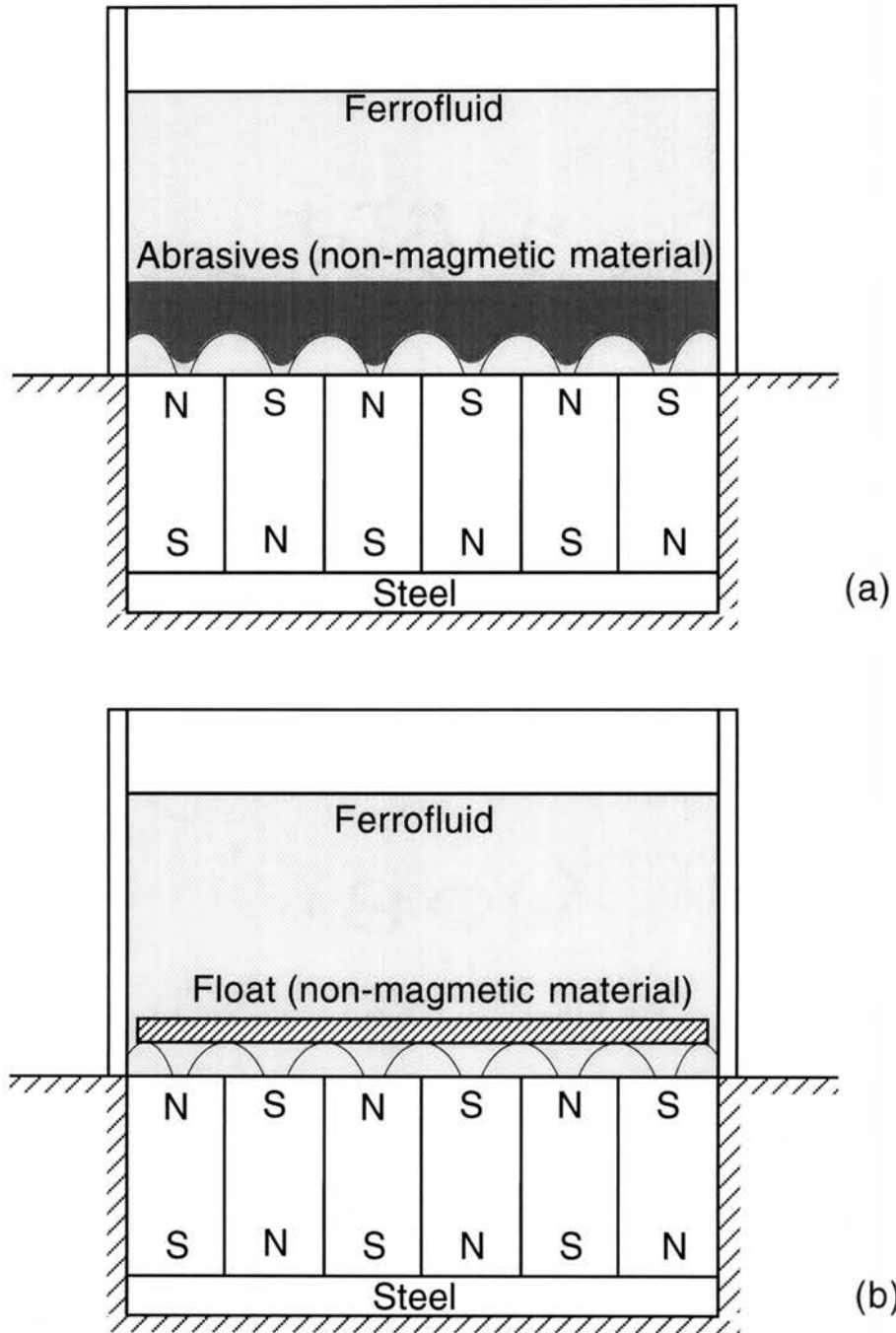
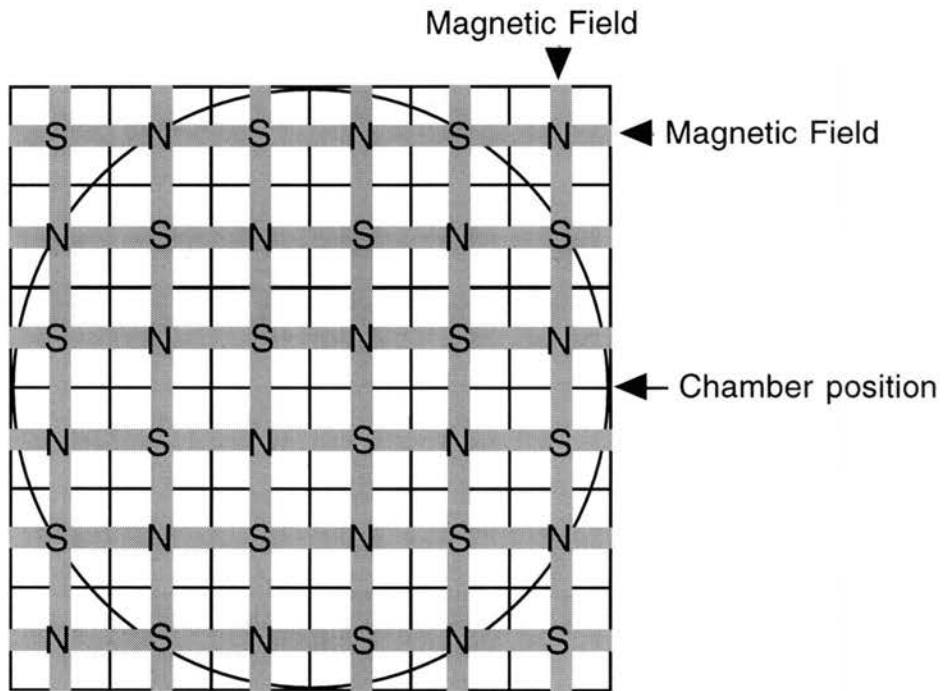
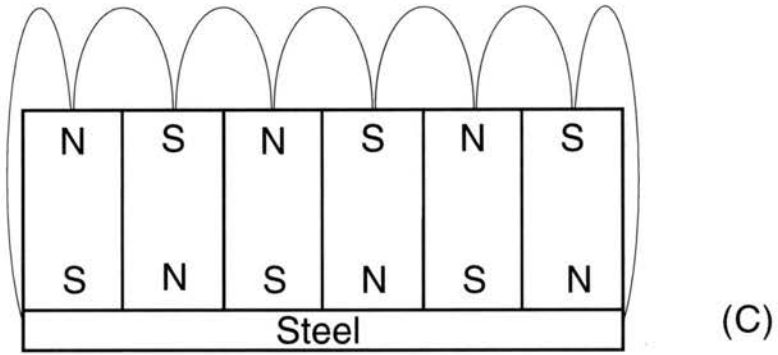


Figure 2.1 When a magnetic field is applied to the magnetic fluid, the magnetic particles move to high field side and push non-magnetic body towards lower field side and thus (a) the abrasive grains and (b) the float being non-magnetic are floated up. (c) Magnet arrangement used in this study



(c) Magnet arrangement used in this study

Magnetic float polishing was first introduced by Tani et al (1984) to polish extremely soft materials, such as Acrylic resin (see Figure 1.8). Material removal is obtained by pressing the abrasive grains against the workpiece due to buoyant levitational force applied by the non-magnetic abrasives. The polishing force was extremely low. Hence, it could be used to finish ( $R_{max}$ : 40 nm) only extremely soft workmaterials, such as acrylic resin with removal rate of 2  $\mu\text{m}/\text{min}$  by SiC (4  $\mu\text{m}$  grain size) abrasive. However, the material removal rates were extremely low or negligible when used for finishing hard materials, such as steels, advanced ceramics, and glasses.

In the following some of the work of various researchers are briefly reviewed. It may also be noted that some of the developments in this field are taking place simultaneously in more than one research laboratory. Also, there is a good collaboration (including mutual visits) between Professor Komanduri of OSU, Professor Shinmura of Utsutomina University, Japan, and Dr. Umehara of Tohoku University in Sendai, Japan.

As previously pointed out there are three groups active in the magnetic float polishing of advanced ceramic balls for bearing application in the world.

They are:

- Kato and Umehara's group in Japan (see Table 2.1)
- Childs' group in the UK (see Table 2.2)
- Komanduri's group in the USA (see Table 2.3)

Table 2.1 MFP research activities in Kato and Umehara's group in Japan

<p>Professor Kato's Group:  (Japan)  N. Umehara  B. Zhang  K. Kato</p>	<p><b>WORKMATERIALS:</b></p> <ul style="list-style-type: none"> <li>• Balls: sintered silicon nitride (1990, 1994)</li> <li>• Rollers: silicon nitride (1992)</li> <li>• Plates: alumina (1992), stainless steel (1993)</li> </ul> <p><b>ACTIVITIES:</b></p> <ul style="list-style-type: none"> <li>• Introduction of a float to increase the polishing load and the material removal rate (1990)</li> <li>• Investigated the effect of the Stiffness of the float on the polishing performance (1990, 1994)</li> <li>• Developed a dynamic model for MFP (1996)</li> <li>• Developed an eccentric apparatus to obtain balls with good sphericity (1996)</li> </ul>
--	---

Table 2.2 MFP research activities in Childs' group in the UK

<p>Professor Childs' Group:  (Leeds , U. K.)  S. Mahmood,  H. J. Yoon,  T.H.C. Childs</p>	<p>WORKMATERIALS:</p> <ul style="list-style-type: none"> <li>• <u>Balls</u>: silicon nitride, zirconia, alumina (1994, 1995)</li> </ul> <p>ACTIVITIES:</p> <ul style="list-style-type: none"> <li>• Design of the magnetic float <u>grinding cell</u> (1992)</li> <li>• <u>Kinematics of the ball motion</u> (1994)</li> <li>• <u>Mechanism of material removal</u> (1995)</li> </ul>
---	---

Table 2.3 MFP research activities in Komanduri's group in the USA

<p>Professor Komanduri's Group:  (U.S.A.) M. Raghunandan Jiang Ming S. R. Baghavatula, M. J. Fox M. Dock Asif Patel Vinoos Thomas Brian Perry Cetin Murat Ali Noori-Khajavi Zhen-Bing Hou N. Umehara T. Shinmura R. Komanduri</p>	<p><b>WORKMATERIALS:</b></p> <ul style="list-style-type: none"> <li>• Balls: silicon nitride, zirconia, stainless steel</li> <li>• Rollers: silicon nitride, stainless steel, stainless tube</li> </ul> <p><b>ACTIVITIES:</b></p> <ul style="list-style-type: none"> <li>• Electromagnet apparatus (1994, 1997)</li> <li>• Permanent magnet apparatus (1996)</li> <li>• FEM analysis of the apparatus (1996)</li> <li>• Mechanisms of material removal (1996)</li> <li>• Chemo-mechanical polishing (1996, 1997)</li> <li>• Thermal analysis of MFP (1997a,b,c)</li> <li>• Taguchi experimental method for optimum polishing conditions (1997)</li> <li>• Methodology for finishing ceramic balls for bearing applications with good sphericity and surface finish using Cr<sub>2</sub>O<sub>3</sub> abrasive (1996)</li> <li>• Methodology for finishing ceramic balls for bearing applications with good sphericity and surface finish using CeO<sub>2</sub> abrasive (1997)</li> <li>• Development of equipment for the finishing of large batch balls (1998)</li> <li>• Finishing of ceramic balls for hybrid bearing that meet the requirements of industry (1998)</li> </ul>
---	--

Umehara and Kato (1990) made a major contribution by introducing the use of a float to produce uniform and sufficiently high polishing force to improve the material removal rates when polishing advanced ceramic balls. Much of their early work dealt with sintered material which is not very dense. Figures 2.2 (a) - (d) show the principle of magnetic float polishing with a float and the effect of the float on polishing load, sphericity, and stock removal, i.e., the variation of polishing load with clearance between the magnet and the balls with and without the float, variation of sphericity with polishing time with and without the float, and variation of the stock removal with polishing time with and without the float [Umehara and Kato, 1990]. It can be seen that the polishing load increases significantly, especially at lower clearances, sphericity decreases significantly with polishing time and the stock removal rate increases with the float compared to that without the float. This work more or less established the need for the float and today all designs of MFP apparatus incorporates this concept.

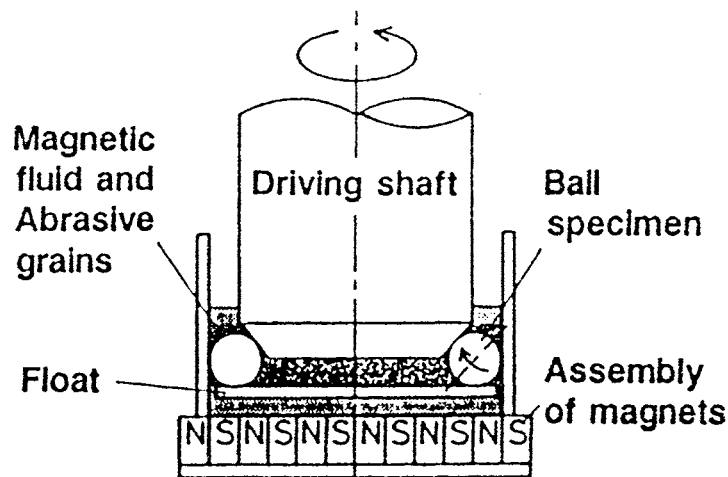


Figure 2.2 (a) Magnetic float polishing set-up [Umehara and Kato, 1990]

NOTE: Clearance bet. Float and magnet.  
 1 mm / 2 mm !!!

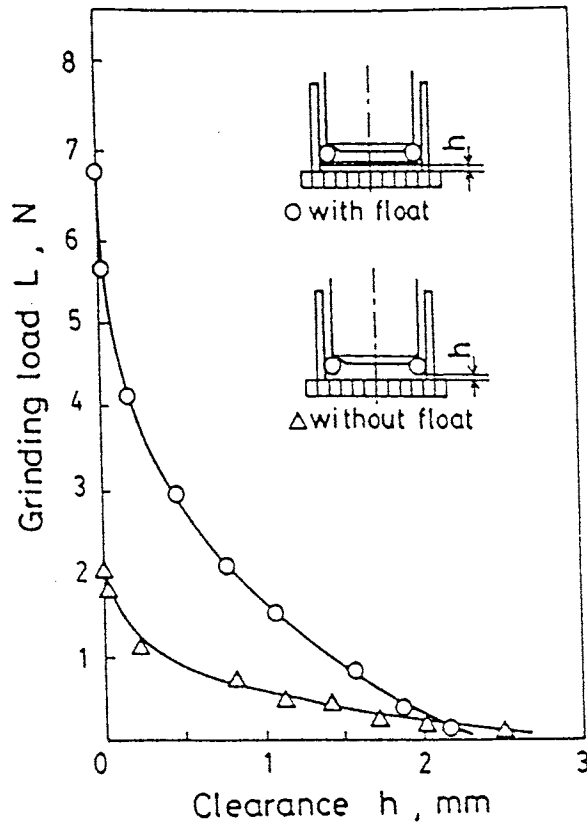


Figure 2.2 (b) Variation of polishing load with clearance  
 [Umehara and Kato, 1990]



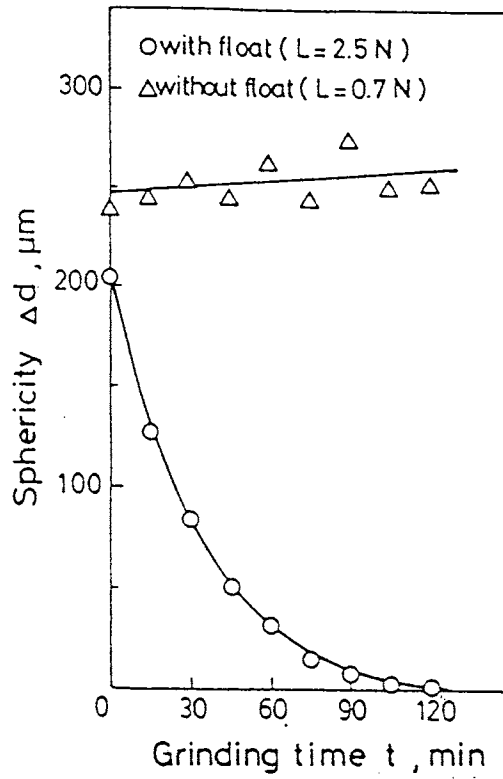


Figure 2.2 (c) Variation of sphericity with polishing time [Umehara and Kato, 1990]

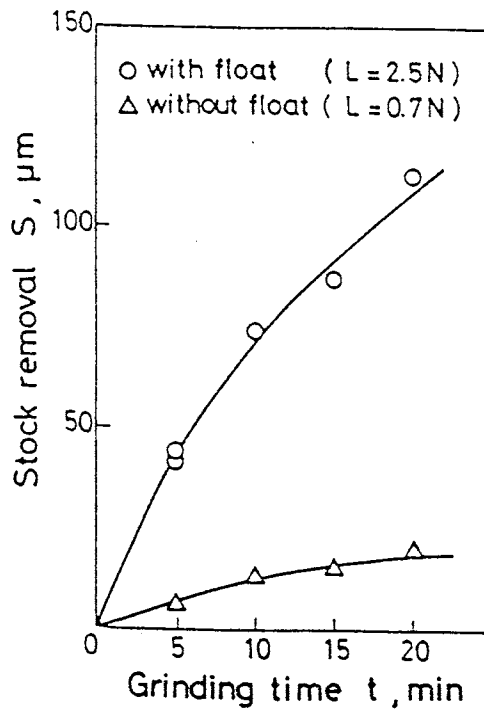
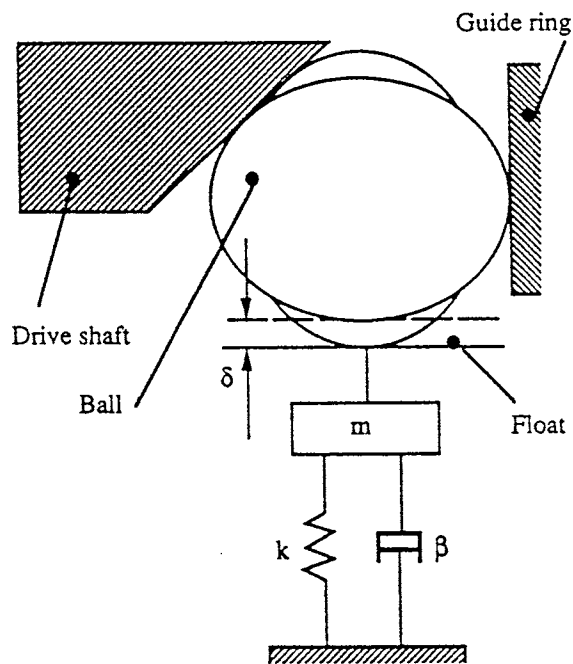


Figure 2.2 (d) Variation of the stock removal with polishing time [Umehara and Kato, 1990]

Zhang, Umehara, and Kato (1996) developed a dynamic model of magnetic float polishing of ceramic balls (see Figure 2.3) for generating good sphericity. They concluded that during the magnetic float polishing, when the larger diameter positions of ball enter the contact area, the load will increase and a larger amount of material will be removed from this place, and this process keeps going until the expected spherical surface is obtained.



$$\Delta P = \kappa \delta$$

$$\kappa = \sqrt{(k - m\omega^2)^2 + (\beta\omega)^2}$$

Figure 2.3 Dynamic model of magnetic float polishing [Zhang et al, 1996]

Zhang et al (1997) investigated an eccentric magnetic float polishing apparatus shown in Figure 2.4. They postulated that the mechanism of the generation of good sphericity of the ball is that polishing should be conducted with uniform distribution of contact track over the whole ball surface. They believe that proper eccentricity between the driving shaft and the guide ring may result in the proper feed motion of the ball for polishing.

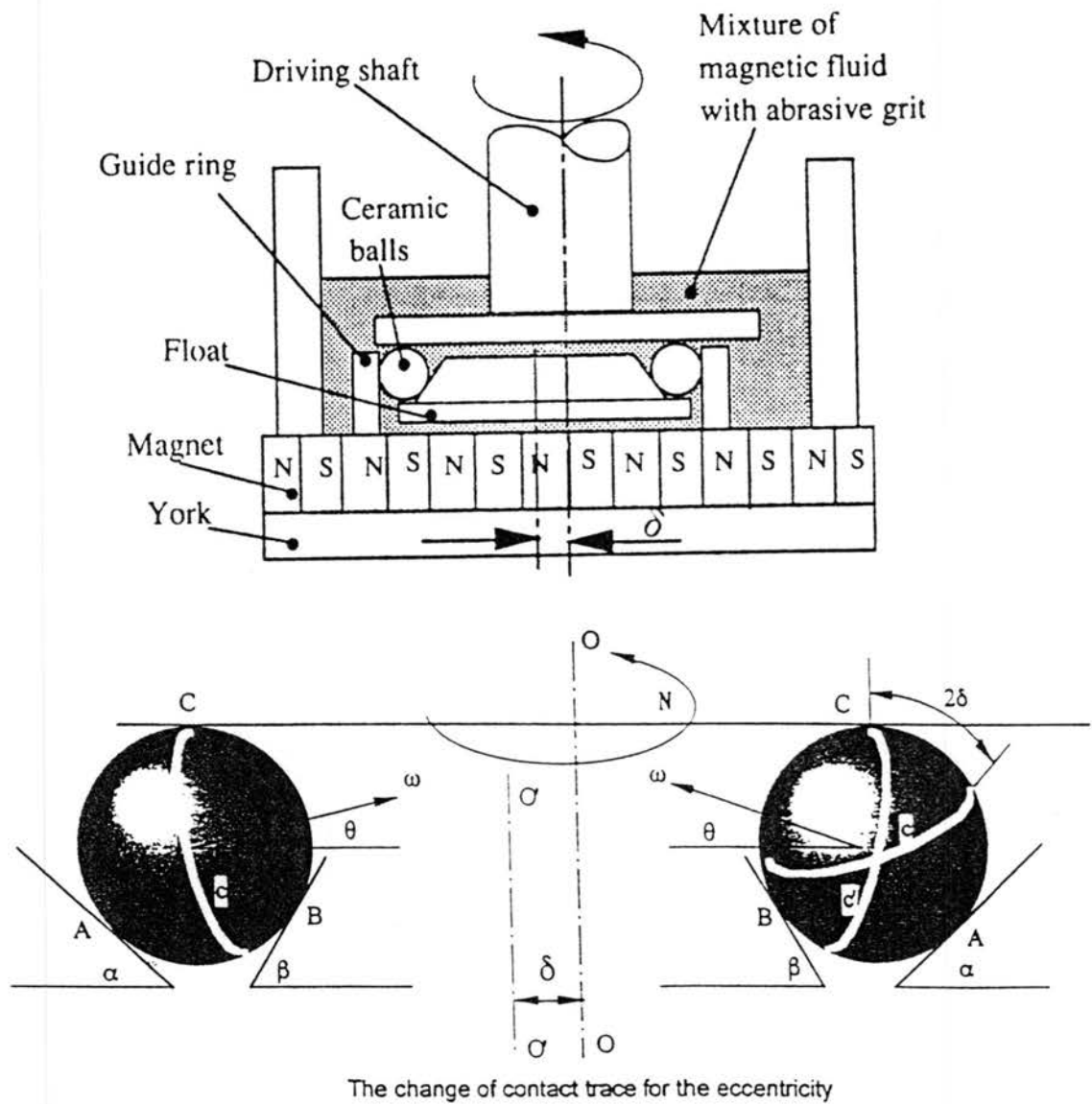
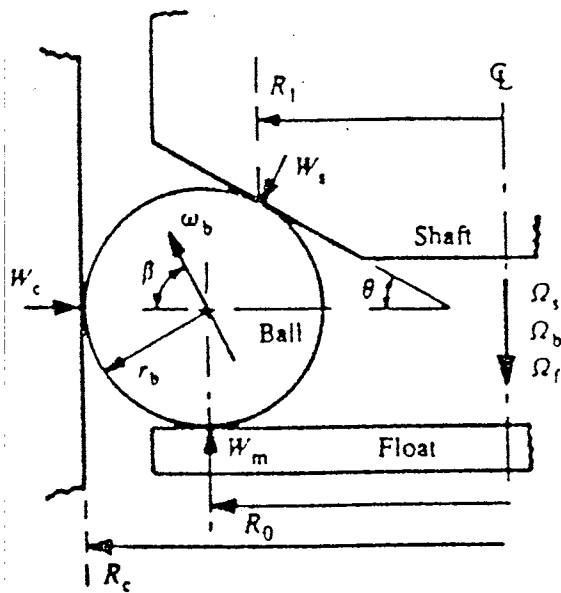


Figure 2.4 Eccentric magnetic float polishing apparatus [Zhang et al, 1997]

Childs et al (1994) developed a kinematic model of ball motion during magnetic float polishing of ceramic balls (shown in Figure 2.5(a) ) to calculate sliding speeds and to estimate the wear (material removal) coefficients. Based on the value of wear coefficients (0.04-0.08), they (1995) concluded that material removal is due to two-body abrasion caused by the abrasives embedded in the drive shaft. They showed evidence of abrasive embedded in the drive shaft in the region where the balls contact (see Figure 2.5(b) and (c) ).



$$R_f = R_c - R_b$$

$$R_s = R_f - R_b \sin \theta$$

$$V_c = (R_f \Omega_b - R_b \Omega_b \sin \beta) - 0$$

$$V_s = R_s \Omega_s - (R_f \Omega_b + R_b \omega_b \cos (\beta - \theta))$$

$$V_f = (R_f \Omega_b - R_b \omega_b \cos \beta) - R_f \Omega_f$$

Figure 2.5 (a) kinematic model of ball motion during MFP [Childs et al, 1994]

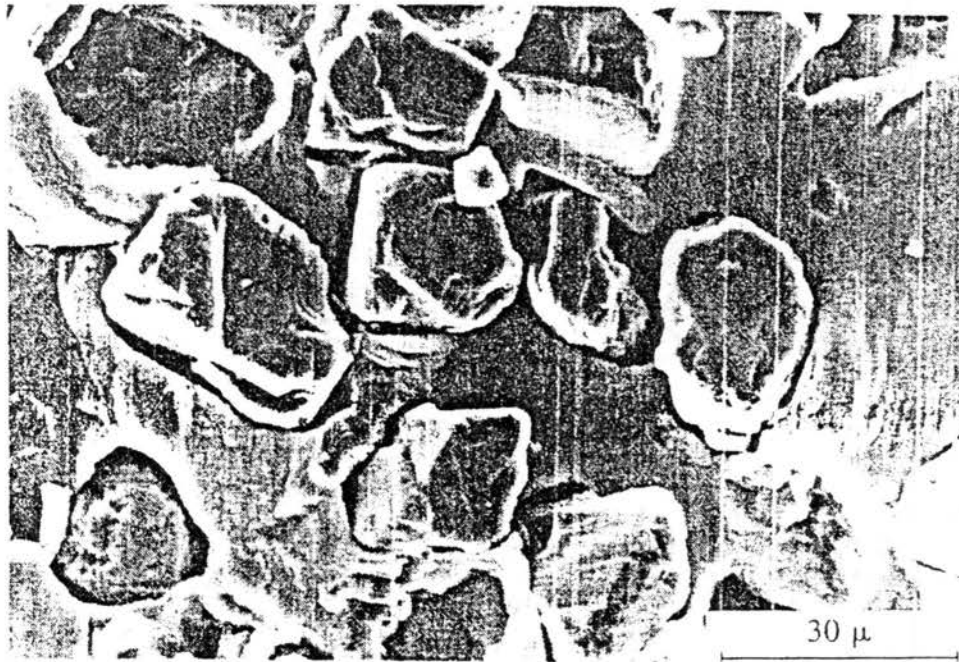


Figure 2.5 (b) Abrasives embedded in the drive shaft [Childs et al, 1995] show two-body abrasion of material removal mechanism in MFP

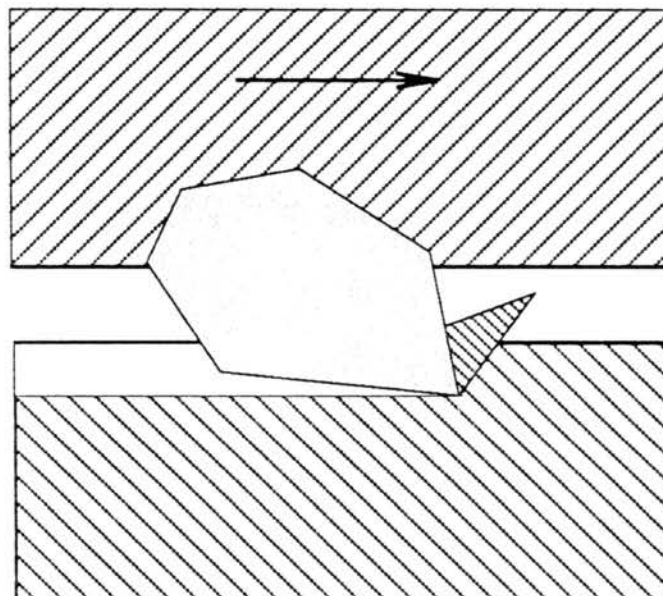


Figure 2.5 (c) Diagram of two-body abrasion

Shinmura, Komanduri, Dock, and Murat have developed an electromagnetic float polishing apparatus. The float forces produced by this apparatus was 40% higher than in the permanent magnet apparatus. Consequently, the material removal rates are 1-2 times that of the permanent magnet set-up [Dock, 1994; Murat, 1996] (see Figure 2.6). The electromagnetic field is generated by passing a DC current through the copper wire wound around a low carbon steel core. The magnetic field is conducted to the ring pole around the polishing chamber by the steel linkage plates. The expected magnetic field for magnetic float polishing is formed between one pole from the steel ring and the other pole from electromagnetic core. The shape of magnetic field in the polishing area is continuous, uniform, and circular (ring). The aluminum base plate is used to separate the steel plate for the magnetic field linkage from the steel table of machine to prevent leakage of the magnetic field contained in this steel plate.

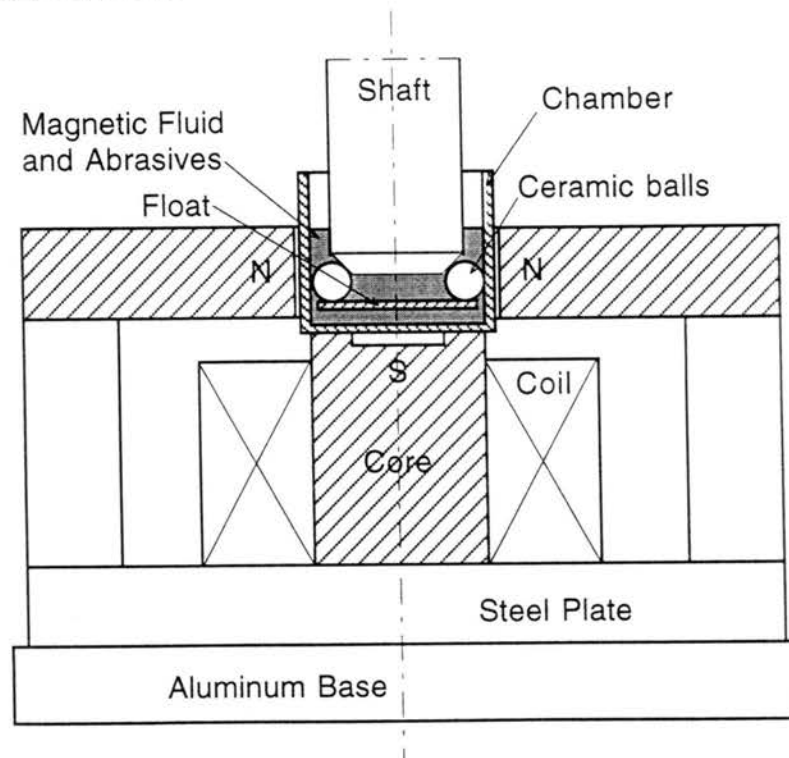


Figure 2.6 Electromagnetic float polishing apparatus

Umehara et al (1992) investigated the magnetic float polishing of Alumina ( $\text{Al}_2\text{O}_3$ ) ceramic flat surfaces. (see Figure 2.7). A minimum surface roughness  $R_a$  of  $0.06 \mu\text{m}$  at the SiC abrasive with a  $1.8 \mu\text{m}$  grain size and flatness of  $0.5 \mu\text{m}$  were achieved. Umehara et al (1993) also studied the magnetic float polishing of stainless steel plates. A minimum surface roughness  $R_a$  of  $0.014 \mu\text{m}$  was achieved with  $\text{Al}_2\text{O}_3$  abrasive ( $2 \mu\text{m}$  grain size) and polyurethane polisher.

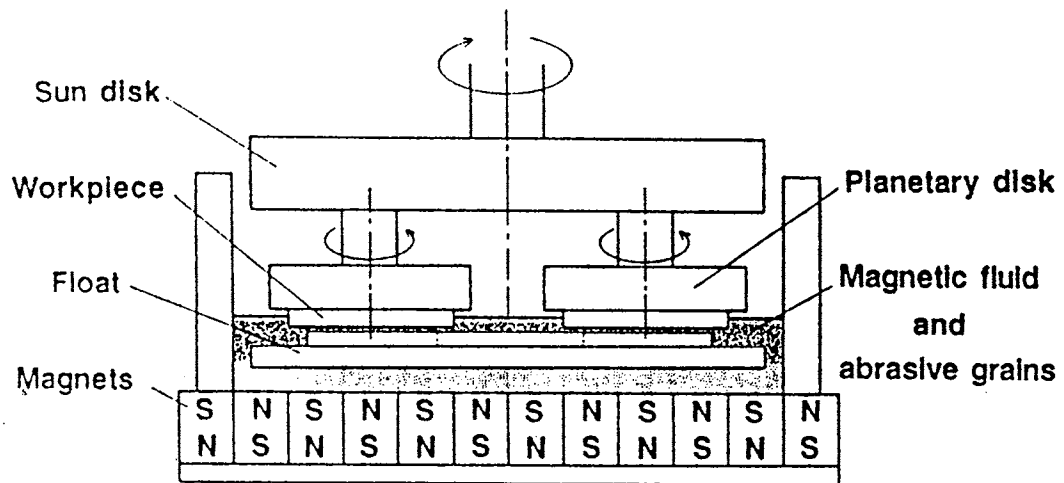


Figure 2.7 Magnetic float polishing of Alumina flat surfaces [Umehara et al, 1992]

Umehara and Komanduri (1996) investigated the magnetic float polishing of HIP'ed Si<sub>3</sub>N<sub>4</sub> rollers. Surface finish of 5 nm Ra was achieved after polishing initially with B<sub>4</sub>C, followed by SiC and Cr<sub>2</sub>O<sub>3</sub>. Figure 2.8 shows the schematic of the apparatus used for this application. There are two magnet assembly rings A and B in this apparatus. Magnetic ring A around the chamber is a hollow cylindrical magnet assembled by individual magnets. Each individual magnet is magnetized in the radial direction and thus the magnetic buoyant force from the magnet assembly ring A not only concentrates the abrasives to the polishing region but also keeps the float at the center similar to a static hydrodynamic bearing. Magnetic ring B at the top of the chamber (fixed to the cover plate) is a ring magnet assembled by individual magnets. Each individual magnet is magnetized in the axial direction. Therefore, the magnetic buoyant force from magnet assembly ring B pushes the float against rollers. The rollers are polished when they are rotated by the driving shaft.



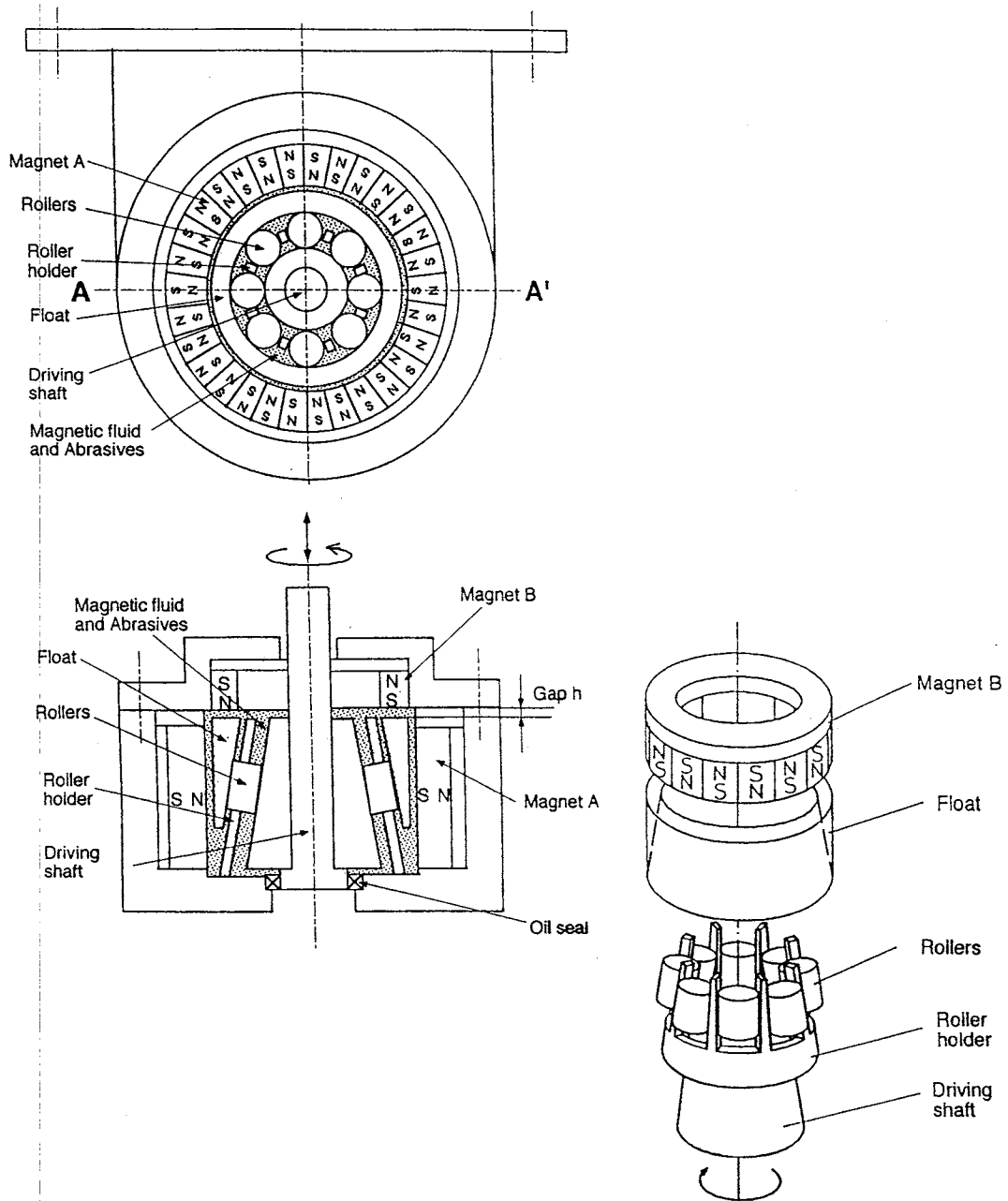
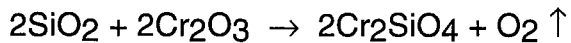
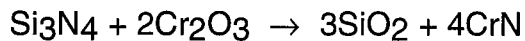
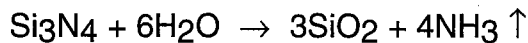


Figure 2.8 Schematic of the magnetic float polishing of HIP'ed Si<sub>3</sub>N<sub>4</sub> rollers apparatus.[Umehara and Komanduri, 1996]

Komanduri (1996, 1997) considered the nature of bonding of advanced ceramics. He pointed that ceramics are different from metals in which plastic deformation, instead of brittle fracture, is the predominant mode of material removal. This is because of the metallic bonding, high symmetry crystal structure, and numerous slip (planes and directions) systems in the case of metals. In contrast, the material removal in ceramic materials during mechanical abrading is predominantly by microfracture due to their high hardness and brittleness. This is because of their strong covalent/ionic bonding, low symmetry crystal structure, and fewer slip systems.

Komanduri et al (1996) reviewed the chemo-mechanical polishing and considered the possibility of chemo-mechanical reaction of finishing silicon nitride balls in magnetic float polishing using soft abrasives for obtaining good surface finish. Chemo-mechanical polishing was first demonstrated by Yasunaga et al (1977-79) for polishing single crystals of silicon using a soft abrasive. Later, Vora et al (1982-83) reported the feasibility of polishing silicon nitride to a high level of finish by chemo-mechanical polishing with  $\text{Fe}_2\text{O}_3$  and  $\text{Fe}_3\text{O}_4$  abrasives. Suga et al (1989) polished silicon nitride using the following abrasives  $\text{CaCO}_3$ ,  $\text{MgO}$ ,  $\text{SiO}_2$ ,  $\text{Fe}_2\text{O}_3$  and  $\text{Fe}_3\text{O}_4$ , and  $\text{Cr}_2\text{O}_3$ . They concluded that  $\text{Cr}_2\text{O}_3$  is a more suitable abrasive for the chemo-mechanical polishing of silicon nitride. However, most of the researchers pointed out that the role of  $\text{Cr}_2\text{O}_3$  is more that of a catalyst than actively participating in the chemical reactions. Wang et al (1994) pointed that the formation of a thin film of the reaction product ( $\text{SiO}_2$ ), usually less than 100 Å thick, resulted in the easy removal of it without directly abrading the hard surface. Thus high material removal rate and low surface damage can be achieved by the formation of softer surface films.

Bhagavatula and Komanduri (1996) studied the mechanisms of material removal from silicon nitride balls polished with Cr<sub>2</sub>O<sub>3</sub> abrasive by analyzing the wear debris from polishing using a scanning electron microscopy (SEM) with an energy-dispersive X-ray microanalyser (EDXA) and a low-angle X-ray diffraction apparatus. As previously pointed out, Cr<sub>2</sub>O<sub>3</sub> has been identified by other researchers [e.g. Kikuchi et al, 1992] as a catalyst rather than its direct involvement in the chemical reactions with Si<sub>3</sub>N<sub>4</sub>. Bhagavatula and Komanduri, based on experimental evidence (Figure 2.9), showed that chemo-mechanical reactions play an important role in the generation of good surface finish in magnetic float polishing Si<sub>3</sub>N<sub>4</sub> balls with Cr<sub>2</sub>O<sub>3</sub> abrasive. Based on this they identified the formation chromium silicate (Cr<sub>2</sub>SiO<sub>4</sub>) and chromium nitrate (CrN) in the chemo-mechanical polishing of Si<sub>3</sub>N<sub>4</sub> balls with Cr<sub>2</sub>O<sub>3</sub> abrasive. The following reactions were considered and a chemo-mechanical polishing mechanism was proposed.



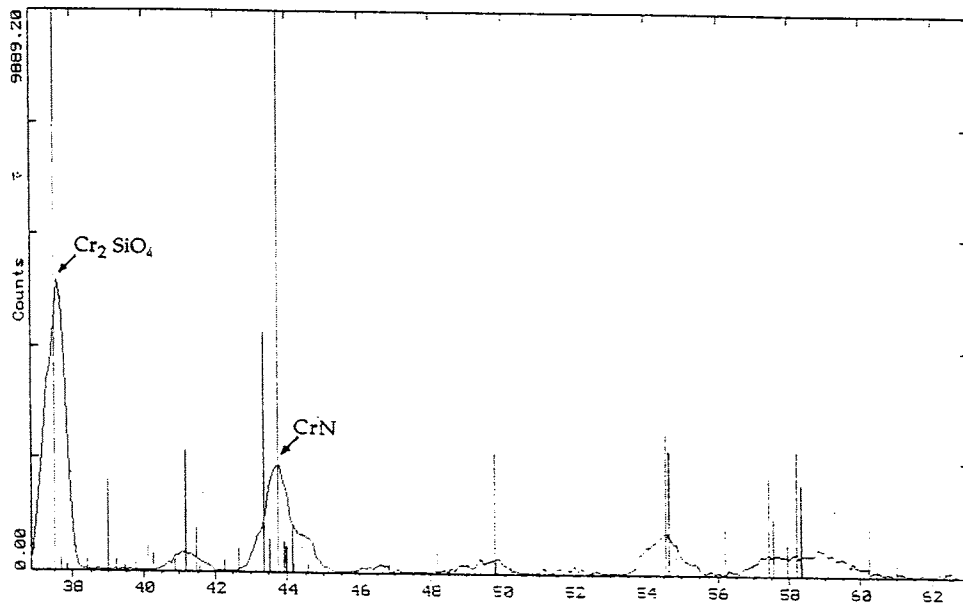


Figure 2.9 X-ray diffraction analysis of the wear debris showing the presence of CrN and Cr<sub>2</sub>SiO<sub>4</sub> [Bhagavatula and Komanduri, 1996]

From the literature review presented in this Chapter it can be seen that magnetic float polishing has been applied and been able to finish advanced ceramic balls with high material removal rates. However, the surface finish and sphericity of these balls have not reached the requirements for bearing applications. It is because the methodology for finishing ceramic balls for bearing application by this method has not been adequately established.

## CHAPTER 3

### PROBLEM STATEMENT

The industry practice is the use of essentially the same technology that is used for finishing *steel* balls, namely V-groove lapping to finish advanced ceramic balls. This includes high loads, low speeds, and the use of diamond abrasive for material removal. In practice, the finishing time is generally long, often several weeks (depending on the quality of the balls required and the state of the manufacturing technology practiced). Because of the high hardness of diamond abrasive and high loads used in conventional polishing, material removal in ceramics will generally be by brittle fracture. The propagation of surface and subsurface damage by brittle fracture can lead to catastrophic failure of the ceramic bearing balls. Also, the use of diamond abrasive will be a significant additional burden on the cost of manufacturing. To overcome this, "gentle" polishing conditions (light loads, high speeds, and avoidance on the use of diamond abrasive) and a process for rapid finishing of Si<sub>3</sub>N<sub>4</sub> balls is needed. In view of the precision finishing applications of the hybrid bearings, these balls should be finished to very high form accuracy and surface finish at the same time meet the specifications of size. A sphericity of 0.15 μm and a surface finish of 4 nm Ra and 40 nm Rt were set as target in this investigation. When this target is reached the technology developed would put OSU second to none in the U.S. and perhaps in the world.

This investigation deals with the development of science and technology of finishing advanced ceramics, such as Si<sub>3</sub>N<sub>4</sub> balls for bearing applications by

magnetic float polishing (MFP) technology. Specifically, a methodology is developed for obtaining high quality (both good sphericity and surface finish)  $\text{Si}_3\text{N}_4$  balls rapidly. To accomplish this, the following specific tasks were undertaken.

1. An instrumented flexible/gentle magnetic float polishing (MFP) apparatus was designed and built to finish (by combined mechanical and chemo-mechanical polishing)  $\text{Si}_3\text{N}_4$  balls for hybrid bearing applications.

2. Optimization of polishing parameters in magnetic float polishing (MFP) was carried out using the Taguchi experimental design and analysis method. The optimum mechanical polishing conditions, such as polishing load, polishing speed, and abrasive concentration were determined using this approach.

3. Various abrasives were investigated systematically to determine their suitability for chemo-mechanical polishing of  $\text{Si}_3\text{N}_4$  material. The purpose was to determine the most effective abrasive to finish silicon nitride bearing balls with extremely smooth and damage-free surfaces. Different magnetic fluids (water-based and oil-based), pH values, and electric conductivities of polishing fluid were also investigated to determine the most effective CMP environment.

4. Possible chemical reactions during CMP process were studied using the Gibbs free energy change (thermodynamic analysis) by employing HSC chemistry software developed in Finland. The temperature under the polishing zone was calculated based on the moving heat source model developed by Hou and Komanduri (1998 a). The CMP and the chemical reaction would proceed on a continuing basis only if the passivating layers are removed by the subsequently mechanical action after chemical reaction.

5. The mechanism of material removal and the surface generation process by both fine mechanical polishing and chemo-mechanical polishing (CMP) of advanced ceramics by magnetic float polishing (MFP) was investigated and discussed.

6. A methodology was developed for rapid finishing of Si<sub>3</sub>N<sub>4</sub> balls by magnetic float polishing technology from the as-received condition to the final stage for hybrid bearing applications with a sphericity of 0.15 μm and a surface finish of 4 nm Ra and 40 nm Rt .

*larger batch polishing !!!*  
7. A prototype apparatus for commercial finishing a larger batch (100 of 3/8 inch) balls and associated monitoring for in-process control of the MFP process will be initiated.

8. Future work includes the extension of magnetic float polishing (MFP) method to finish other advanced ceramics, such as zirconium oxide (ZrO<sub>2</sub>) balls for flow control applications and ferritic stainless steel balls for bearing applications. It may be pointed out that finishing of the latter was found to extremely difficult and time consuming by conventional ball lapping process by a leading industry in the U. S.



## CHAPTER 4

### APPROACH

In this investigation, major emphasis is on the development of technology for finishing Si<sub>3</sub>N<sub>4</sub> balls for hybrid bearing applications with good sphericity (0.15 μm) and extremely smooth (Ra ~4 nm and Rt ~40 nm) and damage-free surfaces. The experimental and analytical work involve the design and development of a polishing apparatus (using ANSYS finite element model), determination of the optimum mechanical polishing conditions (using Taguchi's experimental method for the design and analysis of experiments), and selection of the appropriate abrasive for chemo-mechanical polishing (CMP) after fine mechanical polishing to obtain excellent surface by systematic study of the role of various abrasives and polishing environments for CMP of Si<sub>3</sub>N<sub>4</sub>. In specific, thermodynamic analysis (Gibbs free energy formation) is conducted to identify the chemical species likely to be formed during CMP. Finally the methodology and process for finishing Si<sub>3</sub>N<sub>4</sub> balls from the as-received (sphericity 200 μm) to the final finished condition (AFBMA Grade 3) is developed. The full characterization of the Si<sub>3</sub>N<sub>4</sub> bearing balls including diameter, sphericity, and surface finish are evaluated using micrometer, TalyRond, and TalySurf, SEM, ZYGO laser interference microscope, etc.

#### 4.1 MAGNETIC FLUID POLISHING (MFP) APPARATUS

The magnetic float polishing (MFP) technique is based on the magneto-hydrodynamic behavior of a magnetic fluid that can float non-magnetic materials, such as abrasives suspended in the magnetic fluid. The force applied

by the abrasive on the part is extremely low (1 N/ball) and highly controllable. Figures 4.1 (a) and (b) are a schematic and a photograph of the magnet float polishing (MFP) apparatus (using permanent magnets) for finishing advanced ceramic balls. A bank of permanent magnets (Nd-Fe-B, Residual magnetization: 10500 G) with alternate N and S are arranged below an aluminum float chamber. The float chamber is filled with the required amount of magnetic fluid and appropriate abrasive (5-10%). The magnetic fluid is a colloidal dispersion of extremely fine (100 to 150 Å) subdomain ferromagnetic particles, usually magnetite ( $\text{Fe}_3\text{O}_4$ ), in a carrier fluid, such as water or kerosene. It is made stable against particle agglomeration by coating the surface of the particles with an appropriate surfactant. In this investigation, a water base magnetic fluid (W-40) is used (Saturation Magnetization at 25 °C: 400 Gauss, Viscosity at 27 °C: 25 Cp). When a magnetic field is applied, the magnetic particles in the magnetic fluid are attracted downward to the area of higher magnetic field and an upward buoyant force is exerted on all non-magnetic materials to push them to the area of lower magnetic field. The abrasive grains, the ceramic balls, and the acrylic float inside the chamber (all being non-magnetic materials) are floated by the magnetic buoyant force. A drive shaft is lowered to make contact with the balls and to press them down to reach the desired level of force or height. The balls are held by three point contact between the float chamber wall, the float, and the drive shaft and polished by the abrasive grains under the action of the magnetic buoyancy as the spindle rotates. Damage-free surface on ceramic balls is accomplished by the magnetic float polishing technique because low and controlled magnetic buoyant force (1 N/ball) is applied via the flexible float. The function of the acrylic float used here is to produce more uniform and larger polishing pressure (i.e. the larger buoyancy force near the magnetic poles can

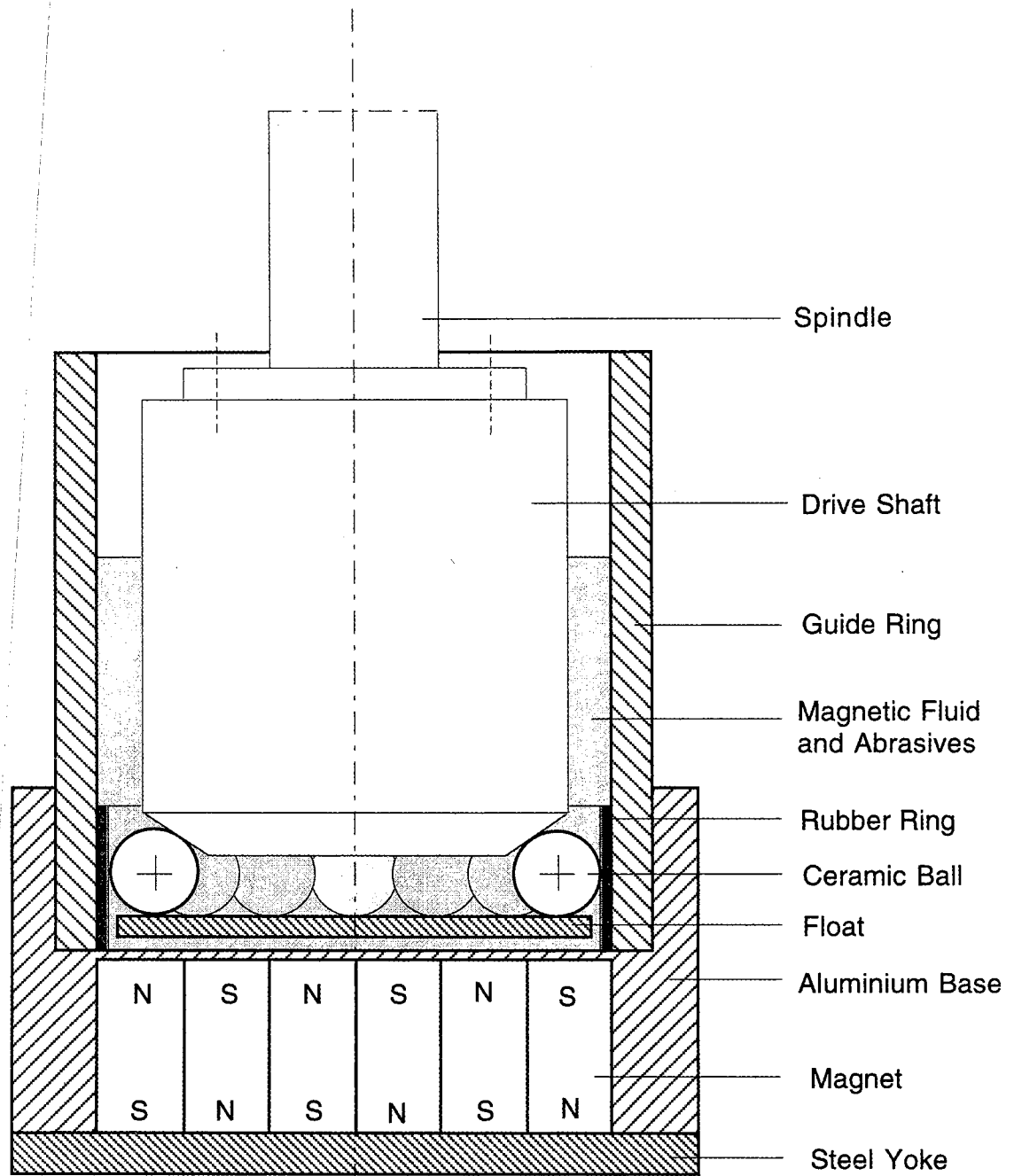


Figure 4.1 Schematic of magnetic float polishing apparatus

be transmitted to the polishing area by this float). An urethane rubber sheet is bonded on to the inner guide ring to protect it from wear. The material of the drive shaft is austenitic stainless steel (a non-magnetic material).

#### **4.1.1 SALIENT FEATURES OF MAGNETIC FLUID POLISHING TECHNOLOGY**

The magnetic float polishing technology has the following characteristics:

1. High material removal rate
2. Excellent surface finish
3. Good sphericity

In addition, the apparatus designed can handle small batches which are particularly useful when only a few balls need to be polished either due to customers demand or due to small amount of material available for evaluation during the materials development program. The process also does not use diamond abrasive and is faster by an order of magnitude or more than conventional V-groove lapping process. Some of these features will be elaborated in the following.

##### **1. High Material Removal Rate**

The material removal by polishing or lapping is due to sliding at the contact region between the workpiece and the abrasives embedded in the tool. The material removal rate during magnetic float polishing ceramic balls is high because there is more sliding in this process than in conventional lapping due to following two reasons: (1) The polishing load in magnetic float polishing is ~100 times lower than in conventional lapping. Hence, the frictional force at the

contact region is significantly reduced. Consequently, there is more sliding than rolling. (2) The drive speed in magnetic float polishing is 100 times higher than in conventional lapping. Thus there will be more sliding taken place in the polishing region due to increased relative speed. The experimental results show that the material removal rate in polishing of ceramic balls by magnetic float polishing method is ~50-100 times higher than by the conventional V-groove lapping method.

## **2. Excellent Surface Finish**

It is reasonable to expect that the ceramic balls finished by magnetic float polishing technology would be free of surface and sub-surface damage because magnetic buoyant force during polishing is extremely small (~ 1 N/ball) and controllable. Also, the chemo-mechanical polishing (CMP) with a softer abrasive is applied to this process during the final stage to improve the surface finish. The hardness of the abrasive used in CMP is generally much lower than the workmaterial. The material removal from the ceramic balls is due to the removal of the reaction product during chemo-mechanical polishing by the frictional action. The chemical reaction is produced by the interaction between the selected abrasive, the work material, and the water from water-based ferrofluid. Thus, the resulting surface on the polished ceramic ball is extremely smooth and damage-free.

## **3. Good Sphericity**

The mechanism for the generation of good sphericity on the balls, be it by lapping or magnetic float polishing, is that when the larger diameter portion of a ball enters the contact area, the load on it will increase and a larger amount of material will be removed from this place. This process continues till the

expected spherical surface is obtained when the abrading tracks are uniformly distributed over the whole ball surface.

In conventional ball lapping, the material from the balls is removed by the V-groove lapping; And the balls arrive at certain location on the lapping plate and are automatically mixed and recirculated in grooves randomly to improve the sphericity. In the magnetic float polishing, there are 3 contact points to each ceramic ball to bring two main motions: the rotation around the axis parallel to the contact area and the spinning around the axis vertical to the contact area. The rotation of the ball is the motion for polishing, and the spinning motion of the ball is the feed for polishing. The spinning motion is critical for obtaining good sphericity. Due to this spinning motion, polishing track distribution over the whole ball surface is very uniform in the magnetic float polishing. Also, because the magnetic float force for polishing is small and flexible, it can modify the sphericity in the very small scale (submicrometer level). Thus, good sphericity can be expected to obtain by magnetic float polishing.

#### **4.2 Silicon Nitride Workmaterial**

Silicon nitride ( $\text{Si}_3\text{N}_4$ ) is a ceramic with predominantly covalent bonding and hexagonal structure [McColm, 1983, Katz, et al, 1985]. The electron configuration of Si [ $3s^23p^2$ ] (excited electron state:  $sp^3$  hybridization) yields the usual tetrahedral arrangement of covalent bond formation with four N atoms producing a  $\text{SiN}_4$  tetrahedral building unit, and these tetrahedral units form the hexagonal  $\text{Si}_3\text{N}_4$  by each corner (nitrogen atoms  $2s^22p^3$ ) being shared with two other  $\text{SiN}_4$  tetrahedrons. So, in the three dimensional silicon nitride

network, each silicon atom is covalently bonded with four nitrogen atoms, and each nitrogen atom is covalently bonded with three silicon atoms.

Silicon nitride has two crystalline phases ( $\alpha$ -Si<sub>3</sub>N<sub>4</sub> and  $\beta$ -Si<sub>3</sub>N<sub>4</sub> respectively) in the microstructure. They are both covalently bonded hexagonal structured materials but  $\beta$ -Si<sub>3</sub>N<sub>4</sub> grain is more elongated than that of  $\alpha$ -Si<sub>3</sub>N<sub>4</sub> ( $\alpha$ -Si<sub>3</sub>N<sub>4</sub>: a=0.78 nm, c=0.56 nm;  $\beta$ -Si<sub>3</sub>N<sub>4</sub>: a=0.76 nm, c=0.29 nm). The  $\alpha$ -Si<sub>3</sub>N<sub>4</sub> is easier to form than  $\beta$ -Si<sub>3</sub>N<sub>4</sub> but it gets converted to  $\beta$ -Si<sub>3</sub>N<sub>4</sub> at high temperature (1400-1800°C). In general, advanced silicon nitride engineering materials are  $\beta$ -Si<sub>3</sub>N<sub>4</sub> because all  $\alpha$ -Si<sub>3</sub>N<sub>4</sub> transform to  $\beta$ -Si<sub>3</sub>N<sub>4</sub> during the shaping process (hot pressing ).

The covalent solid has a low concentration of vacancies and cannot be sintered to high densities merely by heating. Several techniques, such as chemical vapour deposition (CVD), reaction bonding, hot pressing (HP), and hot isostatic pressing (HIP) have been available to obtain dense silicon nitride material [McColm, 1983]. In the following they will be briefly reviewed.

**Chemical Vapor Deposition (CVD) Process:** In the chemical vapour deposition process pyrolytically deposited Si<sub>3</sub>N<sub>4</sub> is formed from SiCl<sub>4</sub> vapor and NH<sub>3</sub> gas. The volatile SiCl<sub>4</sub> and NH<sub>3</sub> gases react and deposit the Si<sub>3</sub>N<sub>4</sub> at the hot substrate. High density Si<sub>3</sub>N<sub>4</sub> layers can be obtained but they are thin and amorphous (at 0°C: SiCl<sub>4</sub> + 6NH<sub>3</sub> → Si(NH)<sub>2</sub> + 4NH<sub>4</sub>Cl; at 1200°C: nSi(NH)<sub>2</sub> →  $\alpha$ -Si<sub>3</sub>N<sub>4</sub>).

**Reaction Bonding Process:** Reaction bonding of Si<sub>3</sub>N<sub>4</sub> material is obtained by heating silicon in a nitrogen atmosphere. Silicon powder is compacted to high density in an inert atmosphere and then heated in a nitrogen atmosphere at ~1400°C to achieve Si<sub>3</sub>N<sub>4</sub> material. The advantage of this

method is that complex shapes can be made. But the final product has about 20% porosity and 300 MPa flexural strength (at 1400°C:  $3\text{Si} + 2\text{N}_2 \rightarrow \alpha\text{-Si}_3\text{N}_4$ ).

**Hot Pressed (HP) and Hot Isostatically Pressed (HIP) Process:** Hot pressed  $\text{Si}_3\text{N}_4$  material is made from a mixture of  $\alpha$ - and  $\beta$ - $\text{Si}_3\text{N}_4$  powders sintered to a high density using either uniaxial or isostatic high pressure. The  $\text{Si}_3\text{N}_4$  powders are mixed with densification aids, such as  $\text{MgO}$  or  $\text{Y}_2\text{O}_3$  to enable liquid phase sintering and then heated to 1700°C at 20 MPa pressure for HP and heated above 1700°C in a nitrogen atmosphere at higher pressures >300 MPa for HIP. The high pressure nitrogen gas can yield the isostatic compression which results in a uniform material. The disadvantage of this method is high cost and only a few shapes of the product can be made. For making bulk products such as balls for bearing application, this technique is commonly used.

The chemical composition and typical properties of NBD-200 silicon nitride ball ( $\beta$ - $\text{Si}_3\text{N}_4$ , uniaxially pressed with 1 wt.%  $\text{MgO}$  as main sintering aid) used in this study are shown in Tables 4.1 and 4.2. A glassy phase is created at the grain boundaries during the high-temperature sintering or hot-pressing of  $\text{Si}_3\text{N}_4$  due to the reaction of  $\text{Si}_3\text{N}_4$  and  $\text{SiO}_2$  with small amounts of  $\text{MgO}$ . This complex glassy phase for sintering is primarily a magnesium silicate modified by Ca, Fe, Al and other impurities initially present in  $\text{Si}_3\text{N}_4$ .



Table 4.1 Chemical composition of NBD-200 Si<sub>3</sub>N<sub>4</sub> ball [Hah, et al, 1995]

Mg	Al	Ca	Fe	C	O	Si <sub>3</sub> N <sub>4</sub>
0.6 - 1.0	≤0.5	≤ 0.04	≤ 0.17	≤ 0.88	2.3 - 3.3	94.1 - 97.1

Table 4.2 Mechanical and thermal properties of Si<sub>3</sub>N<sub>4</sub> ball [Hah, et al, 1995]

PROPERTY	VALUE
Flexural Strength, MPa	800
Weibull Modulus	9.7
Tensile Strength, MPa	400
Compressive Strength, GPa	3.0
Hertz Compressive Strength, GPa	28
Hardness, Hv (10kg), GPa	16.6
Fracture Toughness, K <sub>1c</sub> , MNm <sup>-3/2</sup>	4.1
Density, g/cm <sup>3</sup>	3.16
Elastic Modulus, GPa	320
Poisson's Ratio	0.26
Thermal Expansion Coefficient at 20-1000°C, /°C	2.9 x 10 <sup>-6</sup>
Thermal Conductivity at 100°C, W/m-K	29
Thermal Conductivity at 500°C, W/m-K	21.3
Thermal Conductivity at 1000°C, W/m-K	15.5

### 4.3 Abrasives

Abrasives considered for use in this study are listed in Table 4.3. They are classified into two groups, one predominantly for mechanical polishing and the other for chemo-mechanical polishing depending on their mechanical hardness (higher or less than workmaterial) and chemical activity with respect to the work material in a given environment. Fine grain size diamond, boron carbide (B<sub>4</sub>C), and silicon carbide (SiC) abrasives which are harder than Si<sub>3</sub>N<sub>4</sub>

workmaterial are used for mechanical polishing with high material rates to reach the desired diameter and geometry rapidly. The material removal in this case is considered by mechanical microfracture. Aluminium oxide ( $\text{Al}_2\text{O}_3$ ), chromium oxide ( $\text{Cr}_2\text{O}_3$ ), zirconium oxide ( $\text{ZrO}_2$ ), silicon oxide ( $\text{SiO}_2$ ), cerium oxide ( $\text{CeO}_2$ ), iron oxide ( $\text{Fe}_2\text{O}_3$ ), yttrium oxide ( $\text{Y}_2\text{O}_3$ ), molybdenum oxide ( $\text{Mo}_2\text{O}_3$ ) whose hardness is close to or less than  $\text{Si}_3\text{N}_4$  workmaterial come under the second group. They were investigated and analyzed systematically to find their suitability for the chemo-mechanical polishing to improve the final surface finish and to determine the relationship between surface finish from chemo-mechanical polishing and the abrasives used (for e.g. hardness, pH value, electric Conductivity, thermal conductivity, position in the periodic table etc).

Table 4.3 Abrasives used in this study

ABRASIVE	HARDNESS	
	Mohs	Knoop $\text{kg/mm}^2$
Diamond	10	7000
Boron Carbide ( $\text{B}_4\text{C}$ )	9.3	3200
Silicon Carbide ( $\text{SiC}$ )	9.2	2500
Aluminium Oxide ( $\text{Al}_2\text{O}_3$ )	9	2150
Chromium Oxide ( $\text{Cr}_2\text{O}_3$ )	8.5	1800
Silicon Nitride ( $\text{Si}_3\text{N}_4$ )	8.5	1600
Zirconium Oxide ( $\text{ZrO}_2$ )	8	1200
Silicon Oxide ( $\text{SiO}_2$ )	7	820
Cerium Oxide ( $\text{CeO}_2$ )	6	-
Iron Oxide ( $\text{Fe}_2\text{O}_3$ )	6	-
Yttrium Oxide ( $\text{Y}_2\text{O}_3$ )	5.5	700
Copper Oxide ( $\text{CuO}$ )	3.5	225
Molybdenum Oxide ( $\text{Mo}_2\text{O}_3$ )	1.5	-

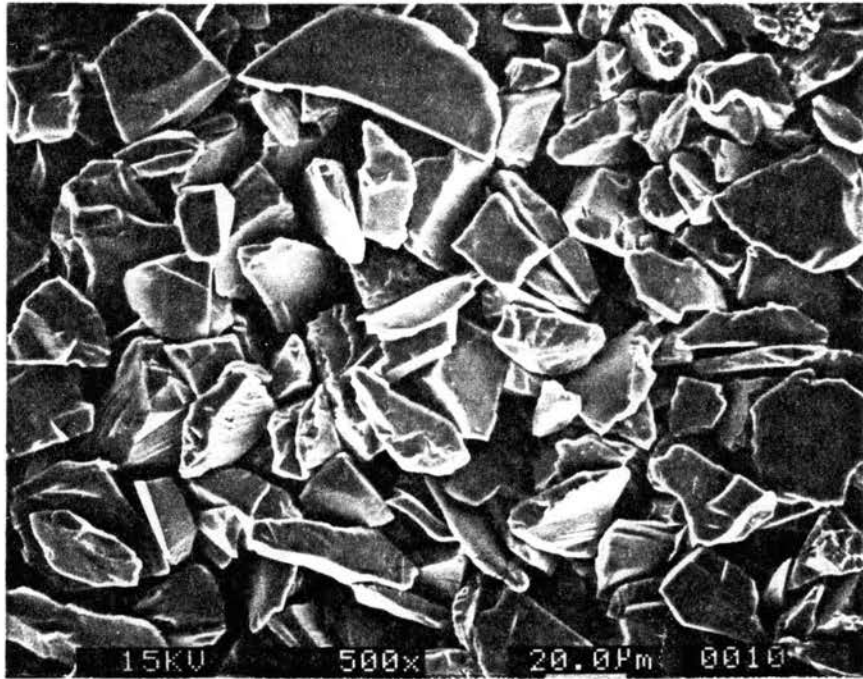


Figure 4.2 (a) SEM micrograph of SiC (#400 grit) abrasives

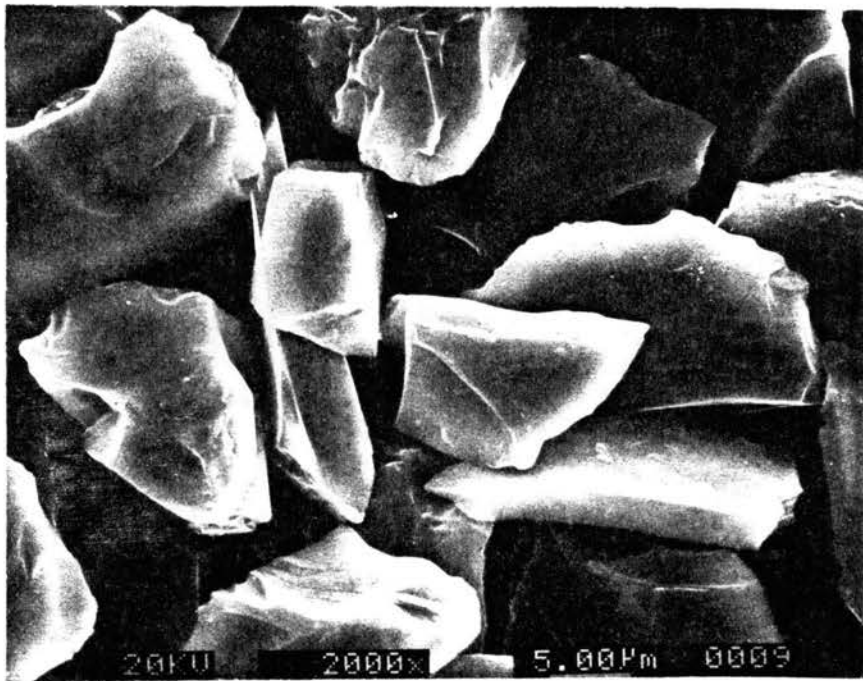


Figure 4.2 (b) SEM micrograph of B<sub>4</sub>C (#500 grit) abrasives

#### 4.4 EXPERIMENTAL WORK

- The polishing shaft was driven by a high-speed, high-precision air bearing spindle (PI Spindle) with a stepless speed regulation of up to 10,000 rpm.
- The magnetic field was measured using a Gauss/Tesla meter.
- The pH and conductivity value of the polishing environment were measured using Cole-parmer pH/mV/Temperature meter and Cole-parmer Conductivity/TDS/Temperature meter, respectively.
- The polishing load was set up by measuring the normal force with a Kistler's piezoelectric dynamometer connected to a charge amplifier and a display (resolution: 0.02 N).
- The material removal rate was calculated by the weight reduction in the balls by measuring the weight before and after polishing at every stage of the test using a precision balance from Brinkman Instruments (resolution: 0.1 mg).
- The ball diameter was measured using a digital micrometer from Mitutoyo (resolution: 1  $\mu\text{m}$ ).
- Full characterization of the bearing balls is required. This includes the size (specific diameter), size variation, sphericity, and surface finish. In this investigation, three balls are randomly selected from each batch and each ball is traced 3 times in approximately three orthogonal planes. The

roundness or sphericity was measured using TalyRond 250 and surface roughness using FormTalysurf 120 L. According to AFBMA, the sphericity of each ball is defined from the maximum value of the roundness measured on three orthogonal planes of the ball. Similarly, the surface finish of each ball is taken as the maximum value of three traces along three orthogonal planes of the ball.

- The roundness of the balls was measured using TalyRond 250 (cut-off: 50  $\mu$ m, Filter: 2CR). The out-of-roundness trace measures the maximum departure (maximum peak-to-valley height) from a true circle and as such it denoted roundness.
- The surface finish of the polished balls was analyzed using:
  - Form Talysurf 120 L (Cut-off: 0.25 mm and 0.8 mm, Evaluation length: 4-6 consecutive cut-off, Filter: ISO 2CR),
  - ZYGO laser interference microscope,
  - ABT 32 scanning electron microscope (SEM).

#### **4.5 EVALUATION OF SURFACE INTEGRATION [Dagnall, 1984, 1986]**

##### **4.5.1 Evaluating Roundness by Number**

The numerical value of the out-of-roundness is the maximum peak-to-valley height (P+V). There are four different reference circles available for this calculation: least square circle (LS), minimum zone circle (MZ), Maximum inscribed circle (MI), and minimum circumscribed circle (MC) as shown in Figure 4.2. The roundness of the balls was measured using TalyRond 250 in this study.

#### 4.5.2 Talyrond 250

Talyrond 250 is a computer controlled stylus instrument manufactured by Rank Taylor Hobson Inc (U.K.). It has a stylus, a variable inductance pick-up (transducer) with rotating worktable (for roundness measurement) and a vertical straightness unit (for vertical straightness measurement). It has two motorized axes for measurement (the worktable and the vertical straightness unit) and one motorized axis for stylus contact. It can evaluate roundness, vertical straightness, squareness, parallelism, flatness, co-axiality, cylindricity, concentricity, eccentricity and runout and capable of conducting harmonic analysis. The roundness limit of error from the worktable and pick-up spindle is about  $0.05 \mu\text{m}$  ( $0.04 \mu\text{m} + 0.0003 \mu\text{m/mm}$  height over the worktable). ?

The deviation from spherical form is determined by rotation of the ball against the transducer with several grams gauge force. The stylus tip, a sapphire ball with a diameter of 2.0 mm, contacts the surface being measured which is fixed on the rotating worktable. When the worktable rotates, the roundness deviation will cause minute movements of the stylus. The variable inductance pick-up will convert this movement of the stylus into variations of an electrical signal. As shown in Figure 4.3, the variable inductance pick-up is the armature that is connected to the stylus and can move between the two coils when the stylus moves. This will alter the inductance of them. These two coils are connected to an ac bridge circuit, the movement of the armature will unbalances this bridge and then will give an output proportional to the movement. The signal is amplified and fed to a recorder. The phase signal

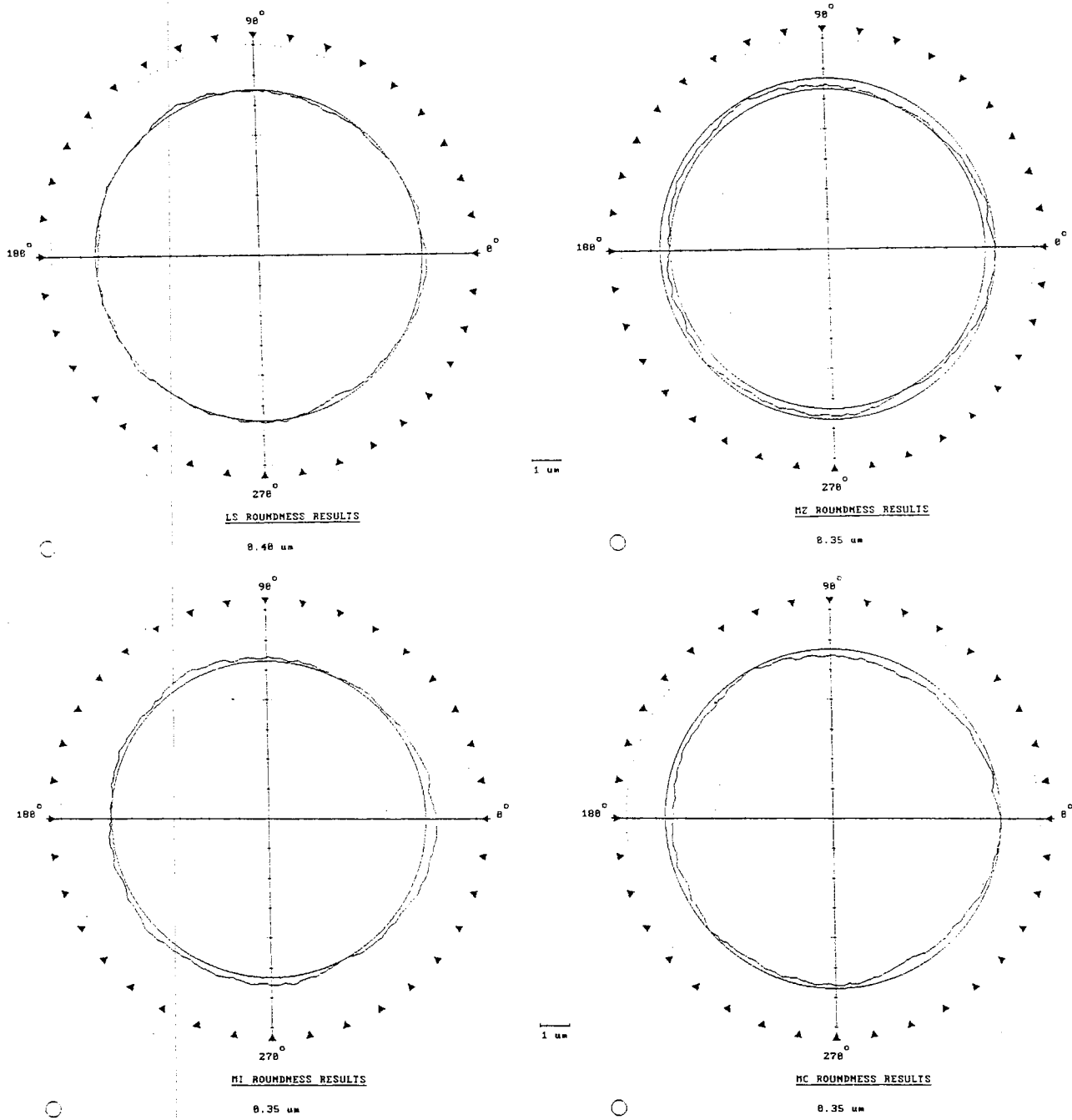
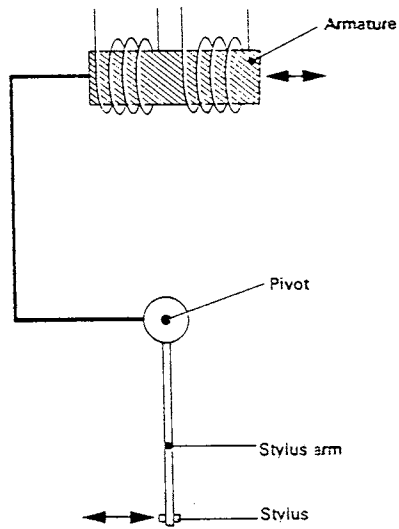
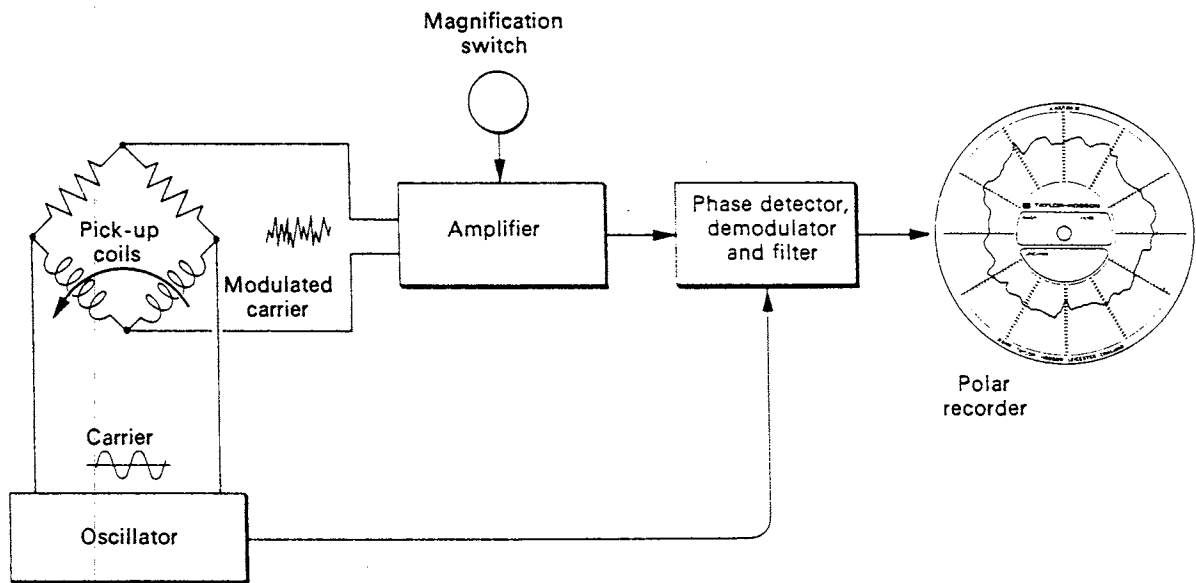


Figure 4.2 Four different reference circles available for Out-Of-Roundness

The numerical value of out-of-roundness is the maximum peak-to-valley height (P+V). There are four different reference circles available for this calculation: least square circle (LS), minimum zone circle (MZ), Maximum inscribed circle (MI), and minimum circumscribed circle (MC).



*Principle of variable inductance pick-up*



*Schematic diagram of electronic measuring system*

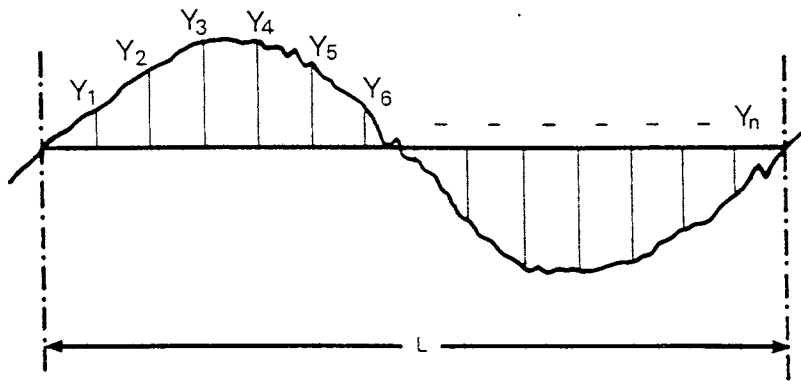
Figure 4.3 The schematic diagram of Talyrond electronic measuring system and the principle of its variable inductance pick-up



which depends on the direction of movement is compared with the oscillator to determine in which direction the recorder pen will move from its zero ( balance) position. 2CR (2-stage CR networks) type filter with a cut-off of 50 upr (undulations per revolution) is used in this study. The 2CR filter has 75% transmission at its cut-off. This means that the amplitudes of the irregularities which have a spacing equal to the the length of the cut-off are reduced to 75% of their true value. The amplitudes of irregularities with longer wavelength are progressively reduced but that of the amplitudes of irregularities with shorter wavelength will be almost unchanged. This filter, which suppresses the out-of-roundness lobes (undulations with approximately equal height and spacing) and leaves the general shape unchanged. It will allow the other surface irregularities to be displayed at a higher magnification.

#### **4.5.3 Evaluating the surface finish by number:**

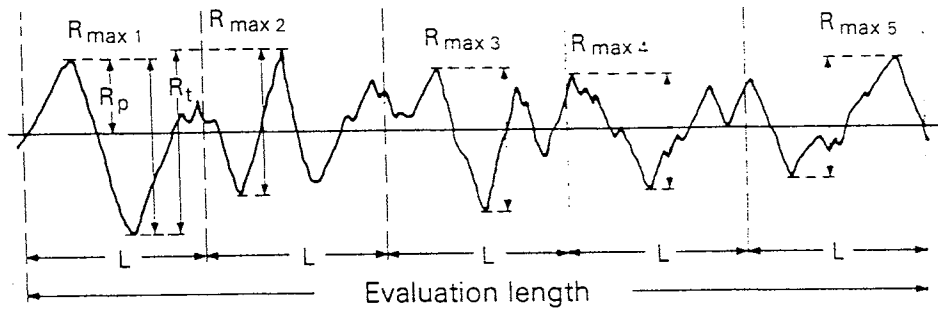
The surface roughness obtained by mechanical polishing generally has approximately a symmetrical profile. However, when the peaks are smoothed preferentially leaving the valleys intact as in fine finishing and chemo-mechanical polishing giving a fairly smooth bearing surface, the surface roughness can be unsymmetrical. Many parameters have been proposed to quantify the various surface characteristics. It is necessary to ensure that these values truly represent the surface features of interest. It is generally recognized that only Ra is not enough to evaluate the surface finish and that both Ra and Rt (or Rmax) may be necessary (see Figure 4.4). The Ra value represents the average roughness is a typical value of the measured surface but information regarding the shape of the irregularities (such as deep surface defects) is averaged out. The Rt value is the vertical distance between the highest and lowest points of the roughness profile. It is not a typical value for the whole



Mathematical derivation of  $R_a$  and  $R_q$

$$R_a = \frac{|y_1| + |y_2| + \dots + |y_n|}{n}$$

$$R_q = \sqrt{\frac{y_1^2 + y_2^2 + y_3^2 + \dots + y_n^2}{n}}$$



Derivation of some peak parameters

$R_{max}$  = Maximum peak-to-valley height within the sampling length  $L$

$R_t$  = The vertical height between the highest and lowest points of the profile within the evaluation length

$R_{pm}$  = The mean value of the  $R_{max}$  of five consecutive sampling lengths

Figure 4.4 Derivation of some surface roughness parameters ( $R_a$  and  $R_t$ )

surface, but can directly represent the irregular surface defects, such as scratches and pits (deep valleys), which can have a significant effect on the surface quality of advanced ceramic materials ( $R_t = R_p + R_v = R_{pv}$ ) for various applications. For polished surfaces, the international standard (IS) recommends that the cut-off (i.e., sampling length) is 0.25 mm or 0.8 mm, and an evaluation length is formed by 4-6 consecutive cut-off.

The surface finish in this study is generally measured using Form Talysurf 120 L. For a stylus instrument, such as TalySurf, the stylus size and shape affect the accuracy of the profile. It would not be possible to trace the complete profile of a deep valley especially the bottom if the size of the valley is smaller than the tip radius. The stylus tip radius of TalySurf 120L used in this study is about 2  $\mu\text{m}$ . However, SEM micrograph can be helpful to identify whether there are surface defects which can be reflected by stylus of TalySulf and whether the value from TalySurf is a reliable for small-damage surface. Talysurf is convenient to use for large area scanning with help by SEM micrograph. The stylus tip radius of AFM is 50-100 nm and can easily be broken and not easy to be operated and used very often. In this study, AFM is used for final high magnification evaluation of some random areas. We also checked surface finish by ZYGO laser interference microscope which is non-contact measurement instrument. For the ZYGO laser interference microscope, the focus range is important and should include both peaks and valleys of the polished surface. Otherwise, the surface values from ZYGO are unreliable. Based on the evaluation by all of Talysurf, SEM, ZYGO and AFM characterization techniques, one can be more confident that the surface finish value shown are a reliable representation of the true surface quality.

#### 4.5.4 Talysurf 120L

Rank Taylor Hobson's Talysurf 120L is used for surface finish measurement in this investigation. It is a computer controlled stylus instrument and has a stylus laser interferometric pick-up (transducer) with a 120 mm traverse unit (for traversing the stylus across the surface of the component to be measured). It is capable of measuring the roughness (by high frequency pass filter) and waviness (by low frequency pass filter) of the surface. Its vertical resolution is 10 nm and the horizontal resolution is 0.25  $\mu\text{m}$  for using standard conisphere diamond stylus with a tip radius of 2.0  $\mu\text{m}$ .

The schematic diagram of the laser interferometric transducer system is shown in Figure 4.5. The force applied to the sample by the stylus over the full range is 0.7-1.0 mN. Measuring speed is 0.5 mm/sec. A straightness datum is incorporated to enable measurements of up to 120 mm long without reference to an external straight line datum. There are three types of filters in the Talysurf, namely, 120L: ISO 2CR, 2CR PC, and Gaussian filter. The ideal filter characteristics of changing abruptly at the selected cut-off length can not be achieved economically in practice. Therefore, the filters are standardized to give a transmission of 75% at its cut-off for 2CR (2-stage CR networks) type filters, and to give a transmission of 50% at its cut-off for Gaussian filters. This means that the amplitudes of the irregularities which have a spacing (wavelength) equal to the the length of the cut-off are reduced to 75% (or 50%) of their true value. The amplitudes of irregularities with long wavelengths are progressively reduced but that of the amplitudes of irregularities with short wavelength will be almost unchanged. The traverse unit requires time to accelerate from rest up to its measuring speed. Using ISO 2CR filter, the first two cut-offs are discarded;

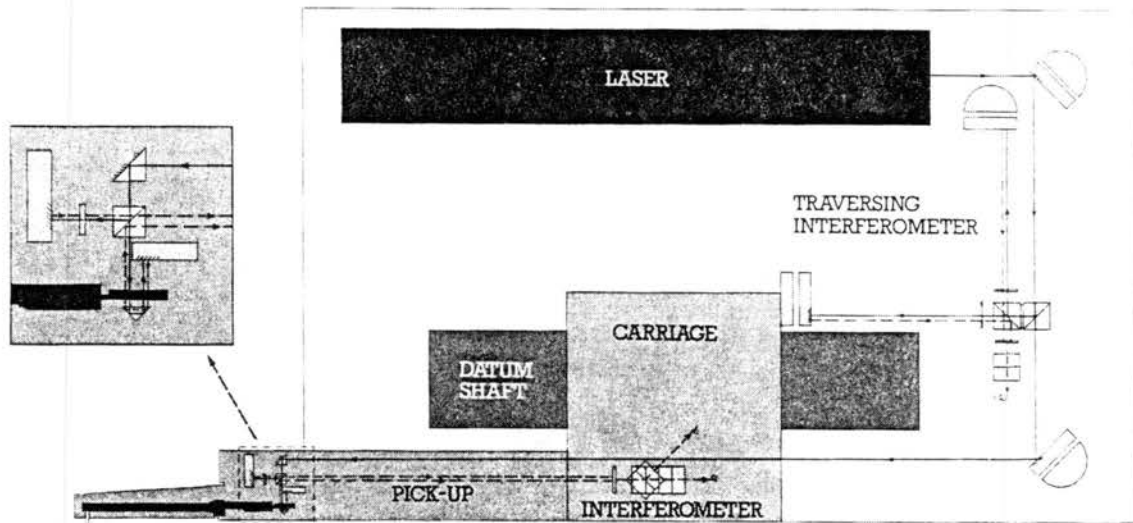


Figure 4.5 The schematic diagram of Form Talysurf traverse unit with laser interferometric transducer system

Due to vertical movement of the stylus, the length of the laser light path changes as it passes through the corner cube prism. When compared to the reference source it effectively changes phase and a Moiré interference fringe pattern can be detected proportional to the laser light wavelength. These fringes are interpolated to obtain the required resolution in the 'Z' axis.

The 'X' axis movement is detected by a pulse train generated by a traversing interferometric transducer system, the Moiré fringe patterns of which occur every half wavelength of laser light, i.e. every  $316.4\text{nm}$ .

2CR PC: the first and last cut-off are discarded; Gaussian: half of the first cut-off and half of the last cut-off are discard.

#### 4.5.5 Grade, Roundness, and Surface Roughness

The AFBMA (Anti-Friction Bearing Manufacturers Association) specification for different grades of metal bearing balls are given Table 4.4. The surface finish requirement for ceramic bearing balls are generally higher than for metal bearing balls. Our target is to obtain AFBMA grade 3 and we have been routinely obtaining Grade 10 without much difficulty by magnetic float polishing (MFP).

Table 4.4 ANSI/AFBMA Grading Charts of Metal Balls for Bearing

ANSI/AFBMA Grade	Lot Diameter Variation ( $\mu\text{m}$ )	Roundness ( $\mu\text{m}$ )	Surface Finish Ra ( $\mu\text{m}$ )
3	0.13	0.08	12
5	0.25	0.13	20
10	0.5	0.25	25
25	1.2	0.6	50
50	2.4	1.2	76
100	5	2.5	127

*good table to include!!*

## CHAPTER 5

### APPLICATION OF TAGUCHI METHOD TO DETERMINE OPTIMUM POLISHING CONDITIONS IN MAGNETIC FLOAT POLISHING

#### 5.1 INTRODUCTION

In this chapter the investigation focuses on the application of Taguchi method for the optimization of MFP process parameters to obtain the best finish possible by final mechanical polishing with a fine B<sub>4</sub>C abrasive. It may be noted that the resulting surface finish obtainable in the final finishing by chemo-mechanical polishing (CMP) is influenced by the previous final mechanical polishing in which fine and harder SiC or B<sub>4</sub>C abrasives are generally used. The surface finish by final fine mechanical polishing should be as good as possible prior to chemo-mechanical polishing. Further improvements in the surface finish can be achieved, for example, by applying CMP technique using CeO<sub>2</sub> abrasive.

Various parameters that affect the quality of the ceramic balls finished by the MFP process, include the magnetic field strength, the workmaterial, the abrasive used (material and grain size), the rotational speed of the shaft, the type of magnetic fluid used (water based or hydrocarbon based), the volume % of the abrasive in the magnetic fluid, and the stiffness of the system. For a given abrasive-workmaterial combination and the MFP system, three polishing parameters, namely, (i) the polishing force, (ii) the abrasive concentration, and (iii) the polishing speed are considered to have major influence on the surface quality. The main objective of this investigation is to determine the effect of

these three parameters on the surface finish during mechanical polishing by fine B<sub>4</sub>C #1500 abrasive (grain size 1-2 μm).

The polishing shaft was driven by a high-speed, high-precision air bearing spindle (PI Spindle) with a stepless speed regulation up to 10,000 rpm. The magnetic field was measured using a Gauss/Tesla meter. The pH value of the polishing environment was measured using a pH/Temperature meter. The polishing load was set up by measuring the normal force with a Kistler's piezoelectric dynamometer connected to a charge amplifier and a display. To calculate material removal rates, the weight reduction in the balls was determined by measuring the weight before and after polishing at every stage of the test using a precision balance. The surface finish of the polished balls was measured using a Form Talysurf 120 L (cut-off: 0.8 mm, evaluation length: 6 consecutive cut-off, Filter: ISO 2CR). The roundness of the balls was measured using TalyRond 250 (cut-off: 50 μm, Filter: 2CR). Table 5.1 lists the test conditions used together with the details of the workmaterial (uniaxially pressed Si<sub>3</sub>N<sub>4</sub>, CERBEC NBD-200 from Norton Advanced Ceramics), the abrasive (B<sub>4</sub>C #1500), and magnetic fluid used (water-based W-40). The polishing shaft diameter is 2.5 inch.



Table 5.1 Test Conditions

Workmaterial	HIP'ed Si <sub>3</sub> N <sub>4</sub> balls (CERBEC) Diameter: 12.7 mm (0.5 inch) Sphericity: 1 μm
Abrasive	Type : B <sub>4</sub> C (NORTON) Size : #1500 (1-2 μm) Concentration : 5%, 10%, 20%
Load, N/ball	0.4 , 0.8 , and 1.4
Speed, rpm	2000, 4000, and 7000
Test Time	45 min/step
Magnetic Fluid	Water-based (W-40) Saturation Magnetization at 25 °C: 400 Gauss Viscosity at 27 °C: 25 Cp

Table 5.2 Test Parameters Used and Their Levels

LEVEL	Parameters		
	A: Load	B: Vol %	C: Speed*
1	0.4 N	5%	2000 rpm
2	0.8 N	10%	4000 rpm
3	1.4 N	20%	7000 rpm

\* Polishing shaft diameter is 2.5 inch.

## 5.2 THE DESIGN OF EXPERIMENTS AND TAGUCHI METHOD

Several approaches are available for the design of experiments to investigate the effect of various parameters on the surface finish obtainable in fine mechanical polishing using MFP process. They include simple single-factor by single-factor approach, i.e. only one factor is changed for a given trial run, the traditional factorial and fractional factorial approaches [Fisher, 1971], and the highly-fractional factorial experimental design, namely, the Taguchi method [Taguchi, 1992; Dehnad, 1989; Roy, 1990; Barker, 1990; Ross, 1996]. Of course, the number of experiments need to be conducted decrease rapidly as one goes from a single-factor by single-factor approach to the factorial design, to the fractional factorial design, to the Taguchi method. This, in turn, will have a significant impact on the time consumed as well as the overall costs.

Compared to the single-factor by single-factor approach, Taguchi method can extract information more precisely and more efficiently. Also, fewer number of tests are needed even when the number of variables are quite large. Although, Taguchi's experimental design and analysis are conducted by highly fractional factorial experimental design (Taguchi Orthogonal Arrays) to determine the influence of the factors and their levels and identify the best combination of parameters, it has been shown that this method yields the same or even better results (in terms of precision) as a complete factorial experiment [Roy, 1990; Barker, 1990; Ross, 1996].

Compared to the traditional factorial and fractional factorial approaches, Taguchi method, as will be shown, overcomes most of their limitations. A full-factorial design of experiments will include all possible combination settings of the factors involved in the study resulting in a very large number of trial runs and

considerable time to accomplish this task. To simplify the experimental effort and reduce the number of tests to a reasonable level, only a small fraction of settings that produces most information from all the possible combinations is selected. This method is known as fractional-factorial design of experiments. Although this shortcut method is well known, its shortcoming is that there are no generally accepted standard guidelines for both the design of experiments and the analysis of the results. Consequently, the experimental design and analysis of the results can be rather complex. Taguchi's method overcomes these limitations by first simplifying and standardizing the fractional factorial designs by developing a set of standard Orthogonal Arrays (OA) which can be used for many experimental situations, and then devising a standard method for the analysis of results. The combination of standard experimental design and analysis techniques used in Taguchi method produces consistency and reproducibility which are not commonly found in other statistical methods. Design of highly fractional factorial experiments, say, for the same problem by two different investigators using Taguchi method, will yield similar data and conclusions. It is, thus, a standardized experimental design methodology that can easily be applied by investigators having particularly no strong statistical background [Roy, 1990].

Taguchi experimental design was developed by Dr. Genichi Taguchi in Japan after World War II. It is considered as a highly effective method for the determination of optimal values for the various parameters involved in a given manufacturing system. The quality of automobiles is particular and various other products in general by the Japanese manufacturers is attributable largely to the widespread application of this method. Since its introduction in the U. S. (first implemented at AT&T Bell Laboratories) in 1980, Taguchi method has been

widely applied and broadly discussed. Several industries including AT&T, Xerox, Ford, and ITT have applied this method in various product realization stages [Dehnad, 1989; Ross, 1996].

This investigation focuses on the use of Taguchi's method to optimize the process conditions in the polishing of ceramic balls for bearing applications. The optimum setting and relative significance of the load, rotational speed, and abrasive concentration (for a given abrasive B4C #1500) on the surface finish ( $R_a$  and  $R_t$ ) of workpiece (NBD-200  $Si_3N_4$  ball) are investigated. The polishing shaft diameter is 2.5 inch.

### **5.3 EXPERIMENTAL APPROACH**

#### **5.3.1 Selection of Parameters and Their Levels:**

As already mentioned, the three process parameters, identified as the most critical variables in the generation of surface finish for a given abrasive (material and size) - workmaterial combination in the polishing process, are (i) the polishing force, (ii) the abrasive concentration, and (iii) the polishing speed. And each factor is investigated at 3 levels to determine the optimum settings for the polishing process in this study. The smallest, standard 3-level orthogonal array  $L_9$  ( $3^4$ ) which has four 3-level columns (for a maximum of four parameters that can be tested) available is chosen for this case. The factors and their levels are given in Table 5.2.

#### **5.3.2 Orthogonal Array (OA) Design:**

Taguchi method employs standard tables known as 'Orthogonal Arrays' for constructing the design of experiments [Barker, 1990]. It may be noted that

the term 'Orthogonal' is used here to indicate balanced and not to be mixed, or separable. Orthogonal Arrays (OA) are generalized from Graeco-Latin squares. The mathematical discovery of OA was originally due to the French mathematician, Jacques Hadamard, who developed it in the 1890s but the technique was not explored for use until World War II [Ross, 1996].

The main functions of the Orthogonal Arrays are the following:

(1) Because of the pairwise balancing property of the orthogonal arrays, any two columns of an OA form a 2-factor complete factorial design. Consequently, whatever is happening of all the other parameters at one level of parameter being studied is also happening in the same way at other levels being studied. The effects of the other parameters on the parameter level being studied can be counteracted (offset) by averaging the responses. That means, the effect of one parameter being studied is separable from the effects of other parameters. So, the contribution and optimum level value of each factor can be determined in the balanced experiment.

(2) Orthogonal array experiments also minimize the number of test runs due to pairwise balancing property. With 4 factors and each at 3 levels, there are  $3^4$  possible combinations and would require 81 trial runs for a factorial experiment, and with 3 factors and each at 3 levels, there are  $3^3$  possible combinations and would require 27 trial runs for the factorial experiment. With the Orthogonal Array (OA) technique, there are only 9 runs required for  $L_9(3^4)$ . Further, the effects of the experimental errors on the parameter being studied as in the case of factorial design or one factor by one factor design can be eliminated (counteracted and offset) as the analysis of Taguchi method takes care of this factor (by the analysis of averaging the level responses).

An orthogonal array (OA)  $L_9(3^4)$  for a 3-level factor used in this investigation is shown in Table 5.3. This array has 9 rows and each row represents a trial condition with factor levels indicated by the numbers in the row. The vertical columns correspond to the factors specified in the study and each column contains three Level 1, three Level 2, and three Level 3 conditions (a total of 9 conditions) for the factor assigned to the column. And each column (factors) has nine possible combinations: (1,1), (1, 2), (1, 3), (2, 1), (2, 2), (2, 3), (3, 1), (3, 2), and (3, 3). We note that any two columns of an  $L_9(3^4)$  not only have these possibilities but also have the same number of times of these possible combinations. Thus, all four columns of an  $L_9(3^4)$  are said to be balanced, *orthogonal* or statistically independent of each other.

### 5.3.3 Experimental Design:

Details of the experimental design and approach are given in Table 4. The factors under consideration, namely, load (N), abrasive concentration (vol %), and speed (rpm) are placed in the first three columns (A, B, C) of the OA  $L_9(3^4)$  leaving the fourth column D open (and is designated for uncontrolled or unknown parameters in this investigation). The outputs, namely, the surface finish (Ra and Rt) values are the test results measured using a Form Talysurf 120 L (cut-off: 0.8 mm, evaluation length: 6 consecutive cut-off, Filter: ISO 2CR).

The vertical columns show the levels of polishing parameters specified in the study and each row represents a trial condition. The performance characteristic value from each trial run (discussed in Section 5.4) are then used to compute the statistical performance characteristic (discussed in Section 5.5) which is affected by any one parameter but independent of the others.

Table 5.3 L<sub>9</sub>(3<sup>4</sup>) Orthogonal Arrays Used

Trial No.	Factors Investigated				Test Results
	A	B	C	D	
1	1	1	1	1	
2	1	2	2	2	
3	1	3	3	3	
4	2	1	2	3	
5	2	2	3	1	
6	2	3	1	2	
7	3	1	3	2	
8	3	2	1	3	
9	3	3	2	1	

Table 5.4 Experimental Design

Trial No.	Factors			Test	Results
	Load ( N )	Abr. Vol %	Speed (rpm)	Ra (nm)	Rt (nm)
1	0.4	5%	2000		
2	0.4	10%	4000		
3	0.4	20%	7000		
4	0.8	5%	4000		
5	0.8	10%	7000		
6	0.8	20%	2000		
7	1.4	5%	7000		
8	1.4	10%	2000		
9	1.4	20%	4000		

\* The fourth column (factor D) is unset and designated as the unknown parameter(s) in this investigation.

## 5.4 EXPERIMENTAL RESULTS AND EVALUATION

The surface quality of the polished ceramic balls under various trial conditions is evaluated in terms of surface roughness (both Ra and Rt) at random of several areas (seven samples  $R_1, R_2, \dots, R_7$  in this study) as shown in Table 5. These repetitive sample data in each trial run (each polishing condition) will further be consolidated into an average value or a signal-to-noise ratio (S/N) to interpret each trial run (each polishing condition) into one evaluation value for the optimum setting analysis study (discussed in Section 5.5).

### 5.4.1 Evaluation of each trial run by average value:

$$\overline{R}_i = \sum_{j=1}^r \frac{R_{ij}}{r} = \frac{1}{r} (R_{i1} + R_{i2} + R_{i3} + R_{i4} + R_{i5} + R_{i6} + R_{i7})$$

where  $i$  is trial number;  $r$  is number of regions where surface roughness values are measured in a trial run.

For example, for Trial No.1

$$\overline{R}_{(Ra)1} = \frac{1}{7} (32 + 37 + 37 + 35 + 33 + 34 + 36) = 35 \text{ nm}$$

$$\overline{R}_{(Rt)1} = \frac{1}{7} (294 + 324 + 318 + 401 + 326 + 302 + 462) = 347 \text{ nm}$$

The average values of the other trial runs are calculated in a similar way and the results are given in Table 5.5. Average value of each trial run can be considered as an average deviation from the target value of zero (Ra and Rt  $\rightarrow$  0).



Table 5.5 Experimental Results

Test No.	Surface Finish, Ra(nm)							Average (nm)	S/N (dB)
	R1	R2	R3	R4	R5	R6	R7		
1	32	37	37	35	33	34	36	35	-30.86
2	37	38	36	39	38	42	38	38	-31.67
3	38	35	35	34	36	32	35	35	-30.89
4	33	29	28	28	29	27	27	29	-29.18
5	31	29	28	27	26	26	24	27	-28.74
6	38	35	42	39	42	40	37	39	-31.84
7	23	24	23	20	22	24	25	23	-27.25
8	35	32	31	38	34	32	30	33	-30.43
9	24	26	33	28	30	27	29	28	-29.03
Test No.	Surface Finish, Rt (nm)							Average (nm)	S/N (dB)
	R1	R2	R3	R4	R5	R6	R7		
1	294	324	318	401	326	302	461	347	-50.9
2	327	498	481	411	399	504	529	450	-53.2
3	395	390	363	385	380	298	513	389	-51.9
4	298	260	346	357	268	251	325	301	-49.6
5	274	254	657	334	283	246	207	322	-50.9
6	405	344	547	547	480	434	368	446	-53.1
7	209	180	210	200	221	250	220	213	-46.6
8	303	297	390	371	334	240	274	316	-50.1
9	229	230	384	214	236	278	228	257	-48.4

#### 5.4.2 Evaluation of each trial run by S/N dB value $\eta$ :

Taguchi method uses the signal-to-noise (S/N) ratio instead of the average value to interpret the trial result data into a value for the evaluation characteristic in the optimum setting analysis. This is because signal-to-noise ratio (S/N) can reflect both the average (mean) and variation (scatter) of the surface quality under one trial run, namely, one polishing condition.

If the S/N ratio is expressed in dB units, it can be defined by a logarithmic function based on the mean square deviation around the target, smaller-the-better, in this study:

$$S/N = - 10 \log_{10} MSD$$

where MSD is the mean square deviation around the target value rather than around the average value. The purpose of using the constant, 10 in the calculation is to magnify the S/N number for easier analysis and the negative sign is used to set signal-to-noise ratio of larger-the-better (a larger signal and a smaller noise) relative to the square deviation of the smaller-the-better. The target value in this study tends to zero ( $R_a$  and  $R_t \rightarrow 0$ ) and all random samples are equally important. Therefore, the mean squared deviation (variance) is calculated from sum of the squares  $(R_{ij} - 0)^2$  of all the data points. As can be seen in the following, this value reflects both the the average,  $\overline{R}_i$  and variance,  $\Delta R_{ij}$  of each trial result data:

$$\begin{aligned} MSD_i = \sigma_{ij}^2 &= \frac{1}{r} \sum_{j=1}^r (R_{ij})^2 = \frac{1}{r} \sum_{j=1}^r (\overline{R}_i + \Delta R_{ij})^2 \\ &= \frac{1}{r} \left( \sum_{j=1}^r \overline{R}_i^2 + 2 \sum_{j=1}^r \overline{R}_i \Delta R_{ij} + \sum_{j=1}^r \Delta R_{ij}^2 \right) \end{aligned}$$

$$= \frac{1}{r} \left( \sum_{j=1}^r \overline{R}_i^2 + \sum_{j=1}^r \Delta R_{ij}^2 \right)$$

$$(\Delta R_{ij} \text{ are normally distributed, so } 2 \sum_{j=1}^r \overline{R}_i \Delta R_{ij} = 0)$$

where  $MSD_i$  is the square of the deviation around the target value of zero ( $R_a$  and  $R_t \rightarrow 0$ ) and reflects the deviation of the trial result from the target value of zero.

$$S/N_i = -10 \log MSD_i = -10 \log \frac{1}{r} \sum_{j=1}^r R_{ij}^2$$

where  $i$  is the number of a trial;  $MSD_i$  is the square of the standard deviation of a trial  $i$ ;  $\sigma_i$  is the standard deviation in a trial  $i$ ;  $r$  is number of regions where surface roughness measurements are made in a trial. First, the  $MSD_i$  is calculated and then substituted in the above equation to obtain the  $S/N$  values.

$$MSD_i = \frac{1}{7} (R_{i1}^2 + R_{i2}^2 + R_{i3}^2 + R_{i4}^2 + R_{i5}^2 + R_{i6}^2 + R_{i7}^2)$$

for example in Test No.1, for  $R_a$

$$MSD(R_a)_1 = \frac{1}{7} (32^2 + 37^2 + 37^2 + 35^2 + 33^2 + 34^2 + 36^2)$$

$$\text{Hence, } S/N(R_a)_1 = -10 \log MSD(R_a)_1 = -30.9 \text{ dB}$$

Similarly for  $R_t$ ,

$$MSD(R_t)_1 = \frac{1}{7} (294^2 + 324^2 + 318^2 + 401^2 + 326^2 + 302^2 + 462^2)$$

$$\text{Hence, } S/N(R_t)_1 = -10 \log MSD(R_t)_1 = -50.9 \text{ dB}$$

Similar calculations are carried out for the other trial runs, the results of which are given in Table 5.5. It is known that smaller average and smaller

variability (smaller MSD) are desirable for the surface finish of the balls. That is, an uneven amount of surface damage is worse than an even amount of surface finish when the average values are the same. This means smaller averages or larger signal-to-noise ratios are better. The evaluation by average value is more a perception while the S/N value is more objective.

## **5.5 EXPERIMENTAL ANALYSIS**

The experimental results are analyzed to achieve the following three objectives:

1. To establish the optimum conditions for the polishing process (5.5.1)
2. To estimate the contributions of individual parameters (5.5.2)
3. To predict the response under optimum conditions

### **5.5.1 Level Average Response Analysis**

The optimum conditions for the polishing process can be identified by studying the average response of each parameter level in the OA (Orthogonal Array) experiments. This is outlined in the following.

#### **5.5.1.1 Level Average Response Analysis Using Average Value of Each Trial Run:**

The level average analysis is based on combining and averaging the response associated with each level for each factor. It may be noted from Table 3 that the 1st level of factor A occurs in experiment numbers 1, 2, and 3, all 3 levels of factors B and C appear once in these three experiments. The 2nd level

of factor A occurs in experiment numbers 4, 5, and 6, all 3 levels of factor B and C also appear once in these three experiments. The 3rd level of factor A occurs in experiment numbers 7, 8, and 9, all 3 levels of factor B and C also appear once in these three experiments. It means the level conditions of factors B and C with different levels of factor A are the same. Hence, it counteracts the effects of the factors B and C on the response of factor A. Thus from the average data of each three experiments wherein one level of factor A occurs in, the optimum value (level) of factor A can be determined.

For example, to compute the average performance of the factor of A at level 1, add results for tests including factor A1: load (0.4 N), and then divide by the number of such tests. In the column for A: load, level 1 occurs in experiment numbers 1, 2, and 3. The average effect of load (0.4 N) is therefore calculated by adding the results of these three tests and dividing by 3:

$$\overline{R_a(A1)} = \frac{1}{3} (35 + 38 + 35) = 36 \text{ nm}$$

$$\overline{R_t(A1)} = \frac{1}{3} (347 + 450 + 389) = 395 \text{ nm}$$

The average effects of the other two levels are calculated in a similar manner. The average effect of each load level under study is displayed in Table 5.6 (a). A<sub>3</sub> (load: 1.4 N) is found to be the optimum condition from the analysis. The average effects of factors B and C are analyzed in a similar way and are given in Tables 5.6 (b) and (c). It is found that B<sub>1</sub> (5 vol% abrasive) and C<sub>3</sub> (7000 rpm) are the optimum conditions. The average effect of each parameter level is shown graphically in Figures 5.1 (a) and (b).

Note that in Tables 5.6 (a) to (c), namely, the surface quality is affected by one parameter only and is independent of the other parameters due to the

Table 5.6 (a) Average Effect of Each Load Level

Load level	Analysis			Average Response	
	Test No.	Ra(nm)	Rt (nm)	Ra (nm )	Rt (nm)
0.4 N	1	35	347	36	395
	2	38	450		
	3	35	389		
0.8 N	4	29	301	32	356
	5	27	322		
	6	39	446		
1.4 N	7	23	213	28	262
	8	33	316		
	9	28	257		

Table 5.6 (b) Average Effect of Each Abrasive Concentration Level

Abrasive vol% level	Analysis			Average Response	
	Test No.	Ra(nm)	Rt (nm)	Ra (nm )	Rt (nm)
5%	1	35	347	29	287
	4	29	301		
	7	23	213		
10%	2	38	450	33	363
	5	27	322		
	8	33	316		
20%	3	35	389	34	364
	6	39	446		
	9	28	257		

Table 5. 6 (c) Average Effect of Each Speed Level

Speed level	Analysis			Average Response	
	Test No.	Ra(nm)	Rt (nm)	Ra (nm )	Rt (nm)
2000 rpm	1	35	347	36	370
	6	39	446		
	8	33	316		
4000 rpm	2	38	450	32	336
	4	29	301		
	9	28	257		
7000 rpm	3	35	389	28	308
	5	27	322		
	7	23	213		

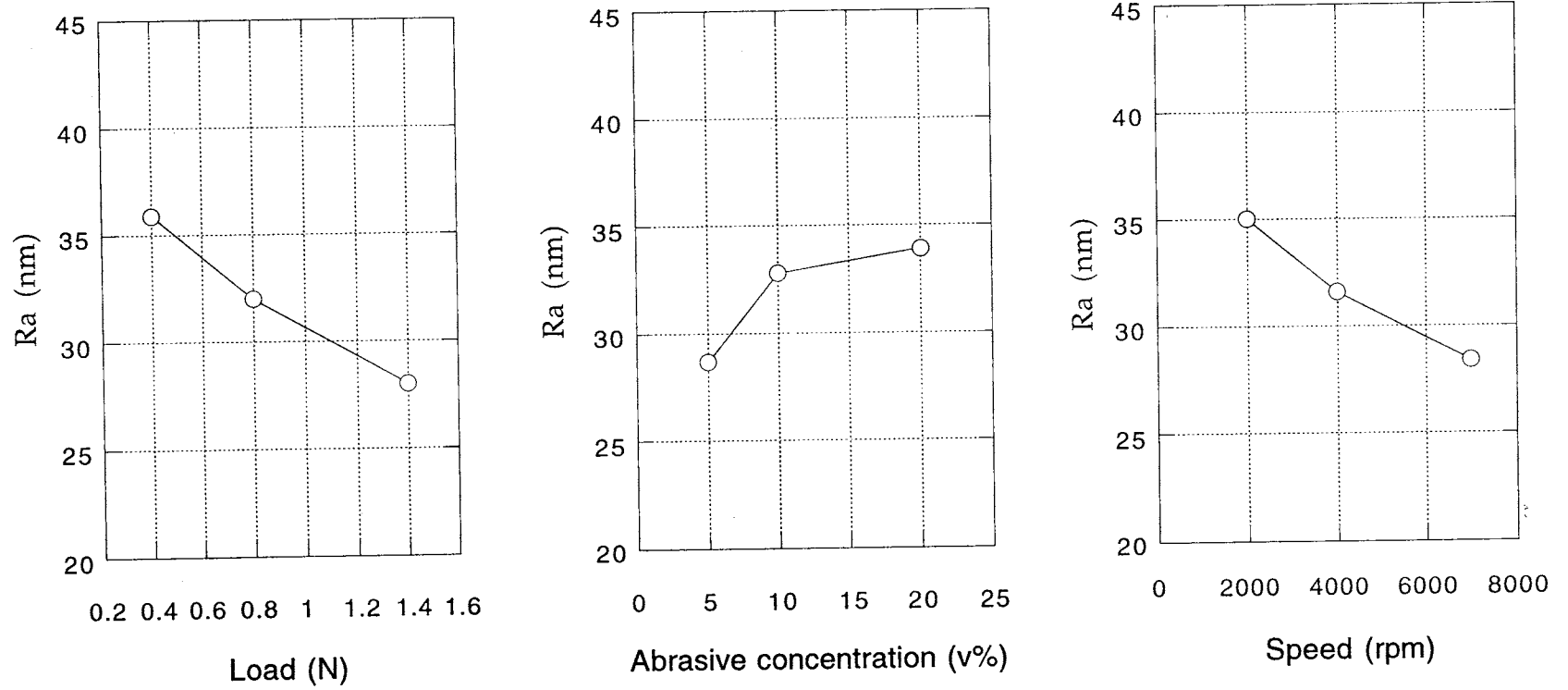


Figure 5.1(a) Plots of the response of each polishing parameter level on the surface finish Ra



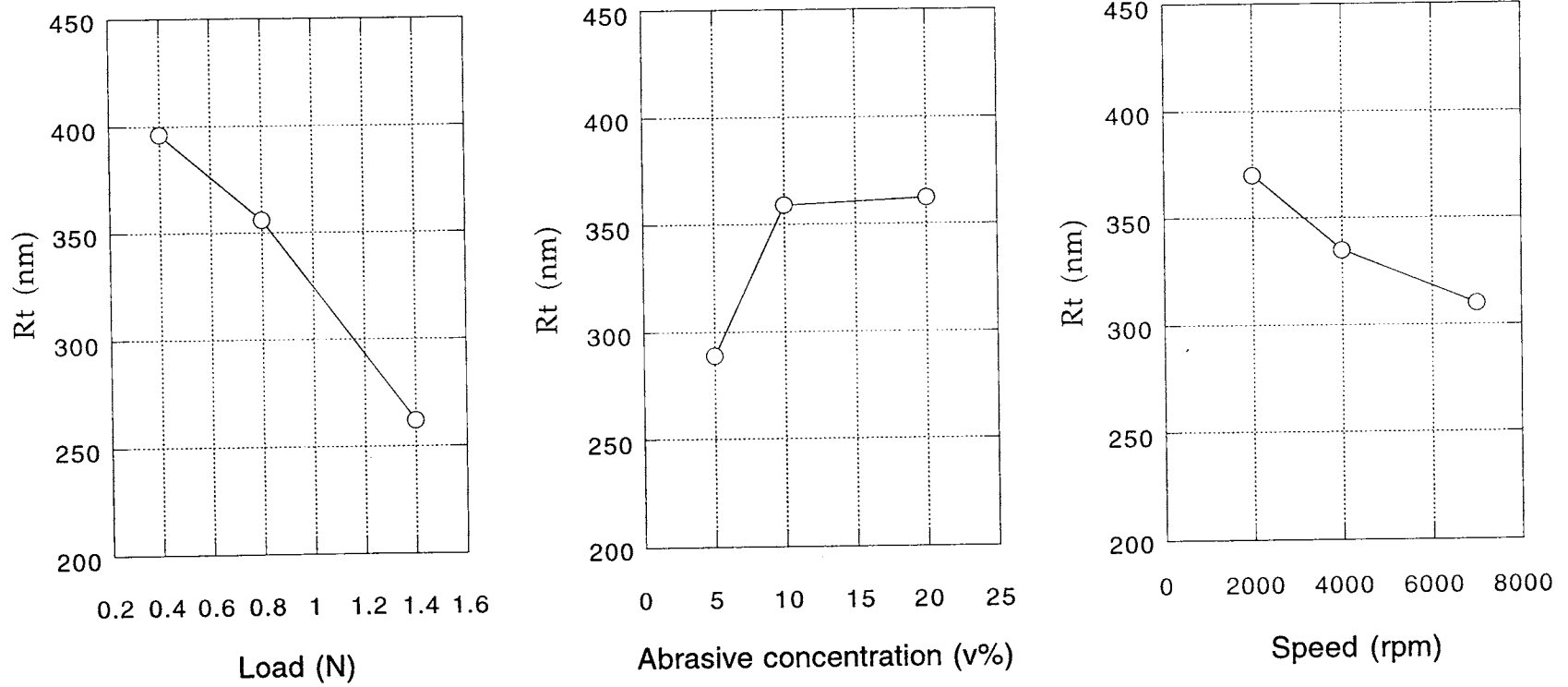


Figure 5.1(b) Plots of the response of each polishing parameter level on the surface finish  $R_t$

pairwise balancing property of the orthogonal design used. For the polishing process, smaller surface finish value ( $R_a$  and  $R_t$ ) of the polished surface is desired. So,  $A_3B_3C_1$  is likely to produce the best results for both  $R_a$  and  $R_t$  and therefore, the optimum conditions are the following : load 1.4 N, vol % of abrasive 5%, and speed 7000 rpm.

#### 5.5.1.2 Level average response analysis using S/N value:

The level average S/N analysis actually is similar to the level average analysis except that S/N values are used instead of the average values. The objective of this analysis is to determine the optimum polishing conditions such that the signal-to-noise (S/N) ratio is as large as possible relative to the mean (the target  $R_a$ ,  $R_t \rightarrow 0$ ) and variation as small as possible. The analysis using the S/N value is more objective, but the S/N value is rather abstract and cannot indicate the physical meaning of the quality/parameter response directly.

Level average S/N analysis is given in Tables 5.7 (a) and (b) by combining and averaging the response for each parameter level. In fact, the analysis presented in Tables 5.7 (a) and (b) is similar to the level average analysis presented earlier but using the S/N values rather than the average values.

Figures 5.2(a) and (b) are S/N response plots using the data from Tables 7 (a) and (b). In these plots, the levels corresponding to the highest S/N values are chosen for each parameter for they indicate the best quality (both the mean and variation are smallest). Thus,  $A_3B_1C_3$  (Table 5.2) is found to give optimum conditions for a large S/N value in conjunction with a small mean and a small variation of both  $R_a$  and  $R_t$ . So, with the range of parameters evaluated in this study, a load of 1.4N, a concentration of 5 vol %, and a speed of 7000 rpm are

Table 5.7 (a) Level average analysis using S/N ratio for Ra

Load level	Test No.	S/N (dB)	Sum. level $Sy_j$	Ave. of level
0.4 N	1	-30.86	-93.42	-31.14
	2	-31.67		
	3	-30.89		
0.8 N	4	-29.18	-89.76	-29.92
	5	-28.74		
	6	-31.84		
1.4 N	7	-27.25	-86.71	-28.9
	8	-30.43		
	9	-29.03		
Abr. Vol% level	Test No.	S/N (dB)	Sum. level $Sy_j$	Ave. of level
5 %	1	-30.86	-87.29	-29.10
	4	-29.18		
	7	-27.25		
10 %	2	-31.67	-90.84	-30.28
	5	-28.74		
	8	-30.43		
20 %	3	-30.89	-91.76	-30.59
	6	-31.84		
	9	-29.03		
Speed level	Test No.	S/N (dB)	Sum. level $Sy_j$	Ave. of level
2000 rpm	1	-30.86	-93.13	-31.04
	6	-31.84		
	8	-30.43		
4000 rpm	2	-31.67	-89.88	-29.96
	4	-29.18		
	9	-29.03		
7000 rpm	3	-30.89	-86.88	-28.96
	5	-28.74		
	7	-27.25		

Table 5.7 (b) Level average analysis using S/N ratio for Rt

Load level	Test No.	S/N (dB)	Sum.level $Sy_j$	Ave. of level
0.4 N	1	-50.9	-156	-52
	2	-53.2		
	3	-51.9		
0.8 N	4	-49.6	-153.6	-51.2
	5	-50.9		
	6	-53.1		
1.4 N	7	-46.6	-145.1	-48.4
	8	-50.1		
	9	-48.4		
Abr. Vol% level	Test No.	S/N (dB)	Sum. level $Sy_j$	Ave. of level
5 %	1	-50.9	-147.1	-49.1
	4	-49.6		
	7	-46.6		
10 %	2	-53.2	-154.2	-51.4
	5	-50.9		
	8	-50.1		
20 %	3	-51.9	-153.4	-51.1
	6	-53.1		
	9	-48.4		
Speed level	Test No.	S/N (dB)	Sum. level $Sy_j$	Ave. of level
2000 rpm	1	-50.9	-154.1	-51.4
	6	-53.1		
	8	-50.1		
4000 rpm	2	-53.2	-151.2	-50.4
	4	-49.6		
	9	-48.4		
7000 rpm	3	-51.9	-149.4	-49.8
	5	-50.9		
	7	-46.6		

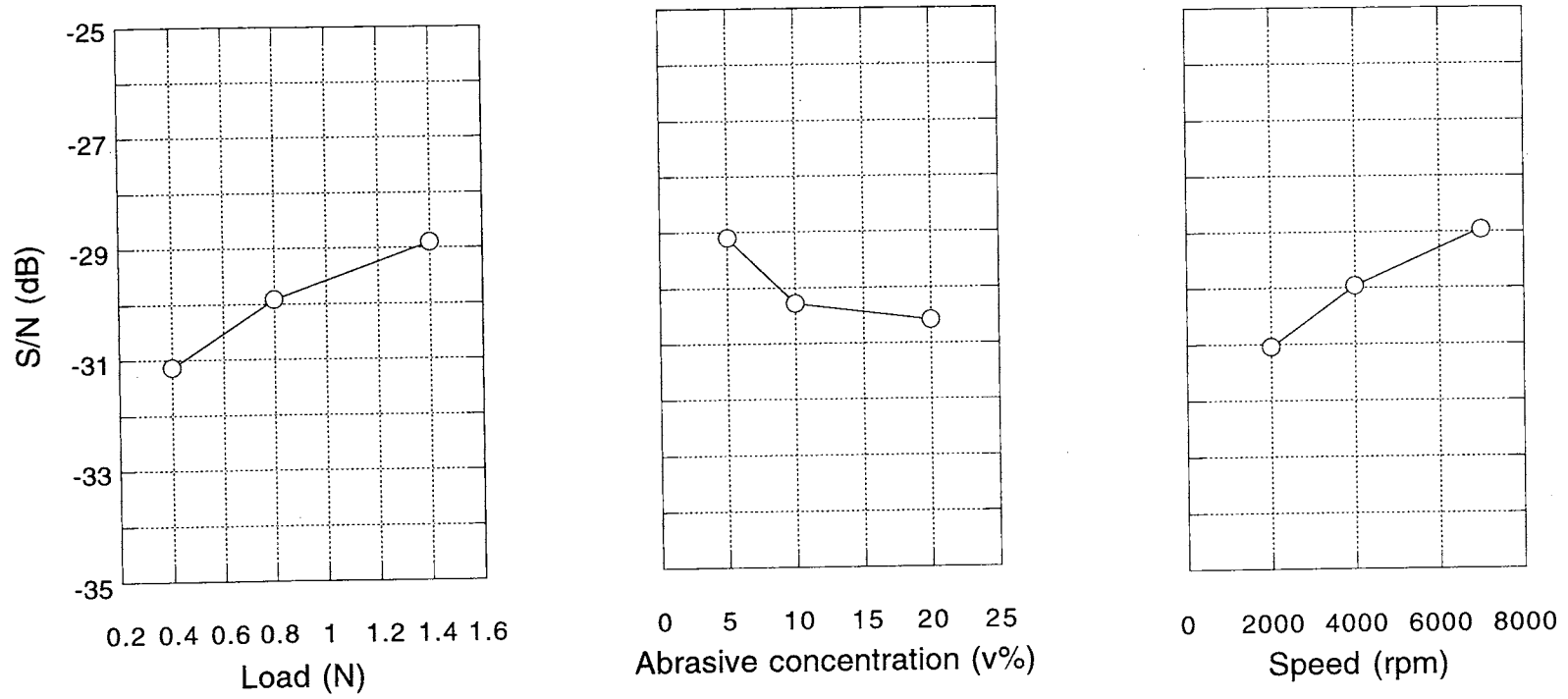


Figure 5.2 (a) Plots of the S/N ratios showing the effect of each parameter level on the surface finish Ra

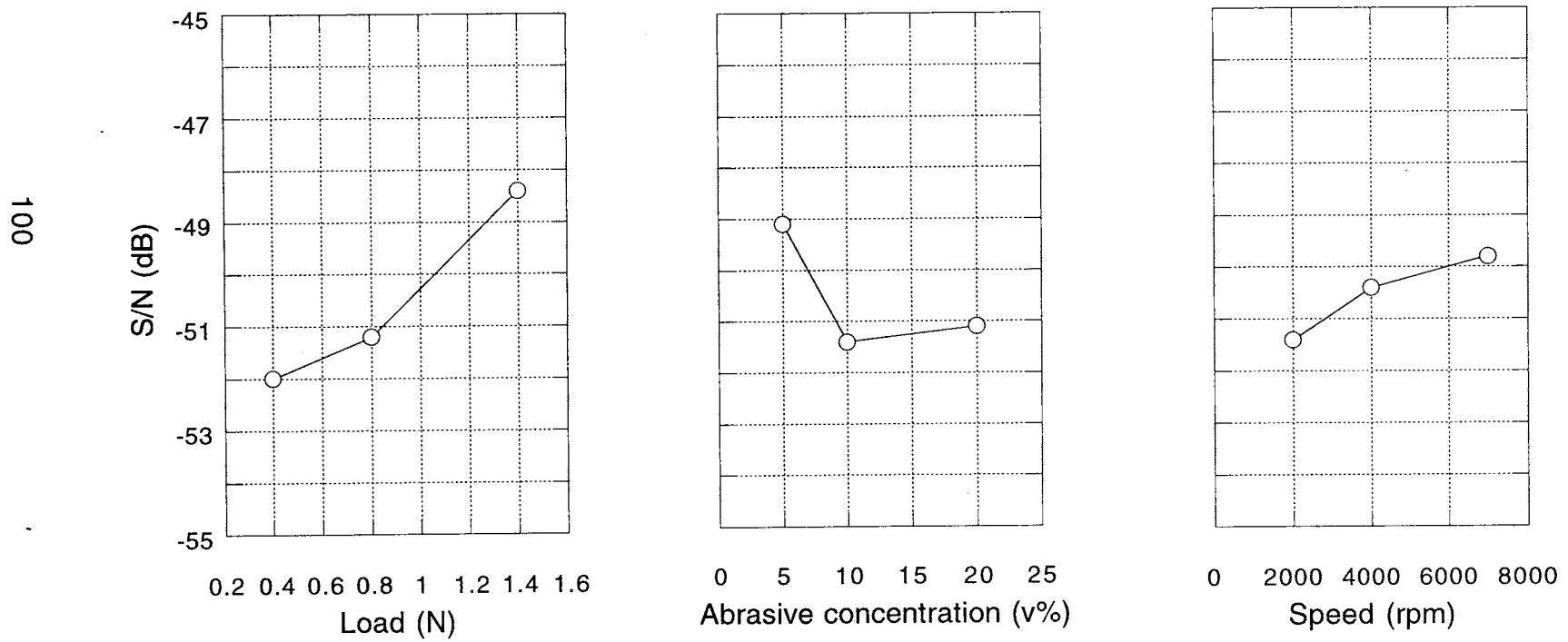


Figure 5.2(b) Plots of the S/N ratios showing the effect of each parameter level on the surface finish Rt

considered as the optimum polishing settings. It is coincidental that the conclusions arrived here from the analysis of S/N values are exactly the same as those drawn from the above simple analysis using the average values.

### **5.5.2 Analysis of variance (ANOVA)**

Analysis of variance (ANOVA) can be used to evaluate the response magnitude (%) of each parameter in the orthogonal experiment. This method was first developed by Fisher in the 1930s [Fisher, 1971]. It is used to identify and quantify the sources of different trial results from different trial runs (i. e. different polishing conditions).

For different trial conditions, the results can be different due to (a) the variations produced by unknown parameters or random interferences (noise factors) (also known as the variations from uncontrolled parameter conditions) and (b) the variations produced by the changing of polishing conditions (also called as the variations from controlled parameter level conditions or testing conditions). Therefore, it is important to identify whether the variations under different trial runs are from the unknown parameters or from different test parameter (control parameters) level settings. This way the influence of the variations in the control parameter settings (different trial run settings or different polishing conditions tested) can be determined and the percent contribution of each parameters can be evaluated to make a decision on how significant is the effect of each parameter (known and unknown) on the polishing results.

Since standard deviations are not additive, the sums of squares of the standard deviation, which are additive  $\sigma_T^2 = \sigma_A^2 + \sigma_B^2 + \sigma_C^2$ , is usually used for the calculation and analysis of the variation or variability from each and all factors (parameters) in ANOVA. The basic property of ANOVA is that the total

sums of the squares (total variation) is equal to the sum of the SS (sums of the squares of the deviation) of all the condition parameters and the error components i. e. adding the variations from each factors,  $SS_T = SS_A + SS_B + SS_C + SS_e$ . Table 5.8 list the values of S/N,  $(S/N)^2$ , and their sums for Ra and Rt respectively which are used in the following calculations for  $SS_T$ ,  $SS_A$ ,  $SS_B$ ,  $SS_C$ , and  $SS_e$ .

(1) Total variation ( $SS_T$ ):

The total variation of the experimental results (for the total number of trial runs,  $n = 9$  in this study) caused by both the controlled (tested) parameter setting variations (i. e. different polishing conditions tested) and uncontrolled (or unknown) parameters can be represented as the sum of the squares (SS) deviation of all the resulting data from the trial runs.

$$\begin{aligned}
 SS_T &= \sum_{i=1}^n (y_i - \bar{y})^2 \\
 &= \sum_{i=1}^n y_i^2 - \sum_{i=1}^n 2y_i \bar{y} + \sum_{i=1}^n \bar{y}^2 \\
 &= \sum_{i=1}^n y_i^2 - 2n\bar{y}^2 + n\bar{y}^2 \\
 &= \sum_{i=1}^n y_i^2 - \frac{G^2}{n} \\
 \therefore SS_T &= \sum_{i=1}^n (y_i - \bar{y})^2 = \sum_{i=1}^n y_i^2 - \frac{G^2}{n}
 \end{aligned}$$

where  $G (= \sum y_i)$  is the sum of the resulting data of all trial runs;  $\sum y_i$  and  $\sum y_i^2$  are taken from Table 5.8; and  $n (=9)$  is the total number of the trial runs. The total trial variance is:  $V_T = SS_T/F_T$ , where  $F_T$  is the number of degrees of



freedom (DOF) of the total variation (i. e the number of trial runs minus one). For example, in this case it is,  $F_T = 9-1= 8$ .

For Ra

$$SS_T = 8112.05 - \frac{(-269.89)^2}{9} = 18.65$$

Similarly, for Rt

$$SS_T = 23009.37 - \frac{(-454.7)^2}{9} = 36.92$$

(2) The trial variation from the the tested parameter setting variation (condition variation)  $SS_k$ :

The variation caused by each parameter from their different level settings can be reflected by the total sum of the squares (SS) of the deviation from the average of all trial results involving this parameter level.

$$SS_k = \sum_{j=1}^t t \times (\bar{y}_j - \bar{y})^2 = \sum_{j=1}^t \left( \frac{Sy_j^2}{t} \right) - \frac{G^2}{n}$$

where k represents one of the tested parameters; j is level number of this parameter K;  $\bar{y}$  is the average of all trial runs;  $\bar{y}_j$  is the average of each of the level under the parameter k; t is the repetition of each level of the parameter k;  $Sy_j$  is sum of all trial results involving this parameter k level j; n ( = 9 ) is the total number of trial runs. Values of  $Sy_j$  for Ra are given in Tables 5.7 (a) and for Rt in Table 5.7 (b).

For Ra

$$SS_{load} = \frac{(-93.42)^2 + (-89.76)^2 + (-86.71)^2}{3} - \frac{(-269.89)^2}{9} = 7.52$$

$$SS_{vol\%} = \frac{(-87.29)^2 + (-90.84)^2 + (-91.76)^2}{3} - \frac{(-269.89)^2}{9} = 3.72$$

$$SS_{speed} = \frac{(-93.13)^2 + (-89.88)^2 + (-86.88)^2}{3} - \frac{(-269.89)^2}{9} = 6.51$$

For Rt

$$SS_{load} = \frac{(-156)^2 + (-153.6)^2 + (-145.1)^2}{3} - \frac{(-454.7)^2}{9} = 21.87$$

$$SS_{vol\%} = \frac{(147.1)^2 + (-154.2)^2 + (-153.4)^2}{3} - \frac{(-454.7)^2}{9} = 10.08$$

$$SS_{speed} = \frac{(-154.1)^2 + (-151.2)^2 + (-149.4)^2}{3} - \frac{(-454.7)^2}{9} = 3.75$$

The variance of each parameter is determined by the (SS) sum of square deviation of each parameter divided by the degrees of freedom (DOF) of this parameter:  $V_k = SS_k / F_k$ . The number of degrees of freedom (or independent comparisons), F, for a parameter is equals to the number of levels (number of observations) for this parameter minus one. For example, in this case,  $F_k = 3 - 1 = 2$ .

(3) The trial variation from the random variations in testing or from unknown parameters,  $SS_e$ :

$$SS_e = SST - SS_{load} - SS_{vol\%} - SS_{speed}$$

For Ra

$$SS_e = 18.65 - 7.52 - 3.72 - 6.51 = 0.9$$

For Rt

$$SS_e = 36.92 - 21.87 - 10.08 - 3.75 = 1.22$$

Variance  $V_e = SS_e/F_e$  where  $F_e = 3 - 1 = 2$ . Actually, the variance of the unknown parameters is equals to the variance of the parameters in column D (uncontrolled parameters) in Table 5.3 and 5.4.

Tables 5.9 and 5.10 shows the results of the analysis of variance (ANOVA) for Ra and Rt, respectively under different trial runs. It can be seen from these tables that for the surface finish Ra, the contribution of factor A (polishing load) (40%) is more significant than factor C (polishing speed) (35%) and both of them are more significant than factor B (abrasive concentration vol%) (20%). For the surface finish, Rt, the contribution of factor A (polishing load) (59%) is more significant than factor B (abrasive concentration vol%) (27%) and both of them are more significant than factor C (polishing speed) (10%). Further, it can be seen that the relative significance of factors B and C are reversed for Ra and Rt.

Table 5.8 Values of S/N and (S/N)<sup>2</sup> for Ra and Rt

Test No.	For Ra		For Rt	
	S/N or $y_i$	(S/N) <sup>2</sup> or $y_i^2$	S/N or $y_i$	(S/N) <sup>2</sup> or $y_i^2$
1	-30.86	952.34	-50.9	2590.81
2	-31.67	1002.99	-53.2	2830.24
3	-30.89	954.19	-51.9	2693.61
4	-29.18	851.47	-49.6	2460.16
5	-28.74	825.99	-50.9	2590.81
6	-31.84	1013.79	-53.1	2819.61
7	-27.25	742.56	-46.6	2171.56
8	-30.43	925.98	-50.1	2510.01
9	-29.03	842.74	-48.4	2342.56
$\Sigma$	-269.89	8112.05	-454.7	23009.37

Table 5.9 Analysis of Variance (ANOVA) for Ra

	DOF	SS	SS %
A: Polishing Load	2	7.52	40%
B: Abrasive Vol%	2	3.72	20%
C: Polishing Speed	2	6.51	35%
D: Unknown	2	0.9	5%
Total	8	18.65	100%

Table 5.10 Analysis of Variance (ANOVA) for Rt

	DOF	SS	SS %
A: Polishing Load	2	21.87	59%
B: Abrasive Vol%	2	10.08	27%
C: Polishing Speed	2	3.75	10%
D: Unknown	2	1.22	4%
Total	8	36.96	100%

## 5.6 OPTIMUM SETTINGS

Experimental results indicate that for the surface finish, Ra and Rt, the polishing force parameter is most significant. However for Ra, the polishing force parameter is followed by polishing speed and then abrasive concentration while for Rt, the polishing force parameter is followed by the abrasive concentration and then polishing speed. The experimental results also indicate that within the range of parameters evaluated, a high level of polishing force (1.4 N N/ball), a low level of abrasive concentration (5%), and a high level of polishing speed (7000 rpm X 2.5 inch) are desirable for improving both Ra and Rt. A comparison of the results obtained by the Taguchi method with single parameter (i. e. one parameter by one parameter) variation using a fine SiC abrasive (1  $\mu\text{m}$ ) yielded similar conclusions regarding optimum conditions. However, Taguchi method can extract information more precisely and more efficiently.

## 5.7 SINGLE-FACTOR BY SINGLE-FACTOR APPROACH

The Talysurf roughness profiles and SEM morphologies of the  $\text{Si}_3\text{N}_4$  ball surface obtained at different polishing loads (0.5, 1, and 1.5 N/ball) with SiC (1  $\mu\text{m}$  grit) abrasive, abrasive concentration 5 vol%, speed 2000 rpm, and test time 45 min/step are shown in the Figures 5.3 (a) - (c) and Figures 5.4 (a) - (c), respectively. It can be seen that both surface finish,  $R_a$  and the depth of surface damage,  $R_t$  decrease (surface quality improves) as the polishing force increases from 0.5 to 1 and to 1.5 N/ball. The considerable microfracture with large and deep pits [Figure 5.3 (a) & 5.4 (a)] were found in the surface polished at 0.5 N/ball load. When the polishing force increased to 1 N/ball or to 1.5 N/ball, the deep microfracture pits disappeared and parallel scratches with some very shallow pits on the surface polishing under a load of 1 N/ball [Figure 5.3 (b) & 5.4 (b)] and long scratches without any pits on the surface polishing under a load of 1.5 N/ball [Figure 5.3 (c) & 5.4 (c)] were observed.

When polishing at low loads such as 0.5 N/ball, the polished surface appears more like that generated by a 3-body abrasion in which deep surface damage is caused due to indentation by the rotary motion of the abrasive. When the polishing force is increased, say from 0.5 N /ball to 1 N/ball and to 1.5 N/ball, the abrasives are embedded in the shaft more deeply and strongly. As a result the polishing process is more like a 2-body abrasion in which material removal on the polished surface is by shallower scratch abrasion by indentation without rotation. Since the shape of the abrasives are generally not uniform, the  $R_t$  value from a 3-body abrasion is larger than that from a 2-body abrasion; Thus the surface quality from a 2-body abrasion is superior to that from a 3-body abrasion. This schematics of a 3-body and a 2-body abrasion models are

shown in Figure 5.5. With increasing polishing force from 0.5 to 1.0 N/ball, the dominant polishing mechanism changes from a 3-body to a 2-body abrasion. The critical of load value for a 2-body abrasion at 2000 rpm is 1 N/ball. The above tests were repeated at 4000 rpm (instead of 2000 rpm). It was found that the surface finish at 4000 rpm was improved especially at the low load, i.e., 0.5 N/ball compared to that at 2000 rpm. This may be due to increase in the minimum depth-of-cut as the speed increases, and therefore the abrasive under the low force will cut along the workpiece surface instead of rolling (3-body abrasion ); or when the speed increases, the number of abrasives passing the polishing area per unit time increases and therefore the material remove per abrasive reduces so that resisting force from material removed is so low as to compel abrasives to rotate causing 3-body abrasion. The 0.5 N/ball load can be considered as the critical value from a 3-body to a 2-body abrasion at 4000 rpm.

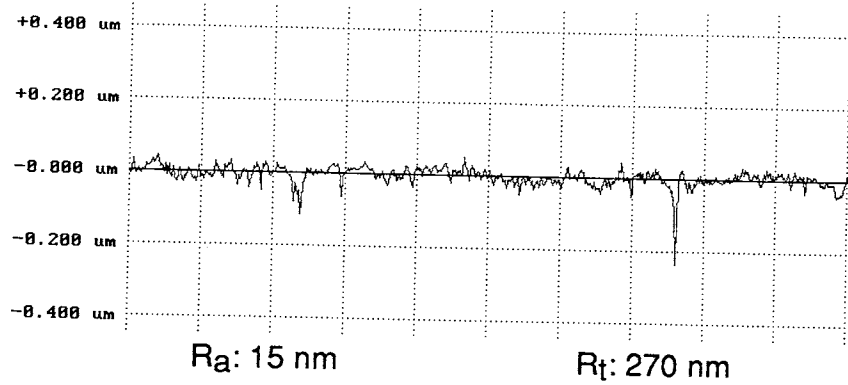


Figure 5.3 (a) Talysurf surface roughness trace after test  
 Load: 0.5 N/ball;  
 Abrasive: SiC (  $1\mu\text{m}$  ); Concentration: 5%;  
 Speed: 2000rpm; Test time: 45 min

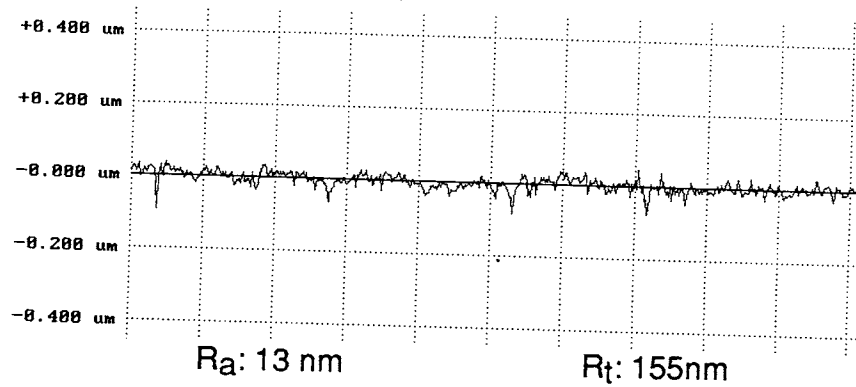


Figure 5.3 (b) Talysurf surface roughness trace after test  
 Load: 1 N/ball;  
 Abrasive: SiC (  $1\mu\text{m}$  ); Concentration: 5%;  
 Speed: 2000rpm; Test time: 45 min

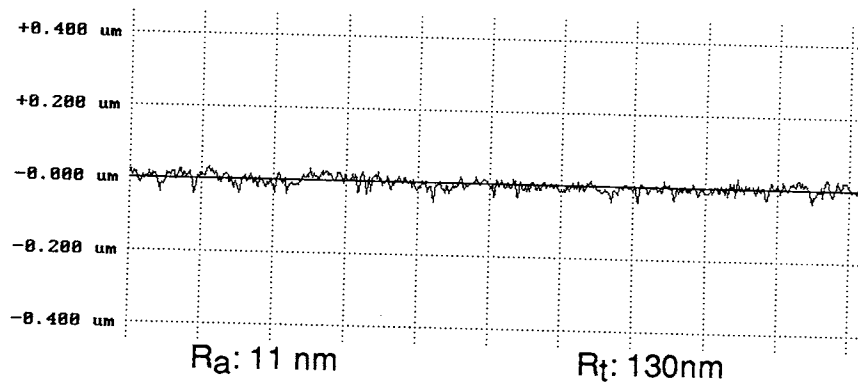


Figure 5.3 (c) Talysurf surface roughness trace after test  
 Load: 1.5 N/ball;  
 Abrasive: SiC (  $1\mu\text{m}$  ); Concentration: 5%;  
 Speed: 2000rpm; Test time: 45 min



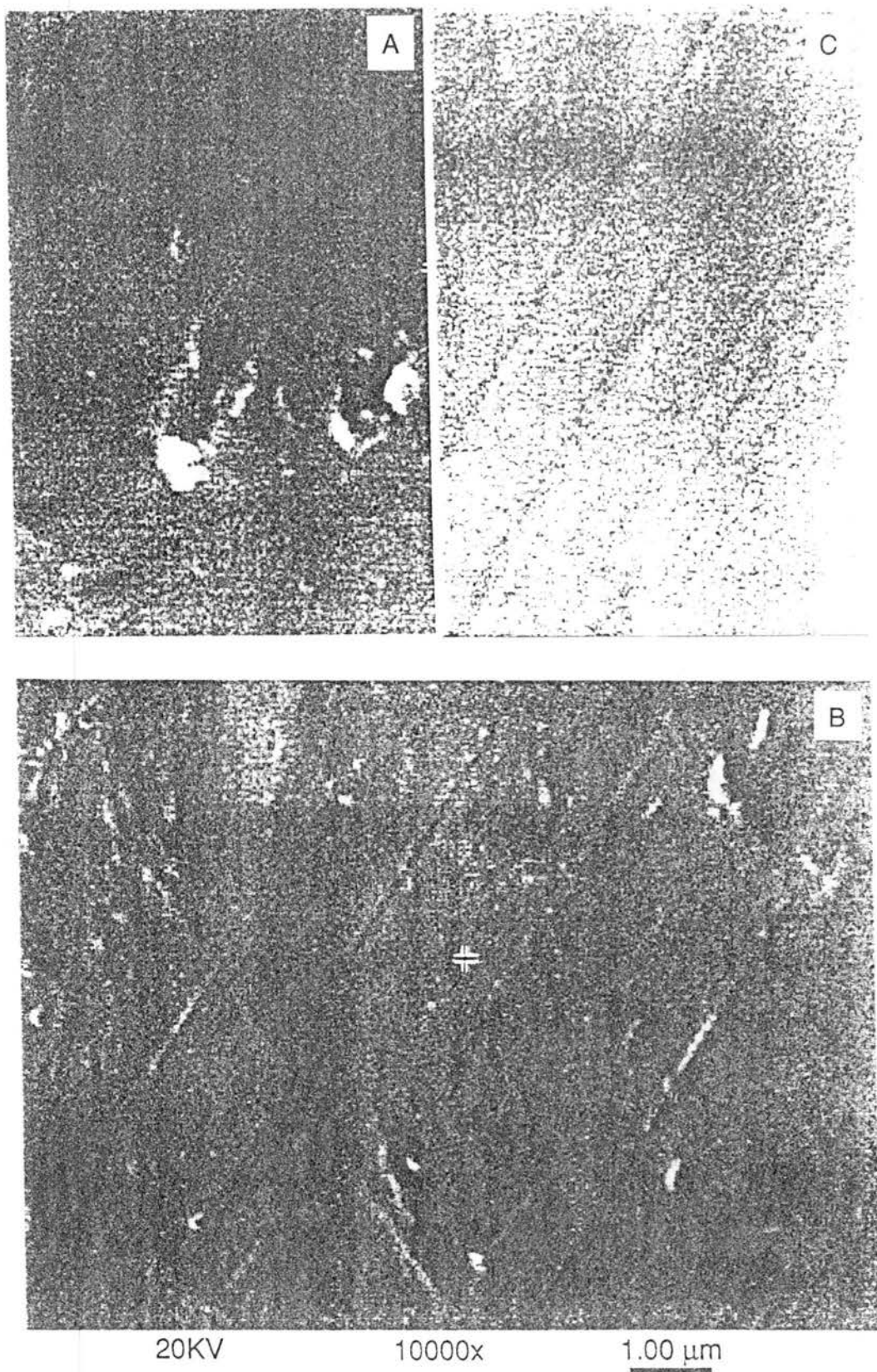


Figure 5.4 SEM morphologies of a  $\text{Si}_3\text{N}_4$  ball surface after polishing with (a) 0.5 N per ball, (b) 1 N per ball, and (c) 1.5 N per ball

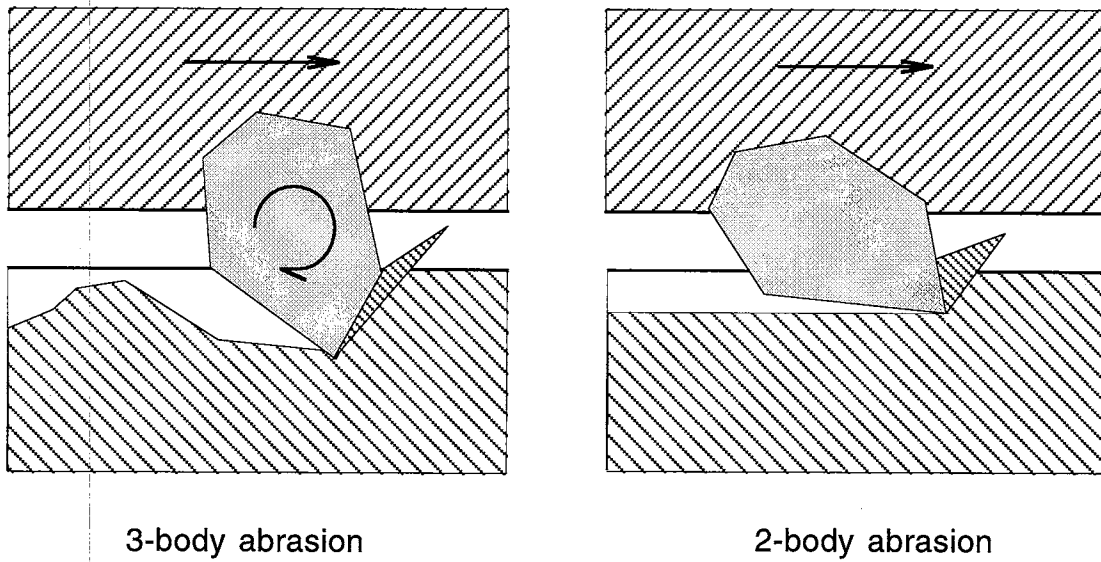


Figure 5.5 The schematic of 3-body and 2-body abrasion models

For 2-body abrasion (grinding),

$$P = FV$$

$$l = \sqrt{Dd}$$

$$t = \sqrt{\frac{4v}{CrV}} \sqrt{\frac{d}{D}}$$

$$Z = vbd$$

where  $l$  = undeformed length of chip,  $t$  = maximum height of chip,  $Z$  = Removal rate,  $b$  = wheel width of cut,  $D$  = wheel dia,  $d$  = wheel depth of cut,  $V$  = wheel speed,  $v$  = work speed,  $C$  = number of cutting grits per sq. in,  $r$  = ratio of the width to the depth of the groove produced by the mean grit.

Talysurf roughness profiles of the  $\text{Si}_3\text{N}_4$  ball surface polished at different drive speeds (2000 rpm, 4000 rpm, and 6000 rpm) are shown in Figures 5.6 (a) - (c), respectively. SiC (1  $\mu\text{m}$  grit) abrasive, 5 vol% abrasive concentration, 1 N/ball load, and a test time of 45 min/step were used in this experiment. As the spindle speed increases, the relative sliding speed between the polished ball and the polishing shaft increases. As discussed before, the number (times) of abrasives embedded in the polishing shaft passing the polishing area per unit time increases; Not only the polished asperities in the polishing area are more uniform but also the material removal per abrasive reduces so that the resistive force from material removal is not high enough to let abrasives embed in the shaft to cause 3-body abrasion during the polishing process. Thus, with increasing spindle speed, the polishing process would change from a 3-body to 2-body abrasion thereby minimizing deep pits from forming in the polished surface. Thus, the depth of surface damage  $R_t$  will decrease as the spindle speed increases. But, it has been noted that overspeed ( $> 6000$  rpm) would cause the polishing process to become unstable due to inertia and thus the surface quality may begin to deteriorate when the spindle speed is increased to very high speeds, e.g. 8000 rpm. In addition, the squeezing of abrasives to the the polished surface can improve the surface finish of metal workmaterials during polishing. When the speed increases to very high value, there is more cutting and less squeezing by the abrasives because the minimum depth-of-cut continues to increase. The squeezing action is very important for improving the surface finish by plastic deformation on the polishing surface on metals, but not in the case of polishing ceramic materials as the material removal mechanism is by brittle fracture rather than plastic deformation.

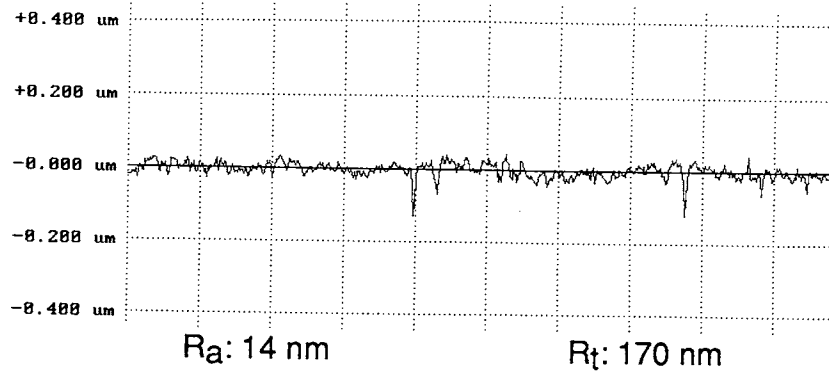


Figure 5.6 (a) Talysurf surface roughness trace after test  
 Speed: 2000rpm;  
 Abrasive: SiC (  $1\mu\text{m}$  ); Load: 1 N/ball;  
 Concentration: 5%; Test time: 45 min.

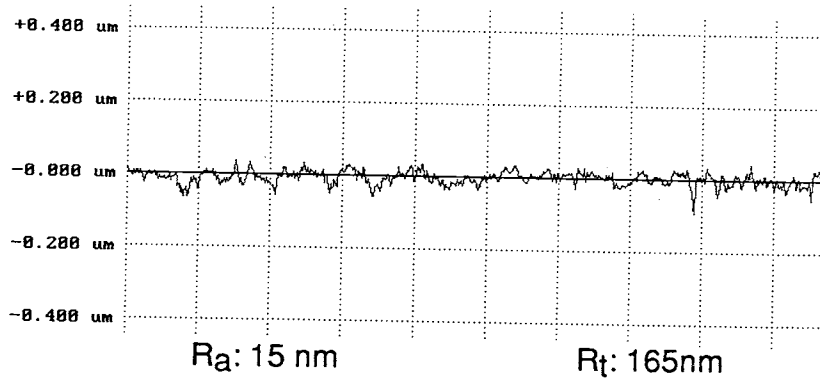


Figure 5.6 (b) Talysurf surface roughness trace after test  
 Speed: 4000rpm;  
 Abrasive: SiC (  $1\mu\text{m}$  ); Load: 1 N/ball;  
 Concentration: 5%; Test time: 45 min.

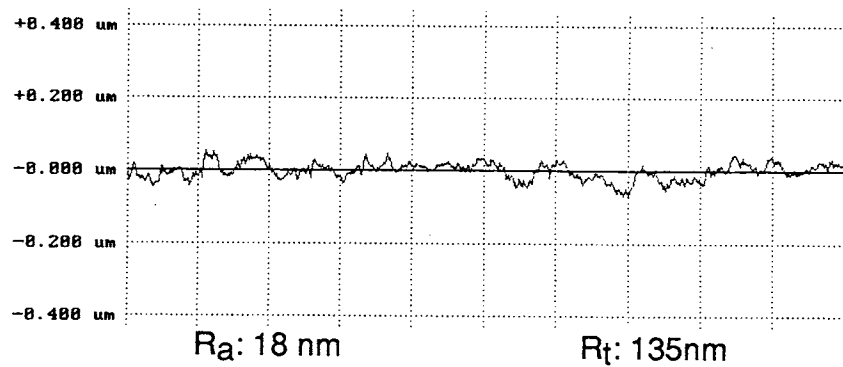


Figure 5.6 (c) Talysurf surface roughness trace after test  
 Speed: 6000rpm;  
 Abrasive: SiC (  $1\mu\text{m}$  ); Load: 1 N/ball;  
 Concentration: 5%; Test time: 45 min.

The Talysurf roughness profiles of  $\text{Si}_3\text{N}_4$  ball surface after polishing with different abrasive concentrations, namely 5 vol %, 10 vol %, and 20 vol %, respectively are shown in Figures 5.7 (a) - (c). SiC (1  $\mu\text{m}$  grit) abrasive, a load of 1 N/ball, speed of 2000 rpm, and test time 45 min/step were the conditions used in this experiment. It can be seen from the Talysurf plots that the surface damage with 5 vol % abrasive concentration is lower than that polished with higher abrasive concentration (10 vol % and 20 vol %). When the amount of abrasives inside the magnetic fluid is low, such as 5 vol %, the abrasives have more freedom and hence the larger size abrasives are more easy to be excluded from the polishing area. But when the density of abrasives increases to 10 vol %, some larger abrasives are pushed into the polishing area. The larger size abrasives can cause significant brittle fracture in the polished surface. As the density of abrasives further increases (i.e., up to 20 vol %), the number of larger size abrasives in the polishing area increases and the polishing force to per abrasive would decrease. Thus the depth of pits and scratches in the surface of the polished ball may decrease and the surface quality may improve.

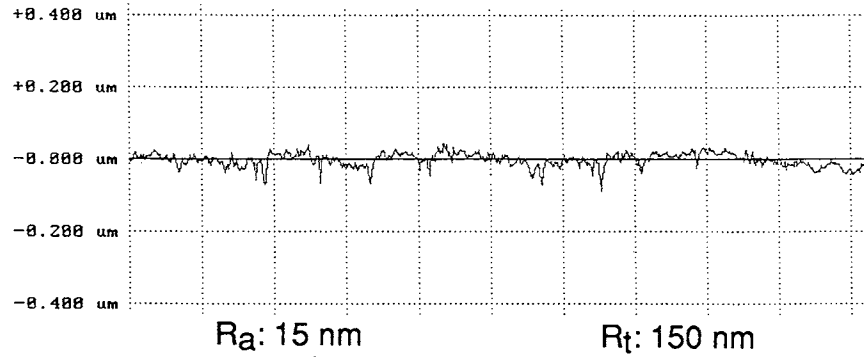


Figure 5.7 (a) Talysurf surface roughness trace after test  
 Concentration: 5%;  
 Abrasive: SiC ( 1 $\mu$ m ); Load: 1 N/ball;  
 Speed: 2000rpm; Test time: 45 min

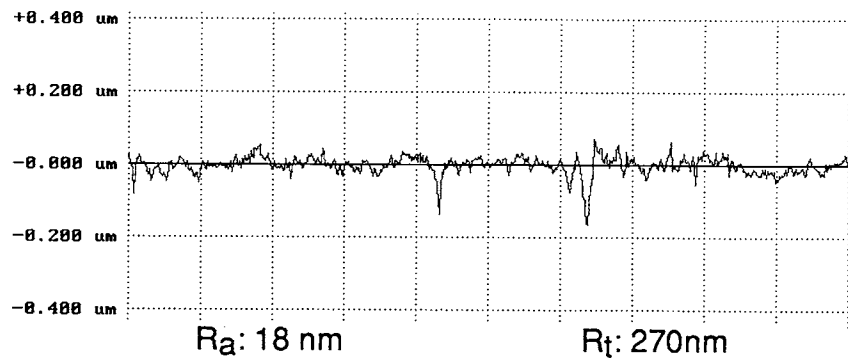


Figure 5.7 (b) Talysurf surface roughness trace after test  
 Concentration: 10%;  
 Abrasive: SiC ( 1 $\mu$ m ); Load: 1 N/ball;  
 Speed: 2000rpm; Test time: 45 min

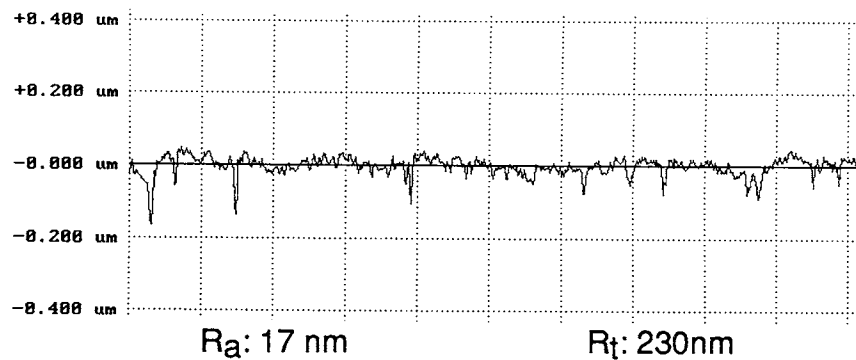


Figure 5.7 (c) Talysurf surface roughness trace after test  
 Concentration: 20%;  
 Abrasive: SiC ( 1 $\mu$ m ); Load: 1 N/ball;  
 Speed: 2000rpm; Test time: 45 min

Polishing tests were conducted with SiC abrasive with four different grain sizes, namely, #400 (23  $\mu\text{m}$ ), #1000 (5  $\mu\text{m}$ ), #1200 (3  $\mu\text{m}$ ), and #8000 (1  $\mu\text{m}$ ) to investigate the effect of abrasive size on the surface finish and material removal rate. The conditions used in this experiment were: abrasive concentration 10 vol %, load 1 N/ball, speed 2000 rpm and test time 45 min/step. The surface finish and the material removal rate obtained from these tests are shown in the Figures 5.8 (a) and (b), respectively. It can be seen that surface finish improves significantly as the given size of the abrasive decreases. Similarly, removal rate decreases significantly as the abrasive size decreases. When the abrasive size decreases, first, the number of abrasives in the polishing area will increase. Therefore, the number of polishing points in the polishing area will increase and become more uniform; second, the force to per abrasive decreases, and therefore the depth and size of brittle fracture from abrasive action of each abrasive decreases. Thus, the surface finish improves and material removal rate decreases due to a decreasing in the the size of brittle fracture with decreasing the abrasive size. The reason that large abrasives are unable to generate good surface finish in the polishing process is that they cause deep ploughing. Further the abrasives are free in the polishing process rather than fixed like in grinding. Free abrasives are easy to fall into the previous scratch groove, and thus the material on the either side of the groove is difficult to remove in the polishing process. Figure 5.9 is a schematic showing the profiles generated after polishing with small size and large size abrasives. The effect of abrasive size on surface finish in polishing is more significant than that in the grinding process.

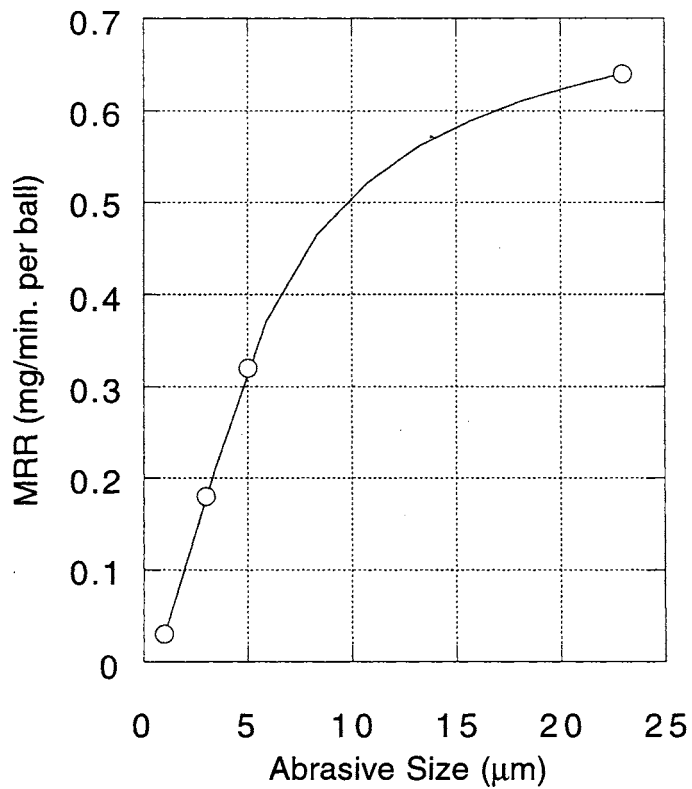
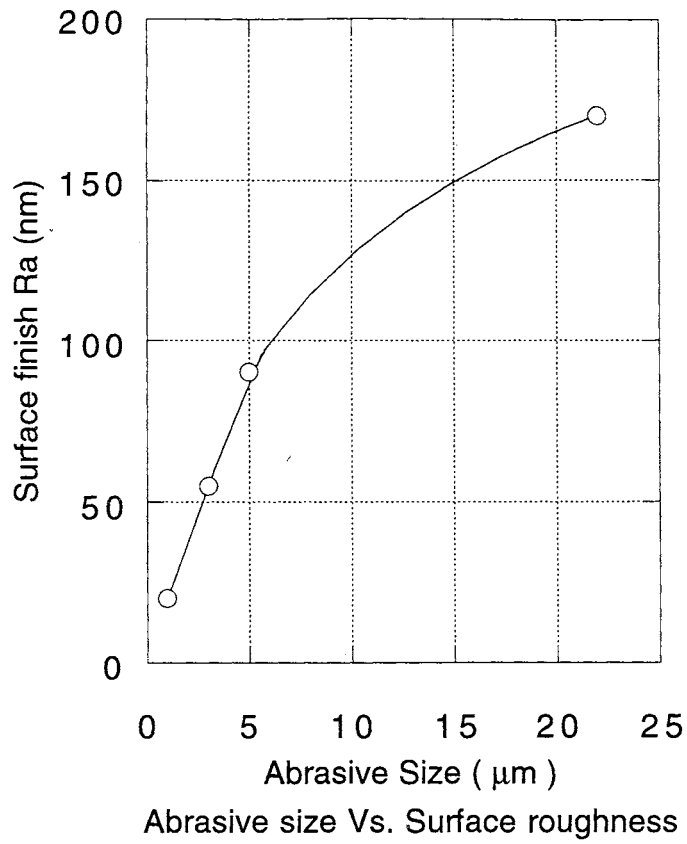
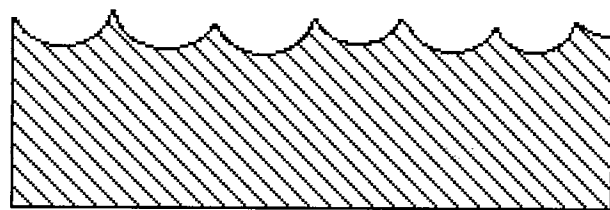
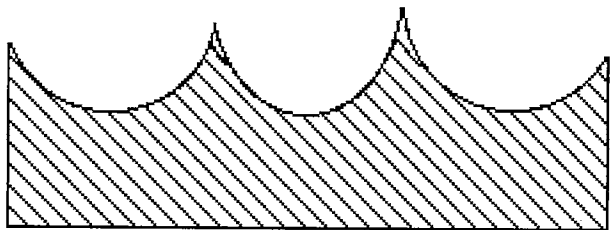


Figure 5.8 Abrasive size Vs. Material removal rate  
 Abrasive: SiC  
 Load: 1 N/ball; Speed: 2000rpm;  
 Concentration: 10%; Test time: 45 min.





(a) by small size abrasive



(b) by large size abrasive

Figure 5.9 Profile of transverse cross-section after polished with small and large size abrasives, respectively

Some polishing tests were conducted to formulate the material removal mechanism in the MFP of  $\text{Si}_3\text{N}_4$  balls with harder abrasives. The surface of the  $\text{Si}_3\text{N}_4$  balls after polishing with  $\text{B}_4\text{C}$  #500 (17  $\mu\text{m}$  grit size) abrasive at 2000 rpm, abrasive concentration 10 vol%, and load of 1 N/ball (Figure 5.10, without ultrasonic cleaning) appears to be covered with microchipping pits/ short scratches; Material removal is by a 3-body abrasion involving brittle microfracture/microchipping. The SEM micrograph (Figure 5.11) of the  $\text{Si}_3\text{N}_4$  ball after polishing with  $\text{B}_4\text{C}$  #1500 (1-2  $\mu\text{m}$  grit size) abrasive at 2000 rpm shows clearly brittle microfractures on the polished surface. A number of scratch abrasion/plowing groove/wear tracks are formed as the polishing speed is increased to 4000 rpm at which condition the polishing process changes from a 3-body to a 2-body abrasion and the length of the sliding distance increases. Figure 5.12 shows that the surface of a  $\text{Si}_3\text{N}_4$  ball after polishing with diamond #500 abrasive at 4000 rpm is mainly covered with scratching abrasion/plowing groove/passing wear tracks in the direction of abrading, and the material removal is by a 2 body abrasion brittle scratching. Different sizes of brittle fracture pits and cracks along and inside the scratching tracks can be seen clearly. There are no evidence of plastic flow, and the material removal in this case is considered to be due to 2-body abrasion involving brittle microfracture with grain dislodgement and cleavage. In the summary, the material removal of  $\text{Si}_3\text{N}_4$  balls polished with harder abrasives such as diamond,  $\text{B}_4\text{C}$ , and  $\text{SiC}$  is by brittle microfracture.

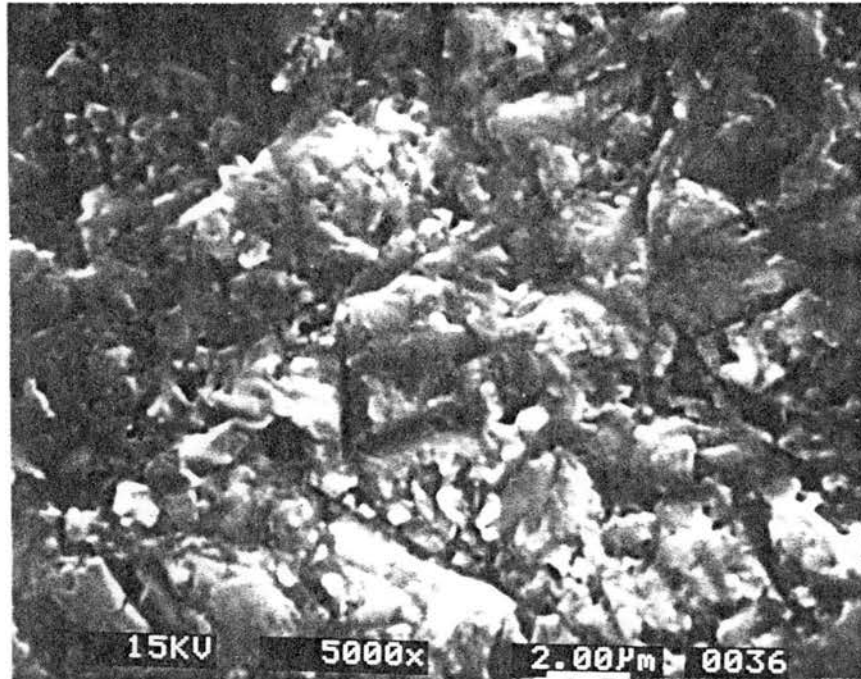


Figure 5.10 SEM micrograph of a  $\text{Si}_3\text{N}_4$  ball surface after polishing with  $\text{B}_4\text{C}$  (# 500 grit) abrasive at 2000 rpm

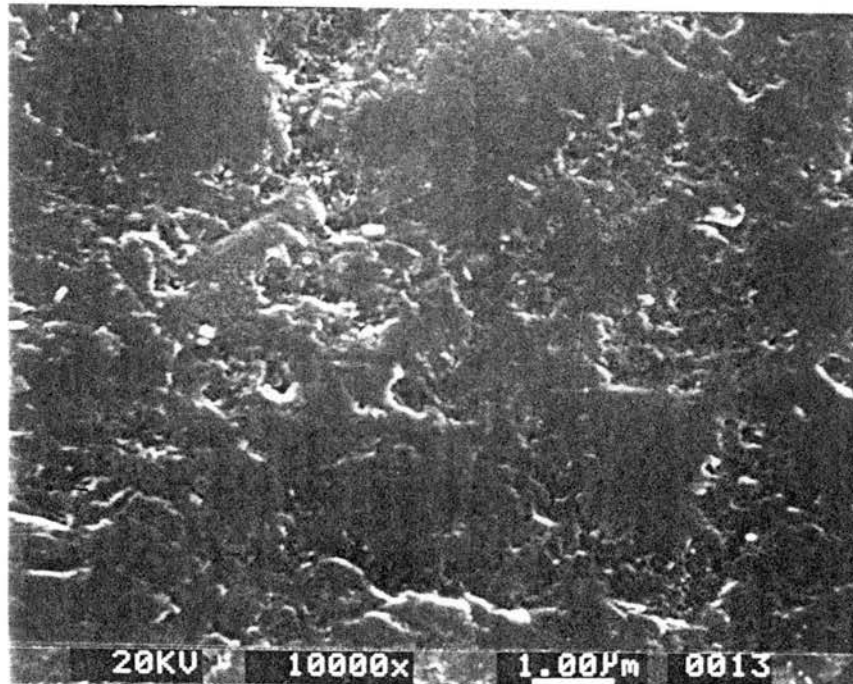


Figure 5.11 SEM micrograph of a  $\text{Si}_3\text{N}_4$  ball surface after polishing with  $\text{B}_4\text{C}$  (# 1500 grit) abrasive at 2000 rpm

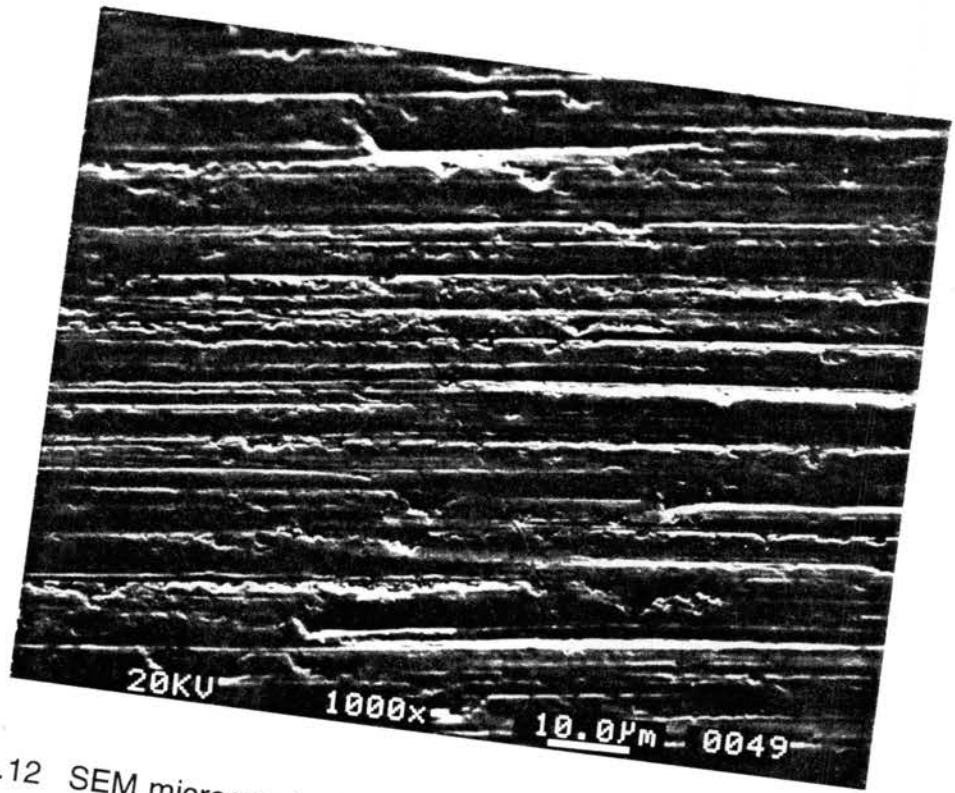


Figure 5.12 SEM micrograph of a Si<sub>3</sub>N<sub>4</sub> ball surface after polishing with diamond (# 500 grit) abrasive at 4000 rpm

## 5.8 BRITTLE FRACTURE MODEL OF MECHANICAL POLISHING

In mechanical polishing with a harder abrasive, brittle fracture pits or/and brittle fracture scratching marks surface are seen on the polished  $\text{Si}_3\text{N}_4$  balls. The material removal mechanism of  $\text{Si}_3\text{N}_4$  balls polished with a harder abrasive such as diamond,  $\text{B}_4\text{C}$ , and  $\text{SiC}$  is considered to be due to brittle microfracture. The brittle fracture model of elastic/plastic indentation of brittle materials [Marshall et al, 1982; Lawn et al, 1975; Swain et al, 1979] can be extended to mechanical polishing.

There are two principal crack systems initiating from the contact area of an abrasive/indenter into workpiece, i.e., radial/median cracks and lateral cracks (Figure 5.13). *Radial/median cracks are usually associated with strength degradation, and lateral cracks are mainly responsible for material removal.* The cracks propagate when significant elastical stored energy is available in the tensile stress region to extend the crack. During loading [Figures 5.14 (a)-(c)], plastic deformation occurs, and the stress field under the tip of the indenter is compressive. However, a tensile stress does arise at the contact surface and is maximum at the boundary between the elastic and plastic deformation zone. During unloading [Figures 5.14(d)-(f)], the material in the plastic deformation zone is compressed by the surrounding elastic region and tensile stress occurs again around the boundary of the plastic zone. So, the elastic/plastic stress field under the indenter at full load consists of elastic component at full load and the residual component during unloading. The elastic component during loading initiates the median cracks, and the residual stress component during unloading provides the primary driving force for the lateral cracks and the propagation of radial/median cracks. So, the following sequence of events

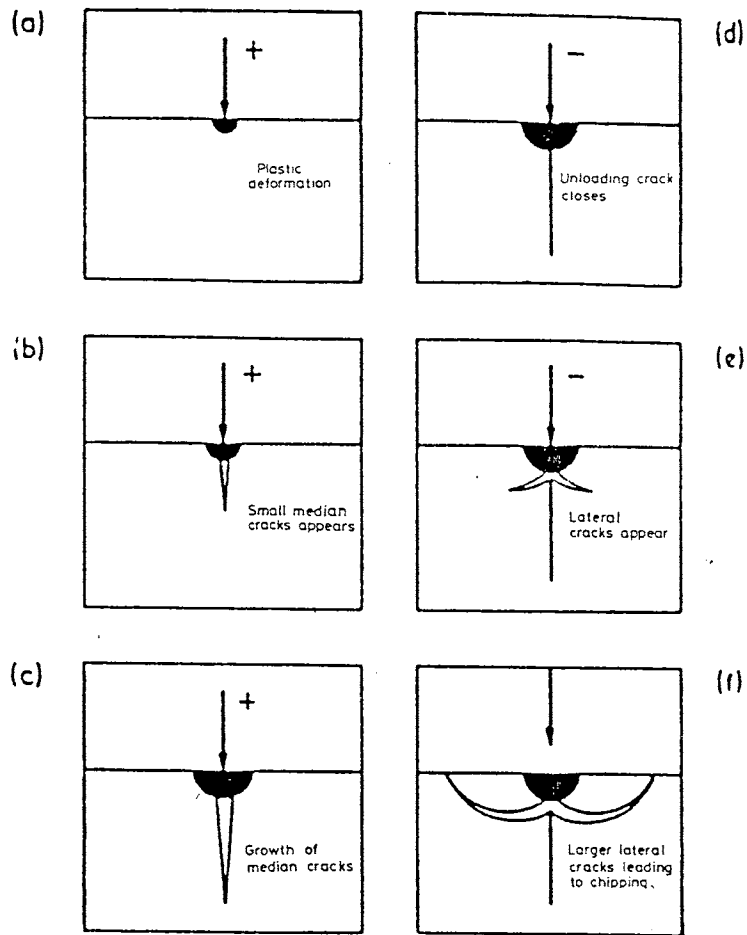


Figure 5.13 Formation of Cracks in a Brittle Surface Under Point Indentation [Lawn and Wilshaw, 1975]

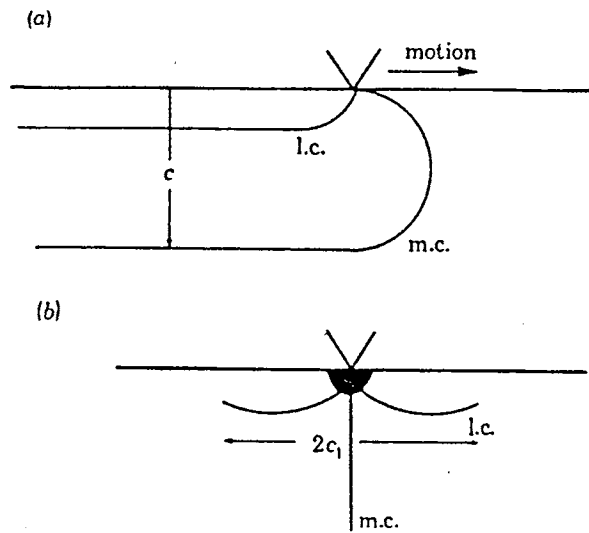


Figure 5.14 Lateral Cracking and Median Cracking of a Moving Point Indentation [Swain, 1979]

are believed to happen during polishing: Elastic/Plastic deformation occurs initially under the abrasive. This is followed by the formation of median cracks during loading. Radial cracks are formed during unloading. Lateral cracks form and propagate parallel to the workpiece surface during the unloading. At high loads (and also depending on the indenter geometry), *the lateral cracks interact with the median/radial crack system and fracture (chipping) occurs*. With a moving sharp indenter/abrasive scratching (2-body abrasion) the brittle material (Figure 5.15), the median and lateral cracks will follow the moving indenter. The median crack plane is along the direction of motion and vertical i.e., into the workmaterial. This is perhaps the reason for the higher flexural strength degradation of advanced ceramics when ground transversely than longitudinally.

The volume removal  $V$  due to lateral cracks by abrasion is given by:

$$V = a \frac{(P)_8^9}{(K_c)_2^1 (H)_8^5} \left(\frac{E}{H}\right)^4 L$$

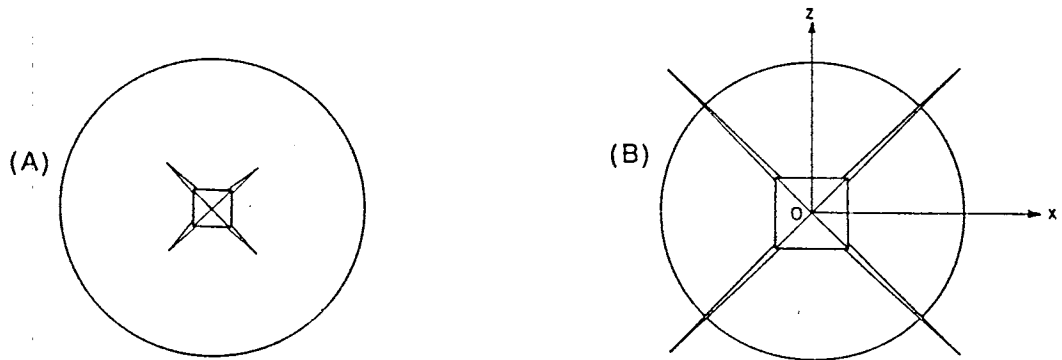
where  $V$  is the removal volume,  $a$  is a material-independent constant,  $P$  is the normal load,  $K_c$  is the toughness,  $H$  is the hardness,  $E$  is the elastic modulus, and  $L$  is the sliding distance.

The minimum threshold load to cause lateral crack is given by:

$$P^* = \zeta \left(\frac{K_c^4}{H^3}\right) f\left(\frac{E}{H}\right)$$

where:

$$\zeta f\left(\frac{E}{H}\right) = 2 \times 10^5$$



(A) Lateral Cracks > Radial Cracks      (B) Lateral Cracks < Radial Cracks

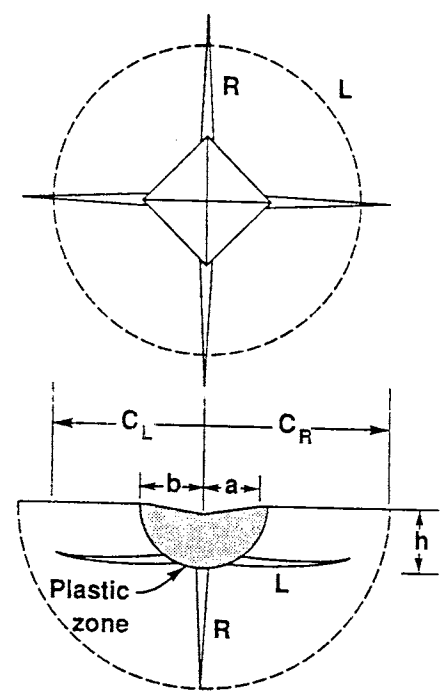


Figure 5.15 Lateral Cracks and Radial / Median Cracking in Vickers Indentation [Marshall et al, 1982]



It can be seen from the above two equations that although a high hardness minimizes the removal rate both below and above the fracture threshold, the threshold force is diminished by increasing hardness. Fracture can be suppressed by high toughness or low hardness. High toughness and high hardness both being desirable for optimum wear resistance leading to low removal rate. For glass, the toughness is  $0.7 \text{ MPa}\sqrt{\text{m}}$  and the hardness is 6 GPa. Hence, the threshold load for glass to cause lateral cracking is:

$$P^* = 2 \times 10^5 \times \frac{(0.7 \times 10^6)^4}{(6 \times 10^9)^3} = 0.2 \text{ N}$$

For silicon nitride ceramic, the toughness is  $5 \text{ MPa}\sqrt{\text{m}}$  and the hardness is 16 GPa. Hence, the threshold load for silicon nitride ceramic to cause lateral cracking is:

$$P^* = 2 \times 10^5 \times \frac{(5 \times 10^6)^4}{(16 \times 10^9)^3} \approx 30 \text{ N}$$

It may be noted that average normal force per abrasive need in grinding and polishing silicon nitride ceramic is very much lower than this critical threshold force for lateral fracture. Generally 1 N per ball is applied in the magnetic float polishing silicon nitride balls. This is equivalent of 0.05-0.1 N per abrasive in this process. However, the material removal is a result of cumulative process rather than an isolated event. The previous tribological contacts (history) have a significant effect on the later material removal process. It has been found that the critical load or depth of cut for cracking to occur will reduce greatly as the number of scratches increases. But the force is small so that there is not enough energy to propagate cracks farther away. Also the interactions between cracks from adjacent points in multipoint grinding and polishing could

reduce the average size of fragments but increase the total amount of material removal. Crack depths for multipoint grinding are only about half that for single-point grinding at the same normal loads because the interactions between neighboring scratches in multipoint grinding could reduce the stress intensity factor. The material is removed by microfracture rather than macrofracture in MFP which uses low polishing force and flexible support system.

## CHAPTER 6

# INVESTIGATION OF CHEMO-MECHANICAL POLISHING (CMP) OF SILICON NITRIDE ( $\text{Si}_3\text{N}_4$ ) WORKMATERIAL WITH VARIOUS ABRASIVES

### 6.1 INTRODUCTION

Surface defects during polishing can be minimized when successively fine abrasive are used but could not be eliminated altogether in mechanical polishing in which the abrasive used is harder than the workmaterial. For example, the best surface finish obtained with a fine  $\text{B}_4\text{C}$  abrasive ( $1\ \mu\text{m}$ ) (harder abrasive) by MFP on HIP'ed  $\text{Si}_3\text{N}_4$  balls was  $\approx 20\ \text{nm}$  Ra and  $\approx 200\ \text{nm}$  Rt (where Ra is the arithmetic average surface roughness and Rt is the peak to valley distance). Similarly, the best surface finish obtained using a fine,  $\text{SiC}$  abrasive ( $1\ \mu\text{m}$ ) (also a harder abrasive than  $\text{Si}_3\text{N}_4$ ) was  $\approx 15\ \text{nm}$  for Ra and  $\approx 150\ \text{nm}$  for Rt [Chapter 5]. To improve the final surface finish to meet to application requirements and for reliable performance of the balls in service, CMP with a soft abrasive for obtaining extremely smooth and damage-free surface has was developed.

### 6.2 CHEMO-MECHANICAL POLISHING (CMP)

Chemo-mechanical polishing (CMP) can be used to finish hard, brittle workmaterials with extremely smooth and damage-free surfaces. CMP depends on the availability for a short duration certain threshold pressure and

temperature at the contact zone of the polishing process to enable a chemical reaction layer to be formed by the interaction of the abrasive, the workmaterial and the environment. This process is considered tribo-chemical polishing when there is absolutely no mechanical action [Fischer, 1988]. In CMP, the selected abrasive is generally softer than the workmaterial. Hence, damage due to mechanical action is minimized or eliminated. Chemical reactions are formed between the workmaterial, the abrasive, and the environment under the conditions of polishing. The reaction products so formed are removed from the workmaterial by subsequent mechanical action of the abrasive.

Wang and Hsu (1994) concluded that the formation of a thin, soft layer of the reaction product ( $< 100 \text{ \AA}$  thick) results in the easy removal of hard workmaterial without directly abrading the surface. Reasonably high removal rates (perhaps not as high as in mechanical abrasion,  $\sim 1/10$ ) and minimal surface damage can be achieved by the formation of brittle surface layers. Chemo-mechanical polishing was first demonstrated by Yasunaga et al (1979) for polishing single crystal silicon using a soft abrasive (barium carbonate,  $\text{BaCO}_3$ ). Later, Vora et al (1982 and 1983) reported the feasibility of polishing  $\text{Si}_3\text{N}_4$  with  $\text{Fe}_2\text{O}_3$  and  $\text{Fe}_3\text{O}_4$  abrasives. Suga et al (1989) polished  $\text{Si}_3\text{N}_4$  using  $\text{CaCO}_3$ ,  $\text{MgO}$ ,  $\text{SiO}_2$ ,  $\text{Fe}_2\text{O}_3$  and  $\text{Fe}_3\text{O}_4$ , and  $\text{Cr}_2\text{O}_3$  abrasives. They concluded that  $\text{Cr}_2\text{O}_3$  was the most suitable abrasive for the CMP of  $\text{Si}_3\text{N}_4$ . Kikuchi et al (1990, 1992) also found  $\text{Cr}_2\text{O}_3$  to be a suitable abrasive for polishing  $\text{Si}_3\text{N}_4$ .

Bhagavatula and Komanduri (1996) studied in detail the mechanism of material removal in the finishing of  $\text{Si}_3\text{N}_4$  balls with  $\text{Cr}_2\text{O}_3$  abrasive by analyzing the wear debris generated during polishing using a scanning electron microscope (SEM) with an energy-dispersive X-ray microanalyser

(EDXA) and a low-angle X-ray diffraction (XRD) apparatus. Prior to their investigation,  $\text{Cr}_2\text{O}_3$  has been identified by other researchers [Kikuchi et al, 1992] as a catalyst rather than its direct involvement in the chemical reactions with  $\text{Si}_3\text{N}_4$ . Bhagavatula and Komanduri, based on the experimental evidence, showed that the role of  $\text{Cr}_2\text{O}_3$  was more than that of a mere catalyst in that it plays an active role in the chemical reaction with  $\text{Si}_3\text{N}_4$  forming chromium silicate ( $\text{Cr}_2\text{SiO}_4$ ) and chromium nitride ( $\text{CrN}$ ). Till recently,  $\text{Cr}_2\text{O}_3$  was considered as the most effective abrasive for CMP of  $\text{Si}_3\text{N}_4$ . The best finish reported was  $\sim 16$  nm Ra and  $\sim 0.54$   $\mu\text{m}$  Rt. There is of course some surface damage that can still be seen with this abrasive due to its mechanical action, in spite of its outstanding chemo-mechanical polishing ability. This is because its hardness is nearly the same or slightly more than that of  $\text{Si}_3\text{N}_4$ . Also, some of the chemical species formed by the reaction of  $\text{Cr}_2\text{O}_3$  with  $\text{Si}_3\text{N}_4$  workmaterial during CMP may not be acceptable environmentally and special care may have to be exercised for the disposal of the fluid.

Chemo-mechanical polishing (CMP) depends on both chemical and mechanical effectiveness of the abrasive in relation to the workmaterial and the environment under the conditions of polishing [Jiang and Komanduri, 1997c]. Since material removal from  $\text{Si}_3\text{N}_4$  workmaterial by this mechanism would not depend on the hardness of the abrasive but on the chemical potentials and removal of the reaction layer, it is possible to remove material by abrasives substantially softer than the workmaterial. Chemo-mechanical action is thus very specific in that proper choice of the abrasive and the environment should be made for a given workmaterial. For efficient removal of material, those that facilitate chemical reactions and efficient mechanical removal would be preferable for CMP. Both thermodynamics and kinetics play an important role

on the rates of chemical reactions. Once the reaction products are formed they should be removed from the workmaterial by subsequent mechanical action of the abrasive.

This chapter presents the results of a systematic investigation of the chemo-mechanical polishing (CMP) of a uniaxially pressed  $\text{Si}_3\text{N}_4$  balls with various abrasives. The abrasives considered include boron carbide ( $\text{B}_4\text{C}$ ), silicon carbide ( $\text{SiC}$ ), aluminium oxide ( $\text{Al}_2\text{O}_3$ ), chromium oxide ( $\text{Cr}_2\text{O}_3$ ), zirconium oxide ( $\text{ZrO}_2$ ), silicon oxide ( $\text{SiO}_2$ ), cerium oxide ( $\text{CeO}_2$ ), iron oxide ( $\text{Fe}_2\text{O}_3$ ), yttrium oxide ( $\text{Y}_2\text{O}_3$ ), copper oxide ( $\text{CuO}$ ), and molybdenum oxide ( $\text{Mo}_2\text{O}_3$ ). The purpose is to determine the most suitable and effective abrasive as well as the environment to finish  $\text{Si}_3\text{N}_4$  balls with extremely smooth and damage-free surfaces for highly reliable performance in such applications as aircraft engine bearings, high-speed spindle bearings. The surface finish obtained on the  $\text{Si}_3\text{N}_4$  balls after CMP by various softer abrasives using magnetic float polishing (MFP) technique is reported. The dual role of chemical and mechanical actions in CMP are elucidated. Thermodynamic feasibility of the chemical reactions formed between the abrasive and workmaterial are investigated based on Gibb's free energy change. The flash temperature generated and the flash duration at the contact zone of the polishing process was calculated using the models developed by Hou and Komanduri [1997a,b] to determine the temperatures for the thermodynamic analysis of the chemical reactions during CMP. The chemical reactions would proceed on a continuing basis only if the passivating layers are removed by the subsequent mechanical action. The kinetic action, which involves the removal of the reaction products from the interface is thus also critical to CMP. A discussion of CMP mechanism

for polishing  $\text{Si}_3\text{N}_4$  with various abrasives is presented based on thermodynamic and kinetic analyses.

### **6.3. EXPERIMENTAL PROCEDURE AND POLISHING CONDITIONS**

The chemical composition and the mechanical and thermal properties of the  $\text{Si}_3\text{N}_4$  workmaterial (NBD-200 uniaxially pressed  $\text{Si}_3\text{N}_4$  balls:  $\beta$ - $\text{Si}_3\text{N}_4$  with ~1 wt.% MgO as a sintering aid) used in this investigation have been given in chapter 4. Table 6.1 gives the properties of the various abrasives used in this investigation for their relative suitability for chemo-mechanical polishing of  $\text{Si}_3\text{N}_4$  balls for bearing applications. Table 6.2 lists the polishing conditions used for each test. There are two types of magnetic fluids, one an oil-based (EMG 909) and the other water-based (W 40, saturation magnetization at 25 °C is 400 Gauss, viscosity at 27 °C is 25 Cp). In this investigation both types were used to compare the effectiveness of the polishing environment. The initial surface finish of the workmaterial for each test was prepared by polishing with  $\text{B}_4\text{C}$  1500 grit abrasive.

As previously pointed out, the chemo-mechanical polishing (CMP) depends on the chemo-mechanical interaction of the abrasive, work material, and the environment. The pH value and the conductivity of the polishing fluid (magnetic fluid + abrasive) would influence the surface finish and material removal rate in CMP as the polishing fluid is part of the electrolytic cell. In this investigation, the pH and conductivity values of the polishing environment were measured using Cole-Parmer pH/Temperature meter and TDS-Conductivity/Temperature meter, respectively.

Table 6.1 Properties of Various Abrasives

ABRASIVE	DENSITY g/cm <sup>3</sup>	HARDNESS	
		Mohs	Knoop kg/mm <sup>2</sup>
Diamond	3.52	10	7000
Boron Carbide (B <sub>4</sub> C)	2.52	9.3	3200
Silicon Carbide (SiC)	3.22	9.2	2500
Aluminium Oxide (Al <sub>2</sub> O <sub>3</sub> )	3.98	9	2150
Chromium Oxide (Cr <sub>2</sub> O <sub>3</sub> )	5.21	8.5	1800
Zirconium Oxide (ZrO <sub>2</sub> )	5.85	8	1200
Silicon Oxide (SiO <sub>2</sub> )		7	820
Cerium Oxide (CeO <sub>2</sub> )	7.13	6	-
Iron Oxide (Fe <sub>2</sub> O <sub>3</sub> )	5.24	6	-
Yttrium Oxide (Y <sub>2</sub> O <sub>3</sub> )	5.01	5.5	700
Copper Oxide (CuO)	6.32	3.5	225
Molybdenum Oxide (Mo <sub>2</sub> O <sub>3</sub> )	4.69	1.5	-

Table 6.2 Test Conditions

Workmaterial	Uniaxially Pressed Si <sub>3</sub> N <sub>4</sub> balls (CERBEC NBD 200) Initial diameter: 12.7 mm (0.5 inch) Initial Sphericity: 1 μm
Abrasive Concentration	10% by volume
Polishing Load	1.2 N per ball
Polishing Speed	2000 rpm
Magnetic Fluid	Oil based (EMG 40), Water based (W 40)



The magnetic field was measured using a Gauss/Tesla meter. The polishing load was set up by measuring the normal force with a Kistler's piezoelectric dynamometer connected to a charge amplifier and a display. To calculate the material removal rates, the weight reduction in the balls was determined by measuring the weight before and after polishing at every stage of the test using a precision balance. The surface finish of the polished balls was measured using a Form TalySurf 120 L (cut-off: 0.8 mm and 0.25 mm, evaluation length: 6 consecutive cut-off, Filter: ISO 2CR). The roundness of the balls was measured using TalyRond 250 (cut-off: 50 upr, Filter: 2CR).

CMP would depend on the availability for a short duration of certain threshold pressure/contact stress and temperature at the contact zone of the polishing process [Yasunaga et al, 1979]. The flash temperature and the flash duration generated at the contact zone of the polishing process enable chemical reaction products to form by the interaction between the abrasive, the work material, and the environment. In this investigation the flash temperatures and the corresponding flash time generated at the contact zone under the conditions of polishing with the most effective abrasive were calculated based on a moving disc heat source model developed by Hou and Komanduri (1997a,b).

Thermodynamic analysis (Gibb's free energy change,  $\Delta G$ ) was conducted to determine the reaction products that could be formed and whether such reactions are thermodynamically feasible. It is well known that for a reaction to occur spontaneously at a given temperature and pressure,  $\Delta G < 0$ . Equilibrium composition and  $\Delta G$  are calculated using the Outokumpu HSC Chemistry Software package developed in Finland. A discussion of the CMP

mechanism for polishing  $\text{Si}_3\text{N}_4$  with various abrasives is presented based on thermodynamic and kinetic analyses.

#### 6.4. CMP TEST RESULTS

Table 6.3 summarizes the average surface finish obtained from polishing  $\text{Si}_3\text{N}_4$  balls by various abrasives used in this investigation. In each test, the surface of the  $\text{Si}_3\text{N}_4$  balls was first polishing with  $\text{B}_4\text{C}$  1500 grit abrasive for 45 min. This was followed by polishing with a given abrasive for a period of 60 or 90 min (see Table V for details). The workpiece is then polished by the same abrasive for the second time for a period of 60 or 90 min to investigate if surface finish could be further improved. The corresponding TalySurf surface finish profiles are shown in Figures 6.1 (a) - (j). It can be seen from this data that  $\text{ZrO}_2$  and  $\text{CeO}_2$  are the most effective abrasives following by  $\text{Fe}_2\text{O}_3$  and  $\text{Cr}_2\text{O}_3$ . Figure 6.2 (a) shows SEM micrograph of a  $\text{Si}_3\text{N}_4$  ball surface after mechanical polishing with a fine  $\text{B}_4\text{C}$  abrasive (2 mm) in which material removal by brittle fractures can be seen clearly and Figure 6.2 (b) after CMP with  $\text{CeO}_2$  abrasive indicating mostly smooth surface with very few shallow pits formed during the previous mechanical polishing by  $\text{B}_4\text{C}$  1500 grit abrasive. It may thus be noted that the resulting surface finish obtainable by CMP is affected by the previous mechanical polishing. The depth of layers to be removed by CMP for smooth surface finish is at least equivalent to the surface roughness (peak-to-valley height,  $R_t$ ) of the previous final mechanical polishing surface.

Table 6.4 gives the average surface finish obtained from polishing  $\text{Si}_3\text{N}_4$  balls by  $\text{ZrO}_2$  and  $\text{CeO}_2$  abrasives after mechanical polishing with  $\text{SiC}$  abrasive (8000 grit). The corresponding TalySurf surface finish profiles are shown in

Table 6.3 Effect of Abrasives on Improving Surface Finish

Abrasive Type	Abrasive Size ( $\mu\text{m}$ )	Test Time (min)	Surface Finish		Effectiveness
			Ra (nm)	Rt ( $\mu\text{m}$ )	
B <sub>4</sub> C 1500	2	45	32	0.280	FAIL
Al <sub>2</sub> O <sub>3</sub>	5	60	46	0.377	
B <sub>4</sub> C 1500	2	45	31	0.295	POOR
CuO	3	60	28	0.241	
CuO	3	90	27	0.240	
B <sub>4</sub> C 1500	2	45	31	0.275	POOR
Y <sub>2</sub> O <sub>3</sub>	20	90	26	0.247	
Y <sub>2</sub> O <sub>3</sub>	20	60	23	0.244	
B <sub>4</sub> C 1500	2	45	30	0.272	POOR
SiO <sub>2</sub>	30	90	22	0.236	
SiO <sub>2</sub>	30	60	22	0.244	
B <sub>4</sub> C 1500	2	45	28	0.270	POOR
Mo <sub>2</sub> O <sub>3</sub>	20	60	22	0.216	
Mo <sub>2</sub> O <sub>3</sub>	20	90	18	0.205	
B <sub>4</sub> C 1500	2	45	29	0.260	GOOD
Cr <sub>2</sub> O <sub>3</sub>	5	90	14	0.208	
Cr <sub>2</sub> O <sub>3</sub>	5	60	12	0.175	
B <sub>4</sub> C 1500	2	45	30	0.274	GOOD
Fe <sub>2</sub> O <sub>3</sub>	3	60	13	0.186	
Fe <sub>2</sub> O <sub>3</sub>	3	90	9	0.167	
B <sub>4</sub> C 1500	2	45	31	0.268	EXCELLENT
CeO <sub>2</sub>	5	60	16	0.172	
CeO <sub>2</sub>	5	90	8	0.100	
B <sub>4</sub> C 1500	2	45	29	0.286	EXCELLENT
ZrO <sub>2</sub>	5	60	18	0.174	
ZrO <sub>2</sub>	5	90	8	0.126	

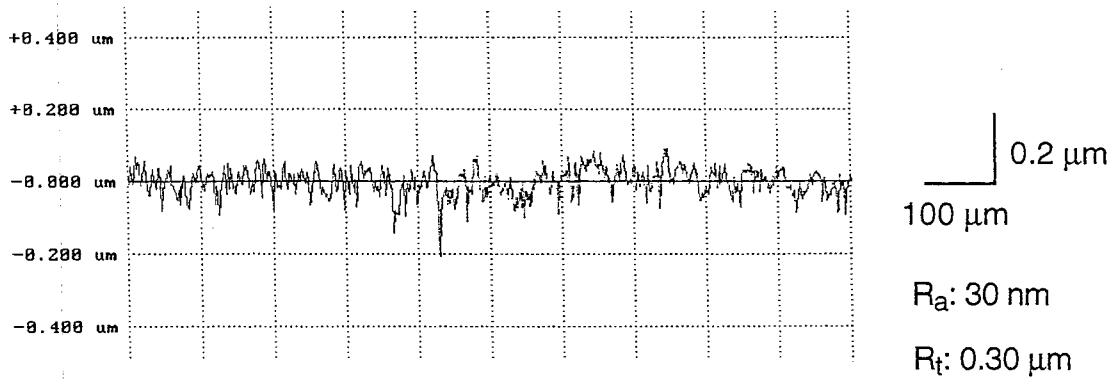


Figure 6.1 (a) Initial surface finish prepared by polishing with  $\text{B}_4\text{C}$  (1500 grit)

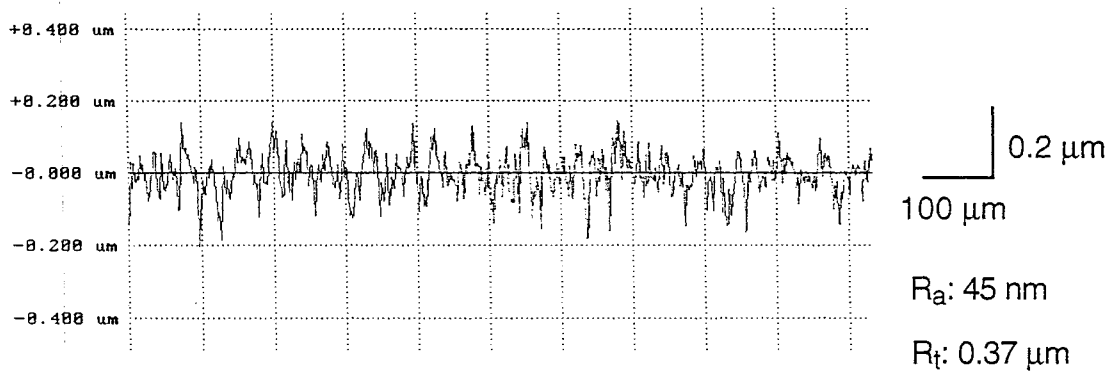


Figure 6.1 (b) Talysurf surface roughness profiles after polishing by  $\text{Al}_2\text{O}_3$

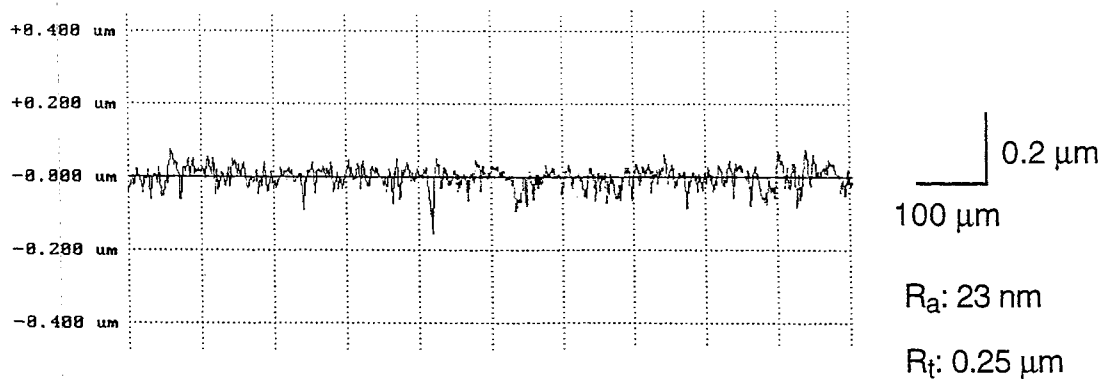


Figure 6.1 (c) Talysurf surface roughness profiles after polishing by  $\text{CuO}$

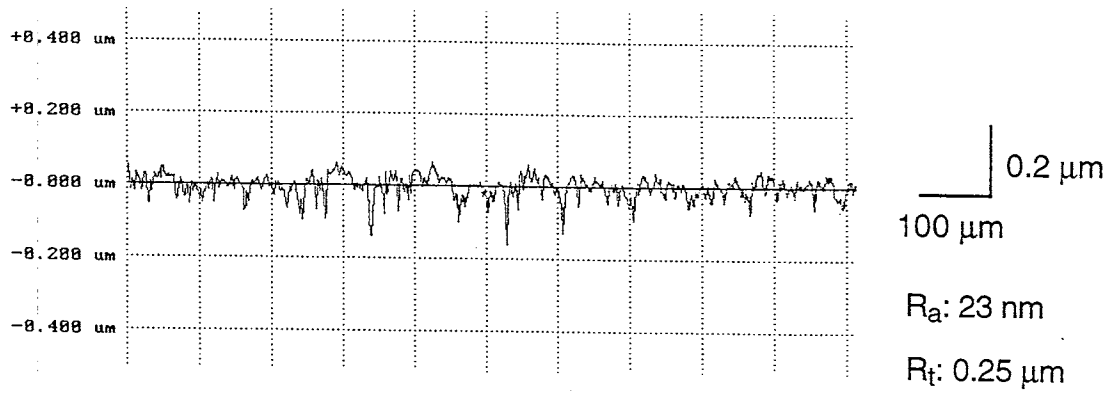


Figure 6.1 (d) Talysurf surface roughness profiles after polishing by  $\text{Y}_2\text{O}_3$

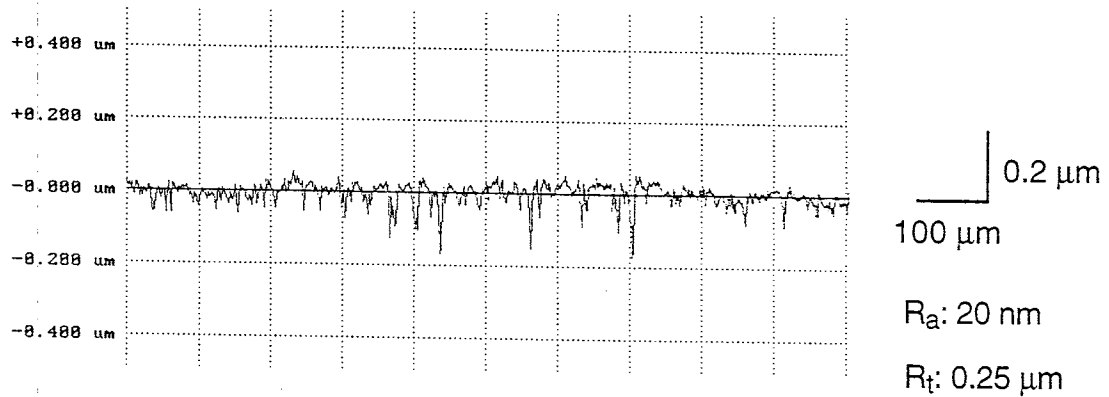


Figure 6.1 (e) Talysurf surface roughness profiles after polishing by  $\text{SiO}_2$

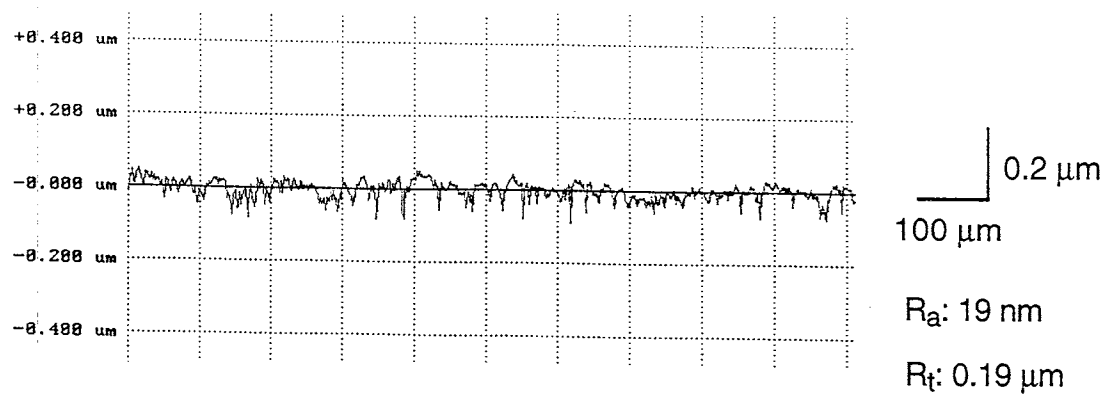


Figure 6.1 (f) Talysurf surface roughness profiles after polishing by  $\text{Mo}_2\text{O}_3$

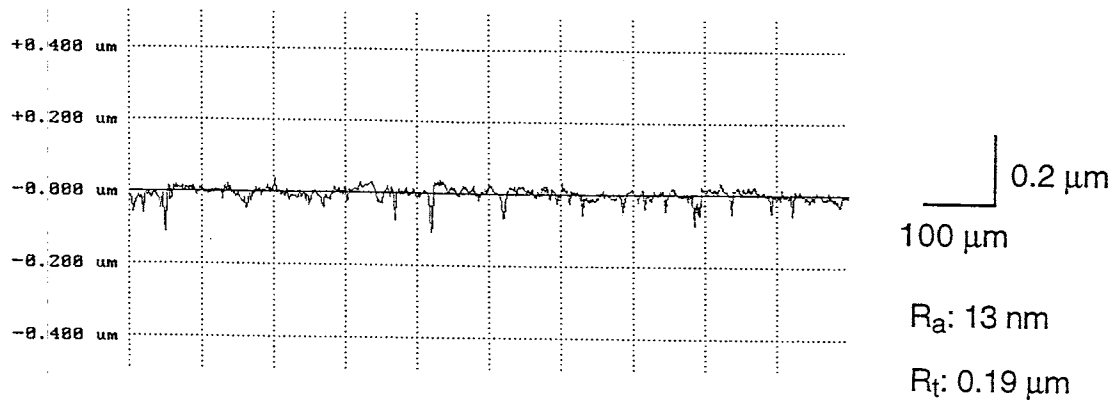


Figure 6.1 (g) Talysurf surface roughness profiles after polishing by  $\text{Cr}_2\text{O}_3$

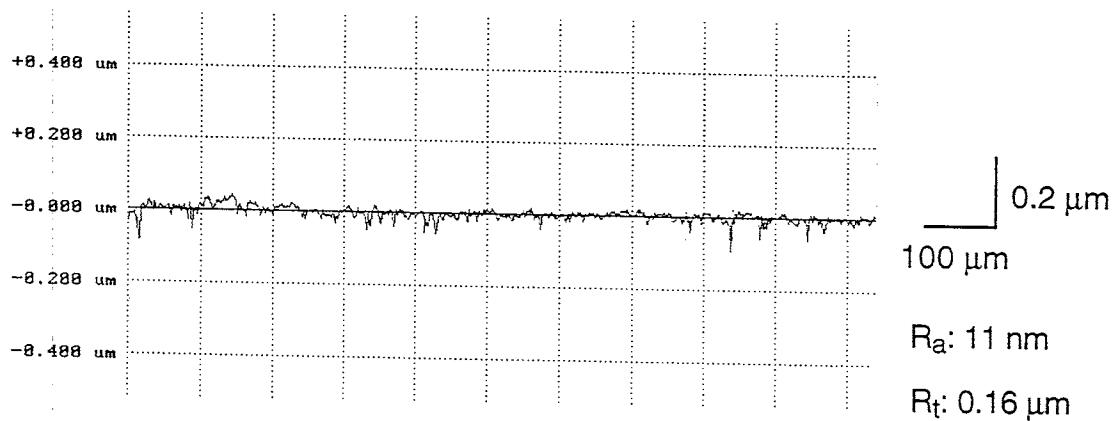


Figure 6.1 (h) Talysurf surface roughness profiles after polishing by  $\text{Fe}_2\text{O}_3$

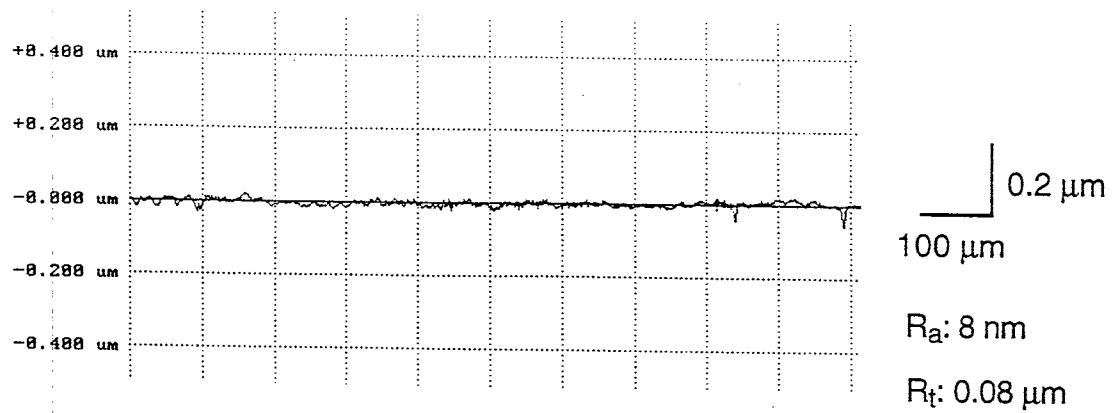


Figure 6.1 (i) Talysurf surface roughness profiles after polishing by  $\text{CeO}_2$

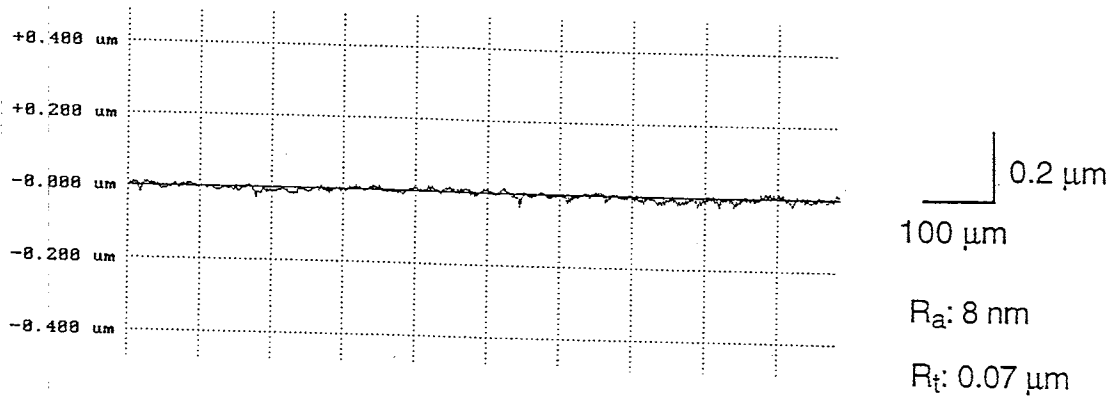


Figure 6.1 (j) Talysurf surface roughness profiles after polishing by ZrO<sub>2</sub>

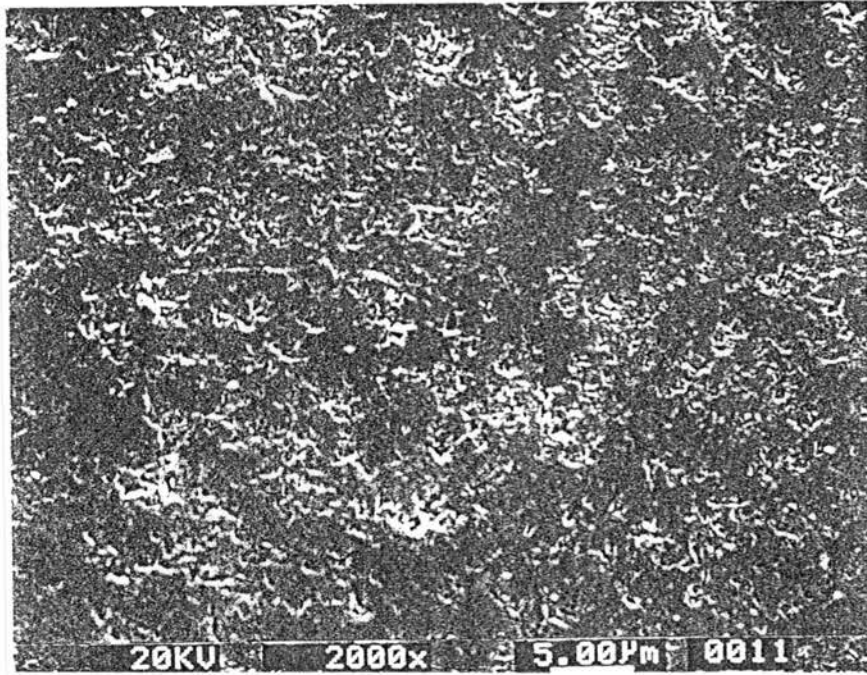


Figure 6.2 (a) SEM micrograph of the surface of a Si<sub>3</sub>N<sub>4</sub> ball finished by B<sub>4</sub>C (1500 grit)

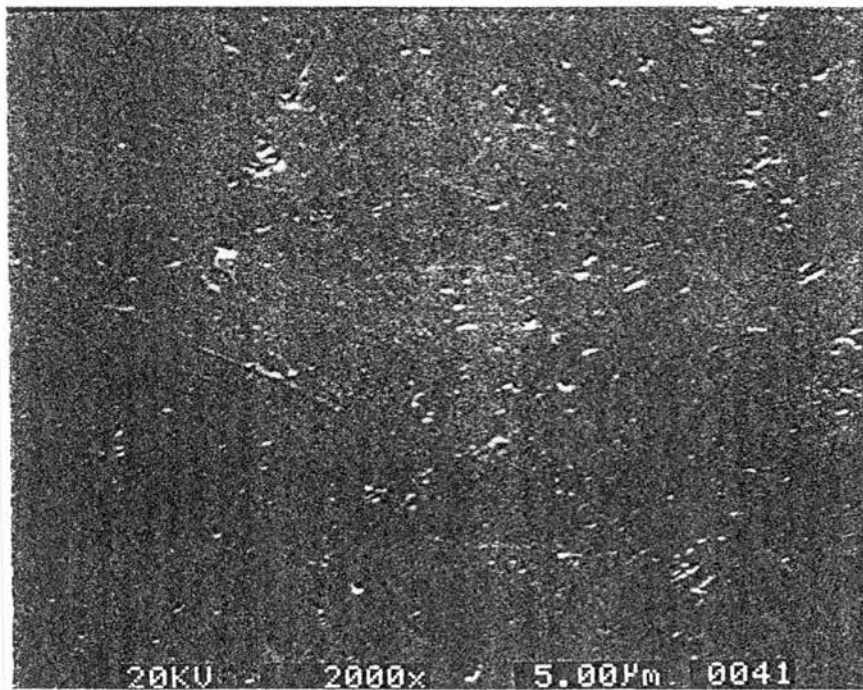


Figure 6.2 (b) SEM micrograph of the surface of a Si<sub>3</sub>N<sub>4</sub> ball finished by CeO<sub>2</sub>



Table 6.4 Surface Finish After CMP

Abrasive Type	Abrasive Size ( $\mu\text{m}$ )	Test Time (min)	Surface Finish		Effectiveness
			Ra (nm)	Rt ( $\mu\text{m}$ )	
SiC 8000	1	60	15	0.15	Excellent
ZrO <sub>2</sub>	5	120	4	0.04	
SiC 8000	1	60	15	0.15	Excellent
CeO <sub>2</sub>	5	120	4	0.03	

Table 6.5 Surface Finish After Polishing With Different Based Mag. Fluid

Abrasive Type	Mag. Fluid	Test Time (min)	Surface Finish		Effectiveness
			Ra (nm)	Rt ( $\mu\text{m}$ )	
B <sub>4</sub> C 1500	W 40	45	30	0.29	POOR
CeO <sub>2</sub> 5 $\mu\text{m}$	EMG 40	60	26	0.24	
B <sub>4</sub> C 1500	W 40	45	30	0.29	EXCELLENT
CeO <sub>2</sub> 5 $\mu\text{m}$	W 40	60	14	0.14	

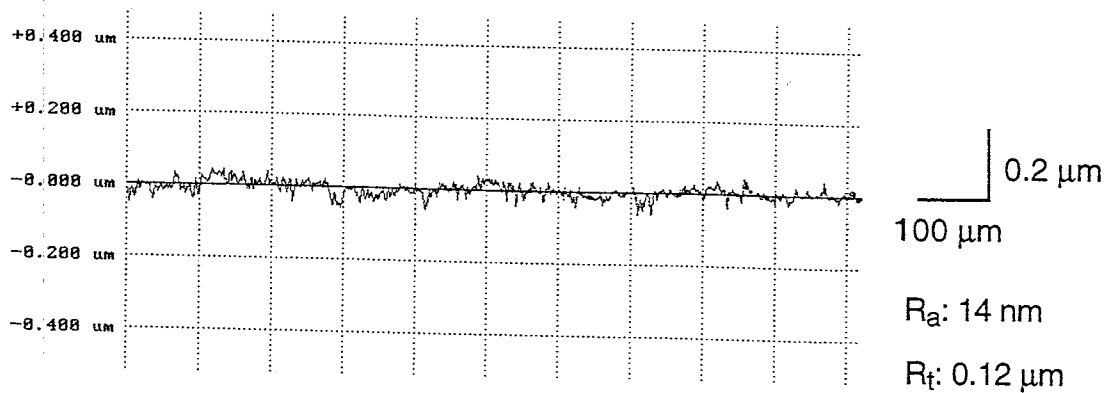


Figure 6.3 (a) Initial surface finish prepared by polishing with SiC (8000 grit)

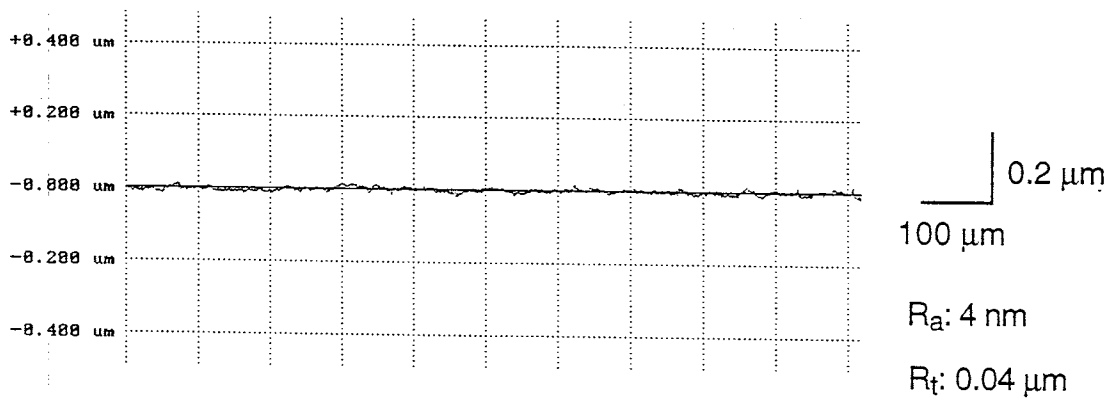


Figure 6.3 (b) Talysurf surface roughness profiles after polishing by  $\text{ZrO}_2$

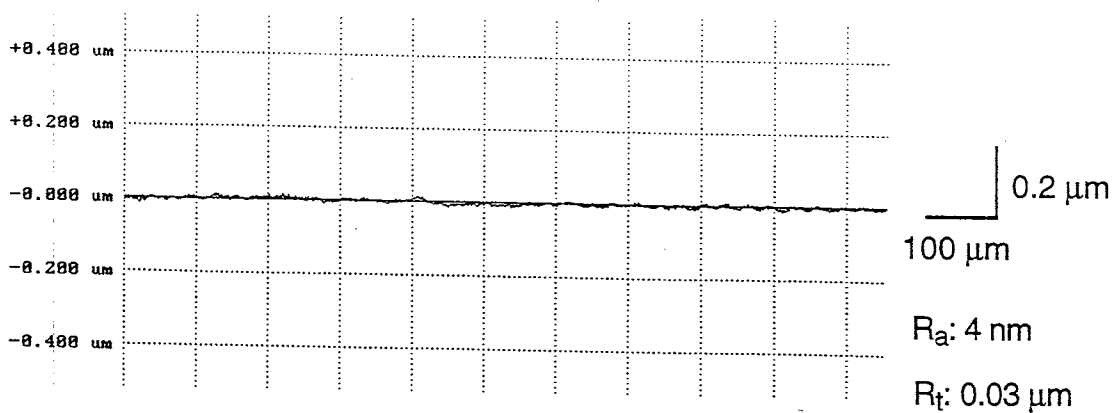


Figure 6.3 (c) Talysurf surface roughness profiles after polishing by  $\text{CeO}_2$

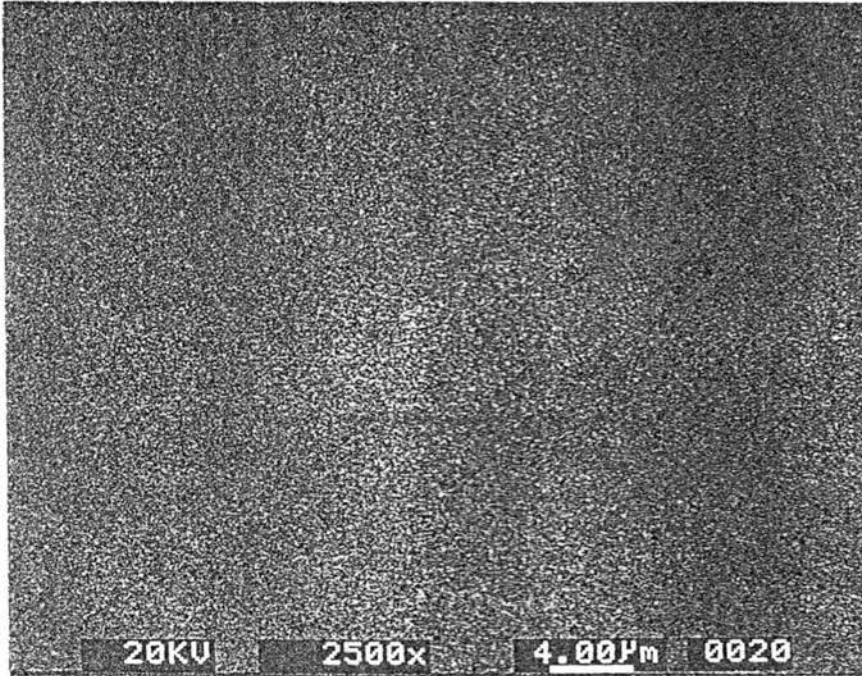


Figure 6.4 SEM micrograph of the surface of a Si<sub>3</sub>N<sub>4</sub> ball finished by SiC 8000 followed by CeO<sub>2</sub>

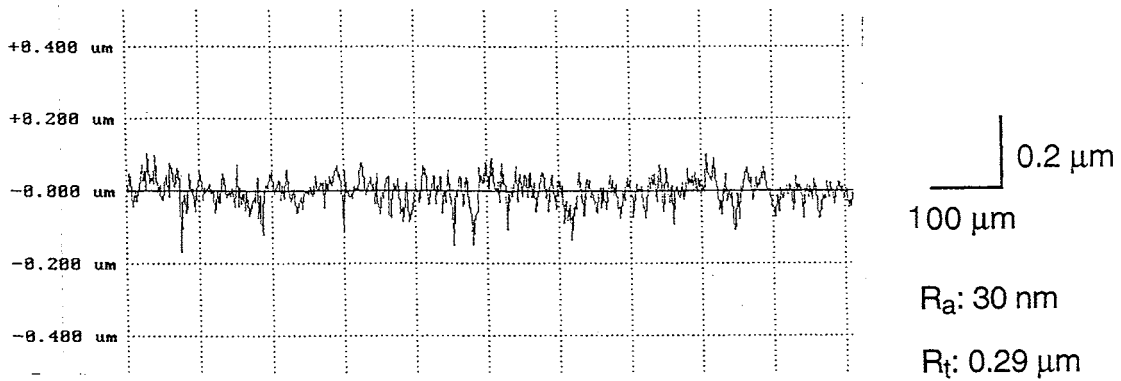


Figure 6.5 (a) Initial surface finish prepared by polishing with  $B_4C$  (1500 grit)

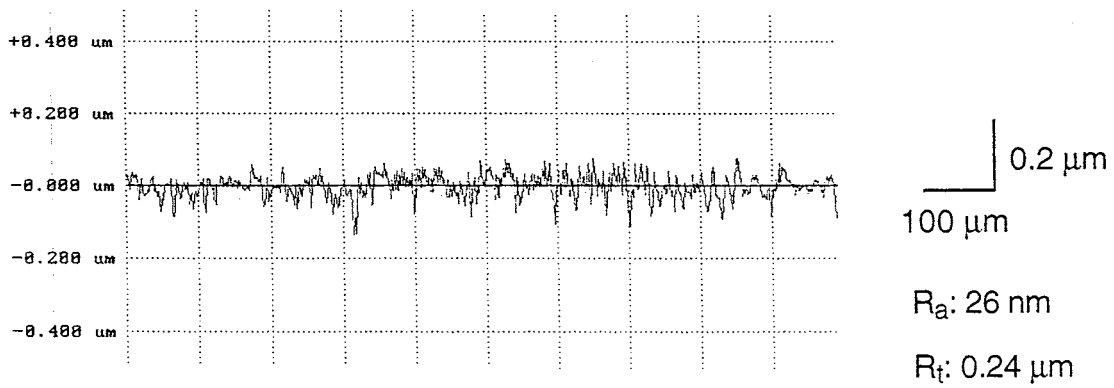


Figure 6.5 (b) Surface finish after polishing by  $CeO_2$  in an oil-based Mag. Fluid

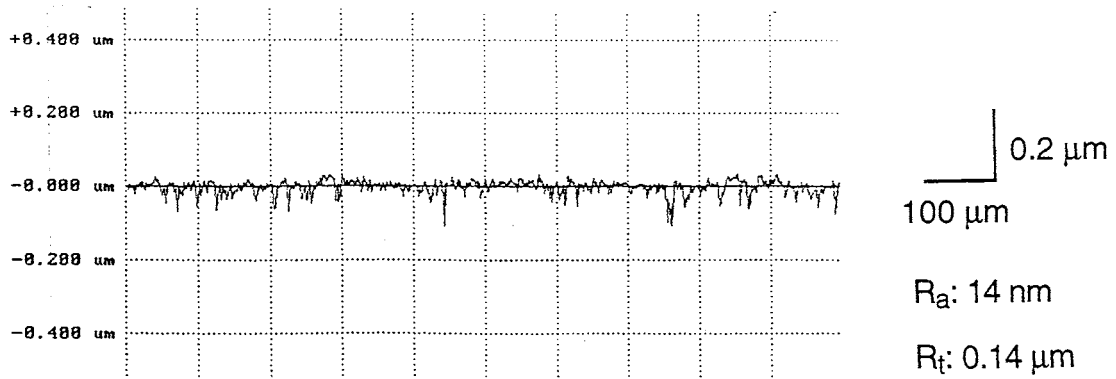


Figure 6.5 (c) Surface finish after polishing by  $CeO_2$  in a water-based Mag. Fluid

Figures 6.3 (a) - (c). Surface finish Ra of ~4 nm and Rt of ~ 40 nm were obtained both for CeO<sub>2</sub> and ZrO<sub>2</sub> abrasives. Figure 6.4 is an SEM micrograph of a Si<sub>3</sub>N<sub>4</sub> ball surface after mechanical polishing with a fine SiC abrasive (8000 grit ) (1 mm) followed by CMP with CeO<sub>2</sub> abrasive indicating extremely smooth surface with practically no surface defects. Since CeO<sub>2</sub> is significantly softer than Si<sub>3</sub>N<sub>4</sub> workmaterial, material removal by direct mechanical action would be extremely difficult, if not impossible. Therefore, the mechanism of material removal must be due to chemo-mechanical action between the abrasive, the workmaterial, and the environment. Since material is removed by the tribo-chemical action instead of mechanical fracture, extremely smooth and damage-free surface can thus be obtained.

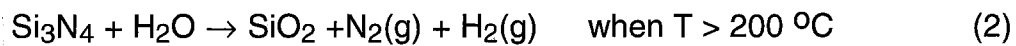
Table 6.5 gives a comparison of the average surface finish obtained from polishing of Si<sub>3</sub>N<sub>4</sub> balls by CeO<sub>2</sub> abrasive with oil-based and water-based magnetic fluid. The corresponding TalySurf surface finish profiles are shown in Figures 6.5 (a) - (c). It may be noted that there is not much improvement between the initial surface finish Figure 6.5 (a) and the finish after polishing in an oil-based magnetic fluid [Figure 6 (b)] but the surface finished in a water-based magnetic fluid [Figure 6.5 (c)] shows a significant improvement in the surface finish. It thus appears that water is essential for CMP of Si<sub>3</sub>N<sub>4</sub> workmaterial. The electrical conductivity measurements of the water-based polishing environment (water-based magnetic fluid plus CeO<sub>2</sub> abrasive) gave values of specific conductivity of 4.8 mS/cm (the current unit of specific conductivity is Seimens (S) which formerly was designated as Mho) and the concentration of the total dissolved solids, TDS of 2.4 ppt. Both the specific conductivity and the concentration of the total dissolved solids, TDS of the oil-based polishing fluid plus CeO<sub>2</sub> abrasive gave zero values. For reference, it

may be noted that the specific conductivity of good city water is 50 mS/cm. The oil film between abrasive and workmaterial may have prevented possible chemical reaction between the abrasive and the workmaterial as well as the removal of the reaction layer formed, if any, thus limiting chemo-mechanical polishing.

## 6.5 DISCUSSION OF CMP

Chemo-mechanical polishing (CMP) is particularly effective in water but in alcohols only when hydroxyl groups are present. During magnetic float polishing (MFP) of  $\text{Si}_3\text{N}_4$  in a water-based magnetic fluid, due to the presence of water environment,  $\text{NH}_3$  and  $\text{SiO}_2$  are formed.  $\text{Si}_3\text{N}_4$  can react (hydrolysis) with water from the water-based polishing fluid leading to the formation of  $\text{SiO}_2$  and  $\text{NH}_3$  (Eqn. 1). At higher temperature ( $> 200\text{ }^\circ\text{C}$ ) dissociation of  $\text{NH}_3$  into  $\text{N}_2(\text{g})$  and  $\text{H}_2(\text{g})$  may result [Jiang and Komanduri, 1997c]. Kanno and Suzuki (1983) identified the formation of  $\text{NH}_3$  during grinding of  $\text{Si}_3\text{N}_4$  powder in water, thus establishing the hydrolysis of  $\text{Si}_3\text{N}_4$ . The thermodynamic analysis presented here strongly suggests the feasibility of this reaction (Eqn. 1). Fischer and Tomizawa (1985), Tomizawa and Fischer (1987), Hah and Fischer (1995) also showed the formation of  $\text{SiO}_2$  and  $\text{NH}_3$  in tribo-chemical polishing of  $\text{Si}_3\text{N}_4$ . But the dissolution of  $\text{SiO}_2$  and  $\text{NH}_3$  (to silicic acid  $\text{Si}(\text{OH})_4$  and ammonium hydroxide  $\text{NH}_4\text{OH}$ ) as a second reaction to stimulate the continuation of tribo-chemical polishing of  $\text{Si}_3\text{N}_4$  in aqueous solutions does not seem to be thermodynamically feasible from Gibbs free energy analysis [Jiang and Komanduri, 1997c]. Silica ( $\text{SiO}_2$ ) in the amorphous state is almost insoluble or at best slightly soluble (100-150 ppm of solubility in a neutral

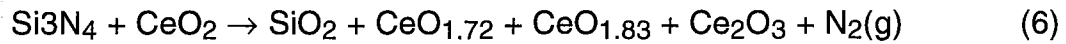
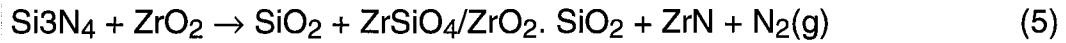
solution at room temperature) [Honda and Saito, 1996]. The effectiveness of an abrasive for CMP depends on the feasibility of chemical reaction (thermodynamic analysis) with the workmaterial and the kinetic action involving the removal of the reaction product from the workmaterial. The actual material removal in CMP will depend on the kinetic action which removes the reaction products from the interface and the chemical reaction will continue only after the passivating layers are removed.



In CMP, material removal is accomplished by chemical reaction stimulated by frictional heat and the contact pressure at the contact area between the workmaterial and the abrasive. The reaction layer is removed by subsequent mechanical action of the abrasive. Vora et al (1982) reported the feasibility of polishing  $\text{Si}_3\text{N}_4$  to a good finish by CMP with  $\text{Fe}_2\text{O}_3$  and  $\text{Fe}_3\text{O}_4$  abrasives. An oxygen rich silicon oxynitride was reported to have been formed on the polished  $\text{Si}_3\text{N}_4$  samples based on the Auger Electron Spectroscopy (AES) analysis. They concluded that oxidation is a possible mechanism causing CMP of  $\text{Si}_3\text{N}_4$ . Bhagavatula and Komanduri (1996) found that chemical reactions between  $\text{Cr}_2\text{O}_3$  and  $\text{Si}_3\text{N}_4$  occur forming chromium silicate ( $\text{Cr}_2\text{SiO}_4$ ) and chromium nitride ( $\text{CrN}$ ). This was established by analyzing the wear debris collected from polishing using a scanning electron microscope (SEM) with an energy-dispersive X-ray microanalyser (EDXA) and a low-angle X-ray diffraction (XRD) apparatus.

The following reaction products can be shown to be feasible thermodynamically based on the analysis of Gibbs free energy of formation of

the chemical reactions between the Si<sub>3</sub>N<sub>4</sub> workmaterial and various abrasives, namely, Fe<sub>2</sub>O<sub>3</sub>, Cr<sub>2</sub>O<sub>3</sub>, ZrO<sub>2</sub> and CeO<sub>2</sub> :



Here, two types of reactions are considered: 1. oxidation-reduction reaction, and 2. exchange reaction (exchange of both cationic and anionic i.e silicate, etc.). Si<sub>3</sub>N<sub>4</sub> → Si: SiO<sub>2</sub>, SiO<sub>4</sub><sup>2-</sup> and N → N<sup>3-</sup>, N<sub>2</sub>(g), NH<sub>3</sub>(g). Chemical reactions with Si<sub>3</sub>N<sub>4</sub> workmaterial are also feasible thermodynamically with Fe<sub>2</sub>O<sub>3</sub>, Cr<sub>2</sub>O<sub>3</sub>, ZrO<sub>2</sub> and CeO<sub>2</sub> abrasives and water from the water-based magnetic fluid. SiO<sub>2</sub> is the main reaction product leaving the surface of Si<sub>3</sub>N<sub>4</sub> workmaterial.

The kinetic action, which removes the reaction products from the interface is also a critical step in the CMP process. The chemical reaction can continue only after the passivating layers are removed by the subsequent mechanical action of the abrasive. It may be noted that the hardness of abrasives that are most suited for CMP of Si<sub>3</sub>N<sub>4</sub>, namely, Cr<sub>2</sub>O<sub>3</sub>, Fe<sub>2</sub>O<sub>3</sub>, ZrO<sub>2</sub> and CeO<sub>2</sub>, is close to the SiO<sub>2</sub> layer but significantly lower (i.e. Fe<sub>2</sub>O<sub>3</sub>, ZrO<sub>2</sub> and CeO<sub>2</sub>) than or close (i.e. Cr<sub>2</sub>O<sub>3</sub>) to Si<sub>3</sub>N<sub>4</sub> workmaterial. Thus, the Si<sub>3</sub>N<sub>4</sub> workmaterial can hardly be scratched, or damaged by Fe<sub>2</sub>O<sub>3</sub>, ZrO<sub>2</sub> and CeO<sub>2</sub>. Hence, SiO<sub>2</sub> reaction layers formed during chemical action are removed without damaging Si<sub>3</sub>N<sub>4</sub> workmaterial by these abrasives.



In general, the hardness for best polishing abrasive for glasses ( $\text{SiO}_2$ ) is  $\approx 7$  on the Moh's scale, which is very close to the hardness of  $\text{SiO}_2$  [Cook, 1990]. The hardness of  $\text{CeO}_2$ ,  $\text{ZrO}_2$ , and  $\text{Fe}_2\text{O}_3$  abrasives is also close to this value.  $\text{Cr}_2\text{O}_3$  (Mohs hardness 8.5) is harder compared to the hardness of the  $\text{Si}_3\text{N}_4$  workmaterial for CMP. Wallace et al [1996] investigated the CMP of  $\text{SiO}_2$  thin films using X-ray reflectivity. They concluded that stress-corrosion mechanism may be responsible whereby the stress induced by the abrasion of abrasive particle in water strains the bonds in the  $\text{SiO}_2$  thin films. The polished material shows an increased density in the near-surface region. The compaction of the  $\text{SiO}_2$  network leads to enhanced dissolution of  $\text{SiO}_2$  into the polishing slurry and an extremely smooth surface.

It can be seen from above results that the most effective abrasives for polishing  $\text{Si}_3\text{N}_4$  workmaterial are  $\text{CeO}_2$  and  $\text{ZrO}_2$  following by  $\text{Fe}_2\text{O}_3$  and  $\text{Cr}_2\text{O}_3$ . The pH of the polishing slurry used here (abrasives+water-based ferrofluid) ranges from 6 to 6.4 for all the abrasives used; for example the pH of  $\text{ZrO}_2$  + ferrofluid is  $\sim 6$  and for  $\text{CeO}_2$  + ferrofluid is  $\sim 6.2$  except for  $\text{MoO}_2$  which has a pH of  $\sim 5$ . It is found that  $\text{SiO}_2$  abrasive has minimal polishing ability for  $\text{Si}_3\text{N}_4$  in the pH range of 6 [Figure 2(e)]. Also, the hardness of the most effective abrasives are  $\text{CeO}_2$ : Mohs 6,  $\text{ZrO}_2$ : Mohs 8,  $\text{Fe}_2\text{O}_3$ : Mohs 6, and  $\text{Cr}_2\text{O}_3$ : Mohs 8.5. These hardness values are closer to the  $\text{SiO}_2$  reaction layer which has a Mohs hardness of  $\sim 7$ . It is somewhat coincidental that in general the chemical effectiveness and the mechanical hardness of abrasives for polishing *glass*, is also  $\approx 6.5$  Mohs which is close to the hardness of glass ( $\sim$  Mohs 7).

There are other similarities between polishing  $\text{Si}_3\text{N}_4$  workmaterial and polishing glass including the role of water. Cook (1990) after a careful review

and analysis of literature concluded that the best abrasives for polishing glasses are  $\text{CeO}_2$  following by  $\text{ZrO}_2$ ,  $\text{ThO}_2$ ,  $\text{TiO}_2$  and  $\text{Fe}_2\text{O}_3$  in the pH range 7-9 and that  $\text{SiO}_2$  abrasive has little polishing ability for finishing glasses except at very high pH (~ 12-14) values. This is not altogether surprising as the material removal mechanism in the case of  $\text{Si}_3\text{N}_4$  is through the formation of  $\text{SiO}_2$  and in the case of glasses it is naturally  $\text{SiO}_2$ . A similar mechanism may be applicable for the polishing of silicon wafers with  $\text{CeO}_2$ ,  $\text{ZrO}_2$ , and  $\text{Fe}_2\text{O}_3$  in a water-based solution which are effective abrasives for polishing  $\text{Si}_3\text{N}_4$  ceramics and  $\text{SiO}_2$  glasses. So, it is not too surprising to note that the first mirror finished silicon wafers used for integrated circuits were polished with  $\text{CeO}_2$  and  $\text{Fe}_2\text{O}_3$  [Abe, 1991]. Currently, the most widely used abrasive for polishing silicon wafers is colloidal silica, i.e. nanocrystalline  $\text{SiO}_2$  particles in an alkaline (KOH) solution (pH 10). This combination has an advantage of little or no decomposition on the surface of silicon wafers which has a natural oxidation layer of  $\text{SiO}_2$  in air at room temperature. For epitaxial growth, the surface layer and subsurface lattice structure of the semiconducting wafers are required to be free of any chemical change or sub-surface damage in the form of dislocation tangles. This is not the case with glasses and advanced ceramics ( $\text{Si}_3\text{N}_4$ ) for optical and mechanical applications. However,  $\text{SiO}_2$  layer on a silicon substrate is an excellent insulator and can be used for isolation and passivation purposes which is an advantage for Si for electronic application.

It is possible that an outer layer of  $\text{SiO}_2$  and an intermediate siliconoxynitride may form between  $\text{SiO}_2$  thin layer and  $\text{Si}_3\text{N}_4$  substrate. The oxide scale on MgO uniaxially pressed  $\text{Si}_3\text{N}_4$  forms in layers composed of amorphous and crystalline  $\text{SiO}_2$ ,  $\text{Si}_2\text{N}_2\text{O}$ , and  $\text{MgSiO}_3$  ( $\text{MgO} \cdot \text{SiO}_2$ , from 1 wt.% MgO sintering additive) [Tighe, 1982; Singhal, 1976; Lange, 1979]. It is notable

that  $\text{Si}_3\text{N}_4$  is easily oxidized in an oxygen-containing atmosphere [Ruhle, 1997]. As a result, the surface of  $\text{Si}_3\text{N}_4$  is always covered with a thin silica layer. CMP does not produce a layer that is chemically different from the natural oxidation layer formed in air at room temperature on the  $\text{Si}_3\text{N}_4$  substrate [Jiang and Komanduri, 1997c]. It has been shown in this investigation that several not-so-hard oxides, such as  $\text{CeO}_2$  and  $\text{ZrO}_2$  followed by  $\text{Fe}_2\text{O}_3$  and  $\text{Cr}_2\text{O}_3$  etc are effective abrasives for CMP of  $\text{Si}_3\text{N}_4$  material. This is because of the thermodynamic feasibility of chemical reactions between the abrasive and the  $\text{Si}_3\text{N}_4$  workmaterial but also due to the subsequent kinetic action of removing the reaction products from the surface of the  $\text{Si}_3\text{N}_4$  workmaterial.

In this chapter chemo-mechanical polishing (CMP) studies were conducted using various abrasives to investigate their relative effectiveness in the finishing of uniaxially pressed  $\text{Si}_3\text{N}_4$  bearing balls by magnetic float polishing (MFP) technique. CMP depends both on the chemical and the mechanical effectiveness of the abrasive and the environment with respect to the workmaterial. Among the abrasives investigated for CMP of  $\text{Si}_3\text{N}_4$  balls,  $\text{CeO}_2$  and  $\text{ZrO}_2$  were found to be most effective followed by  $\text{Fe}_2\text{O}_3$  and  $\text{Cr}_2\text{O}_3$ . Extremely smooth and damage-free  $\text{Si}_3\text{N}_4$  bearing ball surfaces with a finish  $R_a$  of  $\approx 4$  nm and  $R_t$  of  $\approx 40$  nm were obtained after polishing with either  $\text{CeO}_2$  or  $\text{ZrO}_2$ . Thermodynamic analysis (Gibbs free energy of formation) indicated the feasibility of the formation of  $\text{SiO}_2$  layer on the surface of the  $\text{Si}_3\text{N}_4$  balls with these abrasives. This is particularly so in a water environment which facilitates chemo-mechanical interaction between abrasive and workmaterial by participating directly in the chemical reaction leading to the formation of a softer  $\text{SiO}_2$  layer. Since the hardness of some of the abrasives which were found to be most effective in CMP, namely,  $\text{CeO}_2$ ,  $\text{ZrO}_2$ , and  $\text{Fe}_2\text{O}_3$  is closer to that of

SiO<sub>2</sub> layer but significantly lower than the hardness of the Si<sub>3</sub>N<sub>4</sub> workmaterial, removal of the SiO<sub>2</sub> reaction layer effectively without scratching and/or damaging the Si<sub>3</sub>N<sub>4</sub> substrate is facilitated by the subsequent mechanical action of the abrasives. The chemical reaction would proceed on a continuing basis only if the passivating layers are removed continuously by subsequently mechanical action. It is found that the CMP ability in an oil-based polishing environment was found to be rather limited. A mechanism similar to the CMP of Si<sub>3</sub>N<sub>4</sub> may be applicable to the polishing of silicon wafers, various glasses, and SiC due to similarities in the material removal processes.

## CHAPTER 7

### ON THE CHEMO-MECHANICAL POLISHING (CMP) OF Si<sub>3</sub>N<sub>4</sub> WITH WATER-BASED CeO<sub>2</sub> SLURRY

#### 7.1 INTRODUCTION

Among various abrasives investigated for the chemo-mechanical polishing (CMP) of Si<sub>3</sub>N<sub>4</sub> balls, cerium oxide (CeO<sub>2</sub>) was found to be the most effective polishing medium (superior than Cr<sub>2</sub>O<sub>3</sub> which was considered as the most effective abrasive from literature review) yielding an extremely smooth and damage-free surface with a finish R<sub>a</sub> of 4 nm and R<sub>t</sub> of 40 nm. Also, after investigating various reaction species in the CMP of Si<sub>3</sub>N<sub>4</sub> with CeO<sub>2</sub> and Cr<sub>2</sub>O<sub>3</sub>, the former is found to be much safer from an environmental point of view. CeO<sub>2</sub> has two important functions in CMP of Si<sub>3</sub>N<sub>4</sub>: (1) It participates directly in the chemical reaction (oxidization-reduction reaction) with Si<sub>3</sub>N<sub>4</sub> workmaterial leading to the formation of a SiO<sub>2</sub> layer; (2) It can remove the SiO<sub>2</sub> reaction layer effectively without damaging the Si<sub>3</sub>N<sub>4</sub> substrate as no abrasion can take place in subsequent mechanic action of CeO<sub>2</sub> on Si<sub>3</sub>N<sub>4</sub> because of the hardness of CeO<sub>2</sub> is closer to that of SiO<sub>2</sub> layer on top of Si<sub>3</sub>N<sub>4</sub> and significantly lower than Si<sub>3</sub>N<sub>4</sub> workmaterial (about 1/3). CeO<sub>2</sub> is found to be very effective in a water environment. The chemical reaction between the Si<sub>3</sub>N<sub>4</sub> workmaterial and the water environment (hydrolysis) also leads to the formation of SiO<sub>2</sub> layer thereby enhancing the CMP of Si<sub>3</sub>N<sub>4</sub>. In this chapter, thermodynamic feasibility of the chemical reactions formed between the CeO<sub>2</sub> abrasive and Si<sub>3</sub>N<sub>4</sub> workmaterial is investigated based on Gibb's free energy change. The flash temperature generated and the flash duration at the contact

zone of the polishing process was calculated using the models developed by Hou and Komanduri [1998a,b]. This is used for the thermodynamic analysis of the chemical reactions during CMP. The CMP mechanism for polishing  $\text{Si}_3\text{N}_4$  with  $\text{CeO}_2$  abrasives is presented based on thermodynamic and kinetic analyses.

## **7.2 CERIUM OXIDE ( $\text{CeO}_2$ ) ABRASIVE**

Chemo-mechanical action is very specific and proper choice of the abrasive and the environment should be made for a given workmaterial. Both thermodynamics and kinetics play an important role on the rates of chemical reactions. Once the reaction product is formed it is removed from the workmaterial in subsequent mechanical action by the abrasive. Since material removal by this mechanism does not depend on the hardness but on the chemical potentials, it is possible to remove material by abrasives substantially softer than the workmaterial. Theoretically any abrasive that can react with the workmaterial in a given environment and form a reaction product can be used for chemo-mechanical polishing. However, some abrasives may be harder than the workmaterial and the mechanical action may dominate over chemo-mechanical action. Material removal by mechanical action may be satisfactory in roughing, or even semi-finishing but in the final finishing operation it is preferable to minimize the mechanical action that can affect the surface integrity. This is precisely the reason why diamond abrasive was not considered in this investigation for finishing  $\text{Si}_3\text{N}_4$  balls. Similarly, some abrasives react with a given workmaterial much more than others. For efficient removal of material, those with the highest reactions rates would be preferable for chemo-mechanical polishing (CMP).

It is well known that cerium oxide is an efficient polishing agent for glass. It is also known that the fluid medium in which it is used is also very critical. For example, when polishing glass,  $\text{CeO}_2$  is particularly effective in water and in alcohols only when hydroxyl groups are present. Thus cerium oxide slurry in water is invariably used for polishing. The oxide contains polyvalent cerium atoms,  $\text{Ce(IV)}$  and  $\text{Ce(III)}$ , which can provide chemical action with the workmaterial. It appears that when  $\text{Ce(OH)}_4$ , i.e.  $\text{CeO}_2 \cdot 2 \text{H}_2\text{O}$  is precipitated fresh, i. e. *in situ*, in the polishing slurry form, a soluble  $\text{Ce(IV)}$  salt is probably involved in an equilibrium reaction :  $\text{SiO}_2 + \text{Ce(OH)}_4 \rightarrow \text{CeO}_2 + \text{Si(OH)}_4$ . The breaking and reforming of Si-O bonds is perhaps aided by the transfer of OH groupings to incipient fracture sites by a transport mechanism using the relatively large and mobile coordination sphere around oxophilic cerium atom [Kilbourn, 1992].

$\text{CeO}_2$  may react chemo-mechanically with both silicon nitride base material as well as the glassy phase that holds silicon nitride particles together. Cerium is the most abundant elements of the rare earths and ranks around 25th in the listing of abundance in the earth's crust of all the naturally occurring elements. So, Ce is not particularly rare as compared to Ni or Cu. Cerium oxide has a high melting temperature (2750 K) but is a very soft material (Mohs hardness: 5-6) and hence cannot scratch  $\text{Si}_3\text{N}_4$ . Ce ions are present in two stable valence states, namely, the tetravalent  $\text{Ce}^{4+}$  (Ceric) and the trivalent  $\text{Ce}^{3+}$  (Cerous). The tetravalent ceric ion is a strong oxidizing agent but can be reduced by ferrous salts, hydrogen peroxide. When associated with oxygen, it is completely stable as  $\text{CeO}_2$ .  $\text{Ce}_2\text{O}_3$  is unstable in air, water, and the like and readily converts to  $\text{CeO}_2$ . Ceria has the  $\text{CaF}_2$  structure with 8-coordinate cations and 4-coordinate anions. It can be visualized as a close-packed cubic

array of metal atoms with oxygen filling all the tetrahedral holes. Ceria has been tested for acute effects and found to have very low toxicity [Kilbourn, 1992]. Hence, its use is safe from an environmental point of view.

### **7.3 CMP OF Si<sub>3</sub>N<sub>4</sub> WITH WATER-BASED CeO<sub>2</sub> SLURRY**

The chemical composition and the mechanical and thermal properties of NBD 200 HIP'ed Si<sub>3</sub>N<sub>4</sub> balls (supplied by CERBEC) used in this investigation have been shown in chapter 4. The sintering aid is about 1 wt.% MgO. Major impurity is Fe<sub>2</sub>O<sub>3</sub>. Table 7.1 shows the properties of CeO<sub>2</sub> polishing medium. The Si<sub>3</sub>N<sub>4</sub> balls are initially polished with a SiC #8000 (1 mm) abrasive prior to CMP. The polishing conditions are listed in Table 7.2. The pH value of polishing solution [a water-based magnetic fluid (W-40) plus 10 vol.% CeO<sub>2</sub> polishing media is ≈ 6.

Thermodynamic analysis (Gibb's free energy change) was conducted to determine the nature of the reaction products as well as whether such reactions are thermodynamically feasible. For a reaction to occur spontaneously at a given temperature and pressure:  $\Delta G < 0$ . Equilibrium Composition and  $\Delta G$  are calculated using Outokumpu HSC Chemistry Software. A CMP mechanism for polishing Si<sub>3</sub>N<sub>4</sub> balls with CeO<sub>2</sub> will be presented in the following based on thermodynamic and kinetic analysis. A Gibb's free energy change analysis is performed here to determine whether a reaction is spontaneous. It is known, if a reaction is exothermic (Enthalpy change  $\Delta H < 0$ ) and results in increased disorder or randomness (Entropy change  $\Delta S > 0$ ), it will occur spontaneously.



Table 7.1 Properties of CeO<sub>2</sub> Polishing Medium

PROPERTY	VALUE
Hardness, Mohs	6
Density, g/cm <sup>3</sup>	7.13
Elastic Modulus, GPa	165
Poisson's Ratio	0.5
Thermal Conductivity at 100°C, W/m-K	8.4
Thermal Conductivity at 1000°C, W/m-K	0.8

Table 7.2 Test Conditions

Workmaterial	HIP'ed Si <sub>3</sub> N <sub>4</sub> balls (CERBEC) Diameter: 12.7 mm (0.5 inch) Initial Sphericity: 1 μm Initial Finish: Ra=20 nm
Abrasive Concentration	10% by volume
Polishing Load	1.2 N per ball
Polishing Speed	2000 rpm
Magnetic Fluid	Water-based (W-40) Saturation Magnetization at 25 °C : 400 Gauss Viscosity at 27 °C : 25 Cp

However, if one makes a spontaneous contribution and the other makes a nonspontaneous contribution, the relative magnitude of the two contributions determines whether the reaction is spontaneous:  $\Delta G = \Delta H - T \Delta S$ . For a reaction that occurs at constant temperature and pressure: it is spontaneous when  $\Delta G < 0$  for the reaction. The  $\Delta G$ , free energy change is a direct measure of the tendency of a reaction to proceed. It is also called the driving force of the reaction.

Figures 7.1 (a) and (b) are SEM micrograph and Form TalySurf profile of a  $\text{Si}_3\text{N}_4$  ball surface finished by  $\text{Cr}_2\text{O}_3$ , respectively. From the SEM micrograph [Figure 7.1 (a)], it can be seen that while some areas of the surface are very smooth, there are many fine scratches and some pits. The surface finish values obtained by FormTalySurf are  $R_a = 10.7 \text{ nm}$  and  $R_t = 0.149 \text{ }\mu\text{m}$ . A plausible reason for the observed roughness with  $\text{Cr}_2\text{O}_3$  abrasive, in spite of its chemo-mechanical polishing ability is its higher hardness.

Figure 7.2(a) is an SEM micrograph of a  $\text{Si}_3\text{N}_4$  ball surface after polishing with  $\text{CeO}_2$  ( $5 \text{ }\mu\text{m}$ ) showing essentially a smooth surface with no pits, or scratches, or cracks. The corresponding Talysurf surface finish profile [Figures 7.2 (b)] shows a surface finish  $R_a$  of  $4 \text{ nm}$  and  $R_t$  of  $40 \text{ nm}$  (ISO: cut-off  $0.25 \text{ mm}$ , evaluation length  $6 \times 0.25 \text{ mm}$ , ISO 2CR Filter). This is attributed to the use of effective and significantly softer  $\text{CeO}_2$  abrasive which will not scratch  $\text{Si}_3\text{N}_4$  in the polishing but preferably involves in CMP.

Based on the moving disc heat source model developed by Hou and Komanduri, (1998 a,b), the temperature field and flash temperatures generated at the contact zone in magnetic float polishing (MFP) with  $\text{CeO}_2$  (elastic modulus:  $180 \text{ GPa}$ , thermal conductivity:  $0.02 \text{ cal/cm.sec.}^\circ\text{c}$ ) are calculated as

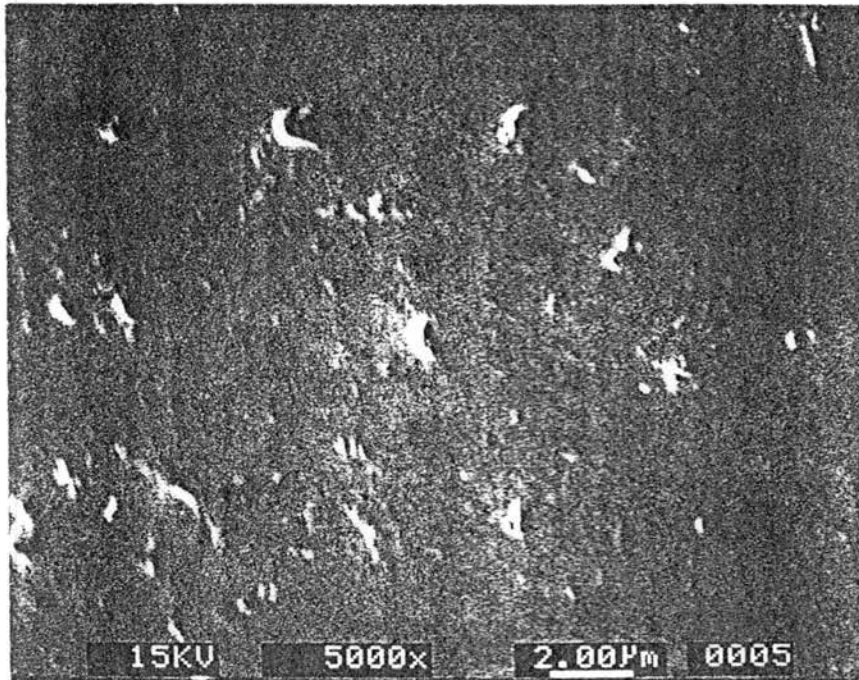


Figure 7.1 (a) SEM micrograph of a  $\text{Si}_3\text{N}_4$  ball surface after finished by  $\text{Cr}_2\text{O}_3$

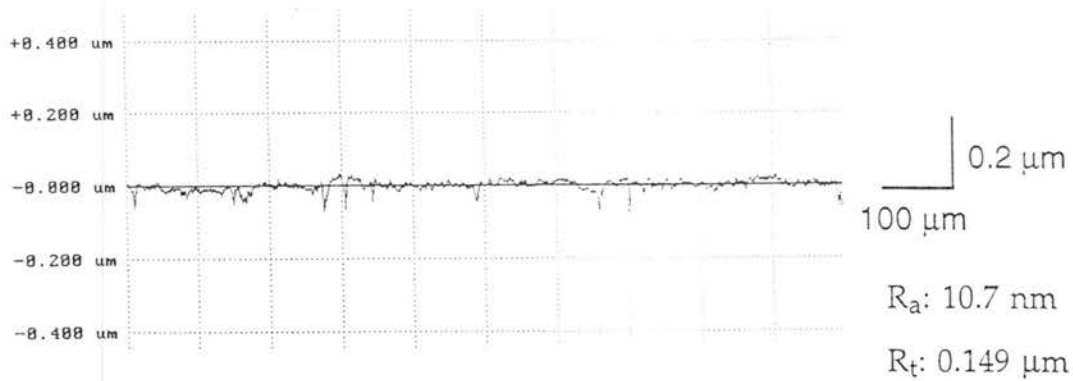


Figure 7.1 (b) Talysurf surface roughness profile of a  $\text{Si}_3\text{N}_4$  ball surface after finished by  $\text{Cr}_2\text{O}_3$

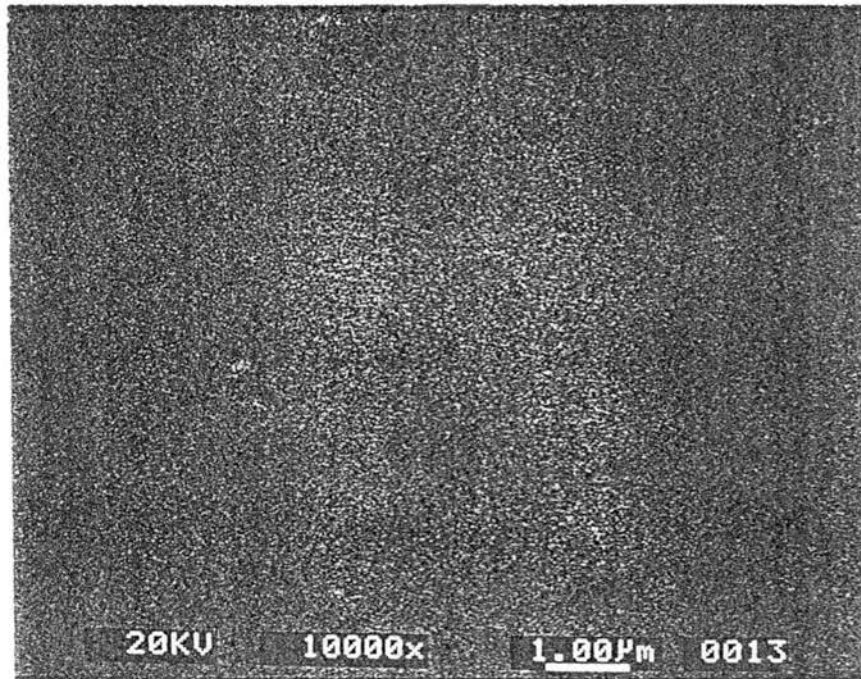


Figure 7.2 (a) SEM micrograph of a  $\text{Si}_3\text{N}_4$  ball surface after finished by  $\text{CeO}_2$

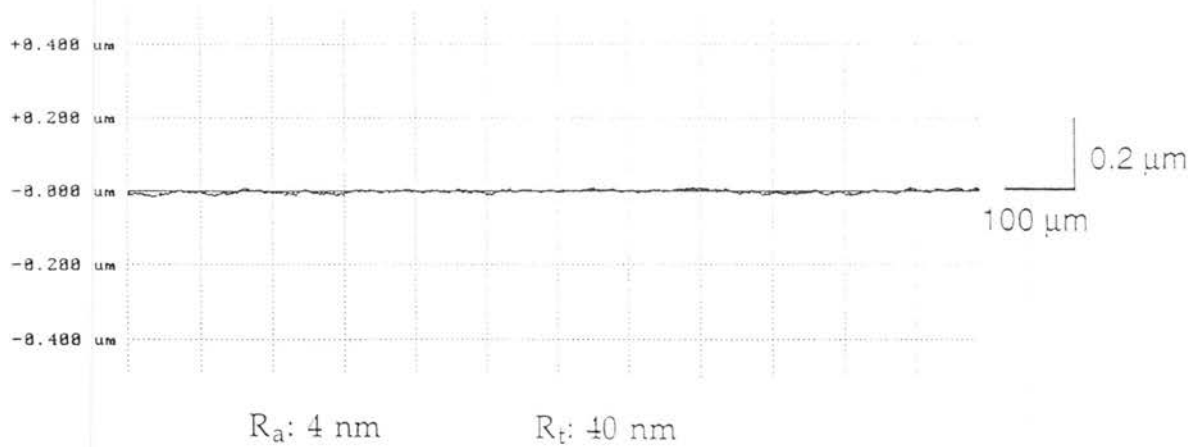


Figure 7.2 (b) Talysurf surface roughness profile of a  $\text{Si}_3\text{N}_4$  ball surface after finished by  $\text{CeO}_2$

shown in Figure 7.3. The related flash times at the area of contact under the polishing conditions are given in Table 7.3. It can be seen that the minimum possible flash temperatures generated and the corresponding flash times are adequate for the generation of specific reactions, such as oxidation, hydrolysis and exchange as shown in following thermodynamic reaction analysis. It is known that for a reaction to occur spontaneously at a given temperature T, the Gibbs free energy change,  $\Delta G$  should be negative.

Table 7.3 Flash Time For Different Flash Temperature  
( $v= 4$  m/sec,  $W =1.2$  N/ball)

Flash Temperature, °C	> 100	> 200	> 300	> 400	> 600	> 800	> 1000
Flash Time, $\mu$ sec	2.2	1.1	0.8	0.6	0.4	0.3	0.2

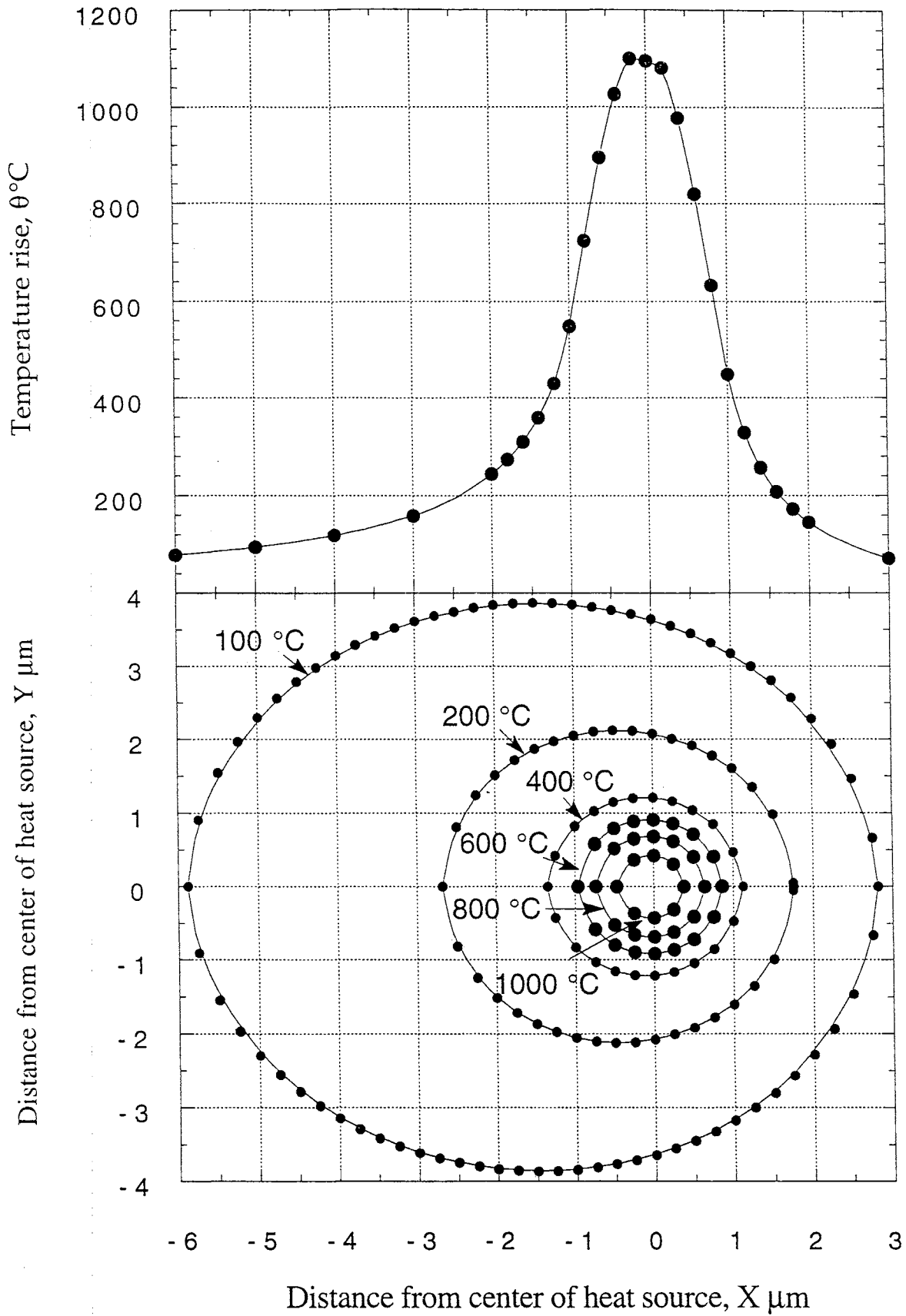


Figure 7.3 (a) Calculated temperature rise on the surface along the X-axis

(b) Isotherms of temperature on the work surface ( $W = 1.25 \text{ N}/\text{ball}$ ,  $v = 4 \text{ m}/\text{sec}$ )

## 7.4 THERMODYNAMIC ANALYSIS OF CMP

It is well known that  $\text{Si}_3\text{N}_4$  can be readily oxidized in an oxidizing atmosphere. As a result, the surfaces of the as-received HIP'ed  $\text{Si}_3\text{N}_4$  balls are invariably covered with a thin layer of silica (see Eqn. 1 in the following Table). For a reaction to occur spontaneously at a given temperature,  $T$ , the Gibbs free energy change,  $\Delta G$  should be negative. In the equations that follow, various chemical reactions of interest, the temperature under consideration,  $T$  (from 0-1000 °C), and the corresponding free energy change,  $\Delta G$  are given.

$\text{Si}_3\text{N}_4 + 3\text{O}_2(\text{g}) = 3\text{SiO}_2 + 2\text{N}_2(\text{g}) \quad (1)$								
T (°C)	0	100	200	300	400	600	800	1000
$\Delta G$ (kcal)	-460.7	-455.4	-450.3	-445.2	-440.2	-430.6	-421.3	-412.4

It may be noted that during the mechanical polishing of  $\text{Si}_3\text{N}_4$  (i. e. prior to CMP) by a harder abrasive, such as SiC and  $\text{B}_4\text{C}$ , the silica surface layer along with a portion of  $\text{Si}_3\text{N}_4$  is removed by brittle fracture or abrasion, thus exposing the base  $\text{Si}_3\text{N}_4$ . In subsequent CMP,  $\text{Si}_3\text{N}_4$  can react with water (hydrolysis) (from the water-based magnetic fluid) leading to the formation of  $\text{SiO}_2$  and  $\text{NH}_3$  (Eqn. 2). Figure 7.4 (a) shows the variation of the mole fraction of various species with temperature at equilibrium based on the thermodynamic calculations of the chemical reaction system consisting of 1 mol of  $\text{Si}_3\text{N}_4$  and 1 mol of  $\text{H}_2\text{O}$ . It can be seen from the figure that at low temperatures (< 300 °C),  $\text{NH}_3(\text{g})$  formation is promoted while at higher temperatures,  $\text{H}_2(\text{g})$  and  $\text{N}_2(\text{g})$  gases are evolved. The  $\text{SiO}_2$  mole fraction as well as  $\text{Si}_3\text{N}_4$  mole fraction, however, seems to be somewhat independent of temperature indicating very little effect, if any, of temperature on the removal rate under these conditions.

Figure 7.4 (b) shows the variation of various chemical species with temperature for 1 mol of Si<sub>3</sub>N<sub>4</sub> and increasing amounts of H<sub>2</sub>O. It can be seen that with increase in the mole fraction of H<sub>2</sub>O, the amount of SiO<sub>2</sub> increases and the amount of Si<sub>3</sub>N<sub>4</sub> correspondingly decreases both accounting for an increase in the material removal due to chemo-mechanical polishing. This shows the beneficial role of H<sub>2</sub>O in CMP. In a similar manner, NH<sub>3</sub>(g), H<sub>2</sub>(g), and N<sub>2</sub>(g) gases also increase with increase in the mole content of H<sub>2</sub>O, as can be anticipated.

Si <sub>3</sub> N <sub>4</sub> + 6H <sub>2</sub> O = 3SiO <sub>2</sub> + 4NH <sub>3</sub> (g) (2)								
T (°C)	0	100	200	300	400	600	800	1000
ΔG (kcal)	-132.7	-140.9	-147.4	-152.6	-156.4	-159.8	-156.9	-146.5

2NH <sub>3</sub> (g) = N <sub>2</sub> (g) + 3H <sub>2</sub> (g) (3)								
T (°C)	0	100	200	300	400	600	800	1000
ΔG (kcal)	9.02	4.28	-0.88	-6.14	-11.53	-22.53	-33.71	-44.96

Eqn. 3 shows that at low temperatures, ΔG is positive indicating the unlikelihood of dissociating NH<sub>3</sub>(g) as N<sub>2</sub>(g) and H<sub>2</sub>(g). Thus NH<sub>3</sub> formation is possible in CMP only when temperature rise at the contact surface is <300 °C [Eqn. 2 and Figure. 3]. Further increase in temperature may result in the dissociation of NH<sub>3</sub> into N<sub>2</sub>(g) and H<sub>2</sub>(g) [Eqn.3 and Figure 3].

It has been reported in the literature, the formation of Si(OH)<sub>4</sub> and NH<sub>4</sub>OH as secondary products due to the reaction between NH<sub>3</sub> (g) and H<sub>2</sub>O, and between SiO<sub>2</sub> and H<sub>2</sub>O in the CMP of Si<sub>3</sub>N<sub>4</sub> (Hah et al, 1996). It can be seen from Eqns. 4 and 5 that these secondary reactions may not be feasible



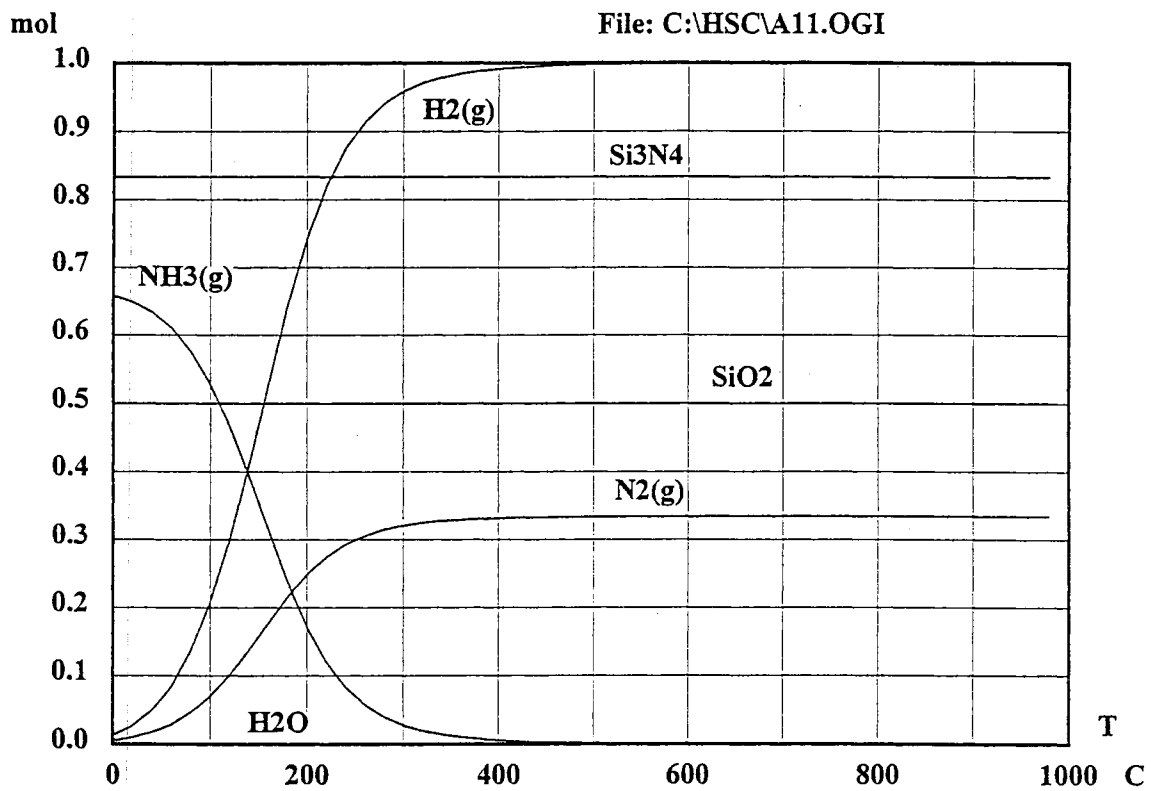


Figure 7.4 (a) Variation of the mole fractions of various species with temperature of the chemical reaction system consisting of 1 mol of  $\text{Si}_3\text{N}_4$  and 1 mol of  $\text{H}_2\text{O}$

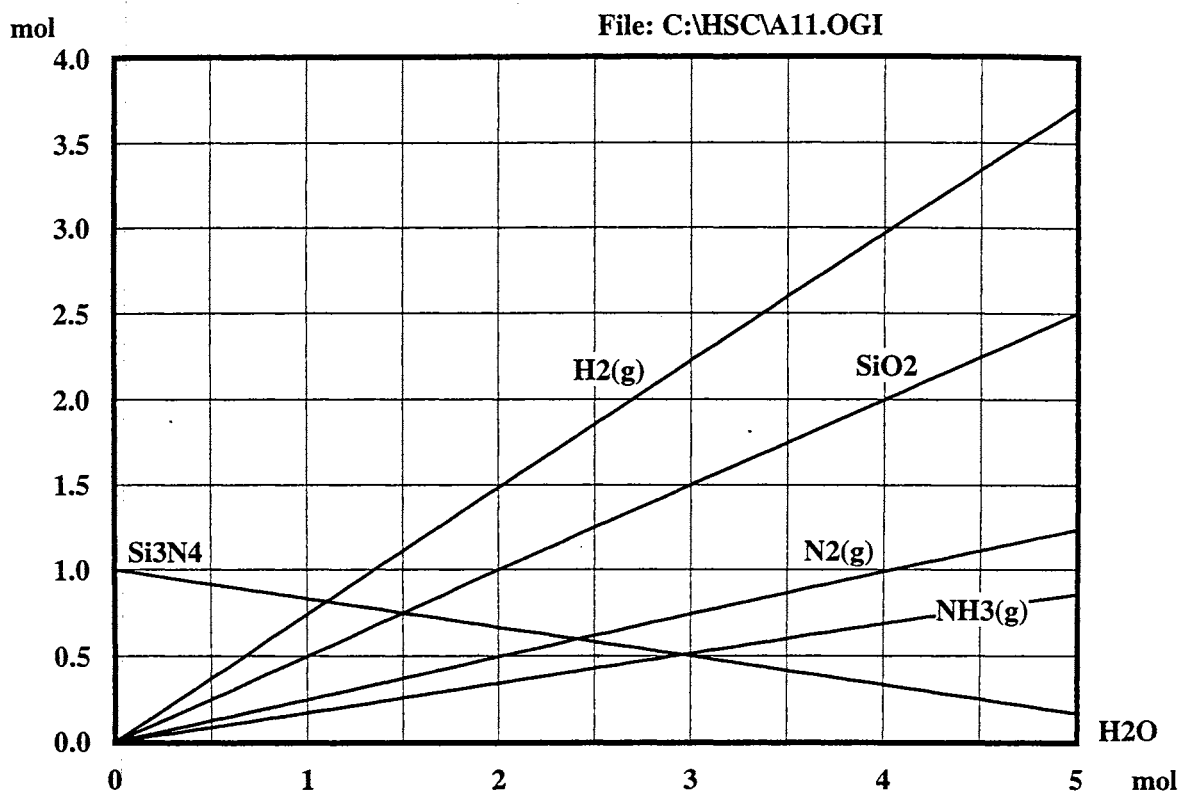


Figure 7.4 (b) Variation of various chemical species with temperature for 1 mol of Si<sub>3</sub>N<sub>4</sub> and increasing amounts of H<sub>2</sub>O.

thermodynamically, as  $\Delta G$  in all cases is positive. If, however, they form, they have to be by other chemical reactions.

NH <sub>3</sub> (g) + H <sub>2</sub> O = NH <sub>4</sub> OH (4)								
T (°C)	0	100	200	300	400	600	800	1000
$\Delta G$ (kcal)	7.6	9.9	11.8	13.7	15.4	18.9	22.8	27.7

SiO <sub>2</sub> + 2H <sub>2</sub> O = Si(OH) <sub>4</sub> (a) (5)								
T (°C)	0	100	200	300	400	600	800	1000
$\Delta G$ (kcal)	50.7	69.3	85.3	104.4	124.5	167.8	215.1	266.4

CeO<sub>2</sub> can also react directly with Si<sub>3</sub>N<sub>4</sub> (oxidization-reduction reaction) forming SiO<sub>2</sub> and N<sub>2</sub> as reaction products. It may be noted that CeO<sub>2</sub> is not stable and will convert to CeO<sub>1.72</sub> and CeO<sub>1.83</sub> at low temperatures and to the more stable form, namely, Ce<sub>2</sub>O<sub>3</sub> at higher temperatures. Figure 7.5 (a) shows the variation of the reaction products with temperature at equilibrium based on the thermodynamic calculations of the chemical reaction system consisting of 1 mol of Si<sub>3</sub>N<sub>4</sub> and 1 mol of CeO<sub>2</sub> and Figure 7.5 (b) is for 1 mol of Si<sub>3</sub>N<sub>4</sub> and with increasing mole fractions of CeO<sub>2</sub>. The reactions of Si<sub>3</sub>N<sub>4</sub> with CeO<sub>2</sub> yielding CeO<sub>1.83</sub>, CeO<sub>1.72</sub>, and Ce<sub>2</sub>O<sub>3</sub> are shown in Eqns. 6-8. From Figure 7.5 (a) it can be seen that the SiO<sub>2</sub> mole fraction is independent of temperature up to  $\approx 300$  °C and increases gradually up to 1000 °C. Thus temperature does not seem to be as effective as mole fraction of H<sub>2</sub>O [compare Figures 7.5 (a) with Figure 7.4 (b)]. However, as the mole fraction of CeO<sub>2</sub> is increased, the amount of SiO<sub>2</sub> increases and the amount of Si<sub>3</sub>N<sub>4</sub> decreases both accounting for the increase in the material removal rate due to CMP.

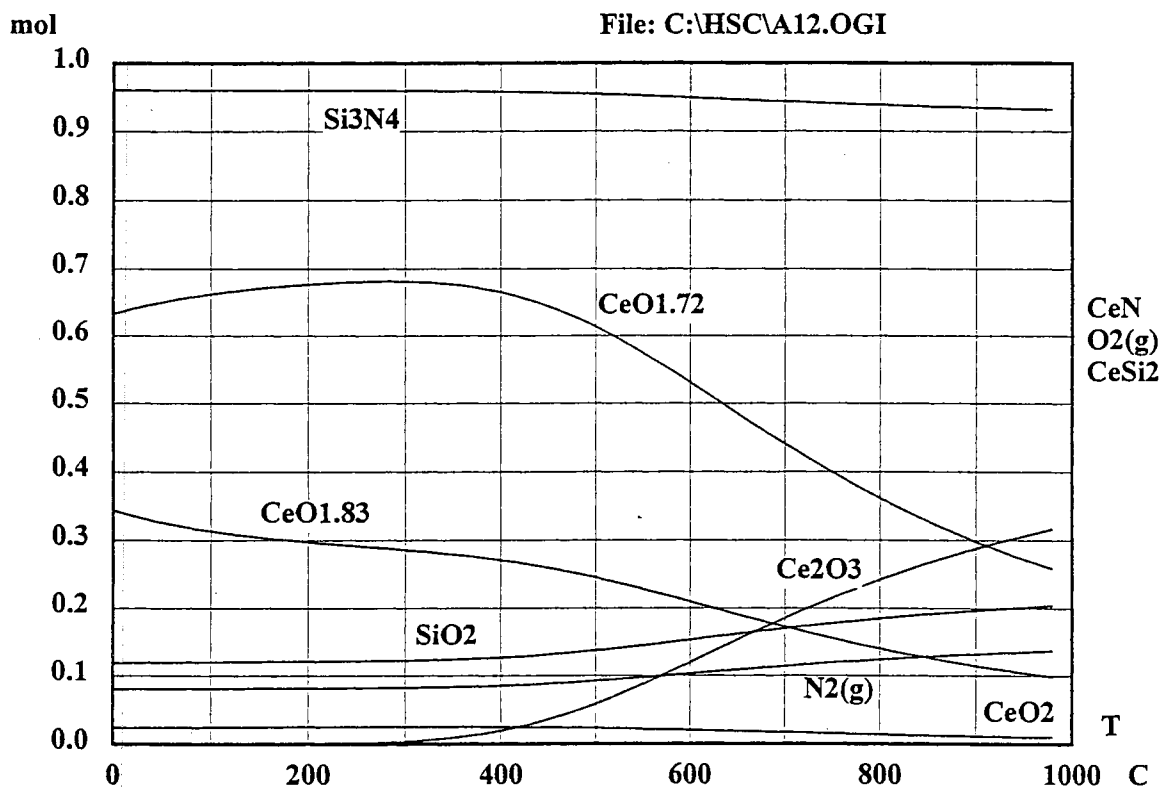


Figure 7.5 (a) Variation of the reaction products with temperature of the chemical reaction system consisting of 1 mol of  $\text{Si}_3\text{N}_4$  and 1 mol of  $\text{CeO}_2$

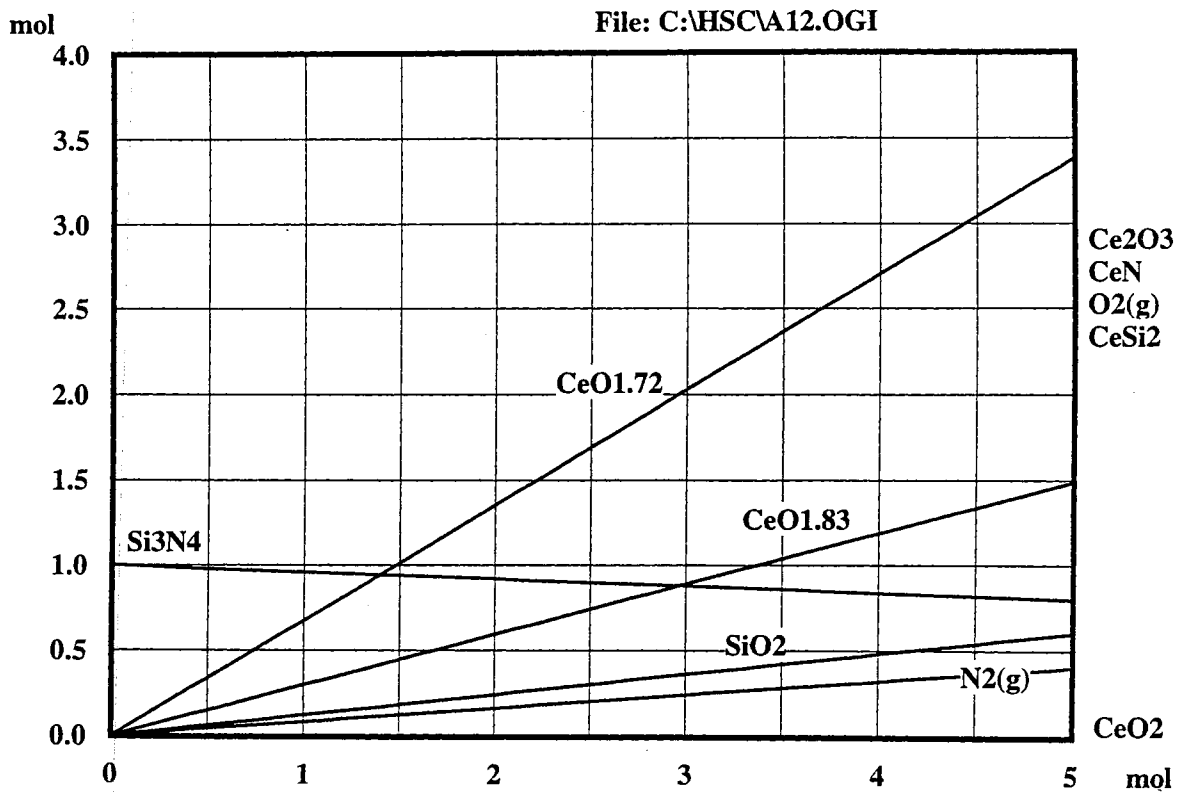


Figure 7.5 (b) Variation of the reaction products with increasing mole fraction of  $\text{CeO}_2$

$\text{Si}_3\text{N}_4 + 35.294 \text{ CeO}_2 = 3\text{SiO}_2 + 35.294 \text{ CeO}_{1.83} + 2\text{N}_2(\text{g})$ (6)								
T (°C)	0	100	200	300	400	600	800	1000
ΔG (kcal)	-47.6	-61.7	-75.7	-89.8	-103.9	-132.9	-163.2	-195.1

$\text{Si}_3\text{N}_4 + 21.429 \text{ CeO}_2 = 3\text{SiO}_2 + 21.429 \text{ CeO}_{1.72} + 2\text{N}_2(\text{g})$ (7)								
T (°C)	0	100	200	300	400	600	800	1000
ΔG (kcal)	-34.6	-47.4	-60.1	-72.7	-85.4	-111.3	-138.2	-166.4

$\text{Si}_3\text{N}_4 + 12\text{CeO}_2 = 3\text{SiO}_2 + 6\text{Ce}_2\text{O}_3 + 2\text{N}_2(\text{g})$ (8)								
T (°C)	0	100	200	300	400	600	800	1000
ΔG (kcal)	35.5	22.3	8.6	-5.5	-19.8	-49.4	-80.0	-111.4

Figure 7.6 (a) shows the variation of the reaction products with temperature for the chemical reaction system consisting of 1 mol of  $\text{Si}_3\text{N}_4$ , 1 mol of  $\text{CeO}_2$ , and 1 mol of  $\text{H}_2\text{O}$  at equilibrium based on the thermodynamic calculations. This diagram provides an insight on the mechanism of chemo-mechanical polishing of  $\text{Si}_3\text{N}_4$  with  $\text{CeO}_2$  showing various chemical species that can be formed during the process. This figure can be considered as a combination of Figures 7.4 (a) and 7.5 (a). It shows that while the  $\text{SiO}_2$  mole fraction is constant upto about  $\approx 300$  °C, it increases with further increase in temperature. A reverse trend can be seen for  $\text{Si}_3\text{N}_4$ , i. e. initially constant followed by a decrease in mole fraction with further increase in temperature, both indicating an increase the material removal rate due to chemo-mechanical action at higher temperatures. It can be seen from the figure that  $\text{NH}_3(\text{g})$  forms

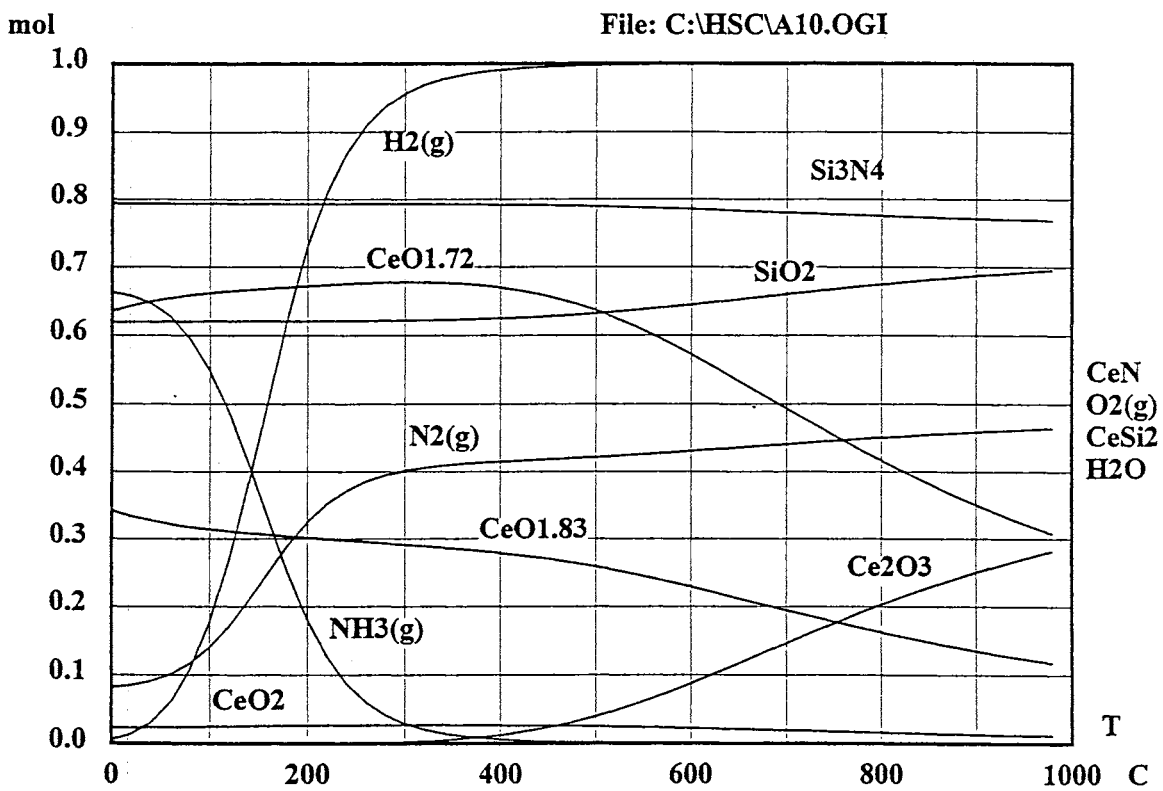


Figure 7.6 (a) Variation of the reaction products with temperature for the chemical reaction system of 1 mol of  $\text{Si}_3\text{N}_4$ , 1 mol of  $\text{CeO}_2$ , and 1 mol of  $\text{H}_2\text{O}$

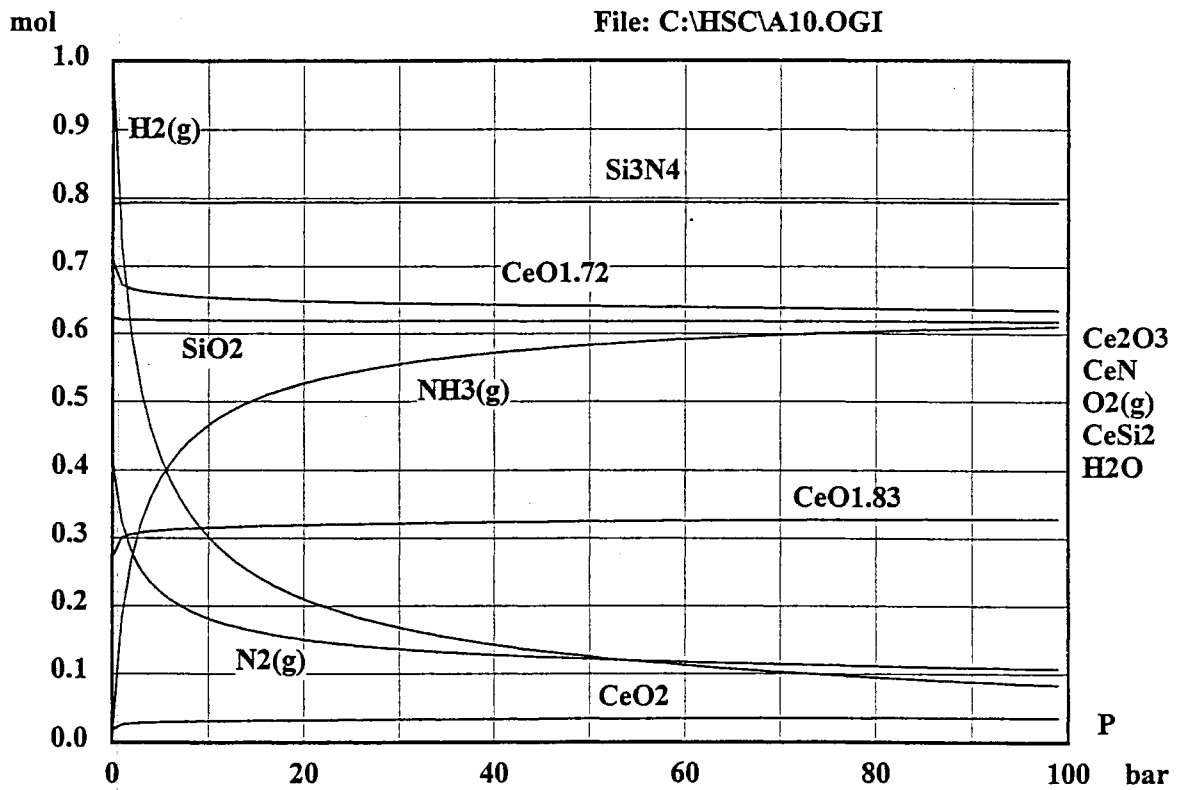


Figure 7.6 (b) Variation of the reaction products with pressure for the chemical reaction system of 1 mol of Si<sub>3</sub>N<sub>4</sub>, 1 mol of CeO<sub>2</sub>, and 1 mol of H<sub>2</sub>O.



at low temperatures ( $< 300\text{ }^{\circ}\text{C}$ ) while  $\text{H}_2(\text{g})$  and  $\text{N}_2(\text{g})$  gases form at higher temperatures, similar to Figure 7.4 (a).

$\text{CeO}_2$  appears to be the most effective polishing medium for CMP of  $\text{Si}_3\text{N}_4$  because of the thermodynamic considerations of its reaction with  $\text{Si}_3\text{N}_4$  as well as its kinetic action of removing the reaction product, namely,  $\text{SiO}_2$  from  $\text{Si}_3\text{N}_4$  workmaterial.

Figure 7.6 (b) shows the variation of the reaction products with pressure at equilibrium based on the thermodynamic calculations of the chemical reaction system of 1 mol of  $\text{Si}_3\text{N}_4$ , 1 mol of  $\text{CeO}_2$ , and 1 mol of  $\text{H}_2\text{O}$ . It can be seen that both  $\text{Si}_3\text{N}_4$  and  $\text{SiO}_2$  more or less remains constant indicating that the formation of  $\text{SiO}_2$  due to chemical reaction is independent of the polishing pressure. It may be noted that an increase in the mole fraction of  $\text{SiO}_2$  and a corresponding decrease in  $\text{Si}_3\text{N}_4$  are an indication of the increase in the material transformed by chemical action. However, the actual material removal will depend on pressure or kinetic action involving the removal of the reaction products to enable the chemical reaction to continue ad infinitum.

It may be noted that the hardness of  $\text{CeO}_2$  is close to  $\text{SiO}_2$  layer but significantly lower than  $\text{Si}_3\text{N}_4$  workmaterial. Thus, the  $\text{Si}_3\text{N}_4$  workmaterial can hardly be scratched, or damaged by  $\text{CeO}_2$ . Hence, almost all the material removal is by chemo-mechanical action between the  $\text{Si}_3\text{N}_4$  workmaterial and the  $\text{CeO}_2$  polishing media in a water environment by the formation of  $\text{SiO}_2$  reaction layer on  $\text{Si}_3\text{N}_4$  and its subsequent removal by mechanical action. The chemical reaction can continue only after the passivating layers are removed by the mechanical action. Thus, the kinetic action, which removes the reaction products from the interface is a very important step in the CMP process. It is

somewhat coincidental, that in general, the Mohs hardness for best polishing abrasives for glasses (SiO<sub>2</sub>) is ≈ 6.5 and the hardness of CeO<sub>2</sub> is ≈ 6 on the Moh's scale. There are other similarities including the role of water and effectiveness of CeO<sub>2</sub> medium for polishing glass. This is not altogether surprising as the material removal mechanism in the case of Si<sub>3</sub>N<sub>4</sub> is through the formation of SiO<sub>2</sub> and in the case of glasses it is naturally SiO<sub>2</sub>. A similar mechanism may be applicable for the polishing of silicon wafers with CeO<sub>2</sub> in a water based solution. It is anticipated that these and other aspects will be addressed in detail in subsequent publications shortly.

It is possible that in the formation of SiO<sub>2</sub> outer layer an intermediate oxynitride (Si<sub>x</sub>O<sub>y</sub>N<sub>z</sub>) may form between SiO<sub>2</sub> thin layer and Si<sub>3</sub>N<sub>4</sub> substrate according to Eqns. 9-11. All three equations are thermodynamically feasible at all temperatures upto 1000 °C.

2 Si <sub>3</sub> N <sub>4</sub> + 17.647CeO <sub>2</sub> = 3 Si <sub>2</sub> N <sub>2</sub> O + 17.647 CeO <sub>1.83</sub> + N <sub>2</sub> (g) (9)								
T (°C)	0	100	200	300	400	600	800	1000
ΔG (kcal)	-68.3	-67.6	-67.2	-66.9	-66.5	-65.0	-62.1	-57.5

Si <sub>3</sub> N <sub>4</sub> + 1.5H <sub>2</sub> O = 1.5 Si <sub>2</sub> N <sub>2</sub> O + NH <sub>3</sub> (g) (10)								
T (°C)	0	100	200	300	400	600	800	1000
ΔG (kcal)	-94.0	-95.6	-98.6	-102.4	-106.7	-116.5	-127.4	-139.4

Si <sub>3</sub> N <sub>4</sub> + SiO <sub>2</sub> = 2 Si <sub>2</sub> N <sub>2</sub> O (11)								
T (°C)	0	100	200	300	400	600	800	1000
ΔG (kcal)	-46.8	-43.2	-40.5	-38.4	-36.5	-33.3	-30.5	-27.9

## 7.5 MECHANISM OF CMP OF $\text{Si}_3\text{N}_4$ WITH $\text{CeO}_2$

Since  $\text{CeO}_2$  is significantly softer than  $\text{Si}_3\text{N}_4$  workmaterial (about 1/3), material removal by mere mechanical action would be extremely difficult if not impossible. Therefore, the mechanism of material removal must be due to chemo-mechanical action between the abrasive, the workmaterial and the environment. In CMP, material removal is accomplished by chemical reaction stimulated by friction energy at the contact area between the workmaterial and the abrasive or water and the reaction layer is removal by subsequent mechanical action of the abrasive [Fischer, 1988]. Since material is removed by the tribochemical action instead of mechanical fracture, extremely smooth and damage-free surface can be obtained as shown in Figure 7.2.

$\text{CeO}_2$  is the most effective abrasive for CMP of  $\text{Si}_3\text{N}_4$  material (both because of its kinetic action to remove the reaction product  $\text{SiO}_2$  and thermodynamic possible of reaction with  $\text{Si}_3\text{N}_4$  workmaterial).  $\text{CeO}_2$  abrasive can form a direct chemical reaction with  $\text{Si}_3\text{N}_4$  workmaterial (oxidization-reduction reaction) and leads to the formation of  $\text{SiO}_2$  as shown in Eqns. 6-8. The oxidation is a possible mechanism causing CMP of  $\text{Si}_3\text{N}_4$ .

Kanno and Suzuki (1983) identified the formation of  $\text{NH}_3$  during grinding of  $\text{Si}_3\text{N}_4$  powder in water, thus establishing the hydrolysis of  $\text{Si}_3\text{N}_4$ . The thermodynamic analysis presented here suggested the feasibility of this reaction (Eqn. 2). During magnetic float polishing (MFP) of  $\text{Si}_3\text{N}_4$  by  $\text{CeO}_2$  due to the presence of water environment (from the water-based magnetic fluid),  $\text{NH}_3$  and  $\text{SiO}_2$  are formed are formed when the temperature at the contact

interface is  $< 300^{\circ}\text{C}$ . Fischer and Tomizawa (1985), Tomizawa and Fischer (1987), Hah and Fischer (1995) also showed the formation of  $\text{SiO}_2$  and  $\text{NH}_3$  in tribochemical polishing of  $\text{Si}_3\text{N}_4$ . But they proposed the dissolution of  $\text{SiO}_2$  and  $\text{NH}_3$  (to silicic acid  $[\text{Si}(\text{OH})_4]$  and ammonium hydroxide  $[\text{NH}_4\text{OH}]$ ) as a second reaction to stimulate the continuation of tribochemical polishing of  $\text{Si}_3\text{N}_4$  in aqueous solutions. Fischer [1988] also pointed out that flash temperatures from the frictional heat is important for the tribochemical reaction at the polishing interface. While the hydrolysis reaction shown in Eqn. 2 is thermodynamically feasible, the dissolution of  $\text{SiO}_2$  and  $\text{NH}_3$  [to silicic acid,  $\text{Si}(\text{OH})_4$  (Eqn. 4) and ammonium hydroxide ( $\text{NH}_4\text{OH}$ )] (Eqn. 5) as reactants to stimulate the tribochemical polishing does not seem to be feasible thermodynamically as  $\Delta G$  (kcal) is positive in all cases. If, in fact, they form, they have to be by other chemical reactions.

It may be noted that the hardness of  $\text{CeO}_2$  is close to the  $\text{SiO}_2$  layer but significantly lower (about 1/3) than  $\text{Si}_3\text{N}_4$  workmaterial. Thus,  $\text{SiO}_2$  reaction layers formed during chemical action are removed without damaging  $\text{Si}_3\text{N}_4$  workmaterial by  $\text{CeO}_2$ . In general, Mohs hardness for best polishing abrasives for glasses ( $\text{SiO}_2$ ) is  $\approx 6.5$ . Hardness of  $\text{CeO}_2$  abrasive is  $\approx 6$  on the Moh's scale and the pH of the magnetic fluid plus  $\text{CeO}_2$  is  $\approx 6$ . It may be noted that Cook (1990) after a careful analysis concluded that the best abrasive for polishing glasses is  $\text{CeO}_2$  and the best polishing environment is with a pH in the range of 6-7. The compaction of the  $\text{SiO}_2$  network leads to enhanced dissolution of  $\text{SiO}_2$  into the polishing slurry and to an extremely smooth surface. The kinetic action, which removes the reaction products from the interface is very important in the CMP process. The chemical reaction can continue only after the passivating layers are removed by the mechanical action.

It is possible that an outer layer of  $\text{SiO}_2$  and an intermediate siliconoxynitride may form between  $\text{SiO}_2$  thin layer and  $\text{Si}_3\text{N}_4$  substrate according to Eqns. 9-11. The oxide scale on MgO uniaxially pressed  $\text{Si}_3\text{N}_4$  forms in layers composed of amorphous and crystalline  $\text{SiO}_2$ ,  $\text{Si}_2\text{N}_2\text{O}$ , and  $\text{MgSiO}_3$  ( $\text{MgO}\cdot\text{SiO}_2$ , from 1 wt.% MgO sintering additive) [Tighe, 1982; Singhal, 1976; Lange, 1979]. It is notable that  $\text{Si}_3\text{N}_4$  is easily oxidized in an oxygen-containing atmosphere [Ruhle, 1997]. As a result, the surface of  $\text{Si}_3\text{N}_4$  is always covered with a thin silica layer as shown by Eqn. 1. The surface after CMP by oxide consists of 0.2-0.5 nm of  $\text{SiO}_2$ , 1.0-1.5 nm of  $\text{SiO}_x\text{N}_y$  on the  $\text{Si}_3\text{N}_4$  substrate. The natural oxidation layer of  $\text{Si}_3\text{N}_4$  at room temperature is no more than 2.5-3.0 nm. Thus, CMP does not produce a layer that is chemically different from the natural oxidation layer formed in air at room temperature on the  $\text{Si}_3\text{N}_4$  substrate [Han and Fischer, 1995]. It has been shown in this investigation that several not-so-hard oxides, such as  $\text{CeO}_2$  and  $\text{ZrO}_2$  following by  $\text{Fe}_2\text{O}_3$  and  $\text{Cr}_2\text{O}_3$  etc are effective abrasive for CMP of  $\text{Si}_3\text{N}_4$  material. This is because of the thermodynamic feasibility of chemical reactions between the abrasive and the  $\text{Si}_3\text{N}_4$  workmaterial but also due to the subsequent kinetic action of removing the reaction products from the  $\text{Si}_3\text{N}_4$  workmaterial.

In summary,  $\text{CeO}_2$  is found to be the most effective abrasive for CMP of  $\text{Si}_3\text{N}_4$  material and is particularly effective in water but in alcohols only when hydroxylgroups are present.  $\text{CeO}_2$  abrasive can directly react chemically with  $\text{Si}_3\text{N}_4$  workmaterial (oxidization-reduction reaction) leading to the formation of  $\text{SiO}_2$  and  $\text{N}_2(\text{g})$ .  $\text{CeO}_2$  is stable only at low temperatures and will convert to  $\text{CeO}_{1.72}$  and  $\text{CeO}_{1.83}$  as the temperature is increased. Further increase in temperature ( $> 300^\circ\text{C}$ ) results in a decrease in the amounts of  $\text{CeO}_{1.72}$  and  $\text{CeO}_{1.83}$  and increase in the more stable form, namely,  $\text{Ce}_2\text{O}_3$  at higher

temperatures . The reactions involved in CMP of Si<sub>3</sub>N<sub>4</sub> with CeO<sub>2</sub> in a water environment are given in Table 7.4. It has been shown that almost all the material removal is by chemo-mechanical action between the Si<sub>3</sub>N<sub>4</sub> workmaterial and the CeO<sub>2</sub> polishing media in the water environment by the formation of SiO<sub>2</sub> reaction layer on Si<sub>3</sub>N<sub>4</sub> and its subsequent removal by mechanical action by cerium oxide abrasive.

Table 7.4 Chemical reaction systems in water-based CMP of Si<sub>3</sub>N<sub>4</sub> with CeO<sub>2</sub>

$\text{Si}_3\text{N}_4 + 35.294 \text{ CeO}_2 = 3\text{SiO}_2 + 35.294 \text{ CeO}_{1.83} + 2\text{N}_2(\text{g})$ (1)								
T (°C)	0	100	200	300	400	600	800	1000
ΔG (kcal)	-47.6	-61.7	-75.7	-89.8	-103.9	-132.9	-163.2	-195.1
$\text{Si}_3\text{N}_4 + 6\text{H}_2\text{O} = 3\text{SiO}_2 + 4\text{NH}_3(\text{g})$ (2)								
T (°C)	0	100	200	300	400	600	800	1000
ΔG (kcal)	-132.7	-140.9	-147.4	-152.6	-156.4	-159.8	-156.9	-146.5
$2\text{Si}_3\text{N}_4 + 35.294 \text{ CeO}_2 + 6\text{H}_2\text{O} = 6\text{SiO}_2 + 35.294 \text{ CeO}_{1.83} + 4\text{NH}_3(\text{g}) + 2\text{N}_2(\text{g})$ (3)								
T (°C)	0	100	200	300	400	600	800	1000
ΔG (kcal)	-180.3	-202.6	-223.1	-242.4	-260.3	-292.7	-320.1	-341.6
$2 \text{ Si}_3\text{N}_4 + 17.647\text{CeO}_2 = 3 \text{ Si}_2\text{N}_2\text{O} + 17.647 \text{ CeO}_{1.83} + \text{N}_2 (\text{g})$ (4)								
T (°C)	0	100	200	300	400	600	800	1000
ΔG (kcal)	-68.3	-67.6	-67.2	-66.9	-66.5	-65.0	-62.1	-57.5
$\text{Si}_3\text{N}_4 + 1.5\text{H}_2\text{O} = 1.5 \text{ Si}_2\text{N}_2\text{O} + \text{NH}_3 (\text{g})$ (5)								
T (°C)	0	100	200	300	400	600	800	1000
ΔG (kcal)	-94.0	-95.6	-98.6	-102.4	-106.7	-116.5	-127.4	-139.4
$\text{Si}_3\text{N}_4 + \text{SiO}_2 = 2 \text{ Si}_2\text{N}_2\text{O}$ (6)								
T (°C)	0	100	200	300	400	600	800	1000
ΔG (kcal)	-46.8	-43.2	-40.5	-38.4	-36.5	-33.3	-30.5	-27.9
$\text{Si}_3\text{N}_4 + 3\text{O}_2(\text{g}) = 3\text{SiO}_2 + 2\text{N}_2(\text{g})$ (6)								
T (°C)	0	100	200	300	400	600	800	1000
ΔG (kcal)	-460.7	-455.4	-450.3	-445.2	-440.2	-430.6	-421.3	-412.4

## CHAPTER 8

### METHODOLOGY FOR FINISHING OF SILICON NITRIDE

#### (Si<sub>3</sub>N<sub>4</sub>) BALLS FOR BEARING APPLICATIONS

##### 8.1 INTRODUCTION

The methodology, involved in the mechanical polishing followed by chemo-mechanical polishing, for the finishing of Si<sub>3</sub>N<sub>4</sub> balls from the as-received condition by MFP is discussed in this chapter. It involves mechanical removal of material initially using harder abrasives (with respect to the workmaterial) of different materials of progressively lower hardnesses and finer grain sizes followed by final chemo-mechanical polishing (CMP) using preferably a softer abrasive for obtaining superior finish with minimal surface or subsurface defects, such as scratches, microcracks, or pits on the Si<sub>3</sub>N<sub>4</sub> balls. High material removal rates (1 μm/min) with minimal subsurface damage is obtained with harder abrasives, such as B<sub>4</sub>C or SiC (relative to Si<sub>3</sub>N<sub>4</sub>) due to the use of a flexible support system, small polishing loads (1 N/ball), and fine abrasives but high polishing speeds (compared to conventional polishing) by rapid accumulation of minute amounts of material removed by microfracture. Final polishing of the Si<sub>3</sub>N<sub>4</sub> balls using a softer abrasive, such as CeO<sub>2</sub> (that chemo-mechanically react with the Si<sub>3</sub>N<sub>4</sub> workmaterial) results in high quality Si<sub>3</sub>N<sub>4</sub> balls of bearing quality with superior surface finish ( $R_a < 4$  nm,  $R_t < 0.04$  μm) and damage-free surface. CMP is very effective for obtaining excellent surface finish on Si<sub>3</sub>N<sub>4</sub> ceramic material and CeO<sub>2</sub> in particular is one of most suitable material for this application.

## 8.2 POLISHING CONDITIONS AND PROCEDURE

The as-received Si<sub>3</sub>N<sub>4</sub> balls (CERBEC NBD-200 from Norton Advanced Ceramics) had a nominal diameter of 13.4 mm. These balls also contained nearly a 200 mm thick x 5 mm wide band of material around the periphery at the parting plane resulting from the uniaxially pressing process. These balls have to be finished to a final size of 12.7 mm (0.5 inch), a sphericity of 0.5 μm, and best finish achievable. All the three factors were considered in the finishing of Si<sub>3</sub>N<sub>4</sub> balls in this chapter with emphasis on the latter aspect, namely, best finish achievable. The large differences in the diameter between the as-received condition to the final size required is to remove all the reaction material that is formed on and near the surface during the hot pressing process. The nominal chemical composition and the mechanical properties of NBD-200 Si<sub>3</sub>N<sub>4</sub> balls have been given in chapter 4.

Table 8.1 gives properties of the various abrasives used in this investigation. As in most finishing operations, there are three stages involved in magnetic float polishing (MFP) of Si<sub>3</sub>N<sub>4</sub> balls, namely, 1) roughing to remove as much material as possible without imparting serious damage to the surface, 2) an intermediate stage of semifinishing where size, sphericity, and surface roughness have to carefully monitored, and 3) final finishing where all three, namely, size, sphericity, and finish have to closely controlled to meet the requirements.

Table 8.2 lists the test conditions used for different stages of polishing. Two coarser, harder abrasives, B<sub>4</sub>C (500 grit) and SiC (400 grit) (i.e. compared to Si<sub>3</sub>N<sub>4</sub> work material) were used during the initial stages of polishing to reach



Table 8.1 Properties of Various Abrasives

Abrasive	Density g/cm <sup>3</sup>	Knoop Hardness kg/mm <sup>2</sup>	Elastic modulus GPa	Melting point, °C
B <sub>4</sub> C	2.52	2800	450	2450
SiC	3.2	2500	420	2400
CeO <sub>2</sub>	7.13	625	165	2500

Table 8.2 Test Conditions

Stage	Abrasive			Abrasive, vol%	Speed, rpm	Load, N/ball	Time, min	Remarks
	Type	Grit Size	Size(μm)					
1	B <sub>4</sub> C	500	17	10%	2000	1.0	-	Roughing (High Material Removal)
	SiC	400	23	10%	2000	1.0	-	
2	SiC	1000	5	10%	2000	1.0	30	Semi-finishing (Sphericity and Roughness)
	SiC	1200	3	10%	2000	1.0	30	
3	SiC	8000	1	5%	4000	1.2	60	Final Finishing (Size, Sphericity, and Finish)
	CeO <sub>2</sub>		5	10%	2000	1.2	120	

\* All abrasives used, except CeO<sub>2</sub>, were obtained from Norton Co.  
CeO<sub>2</sub> is obtained from Aldrich Chemicals.

the desired diameter at high removal rates and at the same time improve the sphericity for proper ball motion. After reaching the diameter close to the desired diameter, an intermediate (semifinishing) stage is utilized as a transition between the roughing and finishing stages, as the material removal rate is of prime concern in the first stage and surface finish in the final stage. The two harder abrasives with a finer grit size were chosen for this intermediate stage, namely, SiC (1000 grit) and SiC (1200 grit). During this stage, the removal rates are much lower and the finish much better than roughing but the emphasis during this stage is the improvement of sphericity. In the final stage (prior to CMP), fine SiC abrasive (8000 grit) is used to approach the required diameter and sphericity and remove almost all the deep valleys from the surface. This is followed by final polishing using a softer, chemo-mechanical abrasive, namely, CeO<sub>2</sub> to produce the balls of required diameter, sphericity, and final surface finish which is extremely smooth and almost damage-free by preferentially removing the peaks from the surface.

The polishing shaft in MFP apparatus was driven by a high-speed, high-precision air bearing spindle (PI Spindle) with a stepless speed regulation up to 10,000 rpm. The magnetic field was measured by Gauss/Tesla meter. pH value of polishing environment was measured by pH/Temperature meter. The polishing load was set up by measuring the normal force with a Kistler's piezoelectric dynamometer connected to a charge amplifier and a display. To calculate material removal rates, the weight reduction in the balls was measured by measuring the weight before and after polishing at every stage test using a precision balance. The surface finish of the polished balls was analyzed using a Form Talysurf 120 L, ZYGO laser interference microscope, a Digital Nanoscope III atomic force microscope (AFM), and an ABT 32 scanning

electron microscope (SEM). The roundness of the balls was measured using TalyRond 250.

In this study, the finished balls are characterized for roundness using a TalyRond 250 (cut-off: 50  $\mu$ m, Filter: 2CR), and for surface features using a scanning electron microscope (SEM), a Form TalySurf 120 L (cut-off: 0.25 mm and 0.8 mm, evaluation length: 4-6 consecutive cut-off, Filter: ISO 2CR), and an AFM. Although the latter three instrument measure or illustrate slightly different surface features, they are basically complimentary in nature. Their combined use provides confidence on the data obtained. In this investigation, three randomly selected balls from each batch are traced 3 times at approximately three orthogonal planes using the TalyRond and Form Talysurf to provide the roundness and surface roughness, respectively. The TalyRond trace measures the maximum departure from a true circle of assumed magnitude and as such it denoted roundness. The sphericity of each ball, according to AFBMA, is defined as the maximum value of the roundness measured on three orthogonal planes of the ball. Similarly, the surface finish of each ball is taken as the maximum value of three traces along three orthogonal planes of the ball.

The surface roughness obtained by mechanical polishing generally has approximately a symmetrical profile. However, when the peaks are smoothed preferentially leaving the valleys intact as in CMP of finishing of  $\text{Si}_3\text{N}_4$  giving a fairly smooth bearing surface, the surface roughness can be unsymmetrical. Many parameters have been proposed to quantify the various surface characteristics. It is necessary to ensure that these values truly represent the surface features of interest. It is generally recognized that only  $R_a$  is not enough to evaluate the surface finish and that both  $R_a$  and  $R_t$  (or  $R_{\text{max}}$ ) may be necessary. The  $R_a$  value represents the average roughness is a typical value of

the measured surface but information regarding the shape of the irregularities (such as deep surface defects) is averaged out. The  $R_t$  value is the vertical distance between the highest and lowest points of the roughness profile. It is not a typical value for the whole surface, but can directly represent the irregular surface defects, such as scratches and pits (deep valleys), which can have a significant effect on the surface quality of advanced ceramic materials ( $R_t = R_p + R_v = R_{pv}$ ) for various applications.

For a stylus instrument, such as TalySurf, the stylus size and shape affect the accuracy of the profile. It would not be possible to trace the complete profile of a deep valley especially the bottom if the size of the valley is smaller than the tip radius. The stylus tip radius of TalySurf 250 used in this study is about  $2 \mu\text{m}$ . However, SEM micrograph can be helpful to identify whether there are surface defects which can be reflected by stylus of TalySulf and whether the value from TalySurf is a reliable for small-damage surface. Talysulf is convenient to use for large area scanning with help by SEM micrograph. We also checked surface finish by ZYGO laser interference microscope which is non-contact measurement instrument. For the ZYGO laser interference microscope, the focus range is important and should include both peaks and valleys of the polished surface. Otherwise, the surface values from ZYGO are unreliable. The stylus tip radius of AFM is  $< 0.08 \mu\text{m}$  and can easily be broken and not easy to be operated and used very often. In this study, AFM is used for final high magnification evaluation of some random areas. Based on the evaluation by all of Talysurf, SEM, ZYGO and AFM characterization techniques, one can be more confident that the surface finish value shown are a reliable representation of the true surface quality.

### 8.3 POLISHING RESULTS

Figures 8.1 (a) to (d) are SEM micrograph, a Form TalySurf profile, an AFM image, and an high magnification AFM image, respectively of a commercially finished best Si<sub>3</sub>N<sub>4</sub> ball surface (considered as a master ball of AFBMA Grade 3). From the SEM micrograph [Figure 8.1 (a)], it can be seen that while some areas of the surface are extremely smooth, there are many fine scratches and some pits. The AFM image of the polished surface [Figure 8.1 (c)] more or less shows the same features with an Ra of 5 nm and Rmax of 220 nm. Even though the TalySurf profile of the smooth region of the polished surface gives an Ra of about 7 nm and Rt of about 70 nm [Figure 8.1 (b)] this may not reflect the actual surface roughness as can be seen from the SEM image [Figure 8.1 (a)]. From the SEM image, several deep pits can be seen the size of such defects at the bottom would be smaller than the stylus tip radius (2 μm) of the Talysulf. As previously pointed out, the values obtained by Talysurf, AFM, and ZYGO would depend on their ability to analyze the data from all the peaks as well as the valleys. If the depth of field is not adequate for a given magnification, the data would be in error on account of this. Consequently, care should be exercised in the quantitative evaluation of the surface finish obtained at these magnifications although relative values and surface topography are helpful in the analysis. Hah, Fisher, and Burk [1985] recently showed the surface finish of a polished surface of a commercial Si<sub>3</sub>N<sub>4</sub> ball (7/16 in diameter) using an AFM, an Ra in the region without defects as 1.8-2.8 nm and the regions including the defects as 11-18 nm (with defect density medium and scratch marks severe). For smaller size balls (1/4 in diameter), they reported an Ra of 2.5 to 4 nm in the region without any defects and 35-40 nm including the regions with defects (with defect density large and scratch marks some).

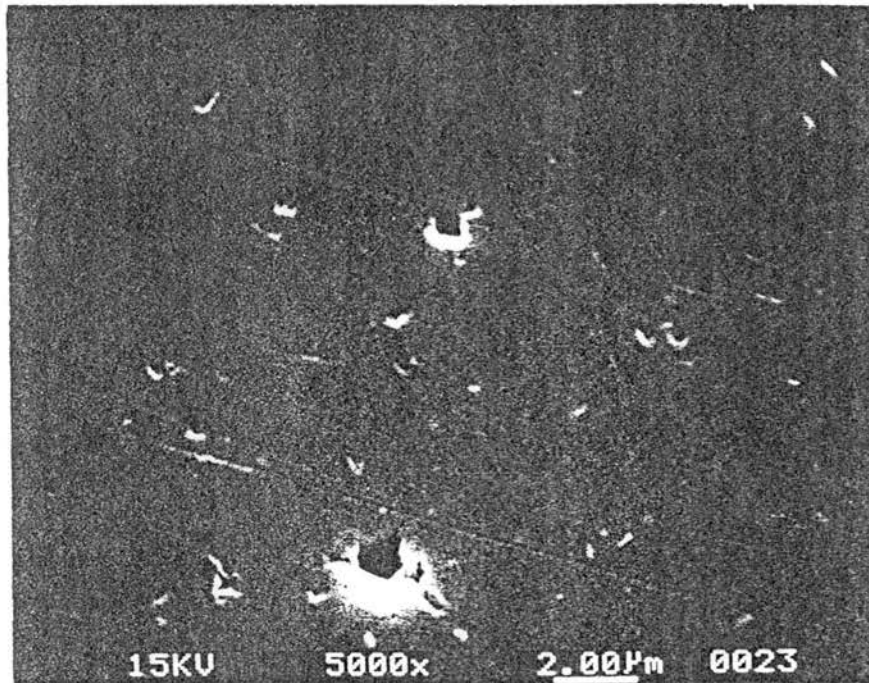


Figure 8.1 (a) SEM micrograph of a commercially finished Si<sub>3</sub>N<sub>4</sub> ball surface

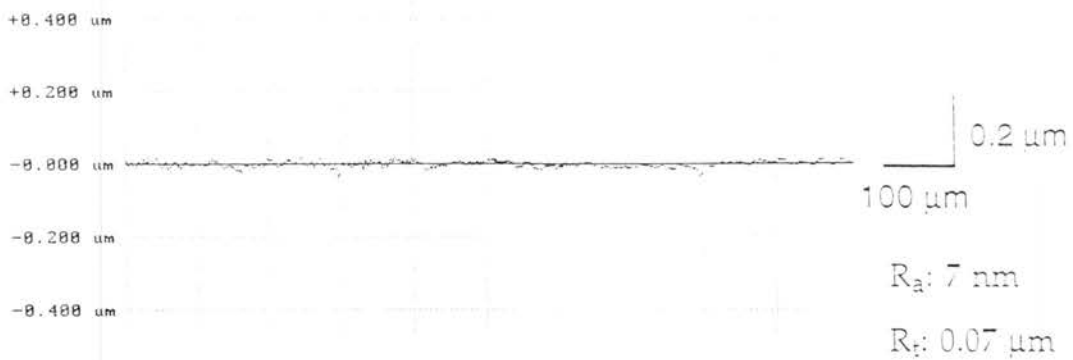
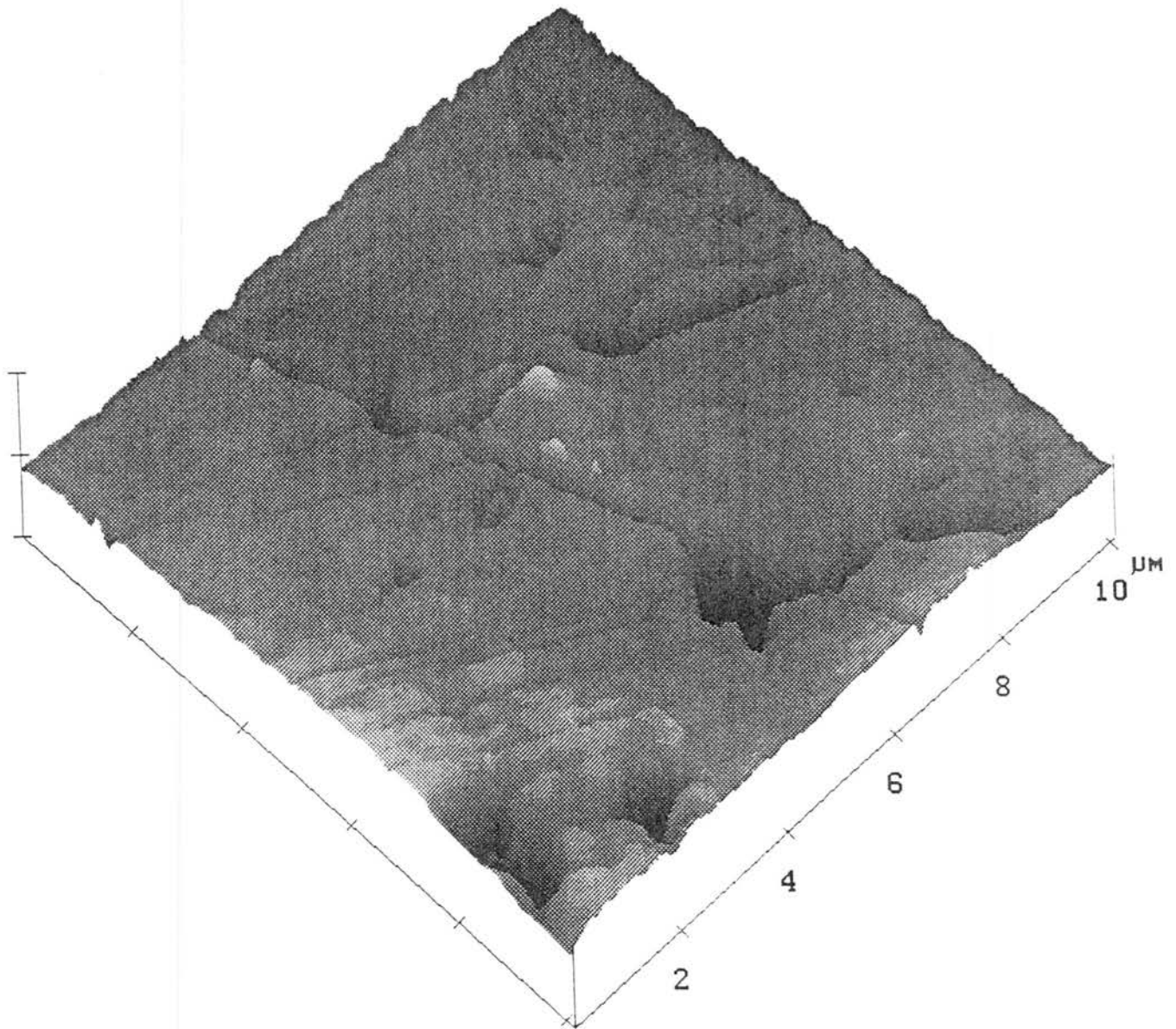
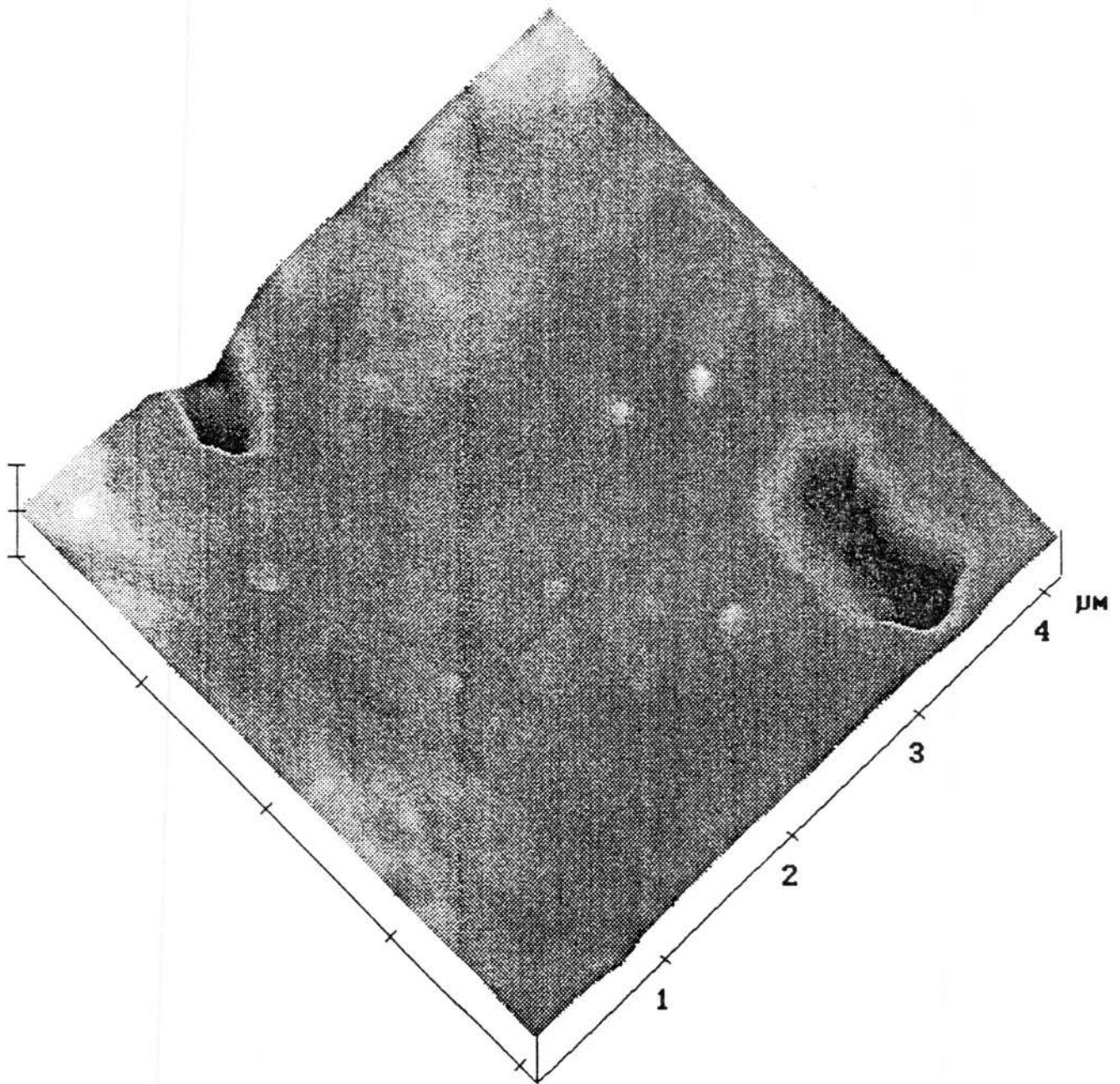


Figure 8.1 (b) Talysurf surface roughness profile of a commercially finished Si<sub>3</sub>N<sub>4</sub> ball surface



Z range	217.78 nm
Mean	-7.276 nm
Rms (Rq)	11.809 nm
Mean roughness (Ra)	5.059 nm
Max height (Rmax)	220.75 nm
Surface area	
Surface area diff	

Figure 8.1 (c) AFM image of a commercially finished Si<sub>3</sub>N<sub>4</sub> ball surface



Z range	75.151 nm
Mean	-4.170 nm
Rms (Rq)	10.087 nm
Mean roughness (Ra)	5.172 nm
Max height (Rmax)	70.897 nm
Surface area	
Surface area diff	

Figure 8.1 (d) AFM image at higher magnification showing smooth area separated by pitting of a commercially finished  $\text{Si}_3\text{N}_4$  ball surface



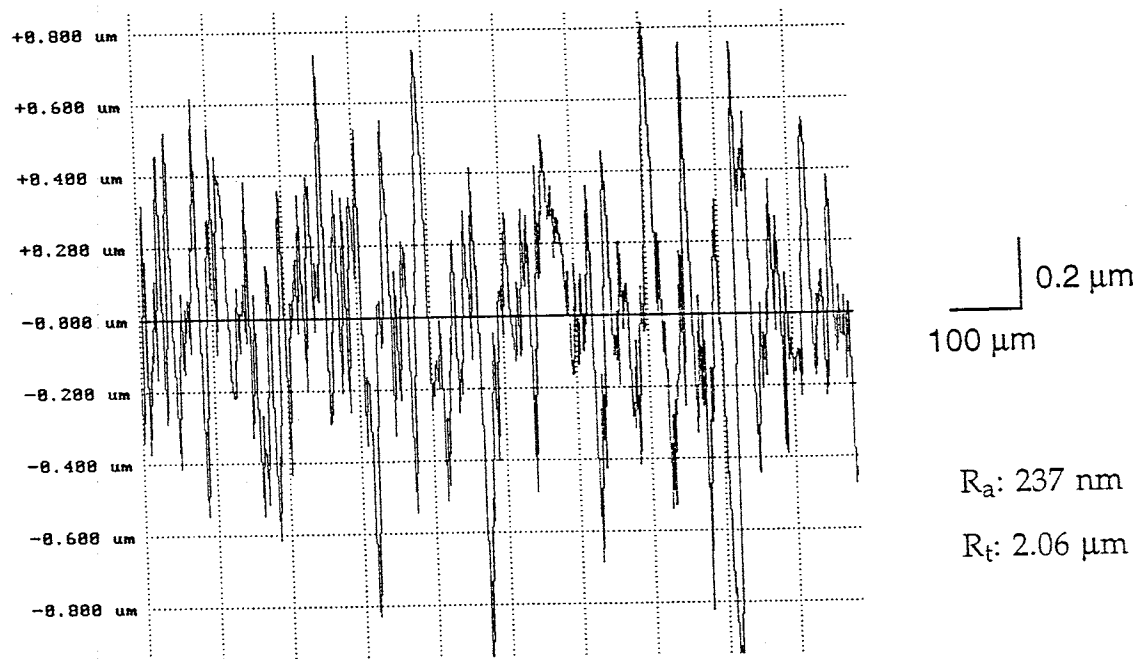
However, the  $R_{max}$  with defects can be many times this value (at least 10 times). Figure 8.1(d) is an AFM image at higher magnification showing deep pits separated by smooth regions of a commercially finished ball.

Table 8.3 gives the average surface finish and material removal rates obtained at progressive stages of polishing. The corresponding Talysurf surface finish profiles are shown in Figures 8.2 (a) - (f). It can be seen that the surface roughness as well as the material removal rates decrease as the hardness and grain size of the abrasive decreases due to a decrease in the size of brittle microfracture. For a harder abrasive with a fine grain size, the material removal is by submicroscopic fracture and therefore results in damage-free subsurface. Further CMP with a softer abrasive, such as  $CeO_2$ , as will be shown, will result in an extremely smooth surface.

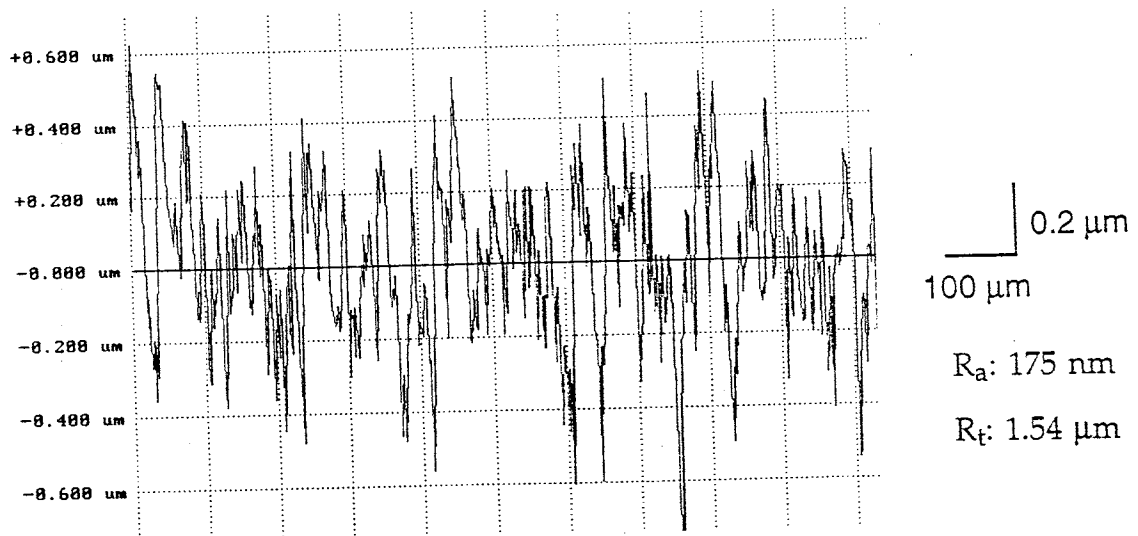
Figures 8.3 show the 3-D plot of the surface roughness using (a) the ZYGO non-contacting laser interference microscope and (b) and (c) AFM, respectively of the final surface polished by softer  $CeO_2$  abrasive. The surface finish values after the final polishing obtained by Form Talysurf are  $R_a$  3.8 nm and  $R_t$  0.029  $\mu m$ , while those obtained by ZYGO are  $R_a$  3.9 nm and  $R_{tm}$  0.021  $\mu m$  for the line scan and by AFM are  $R_a$  1.4 nm and  $R_{max}$  0.018  $\mu m$  for the area scan. The SEM micrographs [Figure 8.4 (b)] show essentially smooth surface with practically no surface defects. Both AFM and ZGYO also provide surface finish by averaging over an area. The evaluation of surface topography by all the characterization techniques considered in this investigation, namely, Talysurf, SEM, ZYGO, and AFM, gives confidence that the final surface is damage-free with a finish of  $R_a$  4 nm and  $R_t$  0.04  $\mu m$  (cut-off: 0.25 mm, evaluation length: 4-6 consecutive cut-off, Filter: ISO 2CR). If one considers the AFM values, the surface finish  $R_a$  would be about 1.4 nm.

Table 8.3 Average Surface Finish and Material Removal Rates  
During Various Stages of Polishing

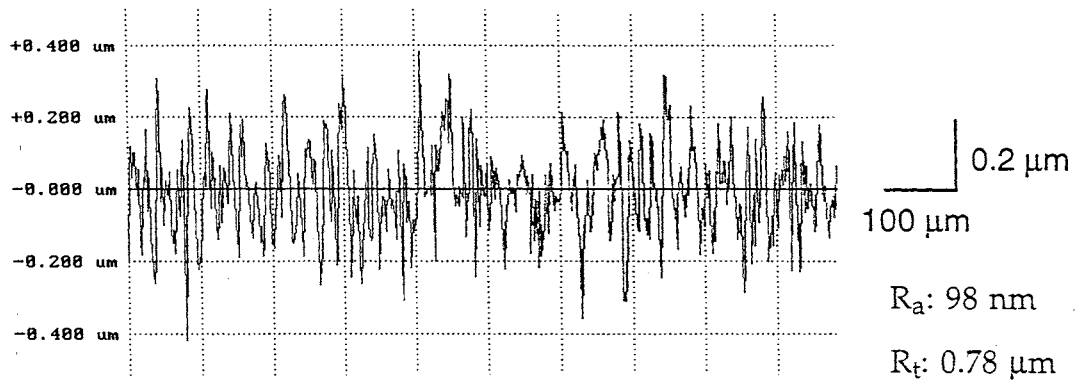
Stage	Abrasive	Surface Finish (Ave.)		MRR per ball		Material Removal Mechanism
		Ra (nm)	Rt ( $\mu\text{m}$ )	mg/min	$\mu\text{m}/\text{min}$	
1	B <sub>4</sub> C 500	225	1.95	0.96	1.2	Microfracture
	SiC 400	170	1.40	0.64	0.8	Microfracture
2	SiC 1000	95	0.80	0.30	0.5	Submicrofracture
	SiC 1200	55	0.50	0.20	0.2	Submicrofracture
3	SiC 8000	15	0.15	0.04	-	Submicrofracture
	CeO <sub>2</sub>	4 nm	0.03 $\mu\text{m}$	0.01	-	Tribo-chemical



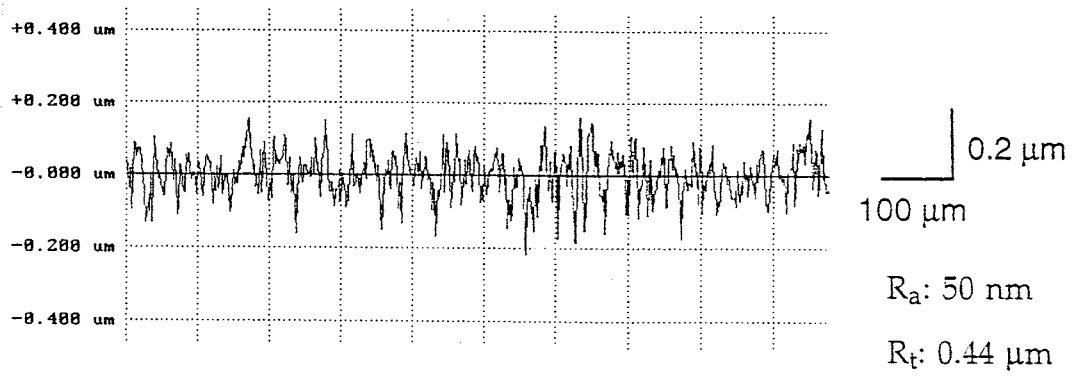
(a)  $\text{B}_4\text{C}$  (500 grit) abrasive



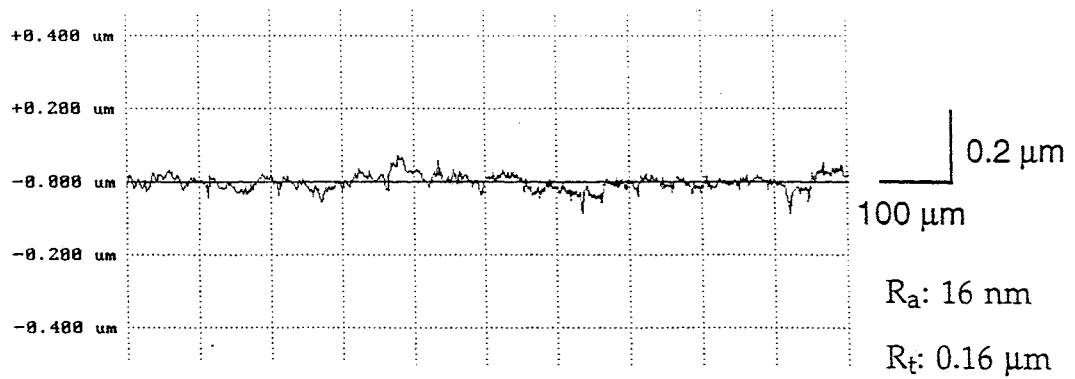
(b)  $\text{SiC}$  (400 grit) abrasive



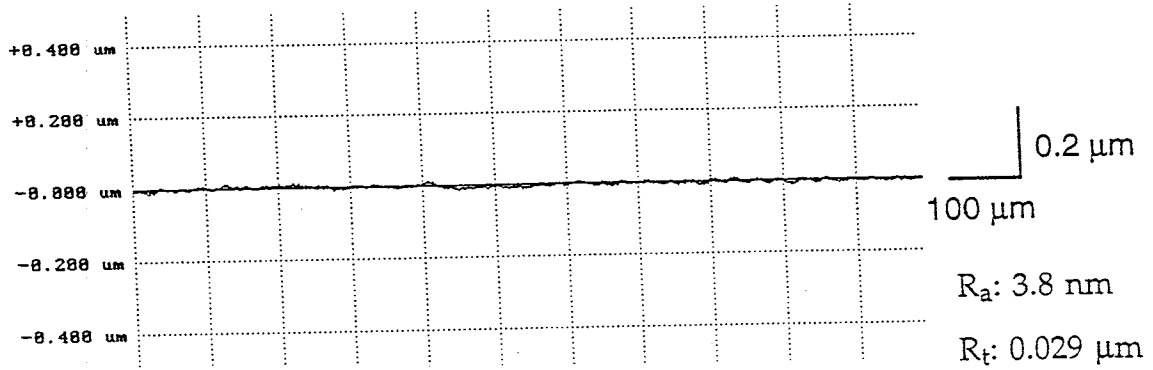
(c) SiC (1000 grit) abrasive



(d) SiC (1200 grit) abrasive



(e) SiC (8000 grit) abrasive



(f)  $\text{CeO}_2$  (5  $\mu\text{m}$ ) abrasive

Figures 8.2 Talysurf surface roughness profiles of a  $\text{Si}_3\text{N}_4$  ball after polishing (a) by  $\text{B}_4\text{C}$  (500 grit) abrasive (b) by  $\text{SiC}$  (400 grit) abrasive (c) by  $\text{SiC}$  (1000 grit) abrasive (d) by  $\text{SiC}$  (1200 grit) abrasive (e) by  $\text{SiC}$  (8000 grit) abrasive (f) by  $\text{CeO}_2$  (5  $\mu\text{m}$ ) abrasive

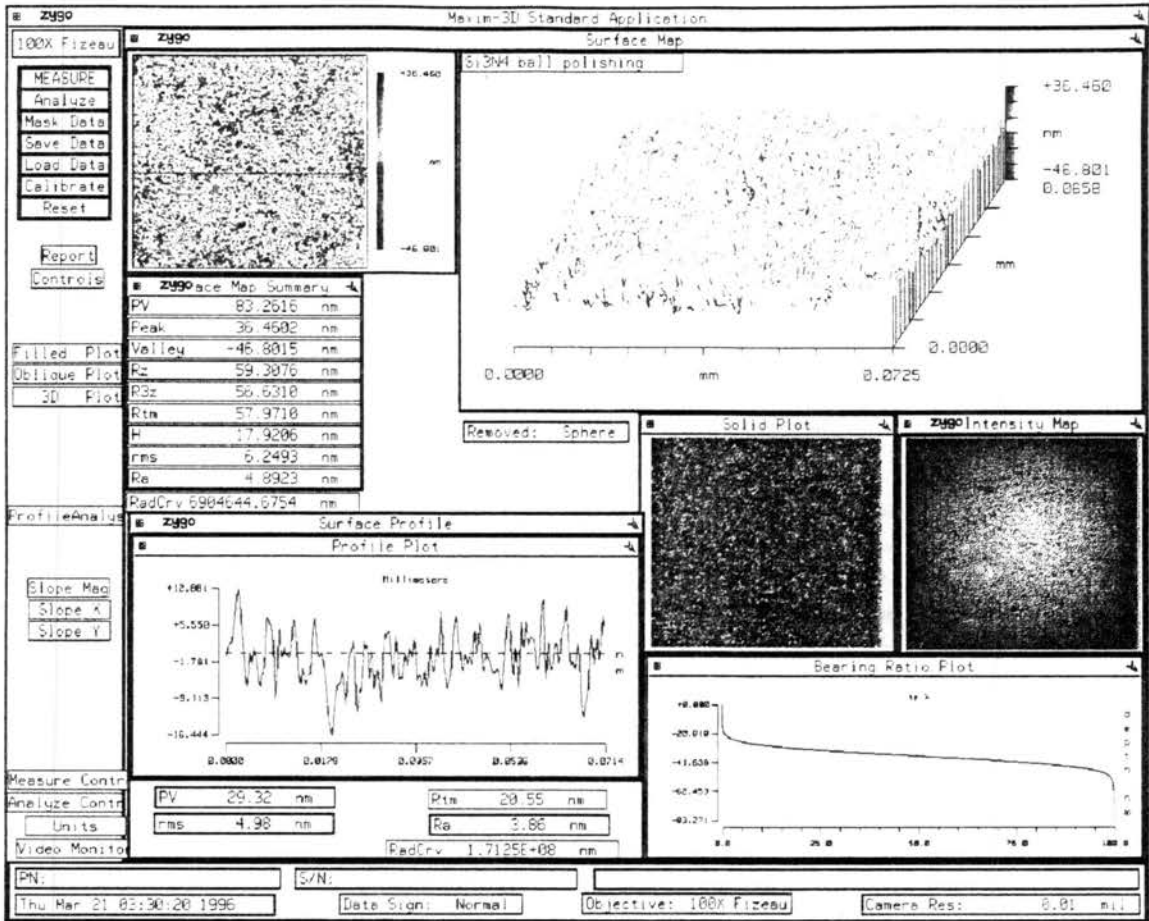
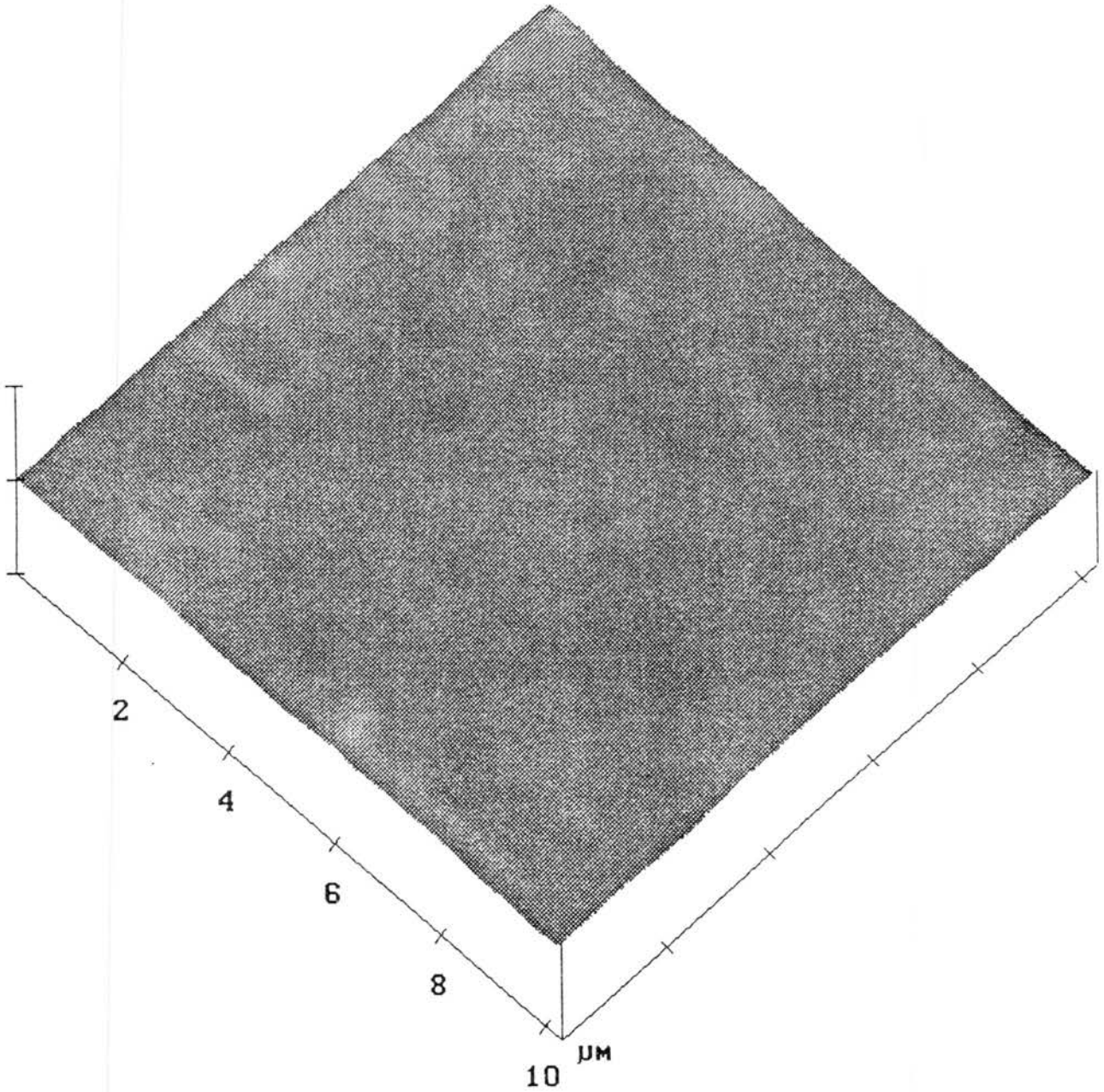
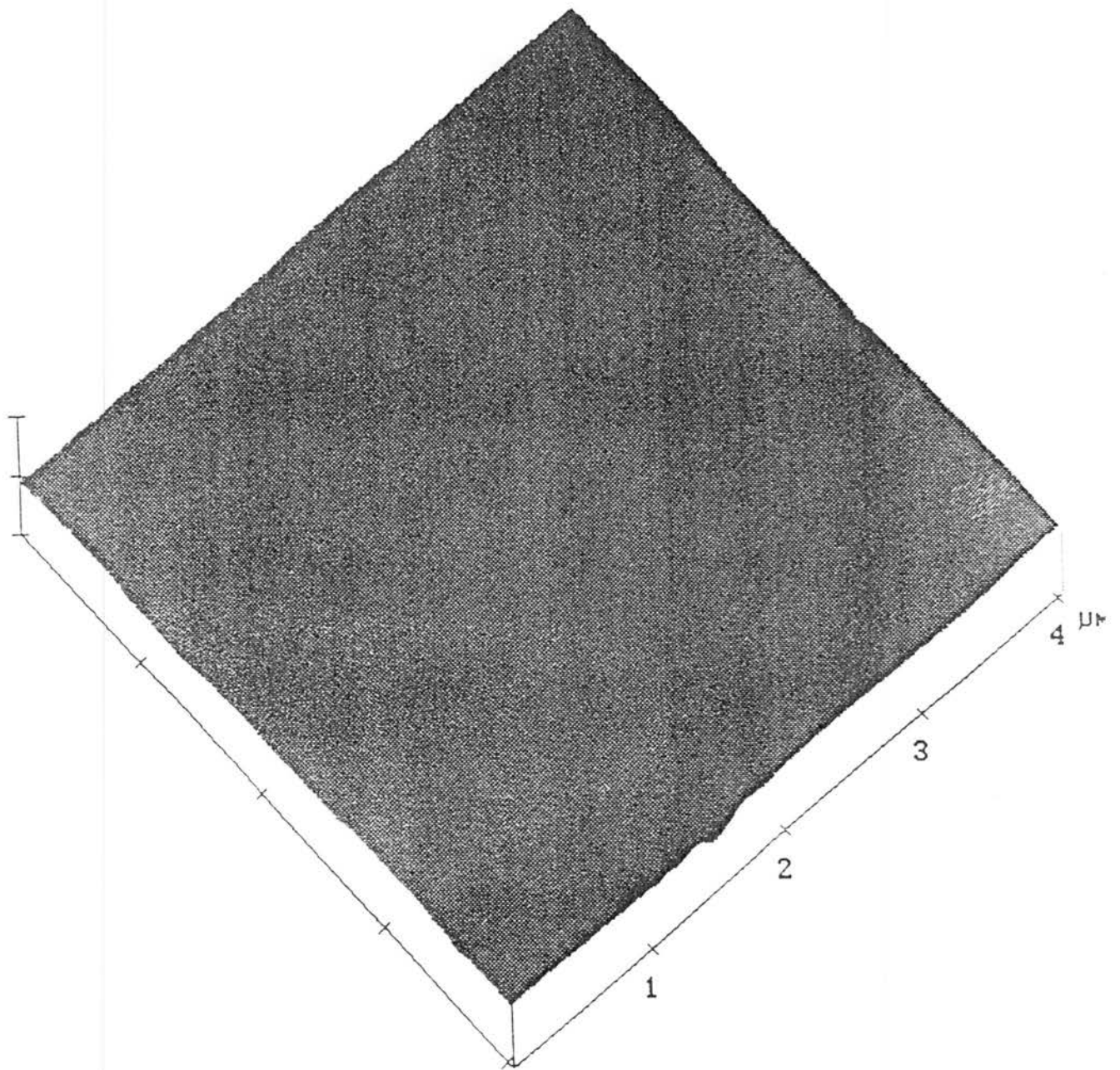


Figure 8.3 (a) ZYGO plot of the surface of a  $\text{Si}_3\text{N}_4$  ball after finishing by softer  $\text{CeO}_2$  abrasive.



Z range	13.986 nm
Mean	-0.097 nm
Rms (Rq)	1.933 nm
Mean roughness (Ra)	1.128 nm
Max height (Rmax)	13.277 nm
Surface area	
Surface area diff	

Figure 8.3 (b) AFM image of the surface of a Si<sub>3</sub>N<sub>4</sub> ball after finishing by softer CeO<sub>2</sub> abrasive.



Z range	19.593 nm
Mean	2.102 nm
Rms (Rq)	3.238 nm
Mean roughness (Ra)	1.386 nm
Max height (Rmax)	18.433 nm
Surface area	
Surface area diff	

Figure 8.3 (c) AFM image at high magnification showing an extremely smooth surface of a  $\text{Si}_3\text{N}_4$  ball after finishing by softer  $\text{CeO}_2$  abrasive.



Figure 8.4 (a) is an SEM micrograph of a  $\text{Si}_3\text{N}_4$  ball surface obtained after mechanical polishing with a finer SiC abrasive (8000 grit size) indicating that the material removal from the workmaterial is predominantly by brittle fracture on a submicroscopic scale under the mechanical action of the abrasive. While some polishing scratches can be seen, the surface is relatively free of pits that would normally form using diamond abrasive. Figure 8.4 (b) is a representative SEM micrograph of a  $\text{Si}_3\text{N}_4$  ball surface after the surface has been finished by CMP with a softer abrasive,  $\text{CeO}_2$ , showing an extremely smooth surface with practically no surface defects, such as pits or scratch marks. Several areas of the  $\text{Si}_3\text{N}_4$  ball surface were scanned and the micrograph shown in Figure 8.4 (b) was found to be a representative of the topography of the surface.

Figures 8.5 (a) and (b) SEM micrographs of the polishing shaft after polishing  $\text{Si}_3\text{N}_4$  balls with B4C 500 and B4C 1500 abrasives. They show that the abrasives are actually not embedded in the shaft as considered by Childs et al [7] but actually abrade the softer stainless steel polishing shaft. Thus, while the action of the abrasives is one of a two body abrasion (i. e. sliding without rotation) as rightly pointed out by Childs, they are not fixed but move relative to the polishing shaft. The material removal is due to the relative speed between the abrasives and the workmaterials.

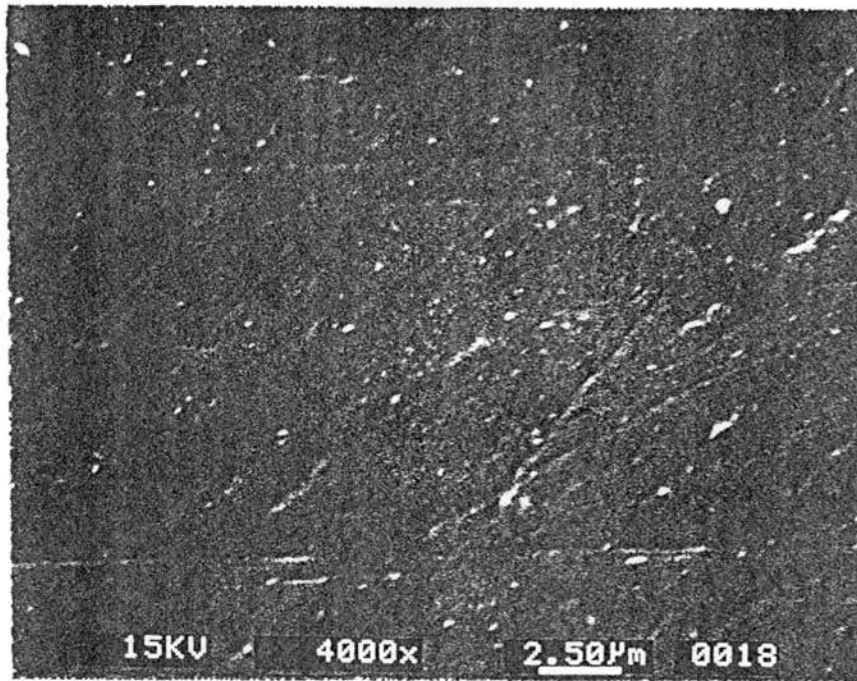


Figure 8.4 (a) SEM micrograph of the surface of a Si<sub>3</sub>N<sub>4</sub> ball after polishing by SiC (8000 grit) abrasive

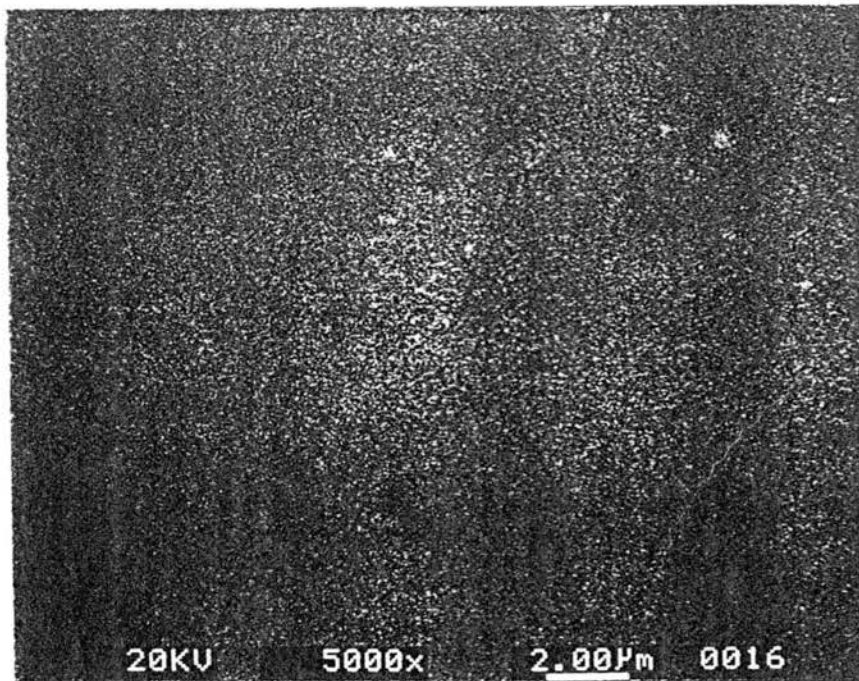


Figure 8.4 (b) SEM micrograph of the surface of a Si<sub>3</sub>N<sub>4</sub> ball after polishing by CeO<sub>2</sub> (5 μm) abrasive

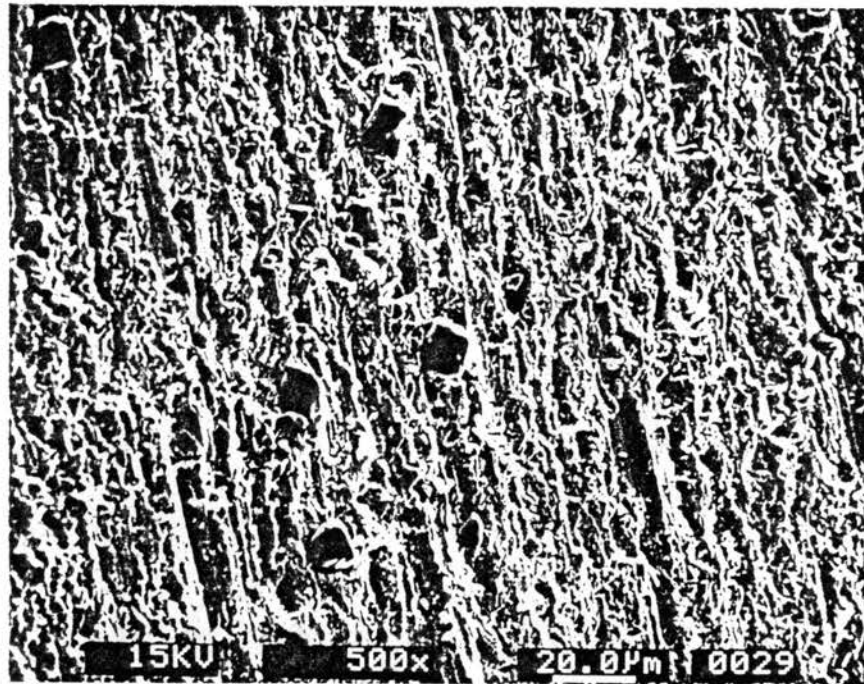


Figure 8.5 (a) SEM micrograph of the stainless steel shaft in contact with  $\text{Si}_3\text{N}_4$  balls in MFP showing the presence of  $\text{B}_4\text{C}$  (500 grit) particles and abrasion marks on the shaft materials.

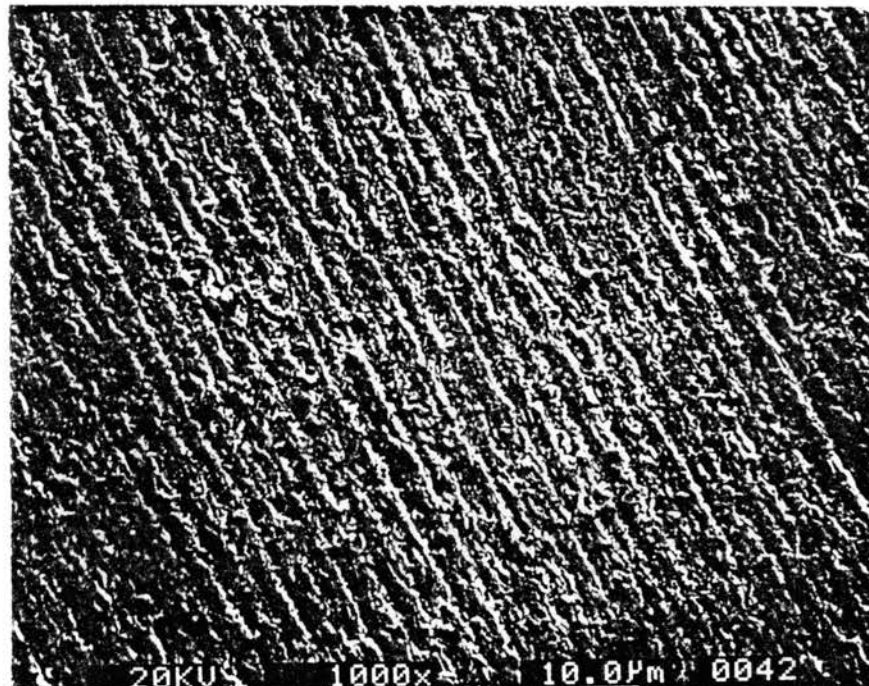


Figure 8.5 (b) SEM micrograph of the stainless steel shaft in contact with  $\text{Si}_3\text{N}_4$  balls in MFP showing the presence of  $\text{B}_4\text{C}$  (1500 grit) particles and abrasion marks on the shaft materials.

## 8.4 DISCUSSION

### 8.4.1 MECHANICAL POLISHING

The mechanism of material removal from the  $\text{Si}_3\text{N}_4$  balls by finer grit, harder abrasives, such as  $\text{B}_4\text{C}$  and  $\text{SiC}$  in MFP process is by mechanical microfracture because of higher hardness of the abrasive and the inherent brittleness of the workmaterial. Under these conditions material removal occurs not by grain pullout, grain fracture, and large fracture but by microfracture by cleavage. While chemo-mechanical action may also occur, its contribution is considered to be much smaller than the mechanical action, namely, microfracture by cleavage.

Childs et al (1995) have shown that in magnetic float polishing(MFP), material removal from the balls is accomplished by the action of the abrasives embedded in the shaft due to sliding at the contact area between the drive shaft and the ball. It is unlikely that when fine abrasives are held between the  $\text{Si}_3\text{N}_4$  balls and the stainless steel shaft that the abrasives will get embedded in the shaft, as in the present case. If this is so, one would never be able to remove material from softer workmaterials with loose abrasives. In an actual situation, the abrasive will abrade the soft stainless steel shaft much more so than the  $\text{Si}_3\text{N}_4$  workmaterial and it appears unlikely that the abrasives will be embedded as Childs et al considered but would be moving relative to the polishing shaft forming abrasion marks in the shaft. In fact wear on the stainless steel shaft is as a result of it and may have to be ground periodically to improve sphericity.

For larger sized abrasives and higher loads, as in conventional polishing with diamond abrasive, the finished surface is effected by the formation of deep pits, grooves and cracks. This will not be the case with finer abrasives and lighter loads. Higher material removal rates without subsurface damage is feasible by magnetic float polishing because of high polishing speeds and very flexible float system used. The low loads used (1 N/ball), while causes microcracking by cleavage, is small enough as to not cause larger cracks, or dislodge grains by grain pullout.

#### **8.4.2 CHEMO-MECHANICAL POLISHING (CMP)**

The mechanism of material removal in the final stages of polishing by softer cerium oxide ( $\text{CeO}_2$ ) is due to CMP. Thermal analysis of flash temperature and flash duration as well as thermodynamic studies of the polishing process strongly suggest the possibility of CMP of  $\text{Si}_3\text{N}_4$  by  $\text{CeO}_2$ . Details of the chemo-mechanical action of the  $\text{CeO}_2$  abrasive with the  $\text{Si}_3\text{N}_4$  balls is the subject in chapter 6-7. Under the mechanical frictional action during polishing, chemical reactions can be initiated between the  $\text{Si}_3\text{N}_4$  balls and the  $\text{CeO}_2$  abrasive in the presence of water (from the water based magnetic fluid) and the material is removed by the chemical dissolution of material resulting in a reaction product that is subsequently removed by the mechanical action of the abrasive. Since the hardness  $\text{CeO}_2$  abrasive is about 1/3 of  $\text{Si}_3\text{N}_4$  workmaterial, it can hardly scratch or damage it and the material is removed by tribological interaction forming a reaction product. Thus, tribochemical action instead of mechanical fracture is credited here for the extremely smooth and damage-free surfaces accomplished on the  $\text{Si}_3\text{N}_4$  balls.

## **8.5 PRECISION MANUFACTURING PROCESS**

Precision manufacturing process for finishing silicon nitride ( $\text{Si}_3\text{N}_4$ ) bearing balls (with good sphericity and excellent surface finish to requirement size) to ANSI/AFBMA 10, 7, 5, and 3 by MFP technology is presented in the following. This process has also been carried out in a large batch polishing apparatus towards implementation of this technology in industry.

### **8.5.1 SURFACE FINISH**

The methodology of fine mechanical polishing followed by chemo-mechanical polishing (CMP) is rather critical for obtaining excellent surface finish of advanced ceramic balls in the MFP process resulting in higher strength workmaterial and reliability of the parts in service.

### **8.5.2 OUT-OF-ROUNDNESS**

It is found that accuracy of both apparatus construction and polishing set-up are critical for obtaining good sphericity of advanced ceramic balls in the MFP process. But these would not have much effect on the surface finish obtainable. In the MFP process, when larger diameter portions of ball enter the contact area, the load will increase and a larger amount of material will be removed from this place. This process continues resulting in improved sphericity.

The accuracies of apparatus construction involved in the geometrical accuracy as well as relative positional accuracy of its main parts. The geometric accuracy depends on the accuracy machine tools used. The relative positional

accuracy depends on the adjustment and set-up of machine tools used in machining process. Regarding polishing set-up accuracy, maintaining coaxiality between rotating axis of the polishing shaft and the polishing guide ring of the MFP apparatus is the most important. In the following these details are discussed briefly:

1. The geometrical accuracy of the main parts of the apparatus:

A. Out-of-roundness of the internal cylindrical surface of the chamber;

B. Out-of roundness of the cylindrical surface of the polishing shaft.

This depends upon the spindle rotational accuracy of the turning machine used for fabricating the chamber and shaft, especially the inaccuracies in the spindle bearing, stiffness, and thermal deformations.

The abrasive wear of the polishing shaft, the polishing float, and the urethane rubber ring during the polishing lead to improper polishing motion of the ball and can result in sphericity degradation. They should re-machined or replaced periodically.

2. Relative positional accuracy of the apparatus:

A. End surface of the shaft, which is the reference surface of the shaft to the drive spindle should be perpendicular to the rotating axis to minimize the additional inaccuracies in the rotational motion; B. The tapered polishing surface of the shaft should be coaxial with rotating axis. To satisfy the above mentioned requirement, i.e., A and B, during final precision machining stages, the machining of shaft cylindrical and conical polishing surface should be accomplished using one chuck mounting, taking the end surface as axial

machining reference. To re-machine the conical polishing surface after wear, the shaft axis should be set up to coaxial to lathe axis by indicating the cylindrical surface of shaft.

C. The axis of chamber wall should be perpendicular to chamber bottom. Polishing chamber is used not only for containing the polishing fluid but also for guiding the ball track as a guide ring. To preserve relation integrity, the machining of chamber should be done within one chuck mounting (without removing the workpiece from the lathe chuck) to machine I.D and O.D. of chamber for their concentricity and machine the end surface to make perpendicularity of the end surface with respect to the chamber walls, which is the reference surface to ensure the chamber walls to perpendicular to the chamber base.

### 3. Polishing set-up accuracy:

A. Coaxiality between drive spindle and polishing shaft: Due to the abrasive wear in MFP process, periodically, the shaft have to be removed and polishing surface have to be re-machined. When the shaft is re-mounted to the drive spindle, great care must be used to aligning the shaft axis with the drive axis. It is preferred re-grinding the shaft without removing the shaft from spindle by setting up a grinding unit.

B. Coaxiality between polishing shaft and polishing chamber: The mounting eccentricity between polishing shaft and polishing guide ring should be avoided. The improper setup or not enough set-up accuracy with even very small enccentricity is the main reason of the low sphericity. Figure 8.6 shows a typical triangle shape of a  $\text{Si}_3\text{N}_4$  ball due to eccentricity between the polishing drive shaft (tool) and guide ring (track).



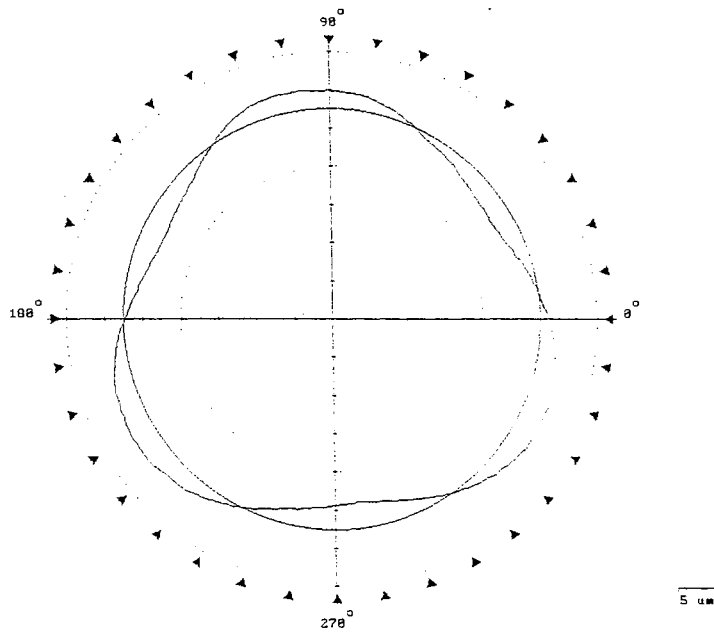


Figure 8.6 TalyRond roundness profile of a  $\text{Si}_3\text{N}_4$  ball with a typical triangle shape after polishing with  $\text{B}_4\text{C}$  #500 due to eccentricity between the polishing drive shaft (tool) and guide ring (track) (Roundness:  $6 \mu\text{m}$ )

The purpose of above mentioned requirements 3. A&B is to keep coaxiality between rotating axis of polishing shaft and polishing guide ring. This is the most frequent problem to cause bad sphericity results.

### **8.5.3 LARGE BATCH MAGNETIC FLOAT POLISHING PROCESS**

Work is underway in the development of an MFP apparatus for finishing a larger batch balls ( ~100 balls of 3/8 in dia.) and associated monitoring for in-process control of the MFP process. The process is carried out in a large batch polishing apparatus for implementation of this technology in industry. The polishing conditions used in large batch MFP (12.5 inch diameter) are in followings: Abrasive: B<sub>4</sub>C #400, SiC 1200, SiC 8000, followed by CeO<sub>2</sub>, Abrasive concentration: 5 vol%, Load: 1 N/ball, and speed: 400 rpm. which is same as the polishing condition used in small batch (2.5 inch diameter). The initial test results yielded a sphericity 0.15 μm and a surface finish Ra 0.010 μm after 20 hour polishing [Komanduri, Umehara, Jiang, and Cao, 1998]. The apparatus shown in Figure 8.7 (guide ring diameter: 12.5 inch) for polishing large batches of advanced ceramic balls has been fabricated in collaboration with Prof. N. Umehara of Tohoku University in Japan.

### **8.5.4 FINISHING PROCESS**

Uniaxial pressed Si<sub>3</sub>N<sub>4</sub> (CERBEC NBD-200) balls are used in this investigation. The as-received balls had a nominal diameter of 13.4 mm and had to be finished to a final size of 12.7 mm (0.5 inch) with (a) a sphericity of 0.25 μm and surface finish of Ra 25 nm for ANSI/AFBMA grade 10; (b) a sphericity of 0.13 μm and surface finish of Ra 20 nm for ANSI/AFBMA

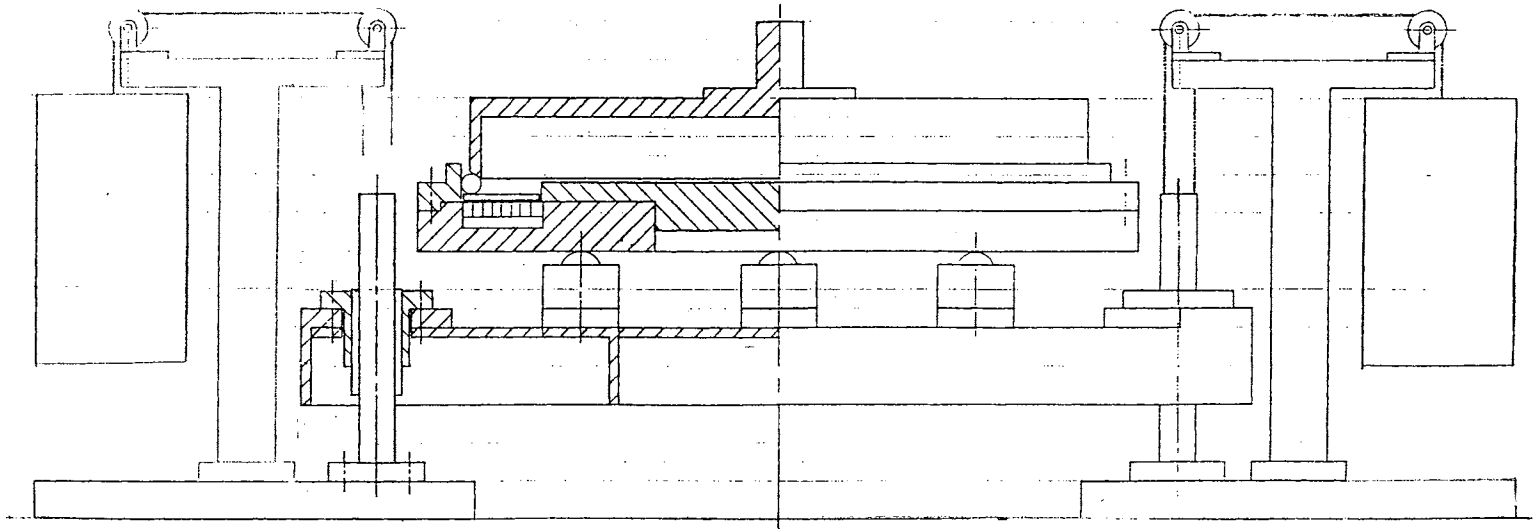


Figure 8.7 Large batch MFP apparatus [Komanduri, Umehara, Jiang, and Cao, 1998]

grade 5; and (c) a sphericity of 0.08  $\mu\text{m}$  and surface finish of Ra 12 nm for ANSI/AFBMA grade 3. Table 8.4 gives the polishing procedure and results.

Figure 8.8 (a) shows TalyRond roundness profile of an as-received  $\text{Si}_3\text{N}_4$  ball showing a 200  $\mu\text{m}$  x 5 mm band at the parting line due to the uniaxial pressing process (Roundness: 200  $\mu\text{m}$ ). Figures 8.8 (b) - (h) show TalyRond roundness profile of a  $\text{Si}_3\text{N}_4$  ball after polishing with  $\text{B}_4\text{C}$  #500 in Tests A - L. The roundness has improved from 200  $\mu\text{m}$  to 0.6  $\mu\text{m}$  after 14 hours of polishing. The diameter was reduced from 13.4 mm to 12.730 mm; The material removal rate was 0.8 - 1.0  $\mu\text{m}/\text{min}$ . Figure 8.9 (a) shows the TalySurf surface roughness profile of a  $\text{Si}_3\text{N}_4$  ball after polishing with  $\text{B}_4\text{C}$  #500, Ra: 0.184  $\mu\text{m}$ , Rt: 1.44  $\mu\text{m}$ .

Figure 8.8 (i) shows the TalyRond roundness profile of a  $\text{Si}_3\text{N}_4$  ball after polishing with SiC #1200 abrasive in Test N. The roundness was improved from 0.6  $\mu\text{m}$  to 0.3  $\mu\text{m}$ . The diameter was reduced from 13.730 mm to 12.706 mm, and material removal rate was 0.2  $\mu\text{m}/\text{min}$ . Figure 8.9 (b) shows TalySurf surface roughness profile of a  $\text{Si}_3\text{N}_4$  ball after polishing with SiC #1200 abrasive in Test N that the surface finish was improved to Ra, 0.05  $\mu\text{m}$  and Rt, 0.5  $\mu\text{m}$ . This is an intermediate stage of semifinishing and the size, the sphericity, and the surface roughness all have to be carefully monitored.

Figure 8.8 (j) shows TalyRond roundness profile of a  $\text{Si}_3\text{N}_4$  ball after polishing with SiC #8000 abrasive in Test O. The roundness has improved from 0.3  $\mu\text{m}$  to 0.2  $\mu\text{m}$ . The diameter was reduced from 12.706 to 12.702 mm, and the material removal rate was 0.05  $\mu\text{m}/\text{min}$ . Figure 8.9 (c) is a TalySurf surface roughness profile of a  $\text{Si}_3\text{N}_4$  ball after polishing with SiC #8000 abrasive showing an improved surface finish Ra of 0.02  $\mu\text{m}$ , and Rt of 0.15  $\mu\text{m}$ . This is the

final mechanical polishing stage where the emphasis was on the required size, sphericity, and good surface finish. The final chemo-mechanical polishing was followed to obtain the final excellent surface finish for increasing the reliability of the parts in service.

Figure 8.8 (k) is a TalyRond roundness profile of a  $\text{Si}_3\text{N}_4$  ball after polishing with  $\text{CeO}_2$  ( $5\ \mu\text{m}$ ) in Test Q. The roundness has improved from  $0.2\ \mu\text{m}$  to  $0.15\ \mu\text{m}$ , the diameter has reduced from  $12.702$  to  $12.700\ \text{mm}$ , and the material removal rate was  $0.01\ \mu\text{m}/\text{min}$ . The sphericity of the balls (i.e. maximum deviation of the roundness of a ball taken in three orthogonal planes) for this batch was found to be  $\sim 0.15\ \mu\text{m}$ . Figure 8.9 (d) is the TalySurf surface roughness of a  $\text{Si}_3\text{N}_4$  ball after polishing with  $\text{CeO}_2$  ( $5\ \mu\text{m}$ ) with a surface finish  $R_a$  of  $6\ \text{nm}$ , and  $R_t$  of  $46\ \text{nm}$ .

Figure 8.10 shows the variation of sphericity with polishing time. It took  $\sim 20$  hours to finish this batch of balls.

Childs, et al, (1995) has indicated that that magnetic fluid grinding is more likely to replace the roughing stage of the polishing than the final stage. In this investigation we have clearly demonstrated that magnetic float polishing (MFP) can replace completely (both roughing and finishing) the conventional polishing starting from the as-received balls and finish them to the final specifications in the same apparatus. The methodology for finishing  $\text{Si}_3\text{N}_4$  balls by MFP is presented for the first time in this study that involves actual finishing time an order or magnitude or more faster than conventional polishing.

Table 8.4 Polishing Procedure and Results

Test No.	Abrasive	Time, min	Diameter (mm)	MRR( $\mu\text{m}/\text{min}$ )	Sphericity ( $\mu\text{m}$ )	Ra ( $\mu\text{m}$ )
A-L	B <sub>4</sub> C #400	12 x 60	12.730/13.4	0.8 - 1.0	0.6/200	0.20
M-N	SiC #1200	2 x 60	12.706	0.2	0.3	0.05
O	SiC #8000	1 x 60	12.702	0.05	0.2	0.02
P-Q	CeO <sub>2</sub>	2 x 90	12.700	0.01	0.15	0.008

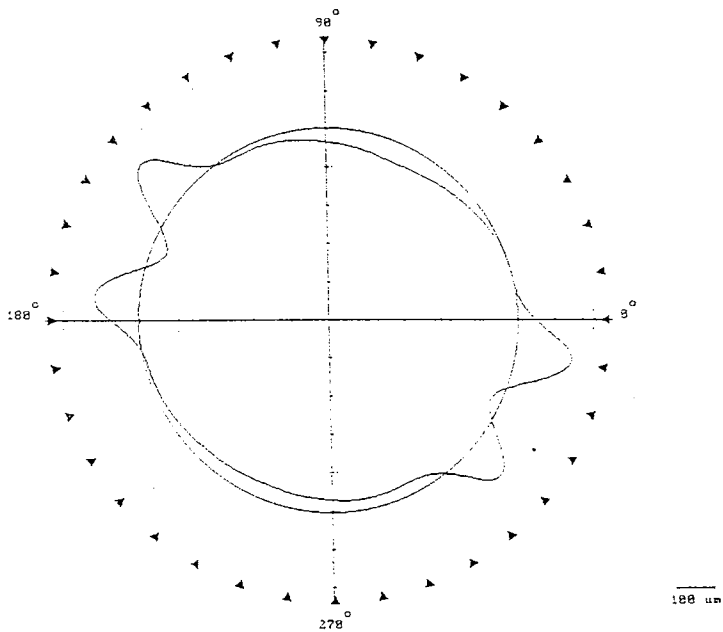


Figure 8.8 (a) TalyRond roundness profile of an as-received  $\text{Si}_3\text{N}_4$  ball showing a  $200\ \mu\text{m} \times 5\ \text{mm}$  band at the parting line due to uniaxial pressing process (Roundness:  $200\ \mu\text{m}$ )

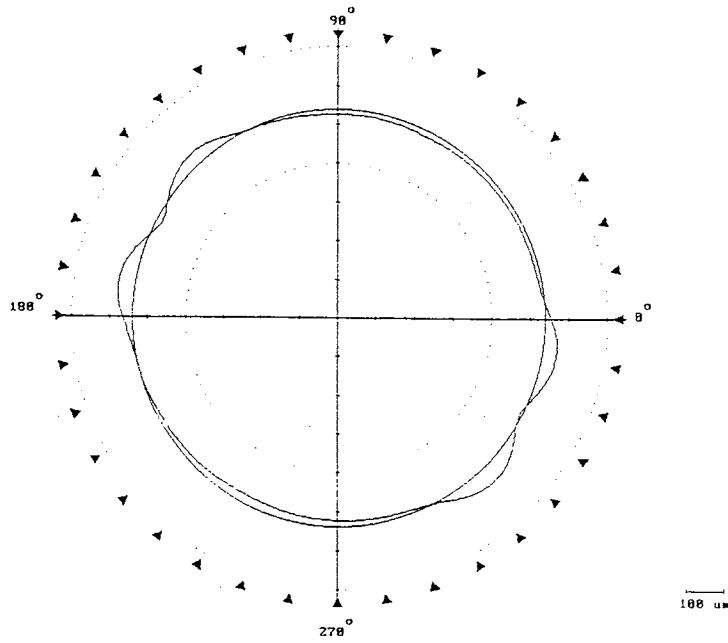


Figure 8.8 (b) TalyRond roundness profile of a  $\text{Si}_3\text{N}_4$  ball after polishing with  $\text{B}_4\text{C}$  #500 in Test A (Roundness:  $82 \mu\text{m}$ )

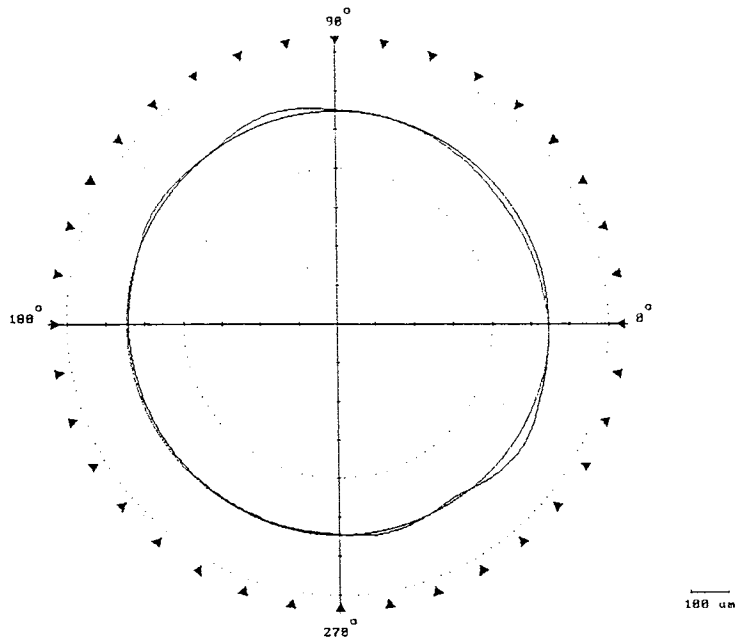


Figure 8.8 (c) TalyRond roundness profile of a  $\text{Si}_3\text{N}_4$  ball after polishing with  $\text{B}_4\text{C}$  #500 in Test B (Roundness:  $46 \mu\text{m}$ )



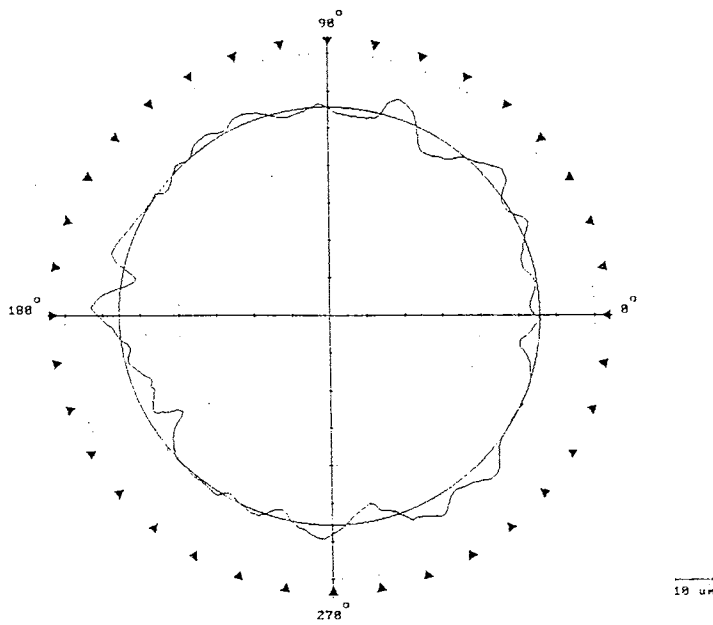


Figure 8.8 (d) TalyRond roundness profile of a  $\text{Si}_3\text{N}_4$  ball after after polishing with  $\text{B}_4\text{C}$  #500 in Test D (Roundness:  $16 \mu\text{m}$ )

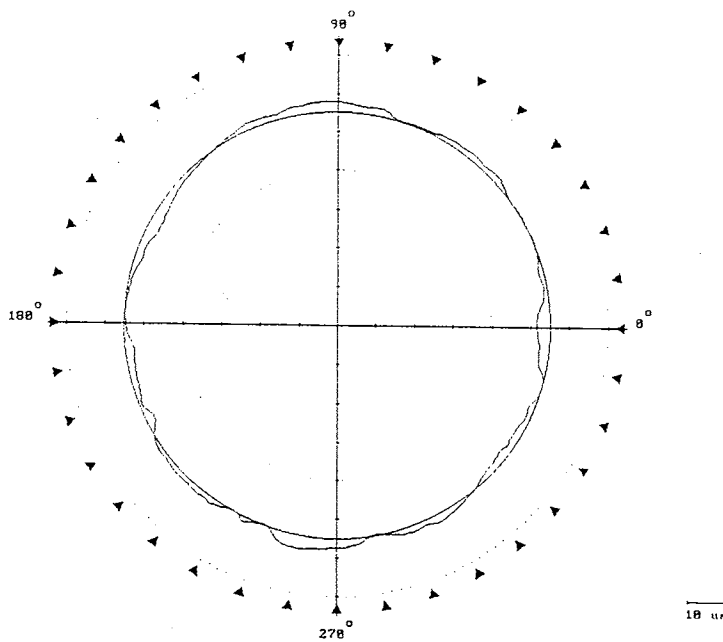


Figure 8.8 (e) TalyRond roundness profile of a  $\text{Si}_3\text{N}_4$  ball after after polishing with  $\text{B}_4\text{C}$  #500 in Test F (Roundness:  $7 \mu\text{m}$ )

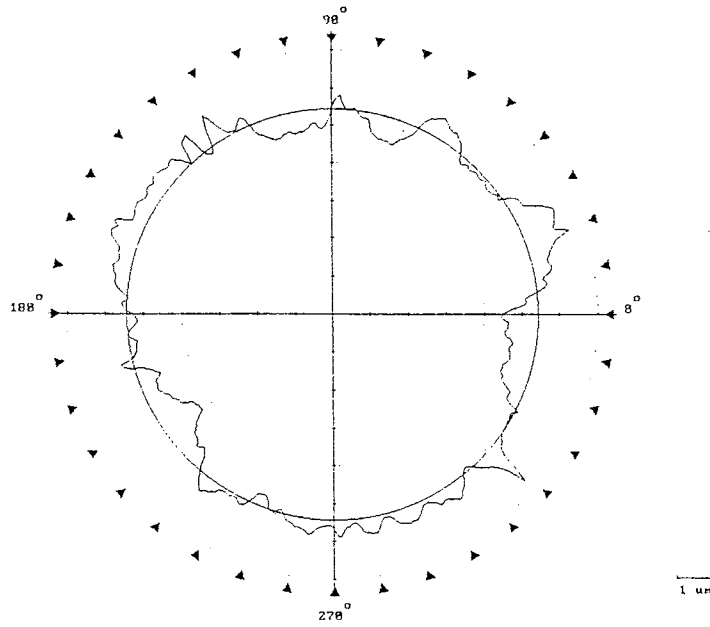


Figure 8.8 (f) TalyRond roundness profile of a  $\text{Si}_3\text{N}_4$  ball after after polishing with  $\text{B}_4\text{C}$  #500 in Test H (Roundness:  $2.4 \mu\text{m}$ )

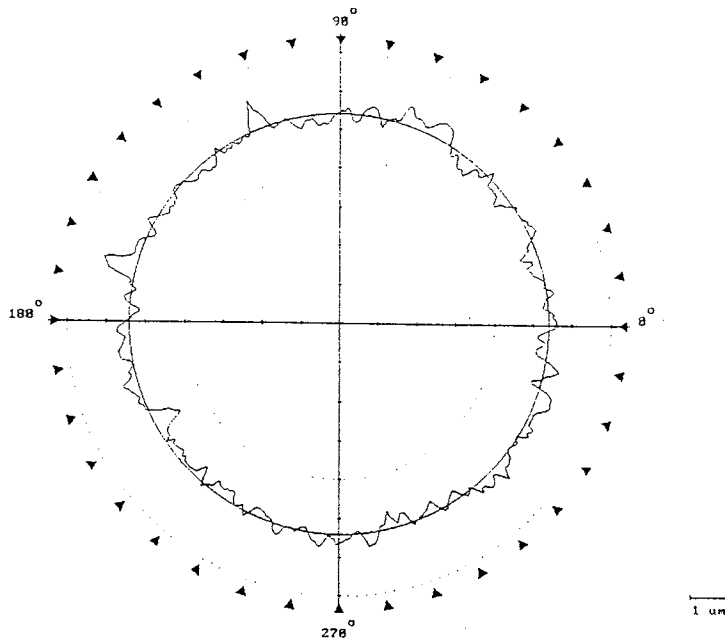


Figure 8.8 (g) TalyRond roundness profile of a  $\text{Si}_3\text{N}_4$  ball after after polishing with  $\text{B}_4\text{C}$  #500 in Test J (Roundness:  $1.6 \mu\text{m}$ )

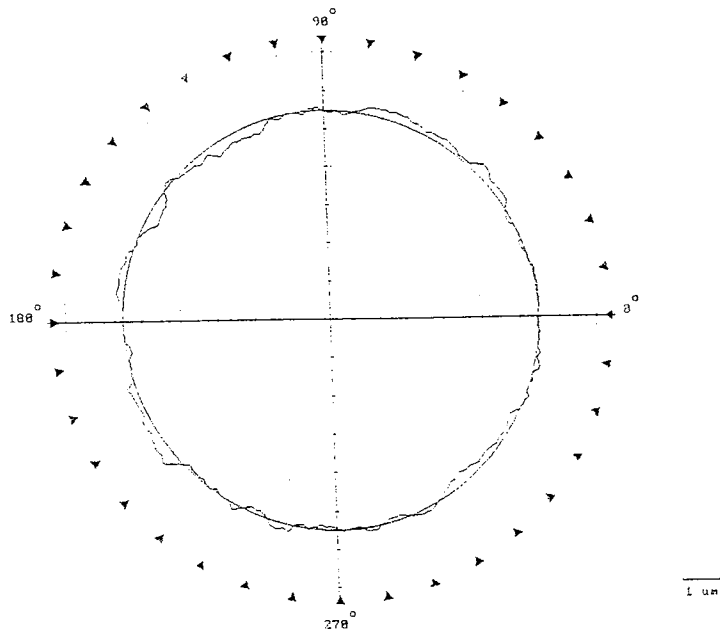


Figure 8.8 (h) TalyRond roundness profile of a  $\text{Si}_3\text{N}_4$  ball after after polishing with  $\text{B}_4\text{C}$  #500 in Test L (Roundness:  $0.6 \mu\text{m}$ )

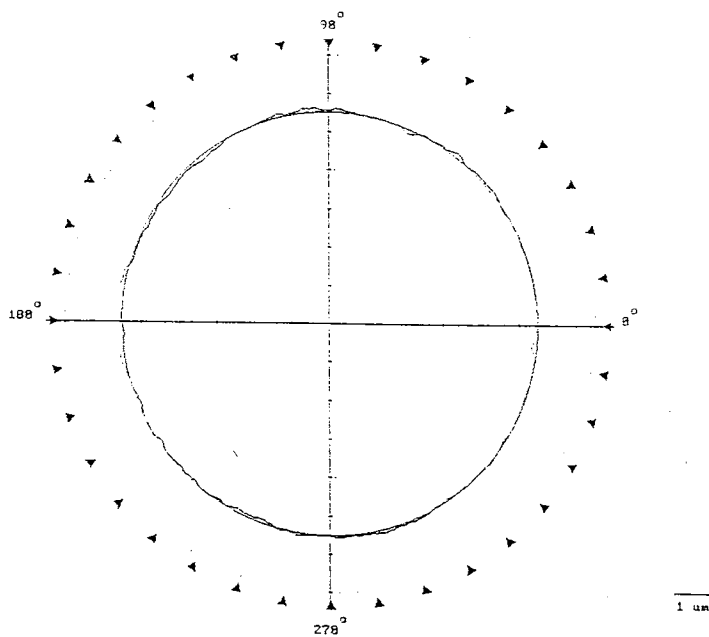


Figure 8.8 (i) TalyRond roundness profile of a  $\text{Si}_3\text{N}_4$  ball after polishing with  $\text{SiC}$  #1200 in Test N (Roundness:  $0.3 \mu\text{m}$ )

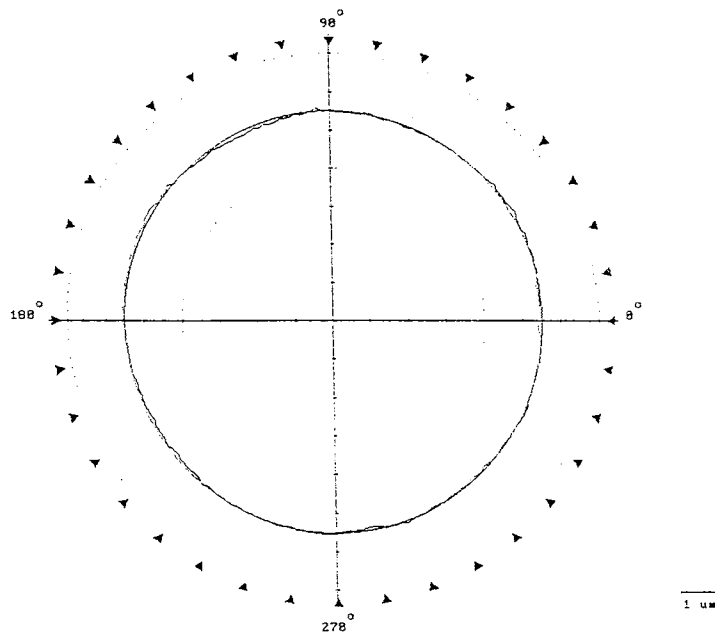


Figure 8.8 (j) TalyRond roundness profile of a  $\text{Si}_3\text{N}_4$  ball after polishing with SiC # 8000 in Test O (Roundness:  $0.2 \mu\text{m}$ )

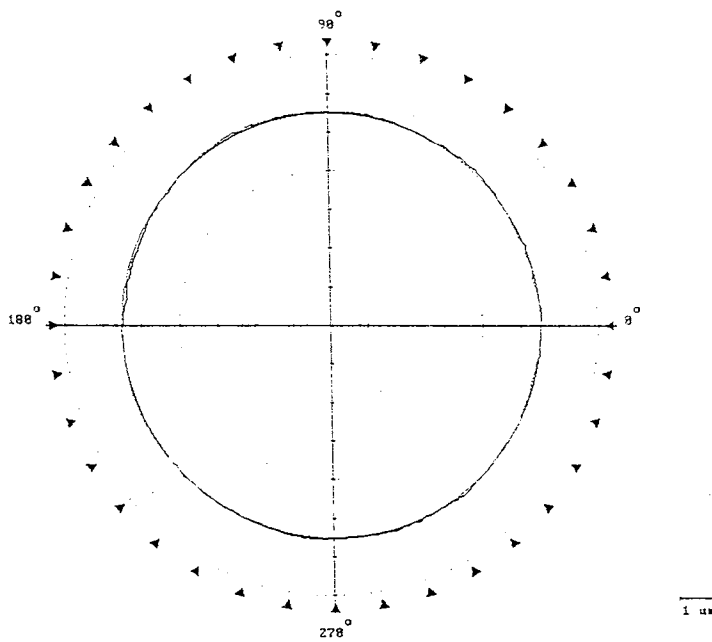


Figure 8.8 (k) TalyRond roundness profile of a  $\text{Si}_3\text{N}_4$  ball after polishing with  $\text{CeO}_2$  ( $5 \mu\text{m}$ ) in Test Q (Roundness:  $0.15 \mu\text{m}$ )

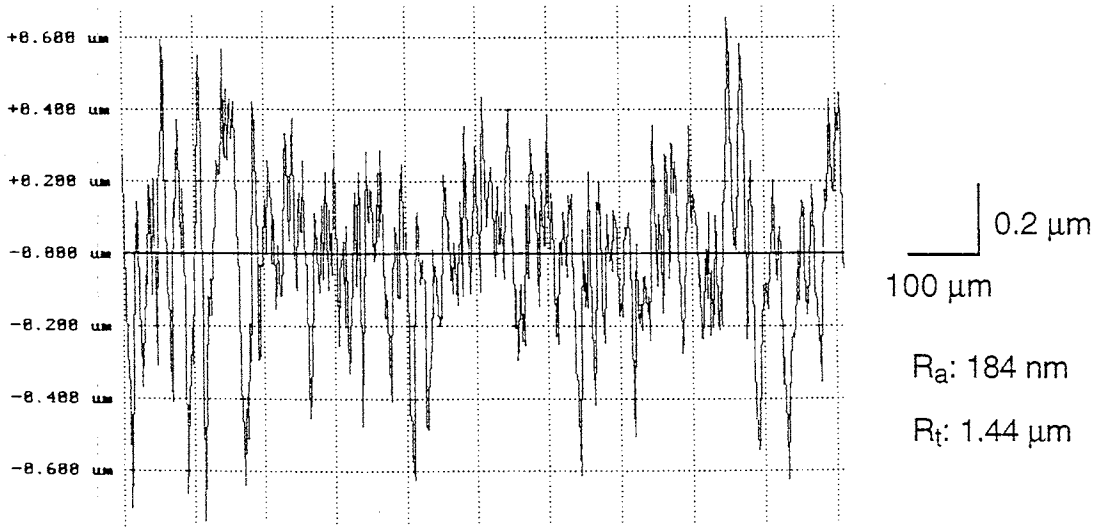


Figure 8.9 (a) TalySurf surface roughness profile of a  $\text{Si}_3\text{N}_4$  ball after polishing with  $\text{B}_4\text{C}$  #500 in Test L

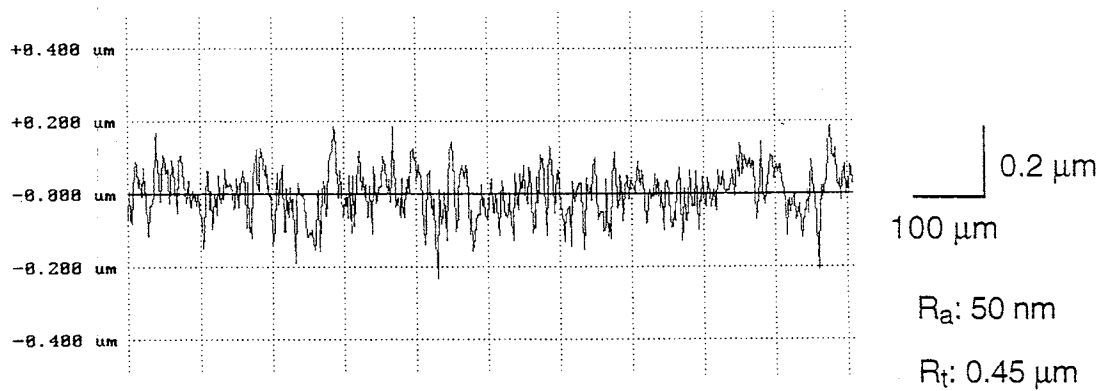


Figure 8.9 (b) TalySurf surface roughness profile of a  $\text{Si}_3\text{N}_4$  ball after polishing with  $\text{SiC}$  #1200 in Test N

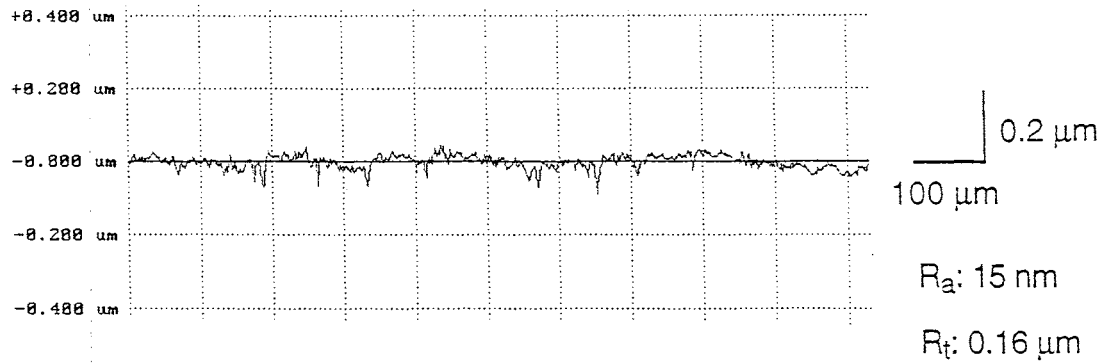


Figure 8.9 (c) TalySurf surface roughness profile of a  $\text{Si}_3\text{N}_4$  ball after polishing with SiC #8000 in Test O

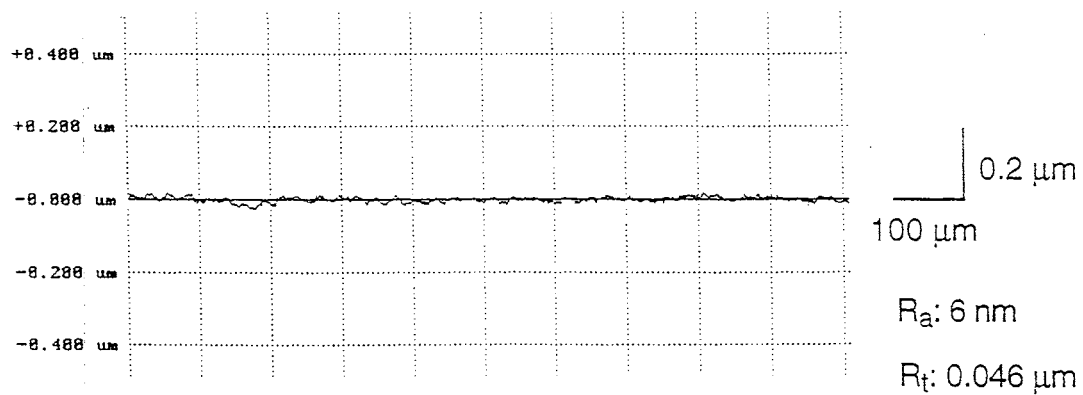


Figure 8.9 (d) TalySurf surface roughness of a  $\text{Si}_3\text{N}_4$  ball after polishing with  $\text{CeO}_2$  (5  $\mu\text{m}$ ) in Test Q

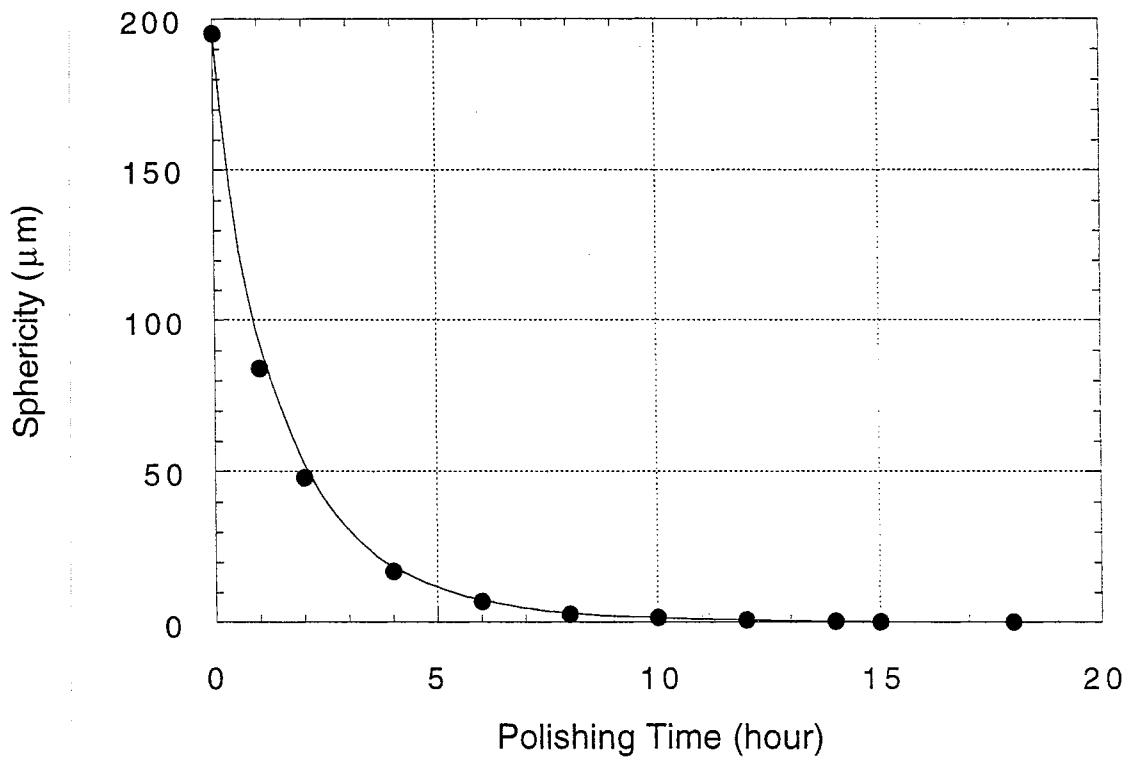


Figure 8.10 Variation of sphericity with polishing time

From the work presented here, it can be seen that magnetic float polishing (MFP) technique can be used for finishing Si<sub>3</sub>N<sub>4</sub> balls from the as-received condition to a sphericity ( $< 0.15 \mu\text{m}$ ), and surface finish Ra  $< 6 \text{ nm}$  without scratches or pits on the surface of balls. The polishing time from the as-received condition to the final requirements is  $< 20$  hours. This, however, does not take into account the time taken for the characterization of the surfaces using various techniques. The methodology developed here incorporates polishing conditions and the use of appropriate abrasives (including grain sizes) that are not severe enough at any stage to cause damage, such as deep pits and cracks in and near the surface, so that the balls can be finished to the requirements without surface or near surface damage. Of course, whether or not the surface can be finished absolutely smooth also depends on the residual porosity of the Si<sub>3</sub>N<sub>4</sub> material.

## **8.6. CONCLUSIONS**

The methodology of fine mechanical polishing followed by chemo-mechanical polishing (CMP) is critical for obtaining excellent surface finish of advanced ceramic balls in the MFP process leading to higher strength of the workmaterial and improved reliability of the parts in service. Both apparatus construction accuracy and polishing set-up accuracy are critical to obtain good sphericity.

MFP is very effective and at the same time economical manufacturing technology. Balls meeting the ANSI/AFBMA 10, 7, 5, and 3 have been finished in our investigation. This technology is now ready for implementation in industry. The process is ready for carrying out both low-volume prototype



production and high-volume standard production to meet the growing demand of next generation precision high-speed, high-temperature ceramic bearings.

## CHAPTER 9

### FUTURE WORK

Future work includes the extension of magnetic float polishing (MFP) technique to finish other advanced ceramics such as zirconia ( $ZrO_2$ ) balls for flow control applications and ferritic stainless steel (AISI 440C) balls for bearing applications. It may be pointed out that finishing of the latter (AISI 440C steel bearing ball) was found to be extremely difficult and time consuming by conventional ball lapping process by a leading industry in the U. S. and the potential for finishing steel balls using MFP method has never been considered by other researchers around the world because of the magnetic nature of steel. Some preliminary test results of MFP of zirconia balls and stainless steel (AISI 440C) balls are presented. It is, however, necessary to improve further to achieve results similar to that with  $Si_3N_4$ .

#### 9.1 FINISHING ZIRCONIA BALLS FOR FLOW CONTROL

Transformation toughened (between metal and ceramics) zirconia ( $ZrO_2$ ) has perhaps the highest fracture toughness among advanced ceramics, i.e., even higher than  $Si_3N_4$  (Table 1.1). The increased toughness tends to stop the cracks from spreading and increases the ball's strength in the stressed area.  $ZrO_2$  is superior in some respects in that it operates well in corrosive and erosive environments, such as molten metals, organic solvents, caustics, and most acids. Because of its high resistance to abrasion and corrosion, it is often

used in check valves for flow control. It is a high-strength material that performs well at temperatures up to 1800 °F. Being lighter than steel ball, it minimizes damage due to mating components. It can operate two to three times longer than metal or carbide balls in certain applications. However, due to higher density compared to Si<sub>3</sub>N<sub>4</sub>, the latter is still prepared for bearing applications.

The properties of zirconia balls used in this investigation are given in Table 9.1. MFP technique was used for finishing ZrO<sub>2</sub> balls. The polishing conditions used are listed in Table 9.2. Because of its relatively high fracture toughness, it is anticipated that there will be more scratching abrasion/ plowing/ wear tracks and less fracture pits in ZrO<sub>2</sub> polished surface than that of Si<sub>3</sub>N<sub>4</sub>.

Table 9.1 Properties of zirconia (Yttria stabilized) balls

Density	6.06 g/cm <sup>3</sup> (0.219 lb/in <sup>3</sup> )
Compressive Strength	794,837 psi
Young's Modulus	21700kgf/mm <sup>2</sup> (30.6 x 10 <sup>6</sup> psi)
Hardness	1250 kgf/mm <sup>2</sup>
Thermal Conductivity	0.007 cal/cm. sec. °C
Thermal Expansion	10.9 x 10 <sup>-6</sup> / °C
Electrical Resistivity	2.2 x 10 <sup>12</sup> cm
Max. useful Temperature	1800 °F
Corrosion Resistance	Zirconia is inert to corrosive materials with the exception of hydrofluoric acid and hot, concentrated sulfuric acid.

Table 9.2 Polishing conditions for MFP of zirconia (ZrO<sub>2</sub>) balls

Workmaterial	Zirconia (Yttria stabilized) Balls
Polishing Tool Material	304 stainless steel
Abrasive	SiC#8000
Magnetic Fluid	Water-based (W-40)
Abrasive vol%	10%
Polishing Load, N/ball	1
Polishing Speed, rpm	2000
Test Time, min/step	90

Table 9.3 shows the preliminary test results of finishing zirconia (ZrO<sub>2</sub>) balls by MFP with SiC #8000 abrasive. The corresponding TalySurf surface finish profiles are given in Figures 9.1(a) and (b). The initial surface of a ZrO<sub>2</sub> ball has a roughness Ra of 0.35 μm and Rt of 2.50 μm [Figure 9.1 (a)]. After 90 min of polishing with SiC (#8000 grit) abrasive, the surface finish is significantly improved (Ra: 0.02 μm, Rt: 0.15 μm) [Figure 9.1 (b)]. Material removal rate was 0.1 μm/min. The surface finish can be further improved by chemo-mechanical polishing (CMP) with an appropriate abrasive.

Table 9.3 Test results of finishing Zirconia (ZrO<sub>2</sub>) balls by MFP with SiC (#8000 grit) abrasive

Initial	Surface	MFP with	SiC 8000
Ra (μm)	Rt (μm)	Ra (μm)	Rt (μm)
0.35	2.5	0.02	0.15

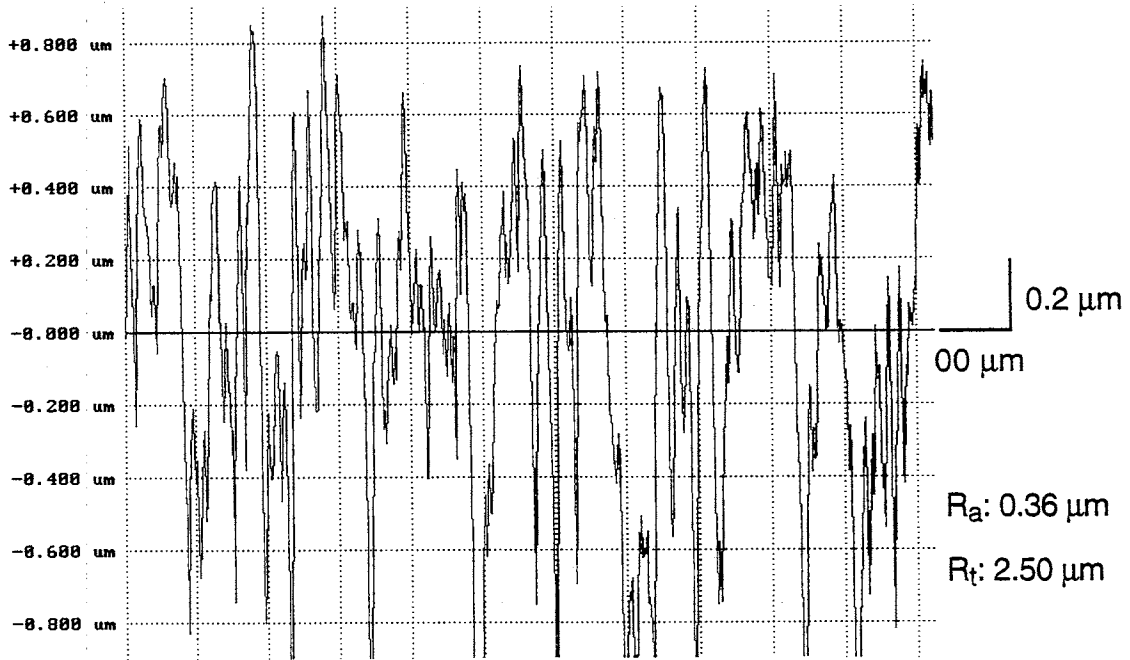


Figure 9.1 (a) An initial surface of a zirconia ( $\text{ZrO}_2$ ) ball

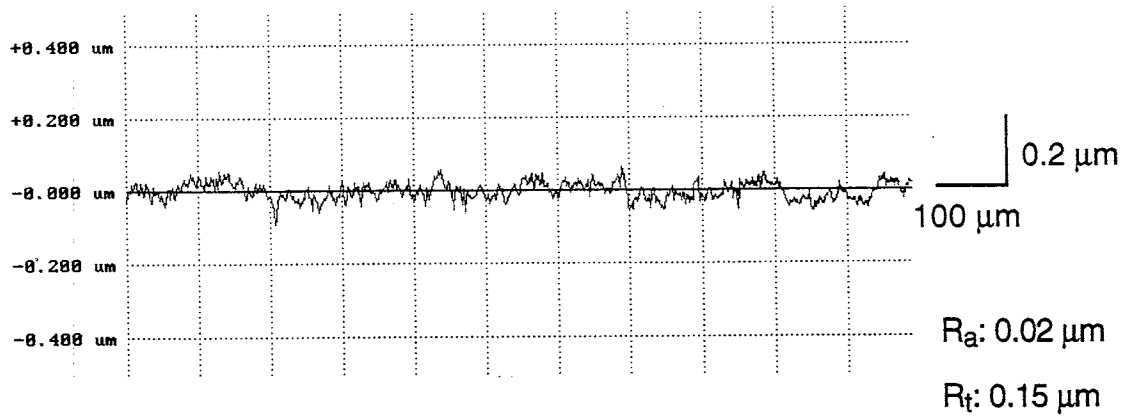


Figure 9.1 (b) A surface of a Zirconia ( $\text{ZrO}_2$ ) ball after polishing with SiC (#8000 grit) abrasive

## 9.2 FINISHING AISI 440C STAINLESS STEEL BALLS FOR BEARING APPLICATIONS

AISI 440C stainless steel is corrosion resistant and hardened steel bearing ball material. The chemical composition and mechanical properties of 440C stainless steel is given in Tables 9.4 and 9.5, respectively.

Table 9.4 Chemical component of AISI 440C

Carbon	0.95 to 1.20%
Chromium	16.00 to 18.00%
Molybdenum	Maximum of 0.75%
Nickel	Maximum of 0.75%
Copper	Maximum of 0.50%
Manganese	Maximum of 1.00%
Silicon	Maximum of 1.00%
Phosphorus	Maximum of 0.04%
Sulphur	Maximum of 0.03%

Table 9.5 Mechanical properties of AISI 440C

Density	0.277 lb/in <sup>3</sup>
Hardness, Rockwell, C	58 - 65
Tensile strength	285,000 psi
Yield strength	275,000 psi
Elongation in two inches	2%
Reduction in area	10%
Modulus of elasticity	29,000,000 psi

AISI 440C (ferritic) stainless steel is a magnetic material. Hence, it can be attracted to the bottom of MFP chamber by the magnetic field from the magnets

under the chamber. However, the AISI 440C steel balls can still be floated up for magnetic float polishing (MFP) when the magnetic buoyant force is higher than the magnetic attractive force of steel balls to the magnets. The acrylic float plays a critical role here as it should push steel balls up after the required amount of magnetic fluid is filled. An appropriate thickness for the acrylic float can reduce or even eliminate the attractive force from the magnets to steel balls by keeping them "further" away from the magnetic poles (where magnetic field intensity is very small or negligible). Also, a larger buoyant force near the magnetic poles of the bottom surface of the float can be transmitted to the ball support area (the top surface of float) by acrylic float. Table 9.6 gives the polishing conditions used in this investigation.

Table 9.6 Polishing conditions used for finishing stainless steel balls by MFP

Workmaterial	SS440 stainless steel balls
Polishing Tool Material	304 stainless steel
Abrasive	B <sub>4</sub> C #1500, SiC#8000 Diamond, Al <sub>2</sub> O <sub>3</sub> , ZrO <sub>2</sub> , Cr <sub>2</sub> O <sub>3</sub>
Magnetic Fluid	Oil-based (EMG 909)
Abrasive vol%	2.5%, 5 %, 10%
Polishing Load, N/ball	0.25, 0.5, 1
Polishing Speed, rpm	2000, 4000, 6000, 8000
Test Time, min/step	30

Table 9.7 shows the results of the tests for finishing stainless steel balls by MFP with B<sub>4</sub>C #1500 and SiC #8000 abrasives. Compared with Si<sub>3</sub>N<sub>4</sub> balls, the influence of polishing parameters on the surface finish of stainless steel

balls is more significant but the optimum polishing conditions are the same, i.e., 5 vol %, 8000 rpm, 1 N/ball. The material removal is by plastic deformation, and plowing can be observed on the polished surface.

Table 9.7 Test results of finishing stainless steel balls by MFP

Abrasive Type	Abrasive Size ( $\mu\text{m}$ )	Abrasive, vol%	Speed, rpm	Load, N/ball	Surface	Finish
					Ra ( $\mu\text{m}$ )	Rt ( $\mu\text{m}$ )
SiC 1200	5	10%	2000	1.0	0.45	4.80
B <sub>4</sub> C 1500	2	10%	4000	1.0	0.13	1.35
B <sub>4</sub> C 1500	2	10%	6000	1.0	0.11	1.20
SiC 8000	1	10%	6000	1.0	0.11	1.20
B <sub>4</sub> C 1500	2	<b>5%</b>	<b>8000</b>	<b>0.5</b>	0.06	0.80
B <sub>4</sub> C 1500	2	2.5%	8000	0.25	0.05	0.95
SiC 8000	1	<b>5%</b>	<b>8000</b>	<b>1.0</b>	<b>0.06</b>	<b>0.60</b>

Tables 9.8 and 9.9 show polishing conditions and test results of finishing stainless steel balls by MFP with a Si<sub>3</sub>N<sub>4</sub> shaft and Cr<sub>2</sub>O<sub>3</sub> abrasive as well as without any abrasive (i.e., only magnetic fluid). Table 9.10 shows a comparison of test results (out-of-roundness) of finishing stainless steel balls by MFP with a 304 stainless steel and a Si<sub>3</sub>N<sub>4</sub> shaft. It can be seen that roundness has improved using the Si<sub>3</sub>N<sub>4</sub> shaft without abrasive to 0.75  $\mu\text{m}$ . This is attributed to the plastic deformation of the balls from the squeezing action between the advanced ceramic shaft and the steel balls.



Table 9.8 Polishing conditions used for finishing stainless steel balls by MFP with a Si<sub>3</sub>N<sub>4</sub> shaft

Workmaterial	SS440 stainless steel balls
Polishing Tool Material	Advanced Silicon Nitride (Si <sub>3</sub> N <sub>4</sub> )
Abrasive	Cr <sub>2</sub> O <sub>3</sub> , without abrasive,
Magnetic Fluid	Oil-based (EMG 909)
Abrasive vol%	0%
Polishing Load, N/ball	1
Polishing Speed, rpm	8000
Test Time, min/step	60

Table 9.9 Test results of finishing stainless steel balls by MFP with a Si<sub>3</sub>N<sub>4</sub> Shaft

Abrasive	Ra (μm)	Rt (μm)
Cr <sub>2</sub> O <sub>3</sub> (1 μm)	0.07	0.8
without abrasive	0.08	0.9

Table 9.10 A comparison of polishing results of finishing stainless steel balls by MFP with 304 stainless steel and Si<sub>3</sub>N<sub>4</sub> shafts

Shaft (Polishing Pad)	Abrasive	Out-of-Roundness (μm)
304 stainless steel	with	> 1.6
Si <sub>3</sub> N <sub>4</sub> advanced ceramic	without	0.75

In summary, in the MFP of steel bearing balls, the results of polishing using SiC, B<sub>4</sub>C, Cr<sub>2</sub>O<sub>3</sub> abrasives are found to be better than that of diamond, Al<sub>2</sub>O<sub>3</sub>, and ZrO<sub>2</sub>. Optimum parameters from surface finish point of view are speed 8000 rpm, abrasive concentration 5 vol % and load 1 N per ball; The roundness of the balls finished by the steel shaft (polishing pad) with abrasives was > 1.6 μm. Use of Si<sub>3</sub>N<sub>4</sub> polishing shaft without any abrasive has yielded an improved roundness to 0.75 μm. However surface roughness was still high (Ra > 60 nm). Further research is needed to improve the surface finish Ra to 20 nm for bearing applications. This may involve using soft polishing shaft for final finishing. It is known that in order to obtain best surface finish on steel bearing balls industry uses a buffing process where semi-finished balls are loaded in a rotating chamber with pieces of leather, fine abrasive, and water for a week. The process for finishing stainless balls by MFP may be as follows: 304 stainless steel (or cast iron shaft) with B<sub>4</sub>C or SiC abrasive (< 5 μm grit size) to reach the diameter and better roundness, and then polishing with Si<sub>3</sub>N<sub>4</sub> shaft without abrasive to final roundness, and then use a soft shaft (buff, leather, wood, felt, polyurethane) with a fine soft abrasive (CaCO<sub>3</sub> ?) for obtaining final surface finish.

## CHAPTER 10

### CONCLUSIONS

1. An effective methodology for finishing silicon nitride balls of required tolerance for bearing application has been presented and supported by experimental results. There are three basic stages involved in polishing, namely, initial roughing stage where the emphasis is on high material removal rate with minimal surface and subsurface damage, intermediate semi-finishing stage where material removal rate, sphericity, and surface roughness have to be closely monitored, and final finishing stage where emphasis is on the required size, sphericity, and finish.
2. The advantage of the magnetic float polishing (MFP) apparatus used in this investigation is that it is capable of finishing a small batch (10-20) balls to the finish requirements without the need for sorting them from a large batch of balls or use different equipment for roughing, semifinishing, and finishing as in conventional lapping. Such an apparatus would be beneficial especially when small batches are needed for specific low volume applications or for evaluation of materials in the development of new materials for bearing applications.
3. Magnetic float polishing (MFP)  $\text{Si}_3\text{N}_4$  balls for bearing applications using fine mechanical polishing followed by chemo-mechanical polishing (CMP) is an efficient and cost effective manufacturing technology for producing high quality due to high polishing speed, small and controlled polishing force, flexible support, and chemo-mechanical action.

4. High material removal rates (1  $\mu\text{m}/\text{min}$ ) with minimal subsurface damage are possible using harder abrasives, such as  $\text{B}_4\text{C}$  or  $\text{SiC}$  due to rapid accumulation of minute amounts of material removed by mechanical microfracture at high polishing speeds and low loads used in the MFP process. Although material removal is by brittle fracture, it occurs on a microscale due to low polishing force, flexible float system, and fine abrasives. The cracks generated are localized and suppressed from propagating into microcracks. Consequently subsurface damage is minimized leading to higher strength of the workmaterial and reliability of the parts in service.
  
4. Experimental design based on Taguchi method has been successfully applied to determine the optimum processing conditions (within the range of parameters and levels tested) for improving the surface quality of the ceramic balls by magnetic float polishing (MFP). The three important parameters for surface quality are identified as the polishing force, the abrasive concentration, and the polishing speed for a given abrasive and its grain size. Among the three parameters tested, the polishing force was found to be the most significant from a consideration of the overall surface finish,  $R_a$  and  $R_t$ . For the surface finish  $R_a$ , the polishing force was found to be most significant followed by polishing speed and then abrasive concentration while for  $R_t$ , the polishing force was most significant followed by the abrasive concentration and then polishing speed.
  
6. The results from Taguchi experimental design also indicate that within the range of parameters evaluated, a high level of polishing force (1.4 N), a low level of abrasive concentration (5%), and a high level of polishing

speed (7000 rpm x 2.5 inch) are optimum for improving both Ra and Rt. A comparison of the results obtained by the Taguchi method with single parameter (i. e. one parameter by one parameter) variation using a fine SiC abrasive (1  $\mu\text{m}$ ) yielded a similar conclusion for optimum polishing conditions, but Taguchi method can extract information more precisely and more efficiently.

7. The best surface finish obtained using fine, harder  $\text{B}_4\text{C}$  abrasive (1-2  $\mu\text{m}$ ) was 20 nm for Ra and 200 nm for Rt; The best surface finish obtained using fine, harder SiC abrasive (1  $\mu\text{m}$ ) was 15 nm for Ra and 150 nm for Rt; To improve the final surface finish, further polishing has to be carried out, involving chemo-mechanical polishing.
8. Chemo-mechanical polishing (CMP) depends on the polishing conditions used, abrasive-workmaterial combination, and the environment used. Among various abrasives investigated for CMP of  $\text{Si}_3\text{N}_4$  bearing balls with magnetic float polishing (MFP),  $\text{CeO}_2$  and  $\text{ZrO}_2$  abrasives were found to be most effective followed by  $\text{Fe}_2\text{O}_3$  and  $\text{Cr}_2\text{O}_3$ . It was also found that CMP of  $\text{Si}_3\text{N}_4$  was particularly effective in a water-based fluid environment.
9. Thermodynamic analysis (Gibbs free energy of formation) indicated the feasibility of chemical reactions between  $\text{CeO}_2$ ,  $\text{ZrO}_2$ ,  $\text{Fe}_2\text{O}_3$ , and  $\text{Cr}_2\text{O}_3$  abrasives and  $\text{Si}_3\text{N}_4$  workmaterial leading to the formation of a  $\text{SiO}_2$  layer. Since the hardness of these abrasives are closer to that of  $\text{SiO}_2$  layer and lower than  $\text{Si}_3\text{N}_4$  workmaterial,  $\text{SiO}_2$  reaction layer is effectively removed without damaging the  $\text{Si}_3\text{N}_4$  substrate by the subsequent mechanical action by the abrasives on the workmaterial. The kinetic action, which removes the reaction products from the interface is critical in the CMP

process. The chemical reaction will be continued only after the passivating layers are removed continuously by the subsequent mechanical action.

10. It is found that there is very little, if any, of CMP occurring in an oil-based polishing environment. The conductivity and dissolution value of an oil-based polishing fluid is nearly zero. The oil film between the abrasive and the workmaterial prevents any chemical reactions between them as well as the removal of reaction layer formed, if any, thus minimizing CMP. It can be seen that CMP of  $\text{Si}_3\text{N}_4$  is particularly effective in a water environment and water is found to be essential for CMP of  $\text{Si}_3\text{N}_4$  workmaterial. Water from water-based polishing fluid not only facilitates chemo-mechanical interaction between the abrasive and the workmaterial but also participates directly in the chemical reaction with the  $\text{Si}_3\text{N}_4$  workmaterial (hydrolysis) leading to the formation of  $\text{SiO}_2$  softer layer thereby enhancing the CMP.
11. An extremely smooth and damage-free surface with a finish  $R_a$  of 4 nm and  $R_t$  of 40 nm has been obtained by  $\text{CeO}_2$  and  $\text{ZrO}_2$  abrasives in the CMP of  $\text{Si}_3\text{N}_4$  balls.  $\text{CeO}_2$  and  $\text{ZrO}_2$  are much softer than  $\text{Si}_3\text{N}_4$  and could not cause any mechanical damage and scratching on the  $\text{Si}_3\text{N}_4$  workmaterials. In the case of  $\text{Cr}_2\text{O}_3$  abrasive, the mechanical abrasion caused by  $\text{Cr}_2\text{O}_3$  could not be eliminated completely, in spite of its chemo-mechanical polishing ability, because  $\text{Cr}_2\text{O}_3$  is slightly harder compared to the  $\text{Si}_3\text{N}_4$  workmaterial. Consequently, while CMP can take place effectively, possibility exists for mechanical abrasion and subsequent microchipping. Further,  $\text{CeO}_2$  and  $\text{ZrO}_2$  and their various reaction products formed during polishing are much safer than the compounds formed by the

reaction of  $\text{Cr}_2\text{O}_3$  with  $\text{Si}_3\text{N}_4$  workmaterial from an environmental point of view.

12. It has been reported that the best abrasives for polishing Glasses are  $\text{CeO}_2$  and  $\text{ZrO}_2$  [Cook, 1990]. There are similarities between polishing glass and polishing  $\text{Si}_3\text{N}_4$  workmaterial including the role of water, polishing environment pH value of 7-9, and abrasive hardness of ~ Mohs 7 for effective polishing. It is somewhat coincidental that, in general, chemical effectiveness and mechanical hardness of abrasives for CMP of  $\text{Si}_3\text{N}_4$  are similar to those for glass. This is not altogether surprising as the material removal mechanism in the case of  $\text{Si}_3\text{N}_4$  is through the formation of  $\text{SiO}_2$  and in the case of glass which is basically  $\text{SiO}_2$  (Mohs 6.5). From an analysis of CMP mechanism for  $\text{Si}_3\text{N}_4$  it appears reasonable to extend this mechanism to the polishing of silicon wafers,  $\text{SiO}_2$  glasses, and  $\text{SiC}$  advanced ceramic. This is based on the similarity of the formation of  $\text{SiO}_2$  on the surface and its subsequent removal by mechanical action.
13.  $\text{CeO}_2$  is found to be the most effective abrasive in the chemo-mechanical polishing of  $\text{Si}_3\text{N}_4$  balls. It has two important functions in CMP of  $\text{Si}_3\text{N}_4$ . (1) it directly reacts chemically (oxidization-reduction reaction) with  $\text{Si}_3\text{N}_4$  workmaterial and leads to the formation of  $\text{SiO}_2$  layer; (2) The hardness of  $\text{CeO}_2$  (Moh 6) is close to that of the  $\text{SiO}_2$  layer (Moh 6.5) and significantly lower (about 1/3) than that of  $\text{Si}_3\text{N}_4$  workmaterial. So, the  $\text{Si}_3\text{N}_4$  substrate can hardly be scratched or damaged by  $\text{CeO}_2$  but the  $\text{SiO}_2$  layer can be removed under subsequent mechanical action of  $\text{CeO}_2$  on  $\text{Si}_3\text{N}_4$  workmaterial. The  $\text{CeO}_2$  polishing media is particularly effective in a water environment. Reaction between  $\text{Si}_3\text{N}_4$  workmaterial and water (from water-based magnetic fluid) also occurs (hydrolysis) and leads to the formation of

SiO<sub>2</sub> layer which is also removed from the Si<sub>3</sub>N<sub>4</sub> substrate by subsequent mechanical action of CeO<sub>2</sub>. The flash temperature generated and the corresponding flash times in the polishing process were calculated using the moving disc heat source model developed by Hou and Komanduri. It can be seen that the possible temperatures generated and flash times at the contact zone of the CMP process are adequate for the generation of specific reactions from previous thermodynamic analysis.

14. The Si<sub>3</sub>N<sub>4</sub> surface after CMP would consist of an outer SiO<sub>2</sub> layer and an intermediate layer of silicon oxinitride (Si<sub>x</sub>O<sub>y</sub>N<sub>z</sub>) on the Si<sub>3</sub>N<sub>4</sub> substrate. The layers composed of amorphous and crystalline SiO<sub>2</sub>, Si<sub>2</sub>N<sub>2</sub>O, and MgSiO<sub>3</sub>/MgO.SiO<sub>2</sub> form by the reaction with the sintering aid (1 wt.% MgO). This is not much different from the surface of Si<sub>3</sub>N<sub>4</sub> workmaterial which invariably has a natural oxidation layer in air even at room temperature.
15. MFP can be a cost effective process for finishing Si<sub>3</sub>N<sub>4</sub> balls for bearing applications. The semifinishing and finishing stages can be accomplished in about 4 hours. The roughing stage depends on the amount of material to be removed from the as-received condition to the final requirements. In any case, a batch of balls can be finished in about 16 to 20 hours compared to several weeks by conventional polishing. Also, diamond abrasive is not required for the process. Faster polishing times and use of abrasives other than diamond would significantly reduce the overall costs of manufacture. Also, implementation of this technology would not be capital intensive as it can be used by incorporating with the existing equipment.



## REFERENCES

- Abe, T., "A Future Technology for Silicon Wafer Processing for ULSI," Precision Engineering, 13/4, Oct. 1991, 251-255
- Ajayi O. O. and K. C. Ludema, "Surface Damage of Structural Ceramics: Implications for Wear Modeling," Wear, 124, 1988, 237 - 257
- Baghavatula, R. S., "Chemo-mechanical Polishing of Silicon Nitride with Chromium Oxide Abrasive," Masters thesis, Oklahoma State University, 1995
- Baghavatula, S. R., and R. Komanduri, "On Chemo-mechanical Polishing of Silicon Nitride with Chromium Oxide Abrasive," Philosophical Magazine A, 74/4, 1996, 1003-1017
- Barker, T. B., "Engineering Quality by Design - Interpreting the Taguchi Approach", Statistics, Vol. 113. Marcel Dekker, Inc, 1990
- Bifano, T. G. and Fawcett, S. C., "Specific Grinding Energy as an In-process Control Variable for Ductile-Regime Grinding," Precision Engineering, 13, 1991, 256-262
- (14) Buchner, K., "A Comparison of Spindle Ball Bearings with Steel or Ceramic Balls for Very High Speed Applications," Creative Use of Bearing Steels, ASTM STP 1195, J. J. Hoo, ED., American Society for Testing and Materials, Philadelphia, 1993. pp. 121-133
- (5) Burrier, H. I. and Burk, C., "Fatigue and Wear Behavior of NBD-200 Silicon Nitride Balls," Ceramic Bearing Development, WL-TR-96-4015 ?

- Chen, Z., Cuneo, J. C., Mecholsky, J. J., and Hu, S., "Damage Processes in  $\text{Si}_3\text{N}_4$  Bearing Material Under Contact Loading," *Wear*, 198, 1996, 197-207
- Childs T.H.C and H.J. Yoon, "Magnetic Fluid Grinding Cell Design," *Annals of CIRP*, 41/1, 1992, 343-346
- Childs, T.H.C., Jones, D.A., Mahmood, S., Kato, K., Zhang, B., and N. Umehara, "Magnetic Fluid Grinding Mechanics," *Wear*, 175, 1994a, 189-198
- Childs, T.H.C., Mahmood, S. and H.J. Yoon, "The Material Removal Mechanism in Magnetic Fluid Grinding of Ceramic Ball Bearings," *Proc. of I. Mech. E. London*, 208, No. B1, 1994b, 47 - 59
- Childs T.H.C., Mahmood S and H.J. Yoon, "Magnetic Fluid Grinding of Ceramic Balls," *Tribology International*, 28, No. 6, 1995, 341 - 348
- Coats, H. P., "Method and apparatus for polishing containers," US Patent 2196058, 1940
- Cook, L. M., "Chemical Processes In Glass Polishing," *J. of Non-Crystalline Solids*, 120, 1990, 152-171 666.105 386
- Dagnall, H., "Let's Talk Roundness," Rank Talyor Hobson Inc, 1984.
- Dagnall, H., "Exploring Surface Texture," Rank Talyor Hobson Inc, 1986.
- David, S. B. and John, M. W., "Chemomechanical Polishing of Silica and Silicon by Fluoride- and Oxide-based Reagents: identification of a reaction intermediate," *J. Mater. Chem.*, 6/2, 1996, 227-232
- Dehnad, K. E. "Quality Control, Robust Design, and the Taguchi Method," Brooks/Cole Pub. Co., CA, 1989
- Dock, M., "Electromagnetic Float Polishing of Ceramic Balls for Bearing Applications," Masters Thesis, Oklahoma State University, 1995

- Dong, X. and Jahanmir, "Wear Transition Diagram for Silicon Nitride," *Wear*, 165, 1993, 169-180
- Evans A. G. and D. B. Marshall, "Wear mechanisms in ceramics," *Fundamentals of friction and wear of materials*, Ed. by Rigney, D. A., ASME Handbook, 1981, 439 - 452
- Fisher, R. S. "The Design of Experiments," Hafner, NY, 1971
- Fischer, T. E. and Tomizawa, H., "Interaction of Tribochemistry and Microfracture in the Friction and Wear of Silicon Nitride," *Wear*, 105, 1995, 29-45
- Fischer, T. E., "Tribochemistry," *Ann. Rev. of Mater. Sci.*, 18, 1988, 303-323
- ⑧ Gardos, M. N., and Pratt, J. R., "Effects of Machining and Finishing on Performance," *Ceramic Bearing Technology*, NIST Special Publication 824, Ed by Said Jahanmir, 1991
- Gardos, M. N., and R. G. Hardisty, "Fracture toughness - and hardness depended polishing wear of silicon nitride ceramics," *Tribology Transactions*, 36, No. 4, 1993, 652-660
- ③ Gottschalk, M. A. and Bak, D. J., "Superbearings: Ceramic Bearing," *Design News*, Dec. 1995
- Hah, S. R., Fischer, T. E. and C. Burk, "Ceramic Bearing Development, Vo.4, Tribochemical Finishing of Silicon Nitride," Technical Report No. WL-TR-96-4018, the Materials Directorate, Wright Patterson AFB OH, March, 1995
- Hah, S. R., "Tribochemical Polishing of Silicon Nitride," Ph.D Thesis, Stevens Institute of Technology, Hoboken, NJ., 1995
- Hashimura, M., "Grinding," *Ceramics Processing State of the Art of R&D in Japan*, Ed by Hirotohi Nogana, Japan Materials Report by Japan Technical Information Service, ASM International, Metals Park, Ohio, 1988
- Hatta, K., "Polishing," *Ceramics Processing State of the Art of R&D in Japan*, Ed by Hirotohi Nogana, Japan Materials Report by Japan Technical Information Service, ASM International, Metals Park, Ohio, 1988

- Hu, K. X. and Chandra, A., "A Fracture Mechanics Approach to Modeling Strength Degradation in Ceramic Grinding Processes," ASME J. of Eng. for Ind., 115, 1993, 73-84
- Honda, F. and T. Saito, "Tribocchemical Characterization of the Lubrication Film at the Si<sub>3</sub>N<sub>4</sub>/Si<sub>3</sub>N<sub>4</sub> Interface Sliding in Aqueous Solutions," Applied Surface Science, 92, 1996, 651-655
- Hou, Zhen-Bing and R. Komanduri, "Magnetic Field Assisted Finishing of Ceramics - Part I: Thermal Model," accepted for publication in Trans ASME, J. of Tribology, 1998
- Hou, Zhen-Bing and R. Komanduri, "Magnetic Field Assisted Finishing of Ceramics - Part II: On the Thermal Aspects of Magnetic Float Polishing (MFP) of Ceramic Balls," accepted for publication in Trans ASME, J. of Tribology, 1998
- Hou, Zhen-Bing and R. Komanduri, "Magnetic Field Assisted Finishing of Ceramics - Part III: On the Thermal Aspects of Magnetic Abrasive Finishing (MAF) of Ceramic Rollers," accepted for publication in Trans ASME, J. of Tribology, 1998
- Inasaki, I., "Grinding of Hard and Brittle Materials," Annals of the CIRP, 36/2, 1987
- Indge, J. H., "The Nitty Gritty of Machining Ceramics," Tooling and Production Magazine, Feb. 1990 626.905 T671
- Indge, J. H., "Lapping: More Science less an Art Form," Ceramic Industry, July 1990, 26-28 666.05 C411
- Imanaka, O., and Okutomi, M., "New Concepts on Surface Finishing and Its Application To Ceramics: Recent Preogress in Ultra-Fine Finishing in Japan," The Science of Ceramic Machining and Surface Finishing II, Eds by Hockey, B. J., and R. W. Rice, National Bureau of Standards Special Publication 562, 1979, 157-169

- Jahanmir, S., Ives, L. K. and Ruff, A. W., and Peterson, M. B, "Ceramic Machining: Assessment of Current Practice and Research Needs in the United States," NIST Special Publication 834, 1992
- Jiang Ming and R. Komanduri, "Finishing of  $\text{Si}_3\text{N}_4$  Balls for Bearing Applications," WEAR 215, 1998, 267-278
- Jiang Ming and R. Komanduri, "Application of Taguchi Method to Determine Polishing Conditions in Magnetic Float Polishing" WEAR 213, 1997, 59-71
- Jiang Ming and R. Komanduri, "On the Chemo-Mechanical Polishing (CMP)  $\text{Si}_3\text{N}_4$  Bearing Balls with  $\text{CeO}_2$ ," submitted to ASME, J. of Materials Engineering and Technology, 1998.
- Jiang Ming and R. Komanduri, "Investigation of Chemo-mechanical Polishing (CMP) of Silicon Nitride With Various Abrasives" accepted for publication in WEAR, 1998.
- Jiang Ming and R. Komanduri, "A New Method for Finishing of  $\text{Si}_3\text{N}_4$  Balls for Bearing Applications," Patent Pending, 1997.
- Jiang Ming and R. Komanduri, "Magnetic Float Polishing Balls Made of Magnetic Materials," Patent Pending, 1997.
- Kachanov, M. and Montagnon, E., "Interaction of a Crack with Certain Microcrack Arrays," Eng. Frac. Mech., 25, 1986, 625-638
- Kato, K., "Tribology of Ceramics. ", Wear, 136, 1990, 117-133
- Kato, K., Umehara N., Adachi S., and S. Sato, "Method for grinding using a magnetic fluid and an apparatus thereof," U.S. patent 4821466, Apr. 18, 1989
- ① Katz, R. N. and Hasnnoosh, J. G., "Ceramics for High Performance Rolling Element Bearings: A Review and Assessment," Int. J. High Technology Ceramics, 1, 1985, 69-79 X

- Kawata, K. and Tani, Y., "Development of High-Concentration Lapping Discs with Low Bonding Strength and Their Application to Mirror Finishing of Brittle Materials," *JSME International Journal*, 36/2, 1993
- Kilbourn, B., T., "CERIUM - A Guide to Its Role in Chemical Technology," Molycorp, Inc., White Plains, NY, U.S.A (1992)
- Kitsunai, H., Kato, K., Hokkirigawa, K., and H. Inoue, "The Transitions Between Microscopic Wear Modes During Repeated Sliding Friction Observed by a Scanning Electron Microscope Tribosystem," *Wear*, 135, 1990, 237 - 249
- Komanduri, R., "On the Mechanisms of Material Removal in Fine Grinding and Polishing of Advanced Ceramics," *Annals of CIRP*, 44/1, 1996
- Komanduri, R., Umehara, N., and M. Raghunandan, "On the Possibility of Chemo-Mechanical Action in Magnetic Float Polishing of Silicon Nitride," *Trans ASME J of Tribology*, 118, 1996, 721-727
- Komanduri, R., Lucca, D. A., and Y. Tani, "Technological Advances in Fine Abrasive Process," *Annals of CIRP*, 46/2, 1997
- Komanduri, R., Umehara, N., Jiang, M., and P. Cao, "Large Batch Magnetic Float Polishing Apparatus," Patent Pending, 1998.
- Kurobe, T. and Imanaka, O., "Magnetic Field-assisted Fine Finishing," *Precision Engineering*, 6/3, 1984, 119-124
- Lange, F. F., "Eutectic Studies in the System  $\text{Si}_3\text{N}_4$  - $\text{Si}_2\text{N}_2\text{O}$ - $\text{Mg}_2\text{SiO}_4$ ," *J. of the Ameri. Ceram. Soci.*, 62, 1979, 617-
- Lawn, B. R. and Wilshaw, R., "Indentation Fracture: Principles and Applications," *J. Materials Science*, 10, 1975, 1049-1081
- Lawn, B. R. and Evans, A. G., "A Model of Crack Initiation in Elastic/Plastic Indentation Fields," *J. Mater. Sci.*, 12, 1977, 2195-2199
- Lawn, B. R. and Evans, A. G., "Elastic/Plastic Indentation Damage in Ceramic: The Median/Radial Crack System," *J. Amer. Ceram. Soc.*, 63, 1980, 574-581.

② Lynch, T. P., "Hybrid Ceramic Bearings Increase Turbine Life: silicon nitride balls in steel races survive conditions that destroy steel bearings," Design News, March 25, 1991. 620.004205 D457

Malkin, S. and Ritter, J. E., "Grinding Mechanism and Strength Degradation for Ceramic components," ASME J. of Eng. for Ind., 111, 1989, 167-173.

Malkin, S. and Hwang, T. W. , "Grinding Mechanisms for Ceramics," Annals of the CIRP, 45/2, 1996

Marshall, D. B., Lawn, B. R., and Evans, A. G. "Elastic/Plastic Indentation Damage in Ceramic: The Lateral Crack System," J. Amer Ceram. Soc., 63, 1982, 574-581

recall 666 M129c  
→ McColm, I. J., "Ceramic Science for Materials Technologists," 1983, 107-114.

→ McColm, I. J., "Ceramic Hardness," Plenum Press, New York, 1990 620.140426 mp9, recalled

Moreland, M. A., "Ultrasonic Machining," Ceramics and Glasses, Engineered Materials Handbook, 4, 1987

Mizuguchi S., Ueda S., Kato K., and N. Umehara, "Microscopic grinding method and microscopic grinding device," U.S. patent 5076026, Dec. 31, 1991

Oliver, R. C., Stephanou, S. E. and R. W. Baier, "Calculating Free-Energy Minimization," Chem. Engr., Feb., 1962, 121-128

Raghunandan, M., "Magnetic Float Polishing of Silicon Nitride Balls," Ph.D. thesis, Oklahoma State University, 1996

Raghunandan, M., Noori-Khajavi, A., Umehara, N., and R. Komanduri, "Magnetic Float Polishing of Advanced Ceramics," Trans ASME, J of Manf. Sci. and Engg 119, (1997) 520-528

Raghunandan, M. and R. Komanduri, "Finishing of Silicon Nitride Balls for High-speed Bearing Applications," Trans ASME, J of Manf. Sci. and Engg 120, (1998) 1-13

Roine, A., "HSC Chemistry for Windows - Chemical Reaction and Equilibrium Software with Extensive Thermochemical Database," published by Outokumpu Research Oy Information Service (97036-ORC-T), Finland, April 30, 1997

Rosensweig, R. E., "Ferrohydrodynamics," Cambridge University Press, Cambridge, U.K., 1985 *check, if I borrow it?*

Ross, P. J., "Taguchi Techniques for Quality Engineering," McGraw-Hill, NY, 1996

Roy, R. K. "A Primer on the Taguchi Method," Competitive Manufacturing Series, Van Nostrand Reinhold, NY, 1990

Ruhle, M. "Microscopy of Structural Ceramics," Adv. Mater., 9/3, 1997, 195-217.

Samuels, L. E., "The Nature of Mechanically Polished Metal Surfaces: the Surface Deformation Produced by the Abrasion and Polishing of 70:30 Brass," J. Inst. Metals, 85, 1956 - 57, 51-62

Shinmura, T., Takazawa, K., and E. Hatano, "Study of Magnetic Abrasive Finishing," Annals of CIRP, 39/1, 1990, 325-328

Shinmura, T., Yamaguchi, H. and T. Aizawa, "A New Internal Finishing Process for Non-ferromagnetic Tubing by the Application of a Magnetic Field - the Development of a Unit Type Finishing Apparatus Using Permanent Magnets," NAMRC, 1993

Singhal, S. C., "Thermodynamics and Kinetics of Oxidation of Hot-Pressed Silicon Nitride," J. of Materials Science, 11, 1976, 500-509

Subramanian, K., Indge, J. H., et al, "Final Shaping and Surface Finishing," Ceramics and Glasses, Engineered Materials Handbook, 4, 1987 *620.11 E52*

Subramanian, K., and Robert, N. K., "Grinding Advanced Ceramics: A Forecast for the 1990s," Ceramic Bulletin, 67/12, 1988 *666.306 A 512L*



- Suzuki, H., Kodera, S., Hara, S., Matsunaga and Kurobe, T., "Magnetic Field-assisted polishing - Application to a Curved Surface," Precision Engineering, 11/4, 1989, 197-202
- Swain, M. V., "Microfracture about Scratches in Brittle Solids," Proc. Roy. Soc. London, A366, 1979, 575-597
- Takazawa, K., Shinmura, and E. Hatano, "Development of Magnetic Abrasive Finishing and Its Equipment," MR 83-678. Proc. of the SME'S 12th Deburring and Surface Conditioning Conference, Orlando , Nov 8-10, 1983
- Taguchi, Genichi "Taguchi Methods - Research and Development," ASI Press, Dearborn, MI, 1992
- Takazawa, K., Shinmura, and E. Hatano, "Advanced Development of Magnetic Abrasive Finishing and Its Equipment," Proc. of the SME'S Deburring and Surface Conditioning Conference '85, Orlando , Sept 23-26, 1985, 30-46
- Tani, Y. and K. Kawata, "Development of High-efficient Fine Finishing Process Using Magnetic Fluid," Annals of CIRP, 33/1, 1984, 217-220
- Taniguchi, N., and Kanekama, N., "On the Ion Beam Sputter machining of Glass," Annals CIRP, 22, 1973, 69-70
- Tighe, N. J., "Analysis of Oxide and Oxide/Matrix Interfaces in Silicon Nitride," National Bureau of Standards, NBSIR 82-2574, 1982
- Usui, E., Modern Cutting Theory, 1990 (in Japanese)
- Umehara N., "Research on Magnetic Fluid Polishing," Ph.D. thesis (in Japanese), Tohoku University, Japan, 1990
- Umehara N. and K. Kato, "Principles of Magnetic Fluid Grinding of Ceramic Balls," Applied Electromagnetics in Materials, 1, 1990, 37-43
- Umehara N., Kato. K and H. Nakano, "Magnetic Fluid Grinding of Ceramic Rollers," Electromagnetic Forces and Applications, Elsevier Science Publishers, 1992, 139 - 142

- Umehara N., Kato. K and I. Kanagawa, "Magnetic Fluid Grinding of Ceramic Flat Surfaces," Electromagnetic Forces and Applications, Elsevier Science Publishers, 1992, 143 - 146
- Umehara N. and K. Kato, "Fundamental Properties of Magnetic Fluid Grinding with a Floating Polisher," Journal of Magnetism and Magnetic Materials, 122, 1993, 428-431
- Umehara N., S. Mizuguchi, K. Kato and S. Nakamura, "Microsurface Finishing of Borosilicate Glass with Magnetic Fluid Grinding," Journal of Magnetism and Magnetic Materials, 122, 1993, 432-4363.
- Umehara, N., "Magnetic Fluid Grinding - a New Technique for Finishing Advanced Ceramics," Annals of CIRP, 43/1, 1994, 185 - 188
- Umehara, N. and R. Komanduri, "On the Material Removal Mechanisms in Polishing of Advanced Ceramics," paper presented at the Annual Meeting of the Japan Society of Tribologists ,1994, (in Japanese)
- Umehara, N. and R. Komanduri, "Magnetic Fluid Grinding of HIP-Si<sub>3</sub>N<sub>4</sub> Rollers," Wear, 192, 1996, 85-93
- Wang, Y. and Stephen M. H., "Wear and Wear Transition Mechanisms of Ceramics," Wear, 195, 1996, 112-122
- Wang, J. C. and S. M. Hsu, "Chemically Assisted Machining of Ceramics," J. of Tribology, 116, 1994, 423 - 429 621. 8905 J86
- Wallace, T. W., Wu, W. L. and R. A., Carpio, "Chemical-mechanical Polishing of SiO<sub>2</sub> Thin Films Studied by X-ray Reflectivity," Thin Solid Films, 280, 1996, 37-42
- Watanabe, J., "Noncontacting Polishing of Semi-conductor Substrate," Precision Machinery, 49/5, 1983, 99
- Xu, H. H. K., Jahanmir, S., and Ives, L. K., "Material Removal and Damage Formation Mechanisms in Grinding Silicon Nitride," J. Mater. Res., 11/7, 1996, 1717-1724

- Yasunaga, N., Obara, A., and O. Imanaka, "Study of Mechanochemical Effect on Wear and its application to Surface Finish," J. of JSPE, 44, 1978, 77-83 (in Japanese)
- Yasunaga, N., Tarumi, N., Obara, A., and O. Imanaka, "Mechanism and Application of the Mechanochemical Polishing Method Using Softer Powder," Science of Ceramic Machining and Surface Finishing - II., Ed. B. H. Hockey and R. W. Rice, NBS Special Publication, No. 562, 1979, 171-
- Yeh, C. H. and Hon, M. H., "Chemical Interaction Between Silicon Nitride and Titanium Carbide Powder," J. Amer. Ceram. Soc., 78/9, 1994, 2395-2340
- Zhang, B., Umehara, N. and K. Kato, "Effect of the Eccentricity Between the Driving Shaft and the Guide Ring on the Behavior of Magnetic Fluid Grinding of Ceramic Balls," Precision Engineering, 61/4, 1995, 587-590 (in Japanese)
- Zhang, B., Kato, K. and Umehara, N., "Dynamic Mechanics of Magnetic Fluid Grinding Process of Ceramic Balls," to be published.
- Zhang, B., Umehara, N. and K. Kato, "Magnetic Fluid Grinding of Ceramic Balls by Off-Setting Drive Shaft and Guide Ring Centers," to be published.

## APPENDIX

### Technical Publications Resulting of This Work

Jiang Ming and R. Komanduri, "Finishing of Si<sub>3</sub>N<sub>4</sub> Balls for Bearing Applications," WEAR 215, 1998, 267-278.

Jiang Ming and R. Komanduri, "Application of Taguchi Method to Determine Polishing Conditions in Magnetic Float Polishing" WEAR 213, 1997, 59-71.

Jiang Ming and R. Komanduri, "Investigation of Chemo-mechanical Polishing (CMP) of Silicon Nitride with Various Abrasives" accepted for publication in WEAR, 1998.

Jiang Ming and R. Komanduri, "On the Chemo-Mechanical Polishing (CMP) Si<sub>3</sub>N<sub>4</sub> Bearing Balls with water-based CeO<sub>2</sub> slurry," submitted to Trans ASME, J. of Materials Engineering and Technology, 1998.

**VITA**  
**MING JIANG**  
**Candidate for the Degree of**  
**Doctor of Philosophy**

**Thesis:** FINISHING OF ADVANCED CERAMIC BALLS FOR BEARING APPLICATIONS BY MAGNETIC FLOAT POLISHING (MFP) INVOLVING FINE POLISHING FOLLOWED BY CHEMO-MECHANICAL POLISHING (CMP)

**Major Field:** Mechanical Engineering

**Biographical:**

**Personal Data:** Born in ChangChen, JiLin, China, on Feb. 17, 1969, the son of ZhuWang Jiang and ZhenChen Jiang.

**Education:** Received Bachelor of Science degree in Mechanical Engineering from HuaQiao University, FuJian, China in July, 1991. Master of Science degree in Mechanical Engineering from HuaQiao University, FuJian, China in July, 1994. Completed the requirements for the degree of Doctor of Philosophy at Oklahoma State University in July, 1998.

**Experience:** Graduate Research Assistant in Mechanical and Aerospace Engineering Department, Oklahoma State University, Stillwater, Oklahoma, 1994 - 1998.